ENVIRONMENTAL ATTACK ON ADHESIVE JOINTS: A FRACTURE MECHANICS APPROACH

by

Panagiotis Frantzis, B.Sc. (Eng), M.Sc., D.I.C.

A thesis submited for the degree of Doctor of Philosophy in the Faculty of Engineering, University of London.

Department of Mechanical Engineering
Imperial College of Science and Technology
London SW7 2BX

February 1989

ABSTRACT

Epoxide resins are widely employed as adhesives and are being increasingly used in engineering industries. The prediction of the strength of such components is therefore vitally important and different approaches and methods are being used to investigate the fracture behaviour of structural adhesives and to predict the durability of adhesive joints when exposed to hostile environments.

The present work firstly describes the development of a relatively simple and inexpensive method to obtain fracture data of adhesive joints. The method is based upon a fracture mechanics approach to the failure of adhesive joints and basically consists of employing a double-torsion joint design. Such adhesive joints have been prepared from steel substrates with a brittle or rubber-toughened epoxide adhesive. By building rigs for subjecting the double-torsion joints to a constant load the test technique is particularly suitable as an accelerated ageing test for examining the resistance of the adhesive joints to attack by moisture. A graphite-gauge method has also been developed to monitor the incubation time for an "interphase" crack to form, and to measure its subsequent velocity, as a function of the applied fracture energy for the different joints exposed in water at the different test temperatures. Secondly, the diffusion and solubility coefficients of water in the different adhesives have been determined, in order to help establish the kinetics of the failure process. Thirdly, scanning electron microscopy and X-ray photoelectron spectroscopy have been employed to identify the locus of joint failure after water attack.These data have been used, together with the fracture mechanics data, to propose a model for the attack of water upon the adhesive joints. Finally, simple butt joints have been subjected to various constant applied loads, in a water bath, and the time to failure measured. This is a typical accelerated ageing test employed in industrial laboratories. The above model, incorporating the fracture mechanics data, has been used in an attempt to predict the lifetimes of these joints, and the theoretical predictions are compared to the experimental data.

CONTENTS

	Page
ABSTRACT	(ii)
CONTENTS	(iii)
ACKNOWLEDGEMENTS	(ix)
LIST OF SYMBOLS	(x)
CHAPTER 1: INTRODUCTION	1
CHAPTER 2: LITERATURE SURVEY	3
2.1 FRACTURE MECHANICS	3
2.1.1 Introduction	3
2.1.2 Energy Balance Approach	4
2.1.3 Stress Intensity Factor Approach	4
2.1.4 G and K Relations	6
2.2 THE DOUBLE-TORSION TEST GEOMETRY	9
2.2.1 Opening Remarks	9
2.2.2 Analysis of the DT Geometry	10
2.2.3 Methods of Calculating Crack Velocity	11
2.3 EPOXIDE RESINS: FRACTURE BEHAVIOUR	14
2.3.1 Introduction	14
2.3.2 Types of Crack Propagation	14
2.3.3 Bulk Fracture Studies	15
2.3.4 Water Diffusion Studies	19
2.4 ADHESIVE JOINTS: FRACTURE BEHAVIOUR	21
2.4.1 Introduction	21
2.4.2 Fracture Behaviour and Environmental Attack	22
2.4.3 Adhesive Joints: Fracture Studies	23
2.5 Mechanisms of Adhesion	27

2.5.1 Introduction 27
2.5.2 Adsorption Theory 27
2.5.3 Electronic Theory 29
2.5.4 Mechanical Theory 30
2.5.5 Diffusion Theory 31
2.5.6 Kinetics of Wetting 31
2.5.7 Summary 32
2.6 ENVIRONMENTAL ATTACK 32
2.6.1 Introduction 32
2.6.2 Early Work 33
2.6.3 Effect of Surface Treatment 34
2.6.4 Effect of Stress 35
2.6.5 Thermodynamic Work of Adhesion and Kinetics of Attack 36
2.6.6 X-Ray Photoelectron Spectroscopy 38
2.6.7 Predictive Models 40
2.6.8 Summary 43
CHAPTER 3: EXPERIMENTAL METHODS 70
3.1 MATERIALS 70
3.2 PREPARATION OF SPECIMENS 71
3.2.1 Preparation of epoxide Polymer used for the DT and Butt Joints 71
3.2.2 Bulk Specimens for Diffusion Studies 71
3.2.3 Bulk Specimens for Fracture Studies 72
3.2.4 Adhesive Joints 72
3.3 FRACTURE EXPERIMENTS ON DT SPECIMENS 73
3.3.1 Introduction 73

3.3.2 Tests Conducted at a Constant Displacement Rate 73
3.3.3 Calibration of the Tensile-Testing Machine 74
3.3.4 Compliance Measurements 74
3.3.5 Calibration of Transducer 74
3.3.6 Compliance Tests 75
3.3.7 Fracture Tests 75
3.3.8 Constant Load Tests 75
3.3.9 Test Equipment 76
3.3.10 Compliance Measurements 76
3.3.11 Calibration of Transducer 77
3.3.12 Compliance Tests 77
3.3.13 Fracture Tests 77
3.3.14 Crack Speed Calculations 79
3.4 FRACTURE EXPERIMENTS ON BUTT JOINTS 80
3.4.1 Introduction 80
3.4.2 Test Equipment 80
3.4.3 Calibration 81
3.4.4 Fracture Tests 81
3.5 SCANNING ELECTRON MICROSCOPY (SEM) 81
3.6 X-RAY PHOTOELECTRON SPECTROSCOPY (XPS) 82
CHAPTER 4: RESULTS AND DISCUSSIONS:
FRACTURE TESTS 92
4.1 INTRODUCTION 92
4.2 CALCULATION OF FRACTURE MECHANICS
PARAMETERS 92
4.2.1 Introduction 92
4.2.2 Stress-Intensity Factor Criterion 92

4.2.3 Fracture Energy Criterion 93

4.2.4 Other Equations 94

4.2.5 Compliance Results 95

4.2.5.1 Bulk Material 95

4.2.5.2 Adhesive Joints 97

4.2.5.3 Conclusions 97

4.3 FRACTURE OF BULK MATERIAL 97

4.3.1 Introduction 97

4.3.2 Types of Crack Growth 98

4.3.3 Values of Stress-Intensity Factor 98

4.3.4 Effect of Structure 99

4.3.5 Summary 99

4.4 FRACTURE OF ADHESIVE JOINTS 101

4.4.1 Introduction 101

4.4.2 Constant Displacement Rate Tests 101

4.4.3 Effect of Test Temperature 101

4.4.4 Effect of Structure 102

4.4.5 Constant Load Tests 102

4.4.5.1 Effect of Environment 102

4.4.5.2 Incubation Time 103

4.4.5.3 Crack Speed 103

4.4.5.4 Effect of Structure 104

4.4.5.5 Conclusions 105

4.5 ADHESIVE BUTT JOINT TESTS 105

4.5.1 Introduction 105

4.5.2 Rubber-modified Epoxide Data 106

4.5.3 Unmodified Epoxide Data 106

4.5.4 Comparison of Butt Joints Fracture Data 106
4.5.5 Butt Joints Fracture Surface 106
4.6 CONCLUSIONS 107
CHAPTER 5: RESULTS AND DISCUSSIONS: DIFFUSION OF WATER STUDIES 148
5.1 INTODUCTION 148
5.2 WATER UPTAKE DATA 148
5.3 CALCULATIONS OF DIFFUSION AND SOLUBILITY COEFFICIENTS 149
5.3.1 Equations 149
5.3.2 Values of Diffusion and Solubility Coefficients 150
5.3.3 Water Ingress Into Joints 152
5.4 SUMMARY 154
CHAPTER 6: RESULTS AND DISCUSSIONS: LOCUS OF JOINT FAILURE STUDIES 177
6.1 INTRODUCTION 177
6.2 VISUAL EXAMINATION OF THE FRACTURE SURFACES OF DOUBLE-TORSION (DT) JOINTS 177
6.3 SCANNING ELECTRON MICROSCOPY OF THE FAILED DT JOINTS 177
6.3.1 Introduction 177
6.3.2 Prior to Environmental Attack 178
6.3.3 After Environmental Attack 179
6.4 X-RAY PHOTOELECTRON SPECTROSCOPY RESULTS 179
6.4.1 XPS Results of Metal Surface Prior to Bonding and Bulk Adhesives 179
6.4.2 XPS Results of Unmodified DT Joints 180

6.4.3 XPS Results of Rubber-modified DT Joints 181
6.4.4 XPS Results of Unmodified Butt Joints 181
6.4.5 XPS Results of Rubber-modified Butt Joints 182
6.5 CONCLUSIONS 182
CHAPTER 7: MECHANISMS AND MECHANICS OF ENVIRONMENTAL FAILURE 201
7.1 INTRODUCTION 201
7.2 MECHANISMS OF FAILURE 201
7.2.1 Thermodynamic Work of Adhesion 201
7.2.2 Kinetics of Failure 203
7.2.2.1 Critical Water Concentration 203
7.2.2.2 Effect of Temperature 204
7.2.3 Effect of Applied Stress 205
7.2.4 Lower Bound Values of Fracture Energy 207
7.3 PREDICTION OF ENVIRONMENTAL ATTACK 208
7.3.1 Introduction 208
7.3.2 Incubation Time 208
7.3.3 Crack Growth Stage 209
7.3.4 Comparison of Theoretical and Experimental Approaches 211
7.4 CONCLUSIONS 212
CHAPTER 8: FINAL CONCLUSIONS 220
CHAPTER 9: SUGGESTIONS FOR FURTHER WORK 223
REFERENCES 224
APPENDICES 236

ACKNOWLEDGEMENTS

I wish to express my gratitude to Dr. A.J.Kinloch for his personal interest and supervision, and Dr. P.S.Leevers for his professional advice on the graphite gauge technique. I am also grateful to the technicians, Mr. M.Rayner, Mr. J. C. Kramer-Hansen, Mr. T.J.Robinson, Mr. R.Wilkins, Mr. G.Senior, Mr. L.W.Morris, Mr. W.Rogers, and Mr. P.Farr, for their valuable assistance. I would also like to thank Dr. J.F.Watts and Mr. S.Greaves from Surrey University, and also my colleagues R.J.Davies and N.G.Cave for their assistance and encouragement.

Finally, I would like to thank the Ministry of Defence for their financial support.

LIST OF SYMBOLS

G	Fracture energy
G_c	Critical fracture energy
α	Crack length
$d\alpha/dt$	Crack speed
K	Stress intensity factor
K_c	Fracture toughness
t	Specimen thickness
F	External force
U	Elastic energy
P_c	Critical fracture load
C	Specimen compliance
σ	Stress at the onset of crack growth
σ_c	Critical stress
r,θ	Polar coordinates at the crack tip
τ	Shear stress
Y	Geometry factor
E	Young's modulus
ν	Poisson's ratio
l_m	Length of moment arm of DT specimens
k	Constant
w	DT specimen width
t_n	Effective DT specimen thickness
B, C_1, A_1, A_2	Constants
y	DT specimen displacement
D	Diffusion coefficient of distilled water
x	Distance into joint

M	Mass of water diffused into the adhesive
t_d	Diffusion time
W_A	Thermodynamic work of adhesion
γ	Surface free energy
C_t	Water concentration at time t
V	Voltage across the graphite gauge
W_o	Initial weight of diffusion samples
W_t	Weight of diffusion samples at time t
C_∞	Concentration of water at equilibrium
E_D	Activation energy for diffusion
R	Gas constant
T	Temperature
D_o	Constant
$J(x)$	Bessel function
γ	Surface free energy
t_{inc}	Incubation time
t_o	Constant
ΔH	Acivation energy for crack propagation to initiate
v^*	Constant
t_{sc}	Time for slow crack growth
t_f	Fracture time ($t_f = t_{inc} + t_{sc}$)
α_o	Intrinsic crack length
α_f	Final crack length
Q	Geometry factor
σ_f	Butt joint applied stress
A	Constant
z	Constant

CHAPTER 1

INTRODUCTION

The use of adhesives in the engineering industry has been rapidly increasing over the last fifty years. As a result, the science and technology of adhesion and adhesives has progressed significantly. Therefore, the prediction of the strength of bonded components is vitally important and different approaches and methods are being used in order to investigate their fracture characteristics. In this type of work, fracture mechanics is a very useful technique for comparing various adhesives, predicting the strength and life-time of bonded components, and generating basic design data.

Due to the increase in the demand of adhesive systems as a means of bonding together engineering components, the phenomenon of adhesion has attracted the interest of many investigators all over the world. As a result, different theories have been suggested that seek to explain adhesion in terms of the properties of the materials involved in the formation of a bond. A literature survey into the adhesion phenomenon has therefore been carried out and has demonstrated that the initial or long-term strength of bonded metal joints is determined by the physical and chemical properties of the adhesive/substrate interface. Therefore, if the properties of the separate adhesive and substrate interfaces are known, one would supose that the properties of a bonded joint could be predicted. However, investigators have not yet been able to demonstrate this, but have only described and attempted to improve those surface aspects which seem to be of primary importance for increasing bond performance. The survey has pointed out that the most hostile environment for adhesive bonds is water, either in liquid or vapour form, and it is the interfacial regions which are attacked and weakened. It has also shown that the rate of loss of joint strength may be a function of water diffusing to the interface through the adhesive layer in a joint. The diffusion properties of the adhesives involved have therefore been shown to play an important role in the formation and destruction of adhesive bonds and models for life prediction studies have been put forward.

The present research programme is therefore concerned with the environmental attack of water on adhesive joints, which consist of mild-steel substrates bonded with an unmodified or rubber-toughened epoxide adhesive. Of particular interest is the application of a fracture mechanics approach to predicting joint durability. The main aims of the present research work were:

1. To design a new test method for assessing the durability of structural adhesive joints exposed to moisture and stresses. This new test would allow the inexpensive determination of the fracture energy, G_c, versus crack velocity, $d\alpha/dt$, relation for a joint.

2. To obtain the G_c versus $d\alpha/dt$ data for an adhesive joint system in a given environment and to assess the reproducibility of the technique.

3. To use the G_c versus $d\alpha/dt$ data to predict the service life of adhesive joints when exposed to a hostile environment.

4. To assess the effect of using an unmodified versus a rubber-modified adhesive.

5. To investigate the mechanisms of joint failure using the scanning electron microscope (SEM) and the X-ray photoelectron spectroscopy (XPS) methods.

CHAPTER 2

LITERATURE SURVEY

The literature survey will first review the basics of fracture mechanics, then consider the detailed joint geometry to be used in the present work (the double-torsion joint geometry). The survey will next discuss epoxide adhesives, especially with respect to the use of fracture mechanics. The final two sections will consider mechanisms of adhesion and the aspect of environmental attack upon adhesive joints.

2.1 FRACTURE MECHANICS

2.1.1 Introduction

It is generally accepted that engineering structures always contain flaws from fabrication or induced during in-service loading. Such flaws act as stress concentrators and may have a significant effect on the properties of the material. In the case of brittle materials it has been found that the measured fracture strengths are well below the theoretical values. This may be explained by the presence of flaws and this hypothesis has led to the development of theories which seek to analyse mathematically the state of stresses in regions where flaws exist. The above theoretical work, which is supported by a large body of experimental work, is termed fracture mechanics and has received considerable attention in recent years. The basic aim of fracture mechanics is to identify fracture criteria that will lead to a more fundamental understanding of the fracture process.

J.F. Knott (1974), D. Broek (1974), J.G. Williams (1984), and A.J. Kinloch and R.J. Young (1983), have recently reviewed this area. Two of the most important criteria are the energy criterion and the stress-intensity factor criterion. The energy criterion is based on a balance between release of strain energy and the requirements of surface energy for the freshly created surfaces. When the crack

propagates there is a strain energy release rate per unit thickness per unit crack extension, G_c, which fulfils the requirements of the new fracture surfaces. The stress intensity factor, K, is a parameter that defines uniquely the stress field around a sharp crack. The criterion states that fracture will occur when K reaches some critical value, say K_c. The value K_c is defined as the fracture toughness and is a material property, whereas K is independent of the material.

2.1.2 Energy Balance Approach

This comes from A.A. Griffith's (1920) and E. Orowan's (1970) work and crack propagation takes place when the work done by an external force, F, and the elastic energy stored in the bulk of the material, U, are converted into fracture energy, G_c:

$$(1/t)(d(F-U)/d\alpha) \geq G_c \qquad (2.1)$$

where t is the thickness of the specimen and $d(F-U)/d\alpha$ is the change in energy per unit crack length. For linear elastic materials it can be shown that the fracture energy may be related to the specimen compliance, C, with the equation (derivation of the equation can be found in Appendix 1):

$$G_c = (P_c^2/2t)(dC/d\alpha) \qquad (2.2)$$

where $dC/d\alpha$ is the change in compliance with crack length α, and P_c is the load at fracture. If the values of the load and the displacement for a given crack length are known then $dC/d\alpha$ for this value can be found and hence G_c can be calculated.

2.1.3 Stress Intensity Factor Approach

The stress intensity factor approach of G.R. Irwin (1970) focuses

attention on the stress state near the crack tip. If a crack is subjected to tensile stresses, σ, along its line of action (Figure 2.1), the stress function solutions will give stresses close to the crack tip of the form:

$$\sigma_{xx} = K_I \cos(\theta/2)/(2\pi r)^{1/2}. [1+\sin(\theta/2)\sin(3\theta/2)]$$

$$\sigma_{yy} = K_I \cos(\theta/2)/(2\pi r)^{1/2}. [1-\sin(\theta/2)\sin(3\theta/2)]$$

$$\sigma_{zz} = (\sigma_{xx} + \sigma_{yy}) \qquad \text{(for plane strain)}$$

$$\sigma_{zz} = 0 \qquad \text{(for plane stress)}$$

$$\tau_{xy} = K_I \cos(\theta/2)/(2\pi r)^{1/2}. [\sin(\theta/2)\cos(3\theta/2)]$$

$$\tau_{xz} = 0$$

$$\tau_{yz} = 0$$

where α is the crack length, r and θ are the polar coordinates at the crack tip, and τ is the shear stress. The parameter, K_I is the stress intensity factor and relates the magnitude of the stress intensity local to the crack tip in terms of the applied loadings and the geometry of the structure. The crack is assumed to be stressed in mode I, i.e. in a tensile (opening) manner shown in Figure 2.2a, although two other types of separation are possible: mode II (edge sliding) and mode III (screw sliding). In mode II (Figure 2.2b) the crack surfaces move normal to the crack front and remain in the crack plane, and in mode III (Figure 2.2c) the crack surfaces move parallel to the crack front and remain in the crack plane. Mode I is the most commonly encountered and is associated with a local displacement in which the crack surfaces move directly apart. Under plane-strain conditions (i.e. a relatively thick specimen) the critical value at fracture is denoted by K_{Ic}, the plane-strain fracture toughness.

In general, stress intensity factors may be written in the following form:

$$K_I = Y\sigma(\alpha)^{1/2} \qquad (2.3)$$

where σ is the applied stress remote from the crack, and Y is a geometry factor. K_I uniquely defines the stress field at the crack tip (it has the dimensions of stress $\sqrt{}$(length)). If fracture is to be related to the intensity factor then it must occur at some critical value of K_I, say K_{Ic}. The condition:

$$K_I \geq K_{Ic} \tag{2.4}$$

therefore represents a fracture criterion. K_{Ic} characterises the intensity of the stress field ahead of a crack and is a material property, often called the fracture toughness K_{Ic} may be expressed in the following form:

$$K_{Ic} = Y\sigma_c(\alpha)^{1/2} \tag{2.5}$$

where σ_c is the applied stress at the onset of crack growth. Y can be calculated for different geometries from experimental or theoretical (analytical and/or numerical) techniques.

2.1.4 G and K Relations

The double-torsion specimen and geometry was suggested by Outwater and developed by J.A. Kies and A.B.J. Clark (1969) and is shown in Figure 2.3 and discussed in detail in Section 2.2.1. Equation (2.2) can be used for a double-torsion specimen geometry (DT) since a compliance calibration may readily be conducted. Further, since the plot of compliance, C, versus crack length, α, is linear, then only the value of the load at fracture is subsequently required from the fracture test to calculate the value of the fracture energy, G_c. The value of $dC/d\alpha$ may first be obtained experimentally and then compared to the theoretical value which may be calculated from the equation (see

Appendix 2):

$$dC/d\alpha = [(1+\upsilon)/E]\ (21_m^2/kwt^3) \qquad \text{(for plane strain)} \qquad (2.6)$$

where E is the modulus of the bulk material. The other symbols in equation (2.6) are the Poisson's ratio, υ, of the adhesive, the moment arm, 1_m, and a constant, k, that depends on the dimensions of the specimen. The constant k depends on the ratio (w/2)/t, where w is the width of the DT specimen.The value of G_c can be obtained, by comparing equations (2.2) and (2.6), from the equation:

$$G_c = P_c^2\, l_m^2\, (1+\upsilon)/E\, kwt^3 t_n) \qquad (2.7)$$

where t is the specimen thickness and t_n is the effective specimen thickness. The stress intensity factor can be calculated from G_c as follows (see also Appendix 3):

(i)Bulk material case

If E is the modulus of the material then:

$$K_{Ic}^2 = E\, G_c/(1-\upsilon^2) \qquad (2.8)$$

and

$$K_{Ic} = P_c\, l_m\, [1/(1-\upsilon)\, kwt^3\, t_n)]^{1/2} \qquad (2.9)$$

(ii)Joints with a crack in adhesive layer

If E_a is the modulus of the adhesive layer, which is assumed to be thin, then:

$$K_{Ic}^2 = E_a G_c/(1-\upsilon^2) \qquad (2.10)$$

and

$$K_{Ic} = P_c l_m [1/(1-\upsilon) kwt^3 t_n)]^{1/2} (E_a/E_s)^{1/2} \qquad (2.11)$$

where E_a is the modulus of the adhesive.

(iii)Joints with a crack at the interface

When the crack propagates at the interface then G_c can still be calculated experimentally from equation (2.2), but for calculating K_c the value of Young's modulus of the system is required:

$$K_c^2 = E' G_c/(1-\upsilon^2) \qquad (2.12)$$

where E' is the Young's modulus of the system. An analysis by J.G. Williams (1984) has shown that for a joint E' may be calculated from the equation:

$$E' = (1/2) [(1/E_a) + (1/E_s) (2\beta-(1/\beta^2)] \qquad (2.13)$$

where E_a is the modulus of the adhesive, E_s is the modulus of the metallic substrate, and β is given by:

$$\beta = (\xi + 1)/(\phi + 1) \qquad (2.14)$$

where

$$\xi = E_s/E_a \tag{2.15}$$

and

$$\phi = [1 + (E_s/2)]\,[((1 + \upsilon_a)/E_a) - ((1 + \upsilon_s)/E_s)] \tag{2.16}$$

where υ_a and υ_s are the Poisson's ratio of the adhesive and substrate respectively. For an adhesive/metal system, β is very close to 1.

It is important to appreciate the above points, otherwise incorrect values of K_{Ic} and G_c may be deduced. However, in the present work interfacial failure is to be expected for the environmental tests and this is the most difficult case to deal with, as may be seen from the above analyses. Therefore, to avoid all these problems, only the parameter G_c will be considered in the present experimental work on joints exposed to environmental attack.

2.2 THE DOUBLE TORSION TEST GEOMETRY

2.2.1 Opening remarks

It has been recently established that the dynamics of crack propagation can be described uniquely by the stress intensity factor (K_{Ic}) at the crack tip (or the fracture energy G_c) and the associated crack velocity ($d\alpha/dt$) for many materials. However, long-term measurements of G_c and crack length, α, cannot be easily made using the existing test techniques, (e.g. single edge-notched, three-point bend, compact tension, double cantilever beam, etc.) because of the cost and complexity of the specimens and equipment for both applying the loads and monitoring the crack growth. This is especially true when testing in the presence of a hostile environment. A suitable test technique, without requiring complex test equipment, is therefore needed to eliminate most of the above difficulties. This technique must also have the ability to allow tests to

be easily carried out in hostile environments without loss of accuracy.

The simplicity of the double torsion test geometry (DT) has led to it being used for many brittle materials and it is ideally suited for the rapid evaluation of the K_{Ic} versus $d\alpha/dt$ or G_c versus $d\alpha/dt$ relations. Further, tests can be easily carried out in hostile environments and on both opaque and transparent materials. The DT specimen is a simple rectangular plate of length l, width w, and thickness t. A side groove is machined along one of its faces and an edge notch, using a flywheel cutter, followed by a sharp notch, using a sharp razor blade, is inserted at one end (Figure 2.3a). The specimen is placed in a box where it rests on the two rollers with its lower face being the one containing the groove. The load (P) is applied via two hemispheres on the upper face, one on each side of the groove. Figure 2.3 shows a schematic representation of the DT test device. The groove is machined to ensure that the crack will propagate along the specimen axis. This groove can be a V-groove or a U-groove.

2.2.2 Analysis of the DT Geometry

The analysis of the DT geometry reveals that evaluation of K_{Ic} (or G_c) does not require a direct knowledge of the crack length and the values ascertained are independent of crack length. This may be confirmed experimentally by a K-calibration. A.G. Evans (1973) has carried out such a calibration for a glass specimen and his results are shown in Table 2.1, indicating that the fracture load is independent of crack length, and hence the determination of the value of K_{Ic} does not involve the crack length. A compliance calibration made by A.G. Evans (1972) shows that the displacement of the loading points per unit load is linearly related to crack length, so that:

$$y = P(B + C_1) \tag{2.17}$$

where B and C_1 are constants that depend on the modulus of the material and the

dimensions of the specimen. The crack front is inclined to the resultant direction of crack propagation so that different values were obtained for the lower and upper face for each compliance measurement. Figure 2.4 shows a schematic represention of the crack front. Figure 2.5 shows the relation between the applied load P and the stresses generated, and the crack profile. The resultant direction of the crack propagation may lead to the conclusion that failure occurs in mode III, i.e. due to shear stresses. This would occur if the crack front was parallel to the direction of the load application. However, it is generally accepted that failure occurs due to the tensile stresses present, i.e. in mode I. However, in any event, obtaining the value of G_c via a compliance calibration will avoid the necessity for a detailed stress analysis to resolve this issue.

2.2.3 Methods of Calculating Crack Velocity

There are three different methods that may be used for the determination of crack velocity. These are summarised below:

(i)Constant displacement method (load relaxation):

In this method the specimen is loaded and held at a constant displacement ($dy/dt = 0$) and the crack growth rate is now given by:

$$d\alpha/dt = -(P_{i,f}/P^2) [\alpha_{i,f} + (C_1/B)] (dP/dt) \qquad (2.18)$$

where:

$P_{i,f}$	is the initial (or final) load
P	is the instantaneous load
$\alpha_{i,f}$	is the initial (or final) crack length, and
B, C_1	have been defined previously, see equation (2.17).

If the initial (or final) values of load and crack length are known, then the crack speed may be found directly from the load relaxation (dP/dt). It was mentioned above that the crack extends more along the lower surface than the upper surface of the specimen. If $\Delta\alpha$ expresses the difference between the two lengths (Figure 2.4) then equation (2.18) becomes:

$$d\alpha/dt = - \phi'(P_{i,f}/P^2) [\alpha_{i,f} + (C_1/B)] (dP/dt) \qquad (2.19)$$

where:

$$\phi' = t/ (\Delta\alpha^2 + t^2)^{1/2} \qquad (2.20)$$

(ii)Constant load method:

The specimen is loaded to a given constant load so that (dP/dt) = 0, and if the initial and final values of the crack length are known, together with the corresponding time intervals, then the crack speed can be calculated from the equation:

$$(d\alpha/dt)_P = [(\alpha_f - \alpha_i) / (t_f - t_i)]_P = (\Delta\alpha/\Delta t)_P \qquad (2.21)$$

This method is very useful for obtaining G_c and $d\alpha/dt$ information at low crack speeds as well as for obtaining crack speeds as a function of the fracture energy (or stress intensity factor). This method is especially relevant as the experiments planned in the present studies will be under conditions of constant load.

(iii)Constant displacement-rate method:

The specimen is loaded at a constant displacement rate, (dy/dt), and the crack will grow at a constant load if crack propagation occurs in a continuous steady manner. The crack

speed is related to the crosshead speed through the slope of the compliance calibration curve by the equation:

$$dy/dt=BP(d\alpha/dt) \qquad (2.22)$$

As can be seen, in all the above methods there is no need to continuously monitor the crack length as the crack grows, but only the initial and final values need to be measured. Since a compliance calibration has already been made, the crack speed may be easily calculated. If tests are to be made using the constant displacement-rate method, then only the crosshead speed of the testing machine is needed as can be seen from equation (2.22). The constant displacement and the constant displacement-rate methods both require expensive equipment, such as a constant displacement-rate tensile-testing machine. If the constant load method is chosen then there may be no need to use such a machine, but a simple rig may be sufficient. Thus, choosing this last method, in principle one may very easily and inexpensively conduct tests to study the fracture behaviour of adhesive joints. The applicability of this technique for the study of adhesive joints in hostile environments will be investigated in the present work.

(iv)Environmental tests:

As stated before, the G_c versus $d\alpha/dt$ diagram (or K_c versus $d\alpha/dt$ diagram), may be used to characterise material behaviour under different conditions, such as test temperature, environment etc. An excellent schematic example of such data is shown in Figure 2.6. This shows a typical K_{Ic} versus $d\alpha/dt$ diagram for crack growth in a ceramic in an hostile environment. There are up to three regions of crack growth, as K_{Ic} varies from K_{Ic} (at the stress corrosion limit) to K_{Ic} (for 'dry' fracture). At low K_{Ic} values, region I, the rate of the chemical reaction near the crack tip controls growth. At intermediate K_{Ic} values, region II, diffusion of the corrosive species to the crack is rate

controlling. At high K_{Ic} values, region III, K_{Ic} is close in value to K_{Ic} ('dry' fracture) and there is a mixture of corrosive and mechanical failure. In the present work, G_c versus $d\alpha/dt$ diagrams for adhesive joints in water will be measured. Apart from allowing the assessment of a given adhesive system, it is also hoped that such data may be employed to predict the lifetime of adhesive joints exposed to an aqueous environment.

2.3 EPOXIDE RESINS: FRACTURE BEHAVIOUR

2.3.1 Introduction

In spite of their high cost the epoxide resins have achieved significant importance as industrial materials and have been reviewed by I. Skeist (1977), W.C. Wake (1982), and H. Lee and K. Neville (1967). They can be used as surface coating materials and for the encapsulation of electronic components, as well as tooling compounds, laminating materials and adhesives. Epoxide resins are highly cross-linked polymers and are used below their glass transition temperature. The properties of the cross-linked resins depend on the curing system used, but their outstanding features are toughness, low shrinkage on cure, high adhesion to most substances and good alkali resistance. They are very brittle materials and their toughness can be increased by the addition of secondary phase particles (for example, rubber particles). This aspect has been reviewed by C.B. Bucknall (1979), and A.J. Kinloch and R.J. Young (1986).

A fracture mechanics approach is used as a failure criterion for these materials and, since they are very brittle and display approximately linear elastic deformation, linear-elastic fracture-mechanics (LEFM) can be applied to describe their failure characteristics.

2.3.2 Types of Crack Propagation

From linear elastic fracture mechanics test methods, three distinct types of crack propagation can be observed in epoxide resins as shown by A.J. Kinloch et al

(1983, 1983a), depending on the test conditions, the composition used, and the type of specimen. These are:

(i)"Stable brittle propagation" - the crack grows in a steady manner under the influence of a constant load depending on the crosshead speed and the testing machine. The fracture surfaces are featureless and the corresponding displacement (or time) against load curve is shown schematically in Figure 2.7a. It is considered that if an epoxy adhesive can be employed which exhibits this type of crack growth then interpretation of the environmental G_c versus $d\alpha/dt$ data will be somewhat easier.

(ii)"Unstable brittle propagation" - the crack propagates in a stick/slip manner. The displacement (or time) against load curve is shown schematically in Figure 2.7b and the values of P_i and P_a correspond to loads at crack initiation and crack arrest points respectively. Crack arrest lines can also be seen on the fracture surfaces. This type of crack growth behaviour is by far the most commonly observed in epoxy materials.

(iii)"Stable ductile propagation" - the crack propagates in a steady manner under a constant load but the fracture surfaces are far rougher than in the first case and torn in appearance, indicating a more ductile process.

2.3.3 Bulk Fracture Studies

D.C. Phillips and J.M. Scott (1974), have conducted tests for the determination of the K_{Ic} versus $d\alpha/dt$ diagram of epoxide resins using the DT test technique. The epoxide resin used was a diglycidyl ether of bisphenol A (DGEBA, Ciba-Geigy "MY750") cured with a liquid anhydride (Ciba-Geigy "HY906") and using a liquid modified tertiary amine (Ciba-Geigy "DY062") as the accelerator. The specimens contained 65, 70, 75, 80 and 90 parts of HY906 to 100 parts of MY750 and 1 part of the accelerator and were cured for 2 hours at 12°C. Some additional specimens of

composition 100:80:1, cured for 10 or 20 hours at the same temperature, were also prepared. The tests were carried out on a tensile-testing machine, but using the relaxation technique. This technique is performed by applying a constant rate of displacement until the crack propagates and then the crosshead of the machine is halted, and therefore the displacement thereafter remains constant. In such tests the load, and hence the stress-intensity factor driving the crack, decreased until the crack was finally arrested. The rate of change of load with time is directly related to the crack speed at that load so that the relaxation curve (load, P, versus time, t) provided all the information necessary to evaluate the K_{Ic} versus $d\alpha/dt$ diagram, since the crack length which corresponded to some point in the relaxation curve was known. In the case of DGEBA epoxide resins, the crack did not always propagate in a continuous manner; some cracks propagated in a stick/slip manner. When stick/slip crack propagation occurred then stick/slip relaxation was obtained experimentally by running the chart recorder at a high rate and expanding the load versus time scale. Now figure 2.9 shows a typical stick/slip relaxation curve obtained during the experiments. The crack speed was calculated from the equation:

$$d\alpha/dt = (1/A_1P)(dy/dt - A_1\alpha\, dP/dt - A_2\, dP/dt) \qquad (2.23)$$

where A_1, A_2 were constants determined from the compliance calibration, dy/dt was the constant crosshead speed of the testing machine and α was the crack length at the point at which P and dP/dt were measured. The crack length at the onset of sudden fracture was measured from the fracture surface, since crack arrest lines were well defined.

Now Table 2.2 shows the modes of fracture of the different compositions that were obtained. When the crack propagated in a continuous manner the crack speed was obtained by filming the crack movement and measuring the crack length from the film. The stress-intensity factor was calculated from the equation:

$$K_{Ic} = P_c l_m [3(1 + \upsilon)/(wt^3 t_n)]^{1/2} \quad (2.24)$$

where the variables have been defined previously. The results are shown in Figure 2.9 where the K_{Ic} versus $d\alpha/dt$ diagram for the different epoxide resins are plotted.

R.J. Young and P.W.R. Beaumont (1975a) measured the variation of crack speed as a function of the stress-intensity factor for crack growth for an epoxy resin containing 42% by volume of irregularly shaped silica particles using the DT test technique. The material investigated was a solid bisphenol-A epoxide resin (Ciba-Geigy "CT200") cured with a white flake phthalic anhydride hardener (Ciba-Geigy "HT901") and filled with silica flour (Ciba-Geigy "Z300"). The ratio of epoxy resin to hardener to filler was 100:30:200 parts by weight. The composite was cured at 135°C for 16 hours. Samples of CT200 cured under the same conditions with HT901 hardener in the ratio of 100:30 parts by weight but without silica were also examined. Tests were performed on a tensile-testing machine at a temperature of 20°C with a relative humidity of 60% and tests to investigate the effect of environments such as distilled water and paraffin at 20°C were also conducted. The thickness of the DT specimens was 7mm and they were machined from sheets of the material in the form of 75mm by 30mm rectangular plates. A V-groove was also machined into the specimens along one face. The data was obtained using the load relaxation method and the critical stress-intensity factor was calculated from the equation:

$$K_c = P_c l_m (1 + \upsilon/wt^3 t_n k)^{1/2} \quad (2.25)$$

where k is a constant which depends on the ratio (w/2)/t. The variation of k with (w/2)/t is shown in Table 2.3. Note that equation (2.25) is not the same as equation (2.9) because plane stress conditions were assumed in the former case. This is not strictly correct, since for thin adhesive layers, plane-strain conditions are more likely and therefore equation

(2.25) involves a slight error.

The results of the K_{Ic} versus $d\alpha/dt$ measurements are shown in Figures 2.10 and 2.11. It can be seen that all the data points on Figure 2.10 fall on two intersecting straight lines. Above a crack speed of about 10^{-5} m/sec the line has a slope of 60 and below this value the slope is 35. In the presence of distilled water the crack speeds were found to increase by nearly one order of magnitude, whereas in paraffin the speeds were reduced by even more (Figure 2.11).

A..J. Kinloch, D.L. Maxwell and R.J. Young (1985), have examined the fracture behaviour of hybrid-particulate composites which contained both rubbery and rigid particles. No attempt was made to measure the crack speeds but all three basic types of crack propagation were observed. The results of the tests performed at different temperatures are shown in Figure 2.12 for a hybrid particulate composite (rubber = 15 phr; glass volume fraction = 0.085). At high temperatures stable ductile crack growth was observed and K_{Ic} steadily decreased with decreasing temperature. At about 0°C crack propagation becomes brittle-unstable in nature, and initiation and arrest values of K_{Ic} were deduced. The critical stress-intensity factor, K_{Ic}, continued to decrease as the temperature was further lowered, but the arrest values were independent of temperature. Stable-brittle crack growth was observed at the very lowest temperature. The increase in K_{Ic} with increasing temperature and the observed transitions in crack propagation behaviour were explained by the phenomenon of crack-blunting in the vicinity of the crack tip. Localised plastic deformations at the crack tip increased as the temperature increased and so progressive crack-tip blunting occurred. At low temperatures, where the yield stress is high, a sharp crack was formed and the value of K_{Ic} was low and stable brittle crack propagation occurred. At high temperatures where the yield stress is lower, higher K_{Ic} initiation values were measured and the rate of release of energy was greater than that required for stable crack growth and hence unstable propagation was observed. At even higher temperatures the degree of crack blunting was so severe that stable ductile

crack growth was again observed but with a relatively high K_{Ic} value.

Finally, a DGEBA epoxy resin cured with TETA hardener has been used by R.A. Gledhill and A.J. Kinloch, and S. Yamini and R.J. Young (1978), for crack propagation studies. The composition of the mixture was 10 parts by weight of TETA to 100 parts by weight of DGEBA. The results showed that crack propagation occurred in a continuous manner and a value of 0.48 $MN/m^{3/2}$ for the critical stress-intensity factor was estimated.

2.3.4 Water Diffusion Studies

The durability of adhesively bonded metal structures in moist surroundings is of extreme importance to the engineering industry: adhesive joints suffer a decrease in strength in moist environment and the process of water transmittion may depend on the rate of water diffusing into the adhesive and the solubility of water in the epoxide. Different investigators have attempted to examine these processes.

D.M. Brewis, J. Comyn and S.T. Tredwell (1987), studied the uptake of water at 25°C and 50°C for some modified phenolic adhesives. The adhesives examined were two nitrile-phenolic adhesives (designated NP1 and NP2) and a vinyl-phenolic adhesive (designated VP). The authors first assumed that water uptake might be Fickian and therefore the concentration of water at points distance x from the centre of the film at some time t_d, C_t, was related to the concentration at equilibrium, C_∞, and the diffusion coefficient at this time via the following equation for one-dimensional diffusion

$$C_t/C_\infty=1-(4/\pi)\sum\{(-1)^n/(2n+t)\}\exp\{-D(2n+1)^2\pi^2t_d/t^2\}\cos\{(2n+1)\pi x/t\} \qquad (2.26)$$

where t was the film thickness for a semi-infinite film in a infinite bath and n is an integer. It was also assumed that equilibrium between the bath and the surface of the film was

established instantaneously on immersion. Integrating the above equation gave the total water content:

$$M_t/M_\infty=1-\sum\{8/(2n+t)^2\pi^2\}\exp\{-(2n+1)^2\pi^2Dt_d/t^2\} \qquad (2.27)$$

where M_t and M_∞ were the masses of diffusant absorbed at time t_d and at equilibrium respectively. At short times equation (2.27) simplifies to:

$$M_t/M_\infty=4/t(Dt_d/\pi)^{1/2} \qquad (2.28)$$

Equation (2.28) indicated that a plot of mass uptake against the square route of time should be initially linear. Figures 2.13 and 2.14 show the results obtained confirming the initial assumption that Fickian behaviour was expected to occur in all cases studied and the diffusion coefficient was calculated from the gradients. Figure 2.13 shows an initial linear region leading to an equilibrium plateau that was observed for the case of NP2 adhesive films at 50°C. The NP1 adhesive films at 50°C first absorbed water to attain a maximum weight and then slowly decreased in weight until a steady value was reached. The films were next dried and a second sorption experiment was undertaken. The authors explained the observation in terms of leaching of some component of the resin from the film. The water in which the film samples had been stored might have been evaporated to dryness leaving a viscous solid of a low molecular weight material.

Table 2.4 shows the diffusion coefficients and equilibrium uptake levels of water in the adhesives. The values of D and C_∞ reported for the case of the NP1 adhesive at 50°C were taken from the second uptake experiments. All diffusion coefficients were found to increase with temperature suggesting that water diffusion in the adhesives examined was an activated rate process. Water solubilities were found to either increase or decrease suggesting that such changes might well depend on whether the heats

of mixing were positive or negative.

D.M. Brewis, J. Comyn, R.J.A. Shalash and J.L. Tegg (1980), investigated the effect of water on some epoxide adhesives in terms of the coefficient of diffusion and the solubility of water on these adhesives. The work undertaken was similar to the work by D.M. Brewis, J. Comyn and S.T. Tredwell (1987). The adhesive used was a diglycidyl ether of bisphenol A and six different hardeners were used to produce thin sheets of the material. The hardeners used and their formulations are shown in Table 2.5. The results of the tests are shown in Table 2.6. The values of the diffusion coefficients, D, and of the equilibrium water uptake masses, M_∞, were calculated in the following manner: the data was presented in terms of plots of fractional water uptake (M_t/M_∞) against ($t^{1/2}/l$), where M_t was the mass of diffusant absorbed at time t and l the sample thickness. All plots showed that the sorption process was Fickian, i.e. the plots were linear up to about $M_t/M_\infty=0.6$, followed by a plateau that was associated with the initial equilibrium uptake. Some typical findings are shown in Figure 2.15. The diffusion coefficients were calculated using equation (2.28) and assuming one-dimensional diffusion process.

Closer examination of the results reported by D.M. Brewis, J. Comyn and S.T. Tredwell (1987), as well as by D.M. Brewis, J. Comyn, R.J.A. Shalash and J.L. Tegg (1980), shows that at 25°C and 50°C the diffusion coefficients of water in most epoxides were an order of magnitude less than in phenolics while the uptake levels were fairly similar. This may therefore suggest that epoxide adhesives have an advantage in durability over phenolic adhesives in that they are less able to transmit water into the glueline or to the adhesive/substrate system. An epoxide adhesive has therefore been chosen as the basic adhesive to be studied in the present experimental programme on the durability of adhesive joints.

2.4 ADHESIVE JOINTS: FRACTURE BEHAVIOUR

2.4.1 Introduction

Epoxide resins have recently become the basis of a new generation of advanced structural adhesives. Such adhesives are usually chemical monomers which polymerise to give high-strength, high modulus adhesives which enable a load bearing joint to be made. Epoxy resins are widely used in industry as a means of joining materials instead of traditional methods such as welding, brazing, riveting, bolting etc. Dissimilar materials can be bonded together efficiently as well as thin sheet materials. An improved stress distribution in a joint is achieved by this method and hence the fatigue resistance of the system is increased. Thick metallic components cannot however be joined together because the strength and toughness of adhesives in tension or shear is low relative to many metals, unless the bonded area is large or they are kept in compression.

Materials prior to bonding often require the use of pretreatments in order to achieve a long service life joint. Dirt, possible contamination, or weak boundary layers can be removed, and in some cases the surface free energy can be increased so that the adhesive spreads and establishes strong inter-molecular adhesion forces, or in other cases the resistance of the interfacial forces to environmental attack can be improved.

2.4.2 Fracture Behaviour and Environmental Attack

Depending on the surface pretreatment and the adhesive used, crack propagation can either occur within the adhesive layer or interfacially between the layer and the substrate. Water is particularly aggressive to adhesive joints. It may be that the energy of the interface is lower in water and therefore a thermodynamically more unstable interface results. Because of this there may be a driving force for the interface to adsorb water and become debonded. In such instances the rate may be determined by the ability of the water to reach the interface. This factor depends upon diffusion of water through the adhesive, wicking effects, pre-existing flaws etc. Also the rate of attack by moisture

can be accelerated if stresses are applied to the joint at the same time, or if the joint is subjected to high temperatures, or both. Such attack leads to loss of joint strength and premature failure.

A fracture mechanics approach to the failure of structural adhesive joints in hostile environments has been developed and has enabled a quantitative description of the failure events to be identified. Although the mechanics of crack growth in such cases is complex, a general description of the failure process in a loaded joint may be established. Figure 2.16b shows a side view of a tapered double cantilever beam joint (TDCB-see below) between the metal substrate and the adhesive. If a cohesive starter crack is introduced then failure usually does not result by the cohesive starter crack propagating through the centre of the adhesive. Instead, first debonding occurs in the adhesive/metal oxide interface region, i.e. very close to the adhesive/substrate interface. Debonding progresses inwards from the edges of the joint, but is limited to the vicinity of the interface at the starter crack tip (Figure 2.16a). Then the crack propagates down the adhesive/metal oxide interfacial region. (However, it should be noted that at relatively high applied loads, and hence high values of G_{Ic}, fracture usually occurs in short times, and in such circumstances there is insufficient time for the water to attack the interface and fracture may occur along the centre of the adhesive).

The interface region therefore is of great importance when a joint is stressed in a hostile environment. The adhesive/oxide interface and/or the oxide layer seems to be the weakest region in a joint and improvements may be achieved by a good substrate treatment so that the resistance of the interfacial forces and the oxide layer to environmental attack is significantly improved.

2.4.3 Adhesive Joints: Fracture Studies

The epoxy resin (i.e. a DGEBA epoxy resin cured with TETA hardener) used by R.A. Gledhill and A.J. Kinloch, and S. Yamini and R.J. Young (1978), was

tested by either using DT bulk specimens or tapered double cantilever beam (TDCB) joints or compact tension tests. A TDCB joint is shown schematically in Figure 2.17. The aim of the investigation was to ascertain whether crack propagation in the adhesive joints is analogous to that in the bulk material. In the case of the DGEBA/TETA adhesive joints, continuous crack propagation was observed and K_{Ic} was estimated to be about the same as for the bulk material (0.48 MN /$m^{3/2}$).

The value of adhesive fracture energy, G_c, for the joints was first determined from the equation:

$$G_c = 4P_c^2 Y/E_s t^2 \qquad (2.29)$$

where P_c was the fracture load, E_s the modulus of the substrate, t the specimen thickness and Y a geometry factor given by:

$$Y = (3\alpha^2/h^3) + (1/h) \qquad (2.30)$$

where α was the crack length. The corresponding value of K_{Ic} was calculated from:

$$K_{Ic}^2 = (E_a G_{Ic})/(1 - \upsilon^2) \qquad (\upsilon = 0.35) \qquad (2.31)$$

The tapered double cantilever beam is used for Mode I loading only and it is an excellent analytical tool for studying the fracture behaviour of adhesives. The kinetics of fracture can be studied and the effect of an applied stress can be analysed. However, the fabrication of the beams is expensive, the beams have to be machined to close tolerances and expensive testing equipment, such as a tensile-testing machine, is needed. The DT test specimens are easier to fabricate and require no close tolerances and tests can be conducted on a tensile machine using one or more of the methods described

elsewhere. If the constant load method is chosen there is no need to use an expensive tensile-testing machine to apply a constant load to the specimen.

Turning to the double-torsion adhesive joint specimens, then no work on DT adhesive joints in hostile environments has been conducted before. However, the DT joint test method has been used by R.H. French and Rishi Raj (1979), to study crack propagation in adhesive joints in a dry environment. The epoxy resins employed were a 3M's "EC-2186" which is a one-part, 100% solids, thermosetting liquid epoxide adhesive, and an impregnated nylon epoxide (American Cyanamid "FM-1000"). Aluminium alloy substrates bonded together with the above epoxides were used and the results of the tests are shown in Figure 2.18. The EC-2186 epoxide adhesive is a lower toughness material than the FM-1000 and the the spread in the data was greater for EC-2186 than for FM-1000. The reason for this spread might be the fact that FM-1000 is a film type adhesive and therefore the bonds were free of defects (air bubbles), but EC-2186 is a paste adhesive and therefore defects might be introduced during fabrication.

Another study has used the DT joint geometry to investigate alumina ceramic specimens bonded together with an epoxy (Ciba Geigy "Araldite B") and cured with anhydride HT901. These studies were conducted by A.C. Moloney, H.H. Kausch and H.R. Stieger (1984), and again no environmental effects were examined. The adhesive was cured for 16 hours at 135°C and the adhesive layer was 0.25mm wide and the tests were conducted on an Instron machine at a constant crosshead speed of about 0.1mm/min. Compliance tests were carried out and the results are shown in Figure 2.19 which suggested that the double-torsion test geometry is a constant compliance geometry. The load at fracture, together with the crack speed, were measured. The following equation was used to calculate K_{Ic}:

$$K_{Ic} = P_c l_m (3(1 + \upsilon)/wt^3 t_n Y)^{1/2} \qquad (2.32)$$

where Y was a geometry factor given by:

$$Y = 1 - 2.26(t/w) + 2.4(t/w)\exp(-\pi w/2t) \quad (2.33)$$

The value of K_{Ic} calculated for the alumina/epoxide bonds was found to be 6.72 MPa/m$^{3/2}$ (value of P_c = 570N, mean load for 24 specimens). K_{Ic} was related to G_{Ic} with the equation for plane-strain conditions:

$$K_{Ic}^2 = G_{Ic} E_s/(1 - \upsilon^2) \quad (2.34)$$

where E_s for the alumina was 320 GPa and this gave a value of 124 J/m^2, which is in good agreement with the fracture energy of the bulk material (G_{Ic} for bulk = 121 J/m^2). It was therefore assumed that equations (2.32) and (2.34) used for calculating K_{Ic} and G_{Ic} were correct and that the modulus of the alumina was the relevant modulus to use in equation (2.34). However, comparison of equation (2.11) to equation (2.32) reveals that this is incorrect in that the latter omits the modulus term and, indeed, the value of K_{Ic} determined from equation (2.32) is much higher than expected. Also, equation (2.34), by comparison with equation (2.10), is incorrect in that the former equation uses E_s instead of E_a. However, the two errors in the two incorrect equations (2.32) and (2.34) cancel each other out and lead to the correct value of G_{Ic} being determined.

2.5 MECHANISMS OF ADHESION

2.5.1 Introduction

Over the last fifty years, or so, the science and technology of adhesion and adhesives has significantly progressed because of the growth in the use of adhesives as a means of bonding together engineering components. An adhesive may be defined as that material whose property is to bond together similar or dissimilar surfaces of materials, when applied between them. Adhesion forces are then set up across the interface of the two materials which resist separation. These forces are refered to as "intrinsic" adhesion forces and the establishment of intimate molecular contact at the adhesive/substrate interface is essential for the development of strong and stable adhesive joints.

The nature of the adhesion, i.e. the force of attraction between the molecules at the interface, has been investigated by scientists and different theories have been proposed. The following survey will discuss the current knowledge on the subject. Adhesive performance is shown to depend upon a number of important factors, each of which under specific conditions may play a dominant role in establishing the observed performance in practice.

2.5.2 Adsorption Theory

Work by such authors as D. Tabor and R.H.S. Winterton (1969), and J.N. Israelachvili and D. Tabor (1972), has demonstrated the existence and importance of the van der Waals' forces. These forces arise from electrostatic dipoles between atoms and molecules. The van der Waals' forces between atoms and non-polar molecules, i.e. molecules without permanent multiple moments, are attractive. For small separations van der Waals' forces are weaker than chemical binding forces, and for large separations they are weak compared with electrostatic forces. However, in the absence of chemical and electrostatic forces they are the main attractive forces between atoms or molecules.

Attractive forces, such as van der Waals' forces, act between solid

bodies in intimate contact. An attempt was made by K.L. Johnson, K. Kendall and A.D. Roberts (1971) to discuss the influence of surface forces acting between body surfaces. When contact is formed between two smooth solid surfaces, adhesion depends on the distribution of elastic forces in the contacting bodies. Under conditions of light loading between elastic solids, surface forces can contribute significantly to adhesion. Experiments were therefore carried out on smooth surfaces of materials with low elastic modulus. Rubber spherical and flat surfaces were made and were brought into contact. Measurements of the diameter of the circle of contact were taken using a low power optical microscope. The surfaces were brought together very gently under zero load, and then a small load was applied through a lever arm system together with a micrometer screw connected directly to one of the rubber surfaces, while the other was held fixed. They showed that, all the results could have demonstrated that van der Waals' attractive forces are present and responsible for the adhesion between elastic bodies, even when contact is made under the influence of different solutions.

E.H. Andrews and A.J. Kinloch (1973), investigated the mechanisms of adhesive failure using adhesive joints made from a cross-linked amorphous rubber and rigid polymeric substrates. They measured the intrinsic adhesive failure energy and compared these values to the values of the thermodynamic work of adhesion for rubber adhering to various substrates. The intrinsic adhesive energy was determined from the adhesive failure energy which in turn was calculated for three types of test-pieces: simple extension (Figure 2.20), pure shear (Figure 2.21), and peeling (Figure 2.22) tests. The thermodynamic work of adhesion, defined as the difference in surface free energies between the separated surfaces and the intact interface, was determined for each rubber-substrate joint using contact angle measurements at room temperature for various pure liquids on samples of the moulded rubbery adhesive sheet and on each substrate. The material used was a rubbery copolymer of styrene and butadiene. The polymeric substrates used were: FEPA (a completely fluorinated ethylene-propylene copolymer), nylon 11, p.e.t. (polyethyleneterephthalate), and FEPC (a completely fluorinated

ethylene-propylene copolymer). The results of the tests showed that there was good agreement between the values of the intrinsic adhesive energy and the thermodynamic work of adhesion for the rubber-untreated substrate joints (see Table 2.7), indicating that the primary mechanism of adhesion might be the formation of interfacial van der Waals' bonds. Therefore, there are several papers published in the literature which provide evidence for the important role of van der Waals' forces as the main mechanism of adhesion. The importance of primary chemical bonds is also reported in the literature, especially with silane-based primers to improve joint durability, as discussed by J. Comyn (1986) and A.J. Kinloch and M. Gettings (1977, 1979).

2.5.3 Electronic Theory

B.V. Deryaguin and others (1955, 1952, 1969), carried out experiments to investigate the adhesion of films on solid substrates. The peeling of films was performed in the dark and he observed that flashes of light and a crackling noise accompanied the peeling process. These observations led him to generate an electrical theory of film adhesion. When two bodies are brought into contact, a double electric layer may be set up at the boundary. Positive charges are distributed over one side of the boundary and negative on the other so that a potential difference is set up across the boundary. If the two bodies in contact are non-conductors the formation of the double layer may still be possible but it may be retarded due to the lack of free movement of charges across the barrier. When an adhesive film is removed quickly from a surface so that separation occurs at the boundary, then the charges of the double layer are separated in the process.

However, it may be generally concluded, from the work of G.V. Harrach and B.N. Chapman (1972), and S.M. Skinner (1953) and A.D. Roberts (1977), that for most adhesive/substrate interfaces, any electrical double layer which is generated does not contribute significantly to the intrinsic adhesion. Indeed, any electrical phenomena observed, for example during the peel test, arise from the failure process

rather than causing the adhesion between the materials.

2.5.4 Mechanical Theory

It has been reported by C.W. Jennings (1972), that when the surfaces of the metallic substrates prior to bonding were mechanically roughened an increase in the measured joint strength was recorded. The explanation of the above observation was that the mechanical treatment might have resulted in a surface topography with cavities suitable for mechanical interlocking between the adhesive and the surfaces of the metallic substrates. Hence,a theory has therefore been developed that proposes that the main source of adhesion between an adhesive and metalic surfaces may be due to mechanical interlocking of the adhesive into the substrate surface irregularities.

However, D.E. Packham et al (1981, 1983), have studied the adhesion of polyethylene to copper metallic substrates whose surfaces had been chemically roughened to produce a very rough, microfibrous oxide surface. The results of the peeling tests showed that high peel strengths were achieved indicating that an improvement in joint strength had been achieved. P.J. Hine, S.EL. Muddarris, and D.E. Packham (1984), studied the effect of chemically roughening the substrate surfaces in joint strength. They used zinc substrates and bonded them together with epoxide adhesives. The results showed that joint strength was increased in the joints whose treated surfaces exhibited the most microfibrous oxide. They concluded that the effect of increasing surface roughness was not so much to give a true "mechanical interlocking" effect but more to form a "micro- composite" interface and so to increase the degree of plastic deformation that the adhesive undergoes. Also K.K. Knock et al (1981), have suggested that the increase in joint strength may not occur due to mechanical interlocking but from other sources.Indeed, they suggested that mechanical interlocking may not occur at all and its contribution to the stability of the interface between the substrate and the adhesive may be of no importance.

2.5.5 Diffusion Theory

This theory has been proposed by R.M. Vasenin (1965a, 1965b) and S.S. Voyutskii (1962, 1963, 1965), carried out tests to investigate the adhesion between high polymers. Polyisoprene and polyisobutylene sheets were brought into contact and the results from peeling tests performed on the materials are shown in Figure 2.23. The strength of adhesion was calculated from the density of the polymer and the polymer molecular weight M. The variation of adhesion strength with time, showed a parabolic law. The author explained this phenomenon as a result of diffusion of speices across the interface of the two polymers. He also emphasized that diffusion can only take place between mutually soluble polymers. The strength of the bonding may be proportional to the number of molecules diffusing at the interface and to the depth of their penetration.

Diffusion of one species into another or into itself, is a function of the solubilities in each other. In the case of the adhesion of polymers to metals, the molecules of metals are immobile and their mutual solubilities are negligible. If it was assumed that diffusion is the major cause of adhesion between the polymer and the metal, it would then be expected that zero bond strength should be achieved at the interface.

2.5.6 Kinetics of Wetting

J.R. Huntsberger (1970), carried out experiments to investigate the dependence of adhesion on the rheological properties of the substrate surfaces. When bonded structures are formed by applying a fluid adhesive between rigid substrates, good adhesion may be achieved if the adhesive can flow around asperities and into the substrate surface irregularities this process is known as the wetting process, Figure 2.24. Indeed, a relatively large fraction of practical problems involving poor adhesive performance may be a result of incomplete wetting at the interface. The kinetics of wetting may therefore play a decisive role in adhesion.

To support this theory, Huntsberger used mild steel substrates to measure the peeling force required to separate poly(n-butyl methacrylate) from these

substrates. The steel substrates were baked for an hour at two different temperatures. The results showed that at temperatures above 72°C cohesive failure was observed and below 72°C the failure was interfacial. Wetting was not completed in the sample baked at 100°C. In this sample, large and numerous unbonded interfacial areas were found at low values of peel force. Any remaining non-wetted areas in the sample baked at 150°C were sufficient small so that fracture occured at higher loads.

2.5.7 Summary

The nature of adhesion between two surfaces has been of major interest to many workers. Different investigators have attempted to identify the major factors that may determine the strength of adhesive joints. As a result of these investigations various theories have been proposed to account for the phenomena observed in practice. The main theory is the adsorption theory which regards adhesion as a purely surface process and explains the formation of a strong bond as a result of the action of molecular forces at the interface: molecular van der Waals' forces and/or chemical bonds. Thus, the formation of primary, i.e. chemical bonds, and secondary, i.e. van der Waals' bonds, attraction forces at the interface of two substances in intimate contact due to the reaction of molecules or atoms and/or chemical groups, may be sufficient in most cases to explain the phenomenon of adhesion. In the case of epoxide resin/metal substrate adhesive systems, the formation of primary and secondary bonds are certainly adequate to explain the good adhesion observed in practice.

2.6 ENVIRONMENTAL ATTACK

2.6.1 Introduction

The above discussions have reviewed the mechanisms of adhesion of joints. The next step is to examine how adhesively bonded systems behave upon exposure to different environmental conditions, i.e. water either in liquid or vapour form, different chemical solutions, temperature, externally applied stresses. The present survey

concentrates its discussions on the case of mild steel/ epoxide adhesive joints, since this adhesive system is being investgated in the present program.

2.6.2 Early Work

C. Kerr, N.C. Macdonald and S. Orman (1967), conducted experiments to investigate the effect of aluminium adhesive joints on exposure to water and ethanol. The substrate material used was pure aluminium alloy with an epoxide adhesive. The results of the tests are shown in Figures 2.25 and 2.26. Figure 2.25 shows the results of failing load in shear for four environments against exposure time. These results clearly indicate that storage of the adhesive joints at 90°C in vacuum, dry oxygen, and dry ethanol, produces no deterioration. Exposure to water, however, results in a decay of bond strength with exposure time. The results suggest that the decay in bond strength was due to the water ingressing into the adhesive joint. Figure 2.26 shows the results obtained from the bulk specimens. Tensile strength and solvent uptake are both plotted against exposure time. The data shows that both tensile strength and the extent of solvent uptake reached equilibrium rapidly in about eight to twelve days when the specimens were exposed to water but the effect on the tensile strength was small. With ethanol, equilibrium was not reached in fifty days and there was a large decrease in tensile strength compared to the fall in the case of water.

Careful consideration of the results shows that water had litle effect on the bulk polymer but a great effect on the joints. To explain their results, Kerr et al assumed that a "boundary layer" had been formed at the polymer/metal interface. The boundary layer had a different chemical nature, degree of crosslinking, and conformational alignment from the bulk polymer. When dry joints were tested, cohesive failure of the polymer was observed, but when they were tested in water, the fracture was close to the polymer/metal interface, but some polymer of undetermined thickness was found to remain on the metal surface. It was therefore claimed that failure occured in the boundary layer after exposure to water at 90°C. This implied that water absorption had a

greater effect on the boundary layer than on the bulk material. The very significant fall in joint strength, compared with the change in polymer strength, was therefore used to postulate that in adhesive joints of this type, i.e. aluminium-alloy single-lap adhesive joints, water molecules rapidly enter the boundary region to interfere with the secondary valence forces responsible for the adhesion between the substrate material and the organic adhesive. However, the work of J. Comyn (1987) does not support this view. This work suggests that the water diffuses through the adhesive layer, see Section 2.3.4.

2.6.3 Effect of Surface Treatment

R.I. Butt and J.L. Cotter (1976),conducted experiments to investigate the durability of adhesive single-lap joints exposed to adverse environments, under laboratory conditions. An epoxy-polyamide adhesive (American Cyanamid "FM1000") was used to bond together aluminium panels of BS2L73 alloy (2 mm thick). The adhesive was cured at 175°C and single overlap joints were tested. The results of the tests performed on the joints are shown on Figure 2.27. The different pretreatments on the aluminium samples were as follows:

(a)Vapour degrease alone or followed by one of the following
(b)Solvent
(c)Chromic-sulphuric acid etch
(d)Alkaline etch
(e)Phosphoric acid etch

The results clearly demonstrate the strong effect of the water on the joints and also that the surface preparation prior to bonding is important. It can also be seen that chromic-sulphuric acid etching is a superior surface pretreatment for improving bond durability. In addition, it was observed that the mode of fracture of the adhesive joints changed progressively from cohesive in the adhesive to predominantly interfacial. These

observations led the authors to the conclusion that the primary role of water in joint degradation is to displace the adhesive from the metal substrate and not to induce cohesive failure of the adhesive.

D.M. Brewis, J. Comyn and J.L. Tegg (1980), investigated the behaviour of single lap joints bonded with an epoxide adhesive when they were exposed to warm moist air for predetermined periods and then subjected to strength measurements. Aluminium alloy (type BS3 L73) substrates were used which were pretreated by one of various methods. The adhesive used was an epoxide resin based on diglycidylether of bisphenol-A (Epitoke 828). The specimens were first placed in an environmental chamber at 50°C and 97-100% relative humidity for predetermined periods.

The results are shown in Figures 2.28 and 2.29 and it can be seen that a linear relationship was found to exist between joint strength and water uptake in the joints. Joint strength increased in the order chromic acid anodize>chromic acid etch>sandblast>degrease. Except for the anodized I joints, all the joints tested displayed a typical decay in joint strength. The strength of anodized I joints increased and the authors explained this behaviour as being due to the absorbed water relieving the internal stresses in the joints.

2.6.4 Effect of Stress

A good example of the effect of stress is the work reported by W.D. Bascom, S.T. Gadomski, C.M. Henderson and R.L. Jones (1977), who have conducted static loading experiments, in moist air and in water, using aluminium butt-joints bonded together with a DGEBA epoxide resin. The results of the tests are shown in Figure 2.30. An exponential decrease in load with time was observed for joints exposed in moist air (40-50% relative humidity) and to water. Because of the large data scatter, there was no direct evidence in the difference between the failure times, but the results clearly demonstrate the decay in load with time. It was concluded that interfacial failure, i.e. failure between the substrate surface and the adhesive, had occurred. Examination of the

interfacial regions revealed, however, that some resin was left on the surface and that it appeared to have failed by a ductile yielding. When cohesive failure occured the fracture surfaces were smooth except that rows of parabolic markings were present. These markings could be associated with the intersection of the main crack front with micro-cracks formed ahead of the crack. Thus, stress accelerates the attack of water upon an adhesive joint. In the present work it is planned to use this effect in designing an accelerated ageing test, and then to proceed and attempt to predict theoretically the results such as those shown in Figure 2.30.

2.6.5 Thermodynamic Work of Adhesion and Kinetics of Attack

R.A. Gledhill and A.J. Kinloch (1974), have carried out experiments to identify the mechanics of environmental failure of joints made from mild steel substrates and bonded with an epoxide adhesive. Emphasis was given to the thermodynamics and kinetics of the failure process. The substrate material was mild steel to specification BS970, EN3B and the adhesive was a diglycidyl ether of bisphenolA (Epitoke 828) cured with HY959 tertiary amine curing agent. The substrate surfaces were first subjected to a liquid and vapour degreasing bath of trichloroethylene, gritblasted and degreased again and finally allowed to cool in air. The cohesive breaking stress of the dumb-bell joints exhibited a rapid decay only when the specimens were immersed in water at 90°C. However, the butt-joint measured strengths decreased considerably as the immersion temperature was increased (the observed losses of butt joint strength were due to the water and not due to the high temperatures imposed, since joints exposed to 40°C, 60°C, and 90°C at 0% relative humidity showed no significant joint strength losses). The initial locus of failure was cohesive through the adhesive but changed gradually to interfacial between the substrate and the adhesive, i.e. a complex locus of failure under the influence of water at different temperatures was observed. Also as the immersion time was increased the interfacial region also increased in size.

Now these authors next considered the thermodynamics of the

processes. If W_A is the thermodynamic work of adhesion, then:

$$W_A=\gamma_x+\gamma_y-\gamma_{xy} \tag{2.36}$$

where γ_x and γ_y are the surface free energies of two phases x and y in contact, and γ_{xy} is the interfacial free energy. If a liquid is present, then the work of adhesion may be written as W_{AL}, where:

$$W_{AL}=\gamma_{xL}+\gamma_{yL}-\gamma_{xy} \tag{2.37}$$

where γ_{xL} and γ_{yL} are the surface energies of the phases x and y in contact with the water. Calculating the terms W_A and W_{AL}, predictions about the environmental stability of the adhesive/metal substrate oxide may be made, if the metal substrate is, say, the x phase, the adhesive the y phase, and the water the L phase. The values of W_A and W_{AL} were +291 mJ/m^2 and -255 mJ/m^2 respectively, i.e. a change from a positive to a negative value. The positive value found for the thermodynamic work of adhesion, indicates thermodynamic stability at the interface, whereas the negative value indicates that an unstable interface has been created as a result of water ingressing into the interface. The authors explained that the large change from the positive to the negative work of adhesion, provided a driving force for the water to displace the adhesive on the metal oxide. The progressive encroachment into the joint of debonded interface, which reduced the joint strength and changed the locus of failure from cohesive to interfacial, was the cause of fracture of the joints.

K. Nakamura, T. Maruno and S. Sasaki (1987), have developed a theory for the decay of the wet shear strength of adhesion in single-lap joints and attempted to correlate the latter with the coefficient of diffusion of water at the interface of the metal/epoxide/metal joints. It was found that in all cases the values of D_s, the diffusion coefficient at the interface of the joints, were higher than D_b, the diffusion coefficient in

the bulk material, leading to the conclusion that moisture absorption first occured at the interface. Water absorption was therefore seen to be determined mainly by water diffusion at the joint interface that was responsible for the decay in wet shear strength.

K. Nakamura, T. Ueda, S. Hosono and T. Maruno (1987), have also applied the theory for the decay in wet shear strength of adhesion developed by K. Nakamura, T. Maruno and S. Sasaki, to lead-alloy/epoxide resin/lead-alloy joints in water at 65°C, 75°C, and 85°C, and they concluded that two main processes that cause bonding breakage may be assumed at the present state: one is that due to water diffusing into the interface, resulting in swelling and/or plasticization of the adhesive (hydrolysis of the adhesive, replacement of adhesive with water molecules), and the other is hydrogen bond breakage by water at the interface.

A. Stevenson (1985), has studied the durability of rubber/metal joints in sea water. It was found that, before exposure to sea water, failure was through the rubber with no bond failure. Exposure to water resulted in the weakening of the bond and failure began to occur at the interface between the steel and the rubber. The interfacial failure area was found to increase as the exposure time of the joint to sea water was increased.

2.6.6 X-Ray Photoelectron Spectroscopy

To illustrate the use of modern surface analytical techniques, some data from F.J. Boerio and D.J. Ondrus (1987), will be discussed in detail, since the locus of joint failure has been investigated by these workers using X-ray photoelectron spectroscopy (XPS) technique. Iron/epoxide resin single-lap joints were made and tested either in dry conditions or after exposure to water at 60°C. A number of the metallic substrates were first pretreated by immersing in dilute aqueous solutions of Γ-amino-propyltriethoxy silane (Γ-APS) at pH 10.4 or 8.0. The results of the analysis are shown in Figures 2.31 and 2.32. Strong bands characteristic of the adhesive and the oxide were observed near 532.9 and 529.6 eV in the adherend O(1s) spectra of the joints which were prepared from adherends primed with Γ-APS at pH 10.4 and tested under dry conditions

(Figure 2.31A). Only a weak band related to the primer was obtained near 102.0 eV in the Si(2p) spectra, indicating that the failure was mostly near the primer/oxide interface but with islands of adhesive left on the surface. The O(1s) and Si(2p) spectra obtained from the analysis of the adhesive failure surface (Figure 2.31B) showed strong bands characteristic of the primer near 532.3 and 102.1 eV supporting the conclusion of failure near the primer/oxide interface.

The O(1s) spectra obtained from the adherend surfaces of joints primed with Γ-APS at pH 10.4 and fractured after immersion in water at 60°C for 7 days, is shown in Figure 2.31C. The spectra showed a strong band near 529.6 eV that were characteristic of the oxide, and the Si(2p) spectra were very weak. The Si(2p) spectra from the adhesive failure surfaces were strong and the O(1s) spectra were observed near 532.0 eV (Figure 2.31D) and were typical of the silane primer, indicating that failure after immersion in water was very near the oxide/primer interface.

Figure 2.32 shows the XPS spectra from the fractured surfaces of the joints made from adherends pretreated with Γ-APS at pH 8.0. Similar spectra for joints tested under dry conditions and after immersion in water at 60°C for 7 days were obtained. The O(1s) spectra from the substrate failure surfaces showed strong bands typical of surface oxides and hydroxides while the Si(2p) spectra were very weak (Figure 2.32A and 2.32C). The O(1s) spectra of the adhesive failure surfaces were near 532.0 eV and the Si(2p) spectra were very strong (Figures 2.32B and 2.32D). It was therefore concluded that the joints prepared from adherends primed with Γ-APS at pH 8.0 always failed very near the primer/oxide interface with very little adhesive left on the adherend failure surface.

Other workers such as A.J. Kinloch et al (1977, 1984), and D. Briggs et al (1976), have also used XPS and this technique will also be used in the present work to investigate the locus of failure.

2.6.7 Predictive Models

It was mentioned in the work by J. Boerio and D.J. Ondrus, that the rate of interfacial debonding may depend on the availability of water at the interface. This, in turn, may suggest that the accumulation of a critical concentration of water in the interface regions may also contribute to the fracture of the joints. The rate of attaining this critical concentration may be related to the rate of water diffusing through the adhesive and may be accelerated by temperature and applied stresses, as the final investigation will suggest.

R.A. Gledhill, A.J. Kinloch and S.J. Shaw (1980), have developed a model for predicting the durability of adhesive joints when they are subjected to external stresses and various temperatures, and attempted to correlate fracture in terms of a critical concentration of water at the interface, as water diffuses through the adhesive. The epoxide resin employed was a diglycidyl ether of bisphenolA, cured with a tertiary amine curing agent. The substrate material was mild steel, and butt joints were made from this material. Square samples of the adhesive (3 cm by 3 cm) of thickness between 0.7 cm and 1.3 cm were also prepared. The bulk samples were dried and weighed and then they were immersed into water baths which were mantained at 20°C, 40°C, 60°C, and 90°C. At various time intervals, the bulk samples were taken out of the water baths, dried, weighed, and then returned to the baths. The purpose of these tests was to find the coefficient of diffusion of the water into the adhesive.

The results of the tests are shown in Figure 2.33, where M_t is the mass of the samples at different times and M_0 is the initial mass. The value of the coefficient of diffusion was estimated from the relation (J. Crank and G.S. Park, 1968):

$$D=0.04919/(t_d/t^2)_{1/2} \qquad (2.38)$$

where D is the coefficient of diffusion, t_d is the time of immersion, and t is the thickness of the specimens. The term $(t_d/t^2)_{1/2}$ is the half-time of the sorption process. Values of D are shown on Table 2.8 together with the equilibrium water concentration, C_∞. Figure

2.34 shows a plot of the coefficient of diffusion as a function of temperature. At the three lowest temperatures, a linear correlation exists, showing the strong dependance of the coefficient of diffusion on the temperature of the water. At the highest temperature, however, the rate of water diffusion is greater, probably due to the fact that the glass transition temperature of the adhesive is lower than the working temperature, and therefore a different mechanism may be involved which permits diffusing speices to penetrate more rapidly than would be expected from the experiments conducted below the glasstransitiontemperature of the adhesive.

Butt joints tested by J. Boerio and D.J. Ondrus, showed areas of interfacial failure and areas of cohesive failure. It was therefore concluded that in the regions where cohesive failure occured, environmental attack had not yet penetrated. The extent of cohesive failure was found to decrease with increasing time of immersion. This observation has lead to the consideration of the water concentration in the adhesive layer as a function of time and distance. Further, it was assumed that the diffusion of water into the adhesive layer was the same as in the bulk adhesive. Thus, the concentration $C^1{}_t$ of water at time t in the adhesive layer may be estimated from the bulk adhesive, using the equation (J. Crank, 1956):

$$C^1{}_t/C_\infty=1-(4/\pi)\sum\{(-1)^n/(2n+1)\}\exp\{-D(2n+t)^2\pi^2t_d/4t^2\}\cos\{(2n+t)\pi x/2t\} \qquad (2.39)$$

where 2t is the depth of the layer, x is the depth from the layer's boundary given by $0\leq x\leq t$ and assuming that the initial concentration of water in the layer is zero. Also, for two-dimensional diffusion, the concentration C_t of the water, may also be given by (J. Crank and G.S. Park, and J. Crank):

$$C_t/C_\infty=1-(1-C^1{}_t/C_\infty)^2 \qquad (2.40)$$

A computer program was written to solve equations (2.39) and (2.40)

and n was allowed to take values 0,1,2,3,4,5,..... until the difference between succesive terms was less than 10^{-5}. Some of the results of this theoretical analysis are shown in Figure 2.35, where the values of D and C_∞ were those obtained from the bulk samples. The water concentration in the adhesive layer is plotted against distance into the joint as a function of time at a particular temperature. Assuming that a critical water concentration value exists, say C_c as Figure 2.35 shows, different environmental crack lengths α_o were estimated and were used to calculate theoretical values of the fracture stress of the butt joints, since:

$$\sigma_f=(E_a G_c/\alpha_o)^{1/2} \qquad (2.41)$$

where σ_f is the fracture stress, E_a is the modulus of the adhesive, and G_c is the fracture energy of the adhesive (values of 2.8 GPa and 0.4 KJ/m^2 respectively) assuming cohesive failure occurs. The theoretical values of σ_f found from equation (2.41) were compared with the experimental values obtained from the fracture of the butt joints, and the results are shown in Figure 2.36. The solid curves are the theoretical values and the points are the experimental values.

The agreement was generally good, indicating that the assumption of a critical concentration of water into the adhesive layer was correct, and also that the model just described can be used for the prediction of the life of different adhesive/metal substrate systems.

2.6.8 Summary

To summarise:

(i)It is very clear from the literature that structural adhesives may have little resistance to environmental attack. The most severe threat to such adhesives is water, either in the form of liquid or vapour, and it has been reported that exposure of adhesive joints to water weakens their strength. It has also been reported that joint strength decay can be accelerated if the temperature of the water is increased and/or if externally applied stresses are present.

(ii)When metals are bonded together with an adhesive, a metal oxide layer is present at the interface. In the case of epoxide resin/mild steel adhesive joint systems, the metal oxide is Fe_2O_3 (ferric oxide), as confirmed by X-ray diffraction studies. In the presence of moisture, the Fe_2O_3 oxide is transformed to Fe_3O_4 which is a weaker oxide. It has also been shown that the oxide layer may be the weakest region in an epoxide/mild steel adhesive system and fracture studies have therefore been concentrated on the nature of the oxide and its behaviour in the presence of different environmental conditions.

(iii)It has been suggested that fracture may initiate due to a crack propagating along the interface region of a joint, i.e. between the substrate metal and the adhesive, when the accumulation of a critical concentration of water at the interface is reached. The rate of this accumulation is governed by the rate of water diffusing through the adhesive. It has also been shown that the rate of water diffusion can be accelerated if the temperature of the water is increased and/or if external stresses are present.

(iv)The mechanisms responsible for the loss in the integrity of the interfacial regions may be:

(a)The rupture of interfacial bonds, i.e. the rupture of the van der Waals'

bonds due to the displacement of the adhesive on the metal oxide by the water and/or the rupture of any covalent bonds . The van der Waals' bonds are formed because of the van der Waals' forces of attraction developed between the molecules or the atoms at contact. In the absence of any other bonds, van der Waals' bonds are responsible for adhesion and for resistance to environmental attack. Covalent bonds are chemical bonds and often called "primary bonds" because they are, or can be made, far stronger than van der Waals' bonds. They usually only arise if a silane primer is employed.

(b)Chemical or physical changes occuring in the oxide structure as a result of water penetration. The original oxide is then transformed into a mechanically weaker oxide leading to the weakening of the interfacial region and therefore to a deterioration of the overall joint performance.

(v)It is evident from the literature that one of the poorest substrate pretreatments is grit-blasting, followed by that of degreasing in a solvent. When the above pretreatment is applied to mild steel substrates prior to bonding, then the forces responsible for adhesion are the van der Waals' "secondary" forces acting along the interface. Thus, in order to prevent the water from rupturing the secondary bonds, stronger interfacial forces have to be induced at the interface which are more resistant to rupture by water. This observation emphasises the importance of the substrate surface pretreatments, and therefore different methods of achieving a good durable bond have been reported, e.g. chromic acid etching, chromic acid anodizing, chromic-sulphuric acid etching. These have increased the durability of adhesive joints by increasing the strength of the interfacial "primary" bonds and/or the water resistance of the oxide.

(vi)Finally, it is very important, especially in the adhesive industry, to be able to predict the life of bonded components when they are exposed to water and subjected to external stresses. Theoretical thermodynamic considerations may be applied for the successful prediction of the life of adhesive joints as well as models which can

also describe the mechanics of environmental failure.

Crack length (cm)	2.0	3.1	4.0	5.2	6.3
Fracture load (kg)	0.92	0.88	0.89	0.90	0.88

Table 2.1: Calibration for glass specimens.

Com-sition	Cure schedule	Fracture mode
100:65:1	2 h at 120°C	Stick-slip
100:70:1	2 h at 120°C	Continuous
100:75:1	2 h at 120°C	Continuous
100:80:1	2 h at 120°C	Stick-slip and continuous
100:80:1	10 h at 120°C	Stick-slip and continuous
100:80:1	20 h at 120°C	Stick-slip and continuous
100:90:1	2 h at 120°C	Continuous

Table 2.2: Fracture mode results obtained by D.C.Phillips and J.M.Scott (1974)

	$(W/2)/t$					
	1	1.5	2.5	4	10	∞
k	0.146	0.196	0.249	0.281	0.312	0.333
Error (%)	53.9	30.4	15.7	8.9	3.4	0

Table 2.3: Variation of κ with (w/2)/t for double-torsion specimens (results obtained by A.G.Evans, 1972, 1973)

Adhesive	Temperature, T (°C)	Diffusion coefficient, $(10^{12}\ D/m^2\ s^{-1})$	$M(\infty)$ (%)
NP1	50	4.7	4.5
	25	3.3	1.50
NP2	50	3.2	1.72
	25	1.6	2.38

(NP1,NP2 are two nitrile-phenolic adhesives of different formulations)

Table 2.4: Diffusion coefficients and equilibrium uptake levels of liquid water in adhesives (results obtained by D.M.Brewis, J.Comyn, and S.T.Tredwell, 1987).

Hardener		Amount of hardener/100 g diepoxide	Mixing temperature (°C)	Substrate temperature (°C)	Curing conditions
di-(1-aminopropyl-3-ethoxy ether)	DAPEE	32.5	80	60	3h at 80°C
triethylene tetramine	TETA	11.0	40	40	3h at 60°C
1,3-diaminobenzene	DAB	13.0	80	80	2h at 80°C then 2h at 150°C
4,4'-diaminodiphenyl methane	DDM	27.0	100	80	2h at 80°C
tris(dimethylaminomethyl)phenol	DMP	60.0	80	50	16h at 50°C
borontrifluoride monoethylamine	BF_3 MEA	4.0	100	80	1h at 130°C then 2h at 180°

Table 2.5: Details of epoxide formulations and curing procedures (used by D.M.Brewis, J.Comyn, R.J.A.Shalash, and J.L.Tegg, 1980).

Equilibrium water uptake (M_∞ (g 100 g^{-1} adhesive))					Diffusion coefficient, D ($10^{-13} m^2 s^{-1}$)			
25°C	45°C	70°C	100°C	Hardener	25°C	45°C	70°C	100°C
5.0	4.7	4.2	4.9	DAPEE	1.3	4.6	36	500
3.8	3.4	3.2	(3.89)*	TETA	1.6	3.2	4.5	170
2.3	3.1	3.2	1.9	DAB	1.9	9.7	13	49
4.1	1.6	1.4	(4.04)*	DDM	0.099	0.06	2.1	20
4.4	4.0	4.0	3.89	DMP	2.0	3.6	21	380
2.3	(2.4)	(2.9)		BF_3MEA	1.6	1.3	0.76	–

Table 2.6: Results of water sorption experiments (by D.M.Brewis, J.Comyn, R.J.A.Shalash, and J.L.Tegg, 1980).

substrate	G_o/mJ m^{-2}	W_A/mJ m^{-2}
FEPA	21.9	48.4
p.c.t.f.e.	74.9	62.5
Nylon 11	70.8	71.4
p.e.t.	79.4	72.3
plasma-treated FEPA	68.5	56.8

Table 2.7: Results for rubber adhering to various substrates. G_0 is the adhesive failure energy and W_A the thermodynamic work of adhesion (results obtained by E.H.Andrews and A.J.Kinloch, 1973).

Environment	$D \times 10^9$ (cm^2/s)	C_∞ (g/100 g)
20°C; 55% R.H.	2.54	0.75
20°C; H_2O	2.43	1.40
40°C; H_2O	6.50	1.60
60°C; H_2O	18.1	2.20
90°C; H_2O	60.7	6.90

Table 2.8: Diffusion coefficient and solubility data for water diffusing into bulk adhesive sample (results obtained by R.A.Gledhill, A.J.Kinloch and S.J.Shaw).

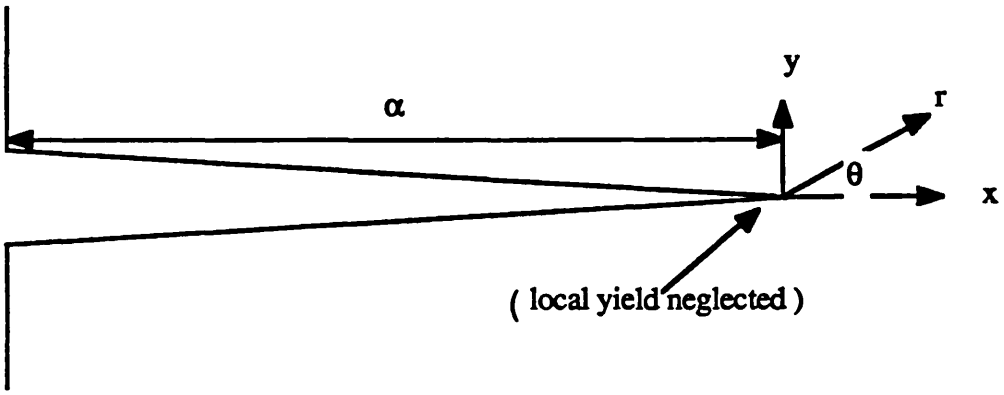
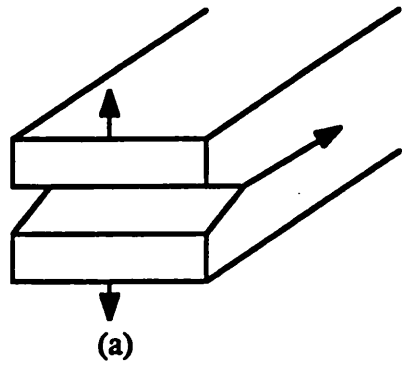


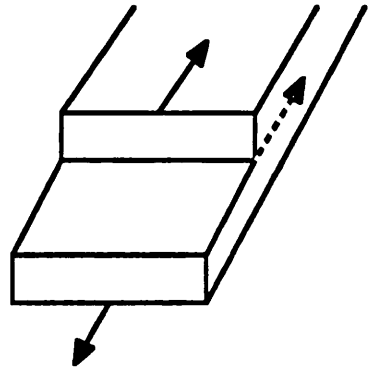
Figure 2.1: A sharp crack in a uniform stressed field-r and θ are the polar coordinates.

Mode I (opening mode)



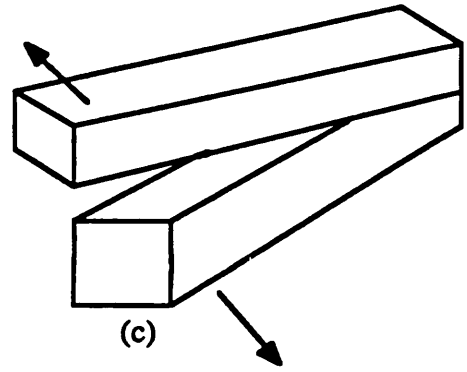
(a)

Mode II (edge sliding)



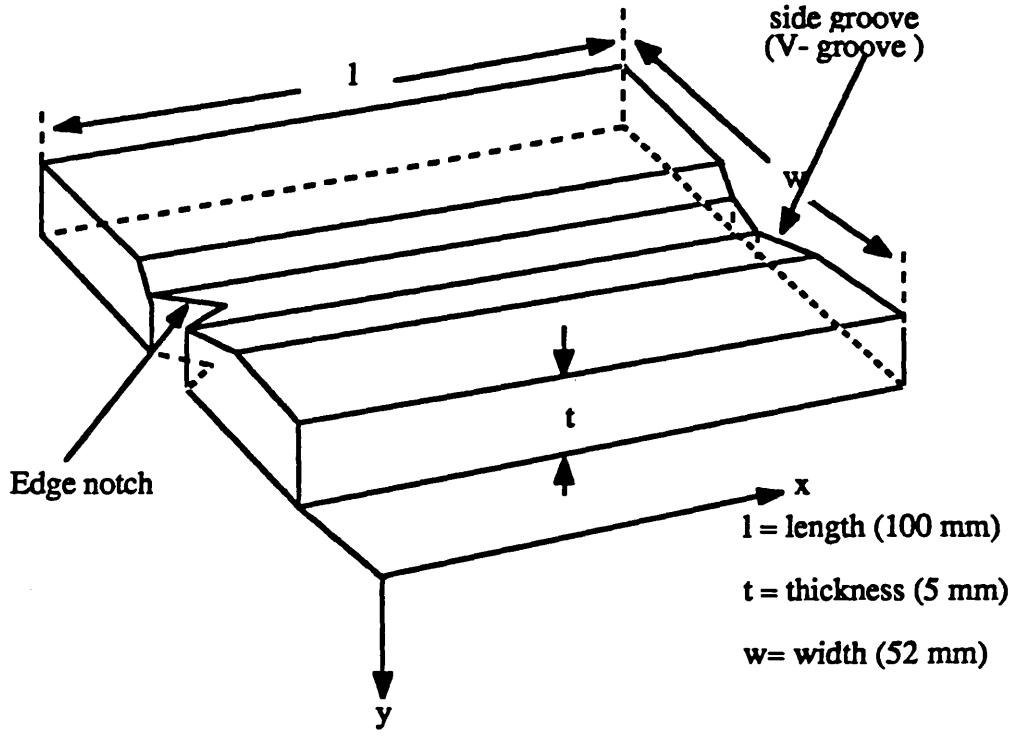
(b)

Mode III (screw sliding)



(c)

Figure 2.2: Modes of loading - (a) opening mode, Mode I, (b) edge sliding mode, Mode II, and (c) screw sliding mode, Mode III.



(a)

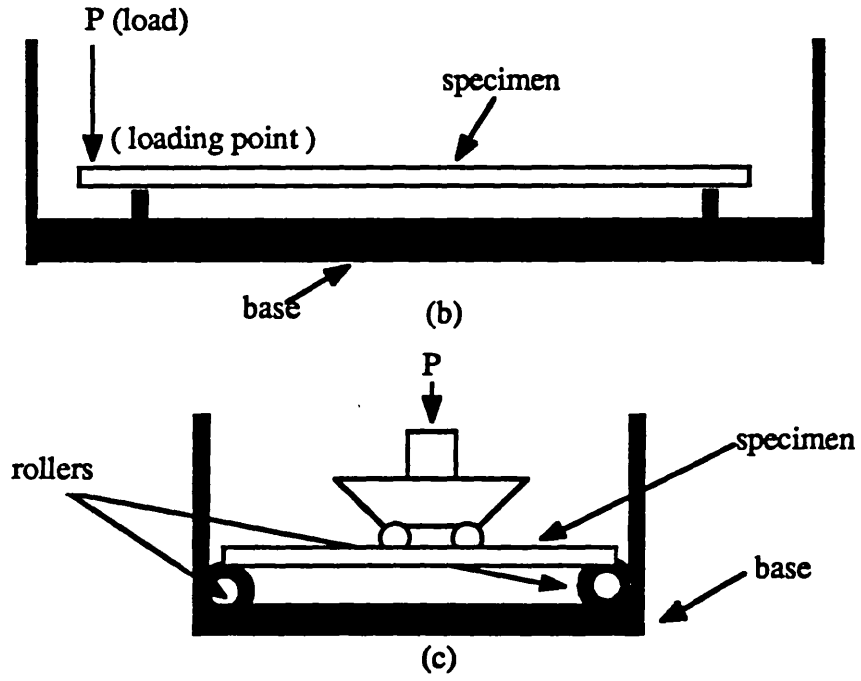


Figure 2.3 : Schematic representation of the DT test device: (a) the DT bulk specimen, (c) end projection,and (b) side projection

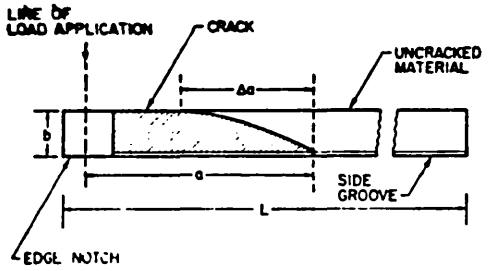


Figure 2.4: Schematic representation of the crack profile showing that the crack extends further along the lower face of the DT specimens.

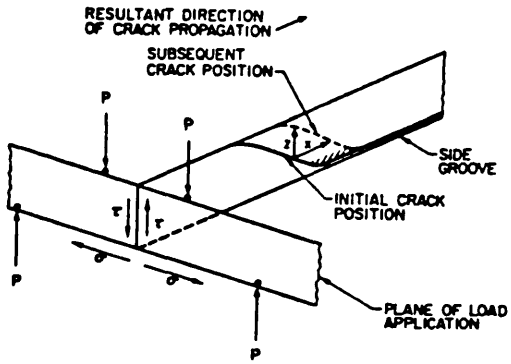


Figure 2.5: Schematic representation of the relationship between the applied load, P, the stresses, σ, (tensile), and τ, (shear), and the crack profile.

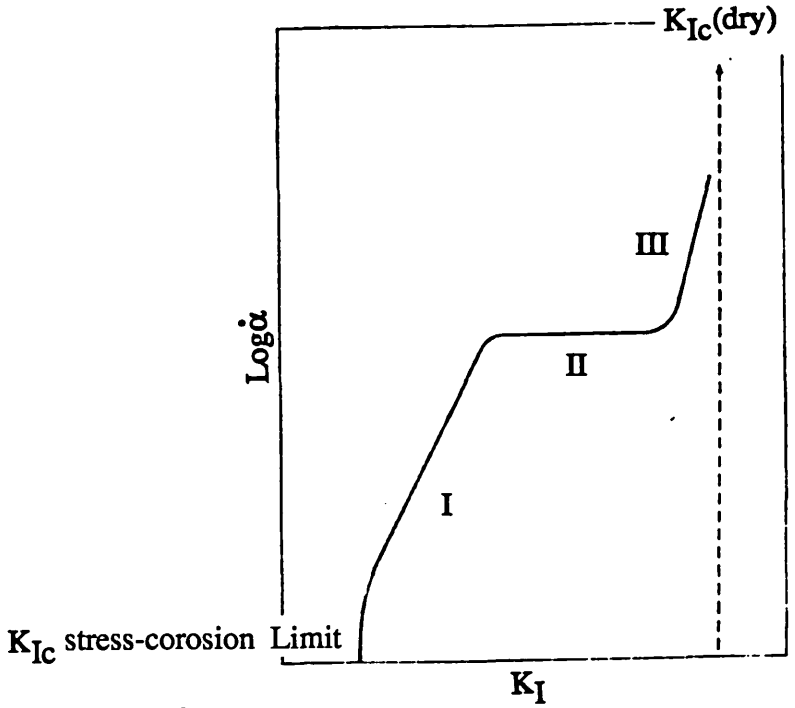


Figure 2.6: Typical log$\dot{\alpha}$ against logK_I graph of a brittle material exhibiting three stages of crack growth.

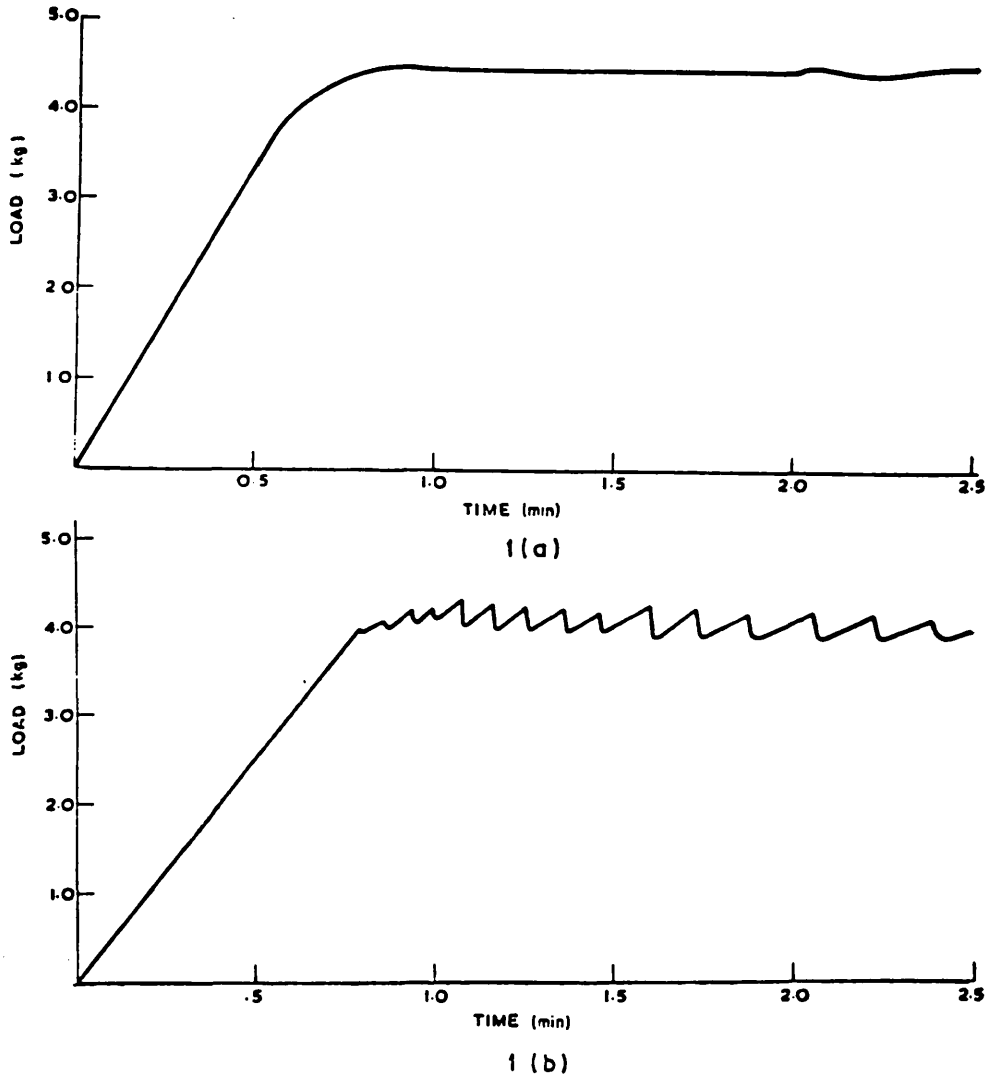


Figure 2.7: Load against displacement (or time) curves for crack propagation in thermosetting polymers - (a) stable continuous propagation and (b) unstable, stick/slip, propagation.

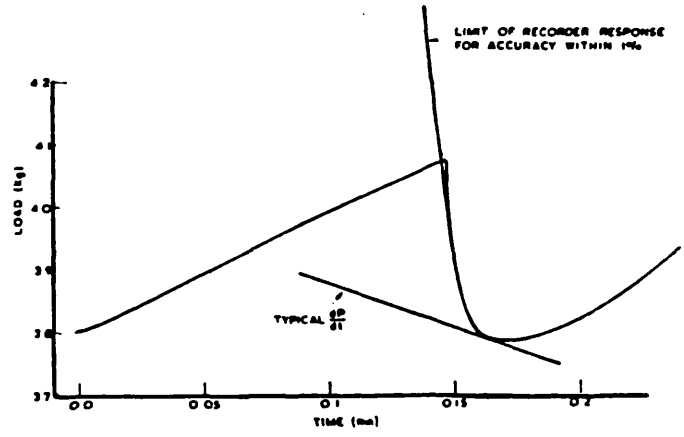


Figure 2.8: Typical stick/slip relaxation curve (results obtained by D.C.Phillips and J.M.Scott, 1974).

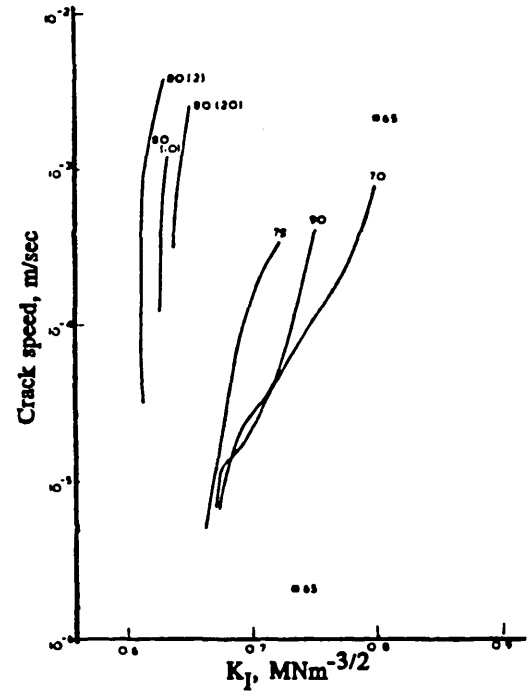


Figure 2.9: K_{IC} versus $\dot{\alpha}$ relationships in epoxide resin (results obtained by D.C.Phillips and J.M.Scott, 1974).

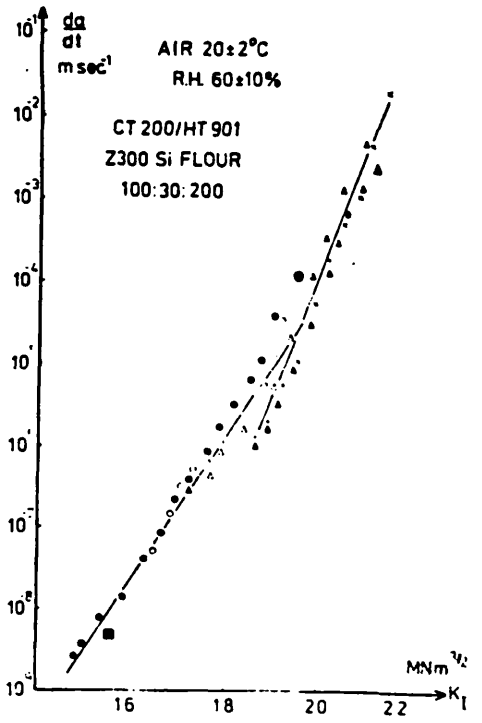


Figure 2.10: Crack velocity as a function of stress intensity factor (results obtained by R.J.Young and P.W.R.Beaumont, 1975a, 1975b).

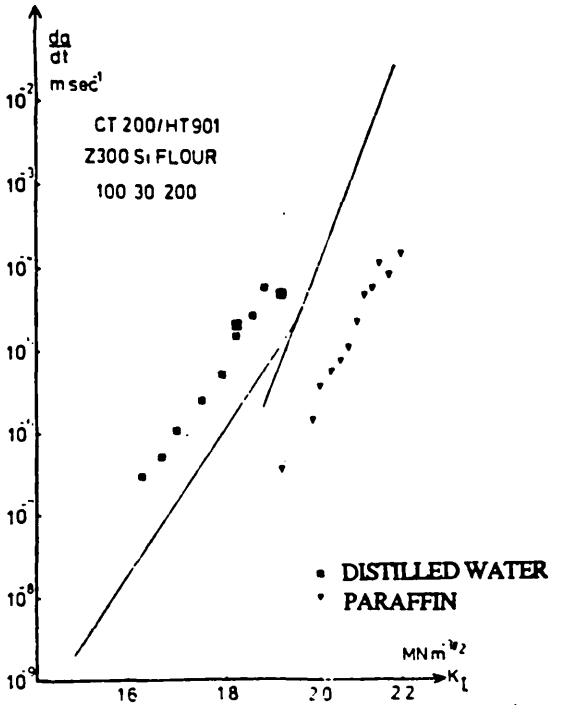


Figure 2.11: Crack velocity as a function of stress intensity factor for the filled resin in distilled water and in paraffin (results obtained by R.J.Young and P.W.R.Beaumont).

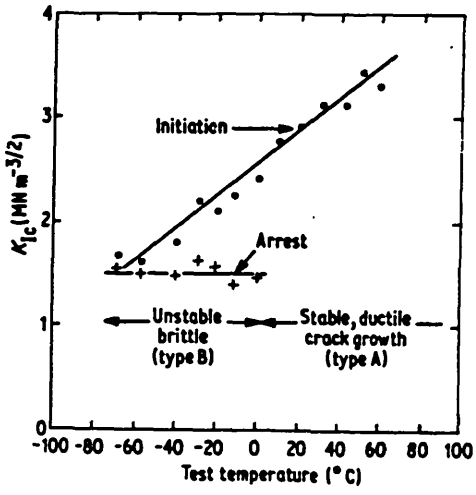


Figure 2.12: Stress - intensity factor , K_{IC},for crack propagation, and observed modes of crack growth as a function of temperature for a hydrid - particulate composite (results obtained by A.L.Kinloch, D.L.Maxwell and R.J.Young, 1985).

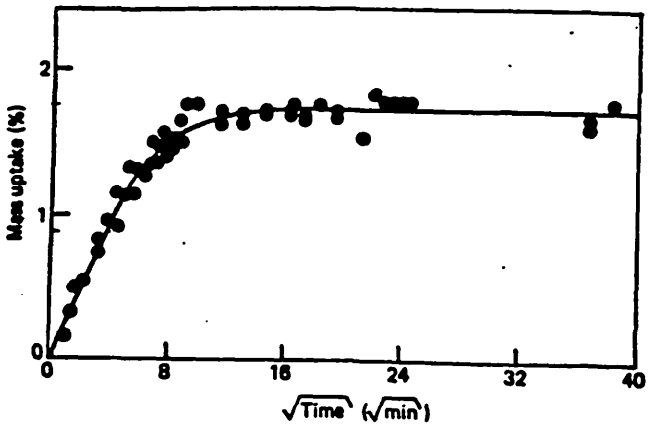


Figure 2.13: Mass uptake of water by a nitrile-phenolic adhesive (NP2) at 50°C (results obtained by D.M.Brewis, J.Comyn, and S.T.Tredwell, 1987).

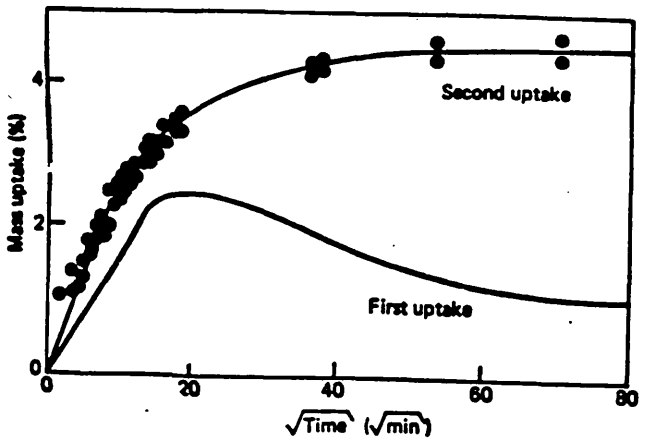


Figure 2.14: Mass uptake of water by a nitrile-phenolic adhesive (NP1) at 50°C (results obtained by D.M.Brewis, J.Comyn, and S.T.Tredwell, 1987).

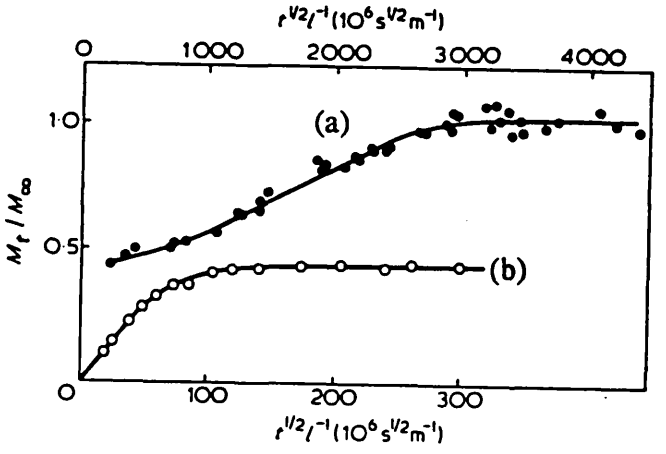
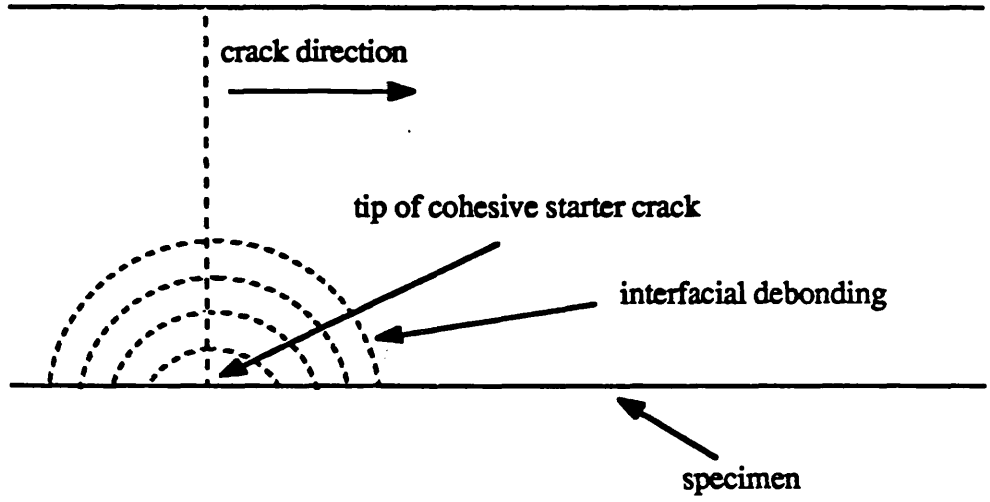
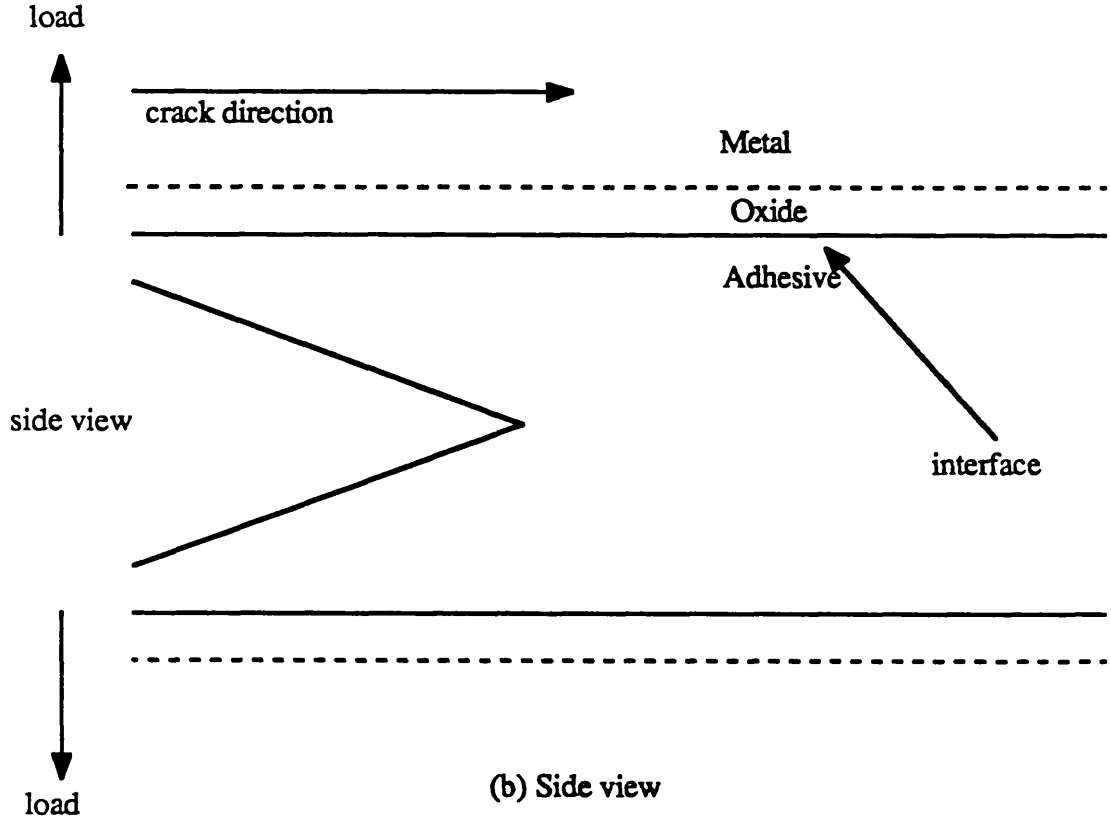


Figure 2.15: Sorption plot for epoxide with DDM hardener at 100°C, (a) long times and (b) short times (by D.M.Brewis, J.Comyn, R.J.A.Shalash, and J.L.Tegg, 1980).



(a) Top view



(b) Side view

Figure 2.16: Mechanism of interfacial attack in an adhesive joint under the application of external stresses in a hostile environment

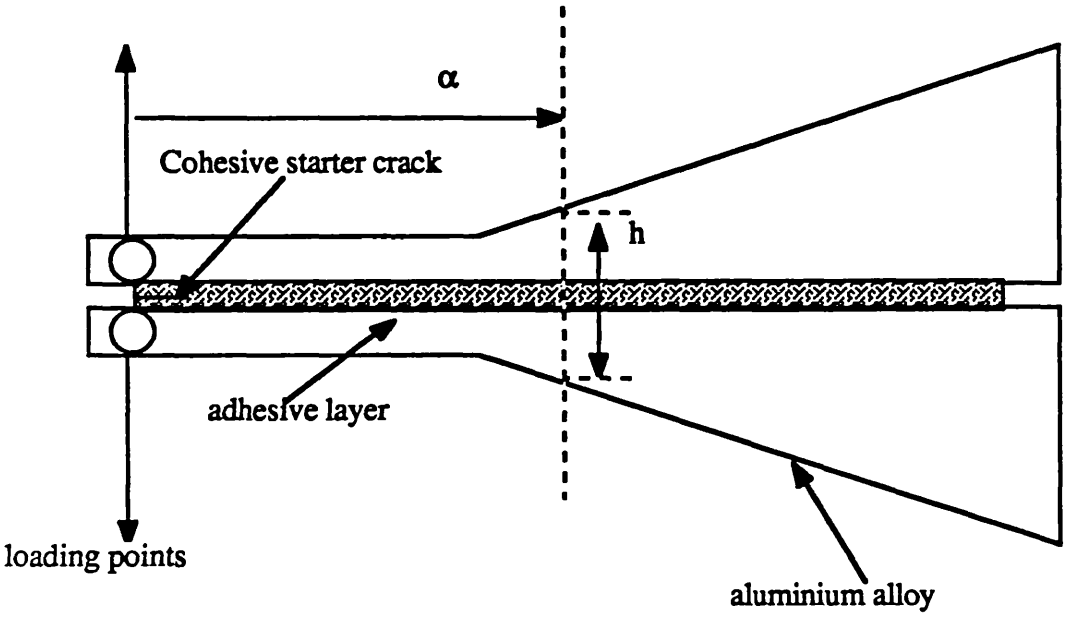


Figure 2.17: Tapered cantilever beam joint employed in the investigation of crack propagation by R.A.Glendhill and A.J.Kinloch, S.Yamini and R.J.Young (1978)

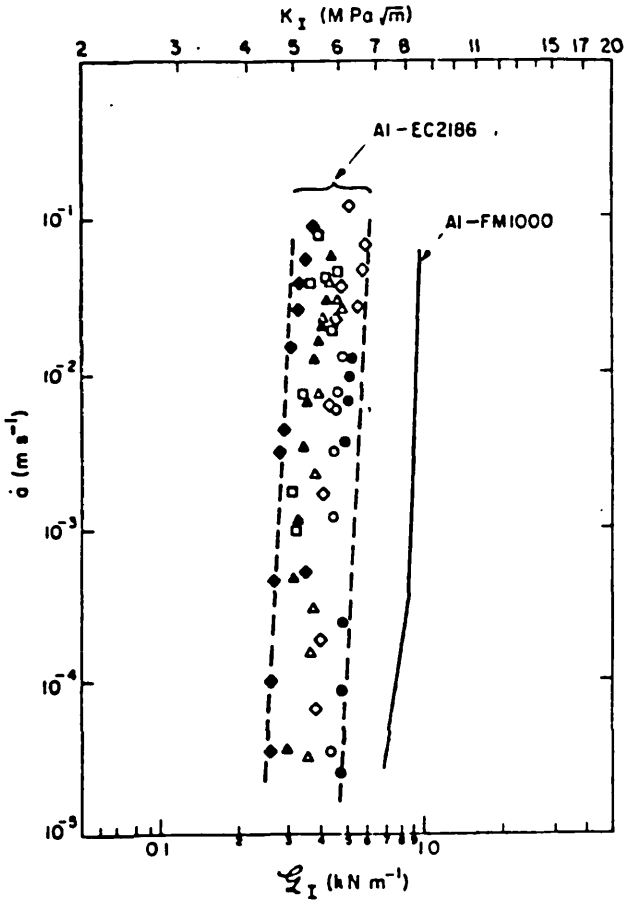


Figure 2.18: Comparison of the fracture properties of two types of adhesive joints (by R.H.French and Rishi Raj, 1979)

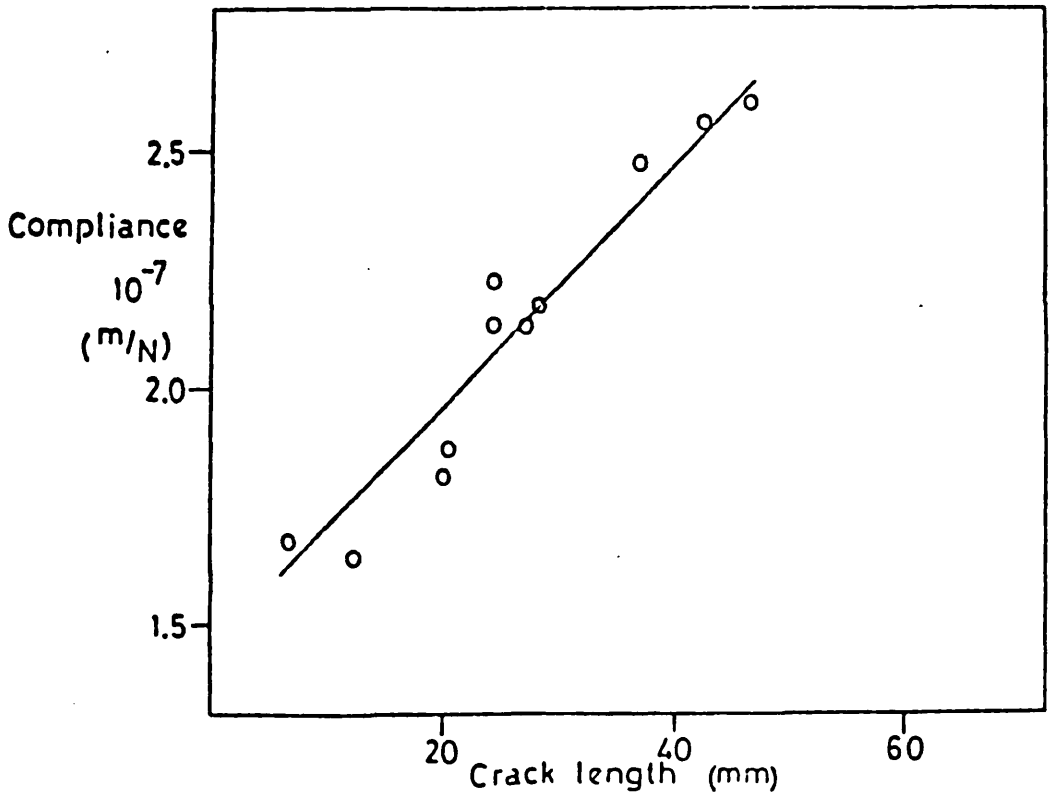


Figure 2.19: Compliance calibration for DT joints (obtained by A.C.Moloney, H.H.Kausch and H.R.Stieger, 1984).

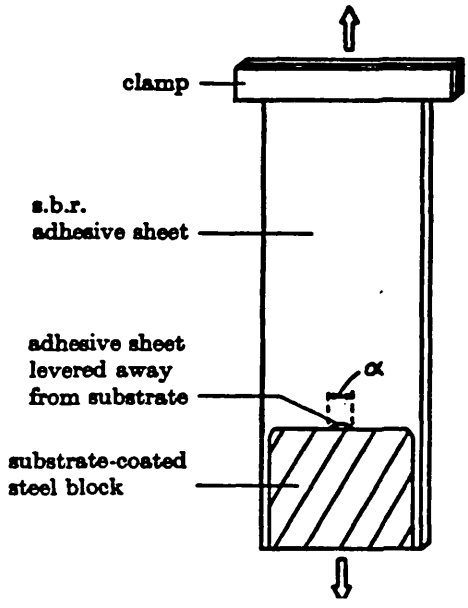


Figure 2.20: Sketch of simple extension test specimen (by E.H.Andrews and A.J.Kinloch, 1973).

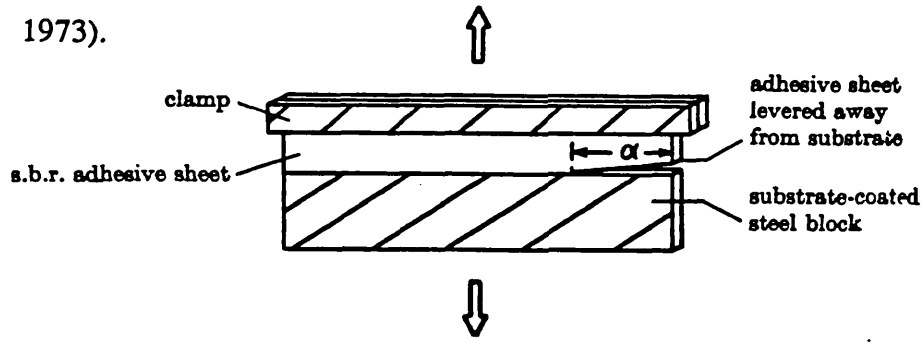


Figure 2.21: Sketch of pure-shear test specimen (by E.H.Andrews and A.J.Kinloch, 1973).

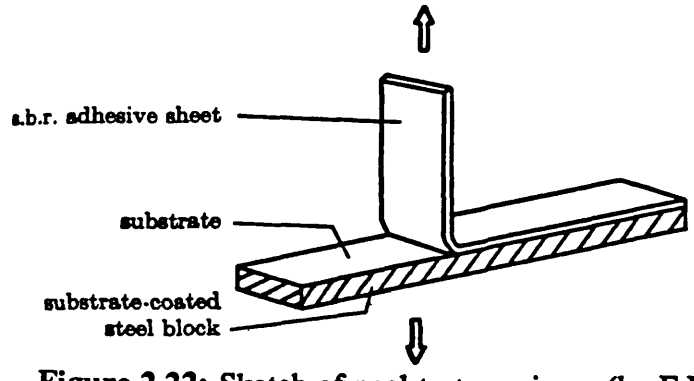


Figure 2.22: Sketch of peel test specimen (by E.H.Andrews and A.J.Kinloch, 1973).

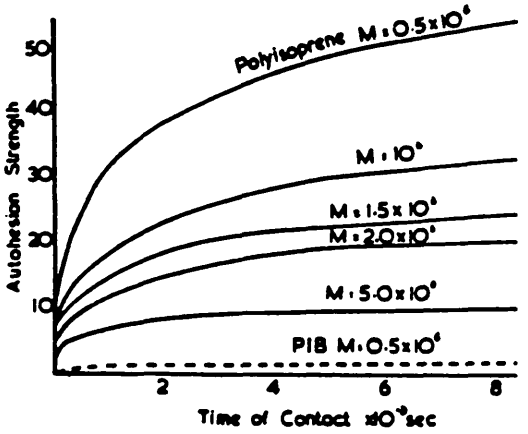


Figure 2.23: Results plotted as a function of time of contact for polyisoprene and polyisobutylene (obtained by R.M.V.Vasenin, 1965).

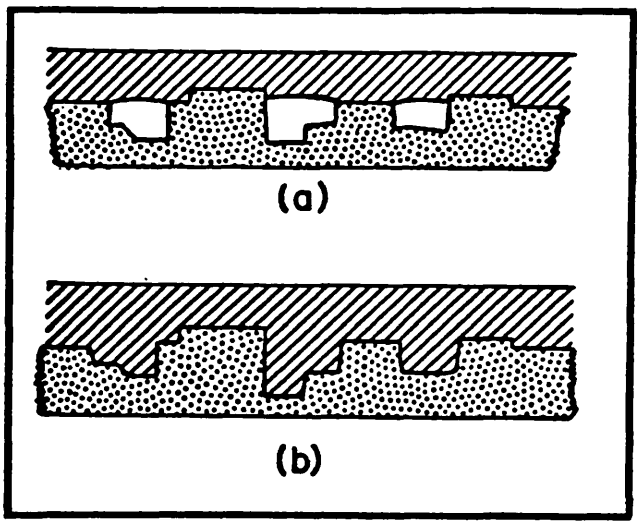


Figure 2.24: Wetting of a solid substrate by a fluid adhesive (suggested by J.R.Huntsberger, 1970)

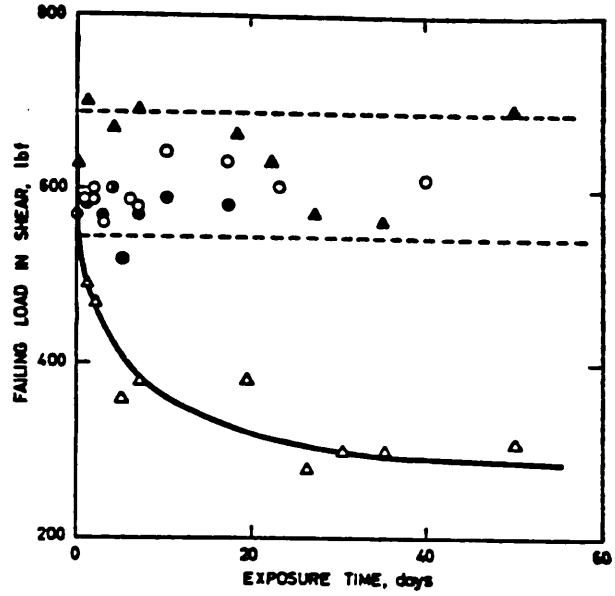


Figure 2.25: Failing load in shear against exposure time at 90°C for formulations A and B at different environments -

Formulation A, o vaccum ● oxygen

Formulation A, Δ water ▲ ethanol

(Results obtained by C.Kerr, N.C.Macdonald and S.Orman, 1967)

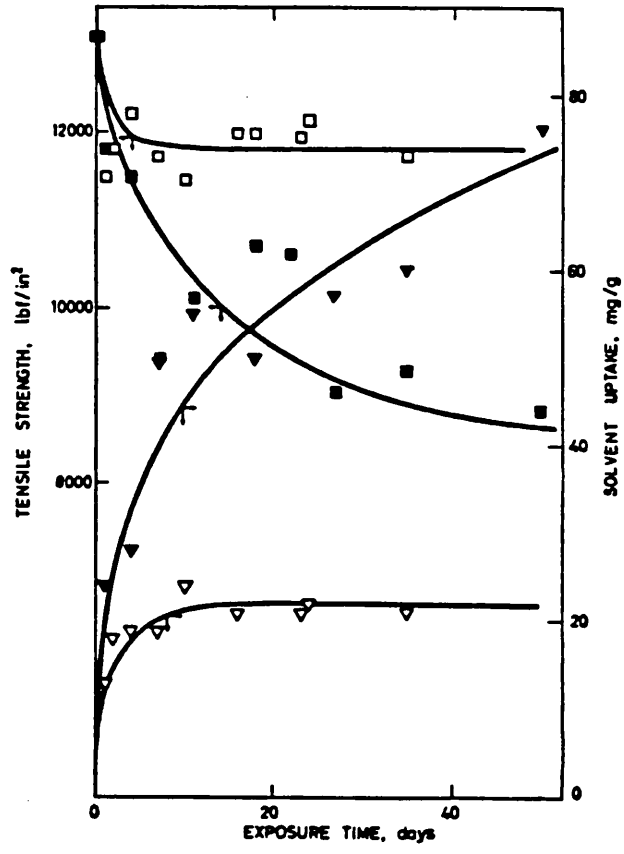


Figure 2.26: Tensile strength against exposure time and solvent uptake results at 90°C -

Water, □ tensile strength ▽ uptake

Ethanol, ■ tensile strength ▼ uptake

(Results obtained by C.Kerr, N.C.Macdonald and S.Orman, 1967)

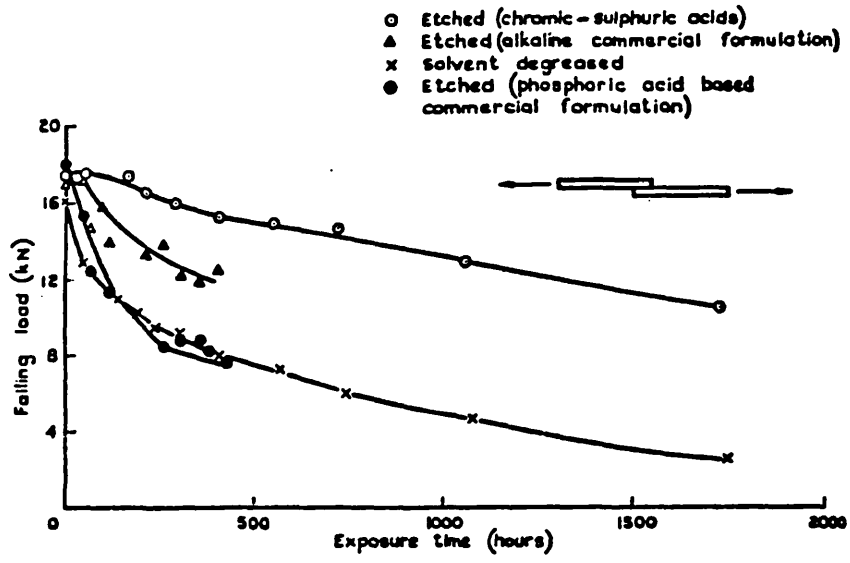


Figure 2.27: Failing load against exposure time results for aluminium joints bonded with an epoxy-polyamide adhesive (FM 1000) at 43°C (results obtained by R.I.Butt and J.L.Cotter, 1976).

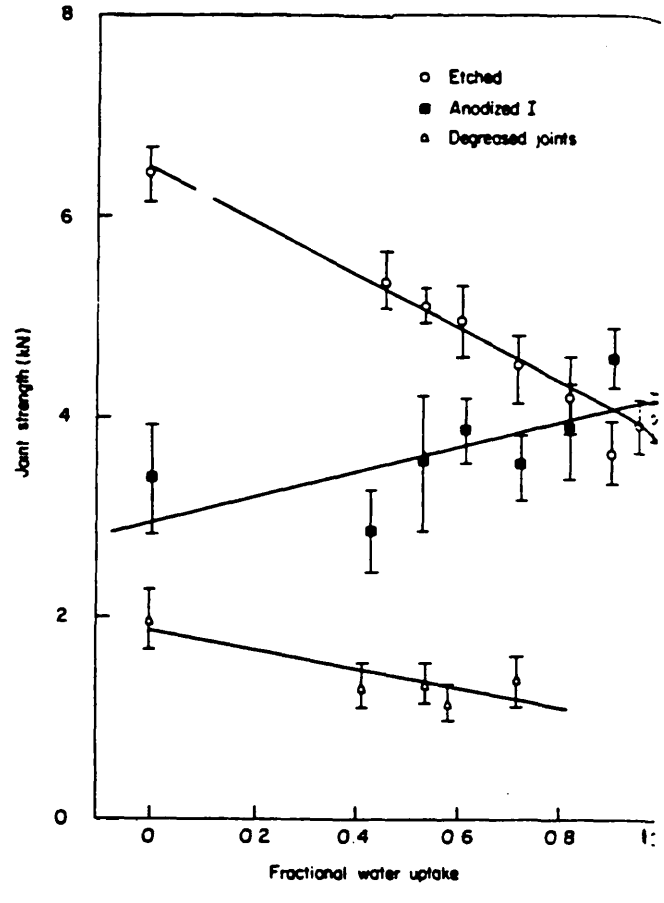


Figure 2.28: Joint strength against water uptake results for etched, anodized I, and degreased joints (results obtained by D.M.Brewis, J.Comyn and J.L.Tegg, 1980).

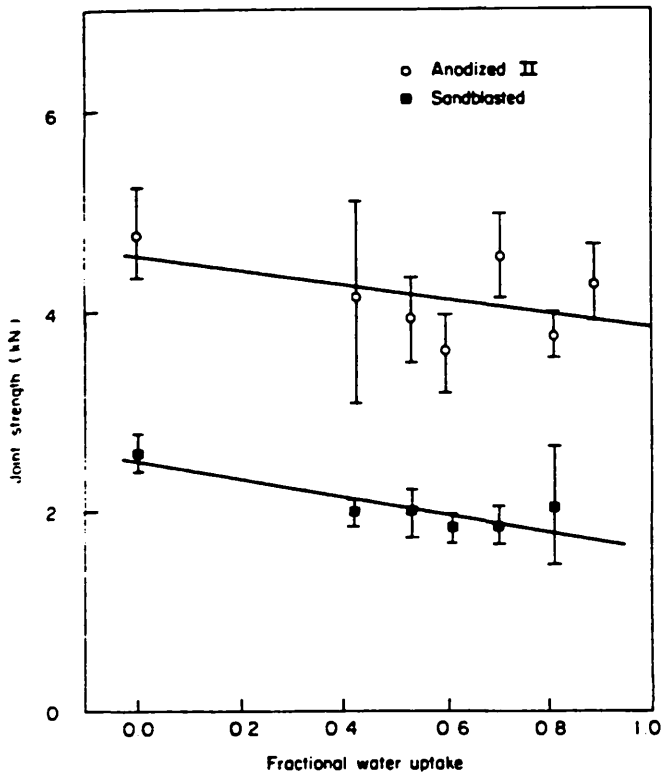


Figure 2.29: Joint strength against water uptake results for anodized II and sandblasted joint (results obtained by D.M.Brewis, J.Comyn and J.L.Tegg, 1980).

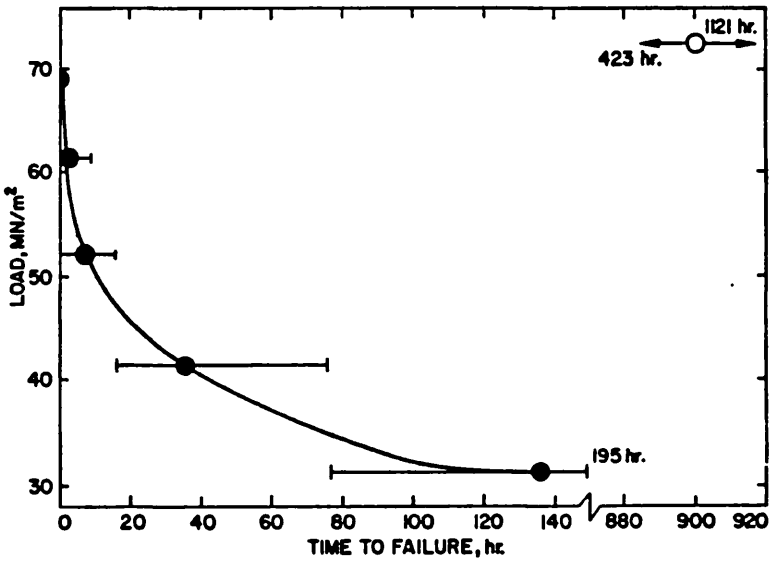


Figure 2.30: Static load against time to failure results (obtained by W.D.Bascom S.T.Gadomski, C.M.Henderson and R.L.Jones, 1977) -

- tested at 50% RH and in water

o tested in dry (<1% RH) air

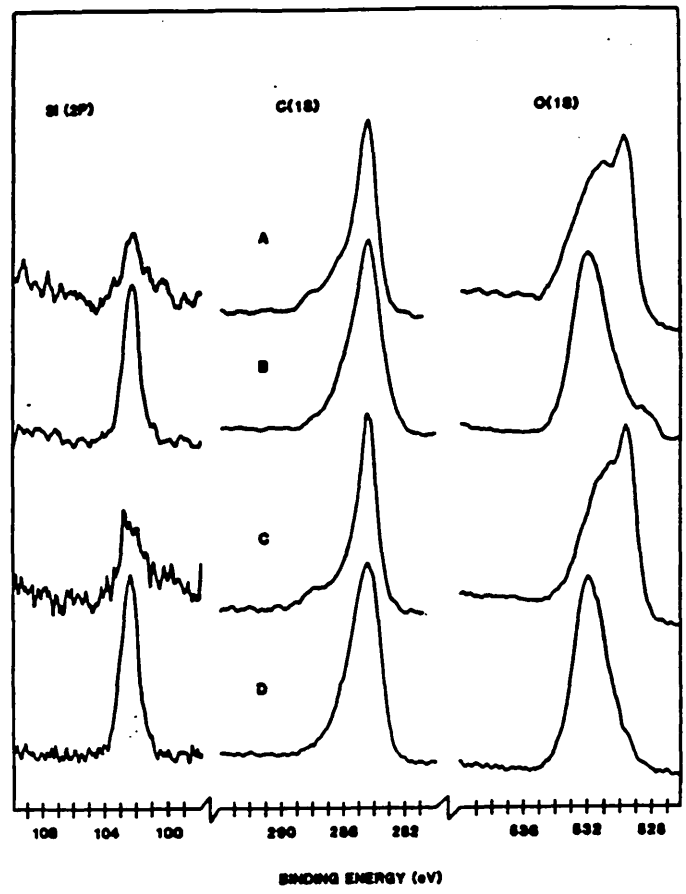


Figure 2.31: XPS spectra obtained from the failure surfaces of an iron/epoxy resin lap joint which was prepared from adherends that were pretreated with Γ-APS at pH 10.4 -

(A) adherend surface before immersion in water

(B) adherend surface of a dry bulk sample

(C) adherend surface after seven days exposure to water at 60°C

and

(D) adherend surface after seven days exposure to water at 69°C



Figure 2.32: XPS spectra obtained from the failure surfaces of an iron/epoxy resin lap joint which was prepared from adherends that were pretreated with Γ-APS at pH 8.0 -

(A) adherend surface before immersion in water

(B) adherend surface of a dry bulk sample

(C) adherend surface after seven days exposure to water at 60°C

and

(D) adherend surface after seven days exposure to water at 69°C

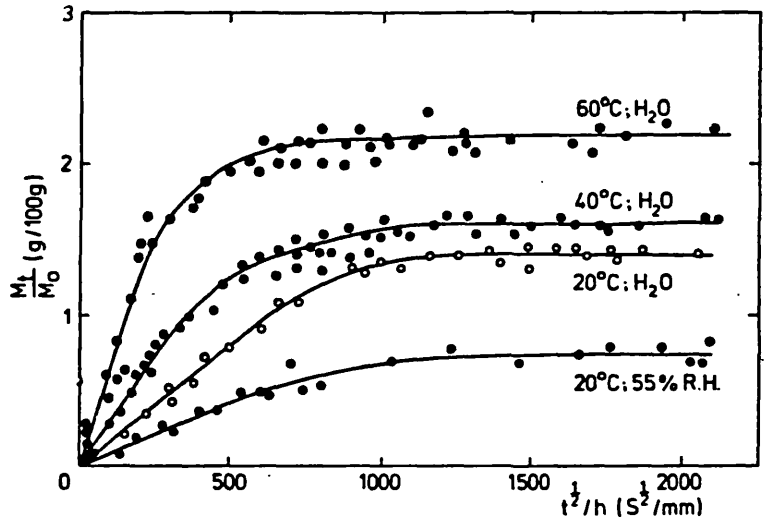


Figure 2.33: Water uptake, M_t/M_o, plotted against time$^{1/2}$/thickness for bulk adhesive samples (results obtained by R.A.Gledhill, A.J.Kinloch and S.J.Shaw, 1980).

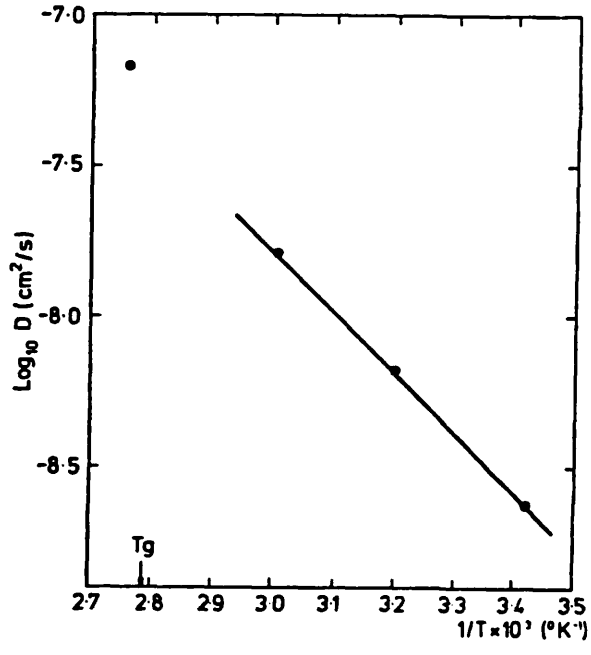


Figure 2.34: Logarithm of diffusion coefficient against the reciprocal of water temperarure (results obtained by R.A.Gledhill, A.J.Kinloch and S.J.Shaw, 1980).

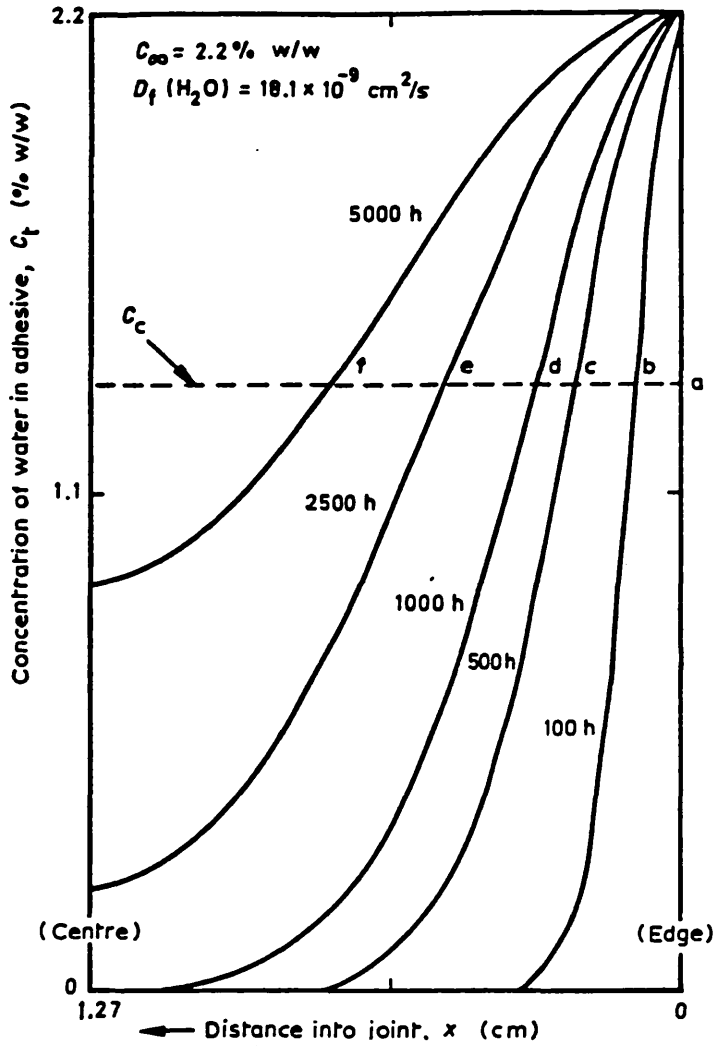


Figure 2.35: Water concentration, C_t, in the adhesive layer as a function of penetration depth for butt joints immersed in water at 60°C (results obtained by R.A.Gledhill, A.J.Kinloch and S.J.Shaw, 1980).

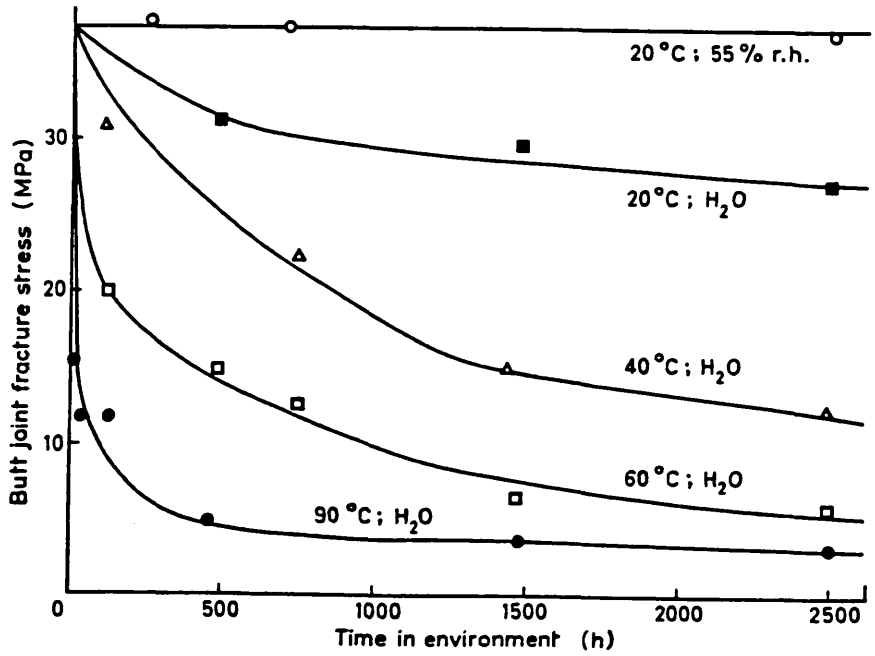


Figure 2.36: Butt joint fracture stress, σ_f, against time in environment. Points are experimental measurements and solid curves are theoretical predictions (results obtained by R.A.Gledhill A.J.Kinloch and S.J.Shaw, 1980).

CHAPTER 3

EXPERIMENTAL METHODS

3.1 MATERIALS

The epoxide resins which have been examined are listed in Tables 3.1 and 3.2 together with the curing agents, the compositions, and the cure schedules. In the first phase of this work, bulk double-torsion (DT) specimens were made from these materials and tested in a tensile-testing machine under dry laboratory conditions at a constant displacement rate of 0.5 mm/min. The purpose of this work was to find an epoxide resin that would give continuous crack propagation, thus enabling G_c versus crack growth rate, $\dot{\alpha}$, fracture data to be readily experimentally determined for the bulk adhesives. In the second phase of the work, unmodified and rubber-modified model adhesives (compositions 2 and 1 respectively in Table 3.1) have been employed in order (i) to investigate the effect of the rubbery phase in the epoxide, (ii) to examine the use of the joint double-torsion (DT) tests in more detail, and (iii) to assist in constructing a new constant-load environmental test method.

The epoxide resin employed for the DT joints and bulk specimens was a diglycidyl ether of bisphenol-A (DGEBA). The curing agent was piperidine which was used at a concentration of 5 parts per hundred of resin by weight (phr). Small particles of rubber-epoxy copolymer were also formed in the unmodified matrix of the epoxide. The rubber was a carboxyl-terminated random copolymer of butadiene and acrylonitrile, CTBN (carboxyl content, 2.37 wt %; acrylonitrile content, 18 wt %; molar mass, 3500 g mol^{-1}) used at a concentration of 15 phr. The epoxide resin was tested either in the form of bulk samples or used to bond mild steel substrates to give two different test geometries: the DT joint for fracture mechanics studies, and the coaxial butt joint for long-term life prediction studies.

3.2 PREPARATION OF SPECIMENS

3.2.1 Preparation of epoxide Polymer used for the DT and Butt Joints

The rubber-modified adhesive mixture was prepared in the following way: 15 phr of rubber (carboxyl-terminated butadiene-acrylonitrite : CTBN) were added to 100 phr of diglycidyl ether of bisphenol A (Ciba Geigy MY750) in a beaker and hand mixed at room temperature. The mixture was then heated in a water bath to 60-70°C and degassed in a vacuum oven at 60°C, until most of the trapped air had been removed. Five phr of piperidine was then added and the mixture was gently hand mixed for about 20 minutes. The final mixture was then ready to be poured into (i) the rubber moulds containing the mild steel substrates, or (ii) into a glass mould of thickness about 1.0 mm, or (iii) into a steel mould of thickness about 6 mm. The substrates and moulds were preheated to 120°C. The moulds were then placed in an oven at 120°C for 16 hours. After 16 hours the moulds were taken out and allowed to cool naturally. The unmodified mixture was prepared in the same way but no rubber was added.

3.2.2 Bulk Specimens for Diffusion Studies

In order to correlate the incubation time and crack speed with the rate of water diffusing into the adhesive joint, diffusion measurements on the rubber-modified and unmodified bulk adhesives were undertaken. Bulk specimens for diffusion studies were prepared from sheets of the materials of thicknesses between about 0.65 and 1.34 mm and cut into rectangles of approximately 20x50 mm. The sheets of the material were obtained using the glass mould which consisted of two glass plates kept together using metal clamps and separated and sealed by thin plastic cards. Tightening of the metal clamps was found to cause fracture of the glass plates when the mould was heated, and therefore the clamps were kept relatively loose which affected the uniformity in the thickness of the sheets from one sheet to another, but for a given sheet a constant thickness was achieved. The samples were weighed and immersed into bottles containing

distilled water. The bottles were then placed into ovens at 40°C, and 55°C, as well as in a temperature controlled room at 25°C. At various intervals, the samples were removed from the bottles, dried, weighed, and returned to the bottles.

3.2.3 Bulk Specimens for Fracture Studies

Bulk double-torsion (DT) specimens were cut from sheets of the materials of thickness 6 mm and were 100 mm long and 53 mm wide. The sheets were obtained using the steel mould. All specimens were side-grooved and the effective thickness, t_n, varied from 4 to 3 mm, but was constant in anyone specimen. Starter cracks were inserted at one end of the specimens using sharp razor blades and tapping them into the material.

3.2.4 Adhesive Joints

Mild steel substrates of about 26 mm width, 100 mm length and 3 mm thickness, were bonded together to give a total width of a double-torsion specimen of about 53.4 mm, i.e. the adhesive layer had a thickness of about 1.4 mm. The steel substrates were first grit-blasted and then degreased in a solvent. The substrates were then placed in pairs into a rubber mould and the adhesive was poured on top of the substrates until it completely covered them. Figure 3.1 shows a schematic representation of the double-torsion specimen. Butt joints were also made from the same materials as the double-torsion joints, and for these joints the mild steel substrates used were about 63 mm in length and 14 mm in diameter and were placed into aluminium moulds into which the adhesive was poured. The aluminium moulds presented sealing problems when the hot adhesives were poured into them and it was not possible to stop the adhesives from running out of the moulds. It was therefore necessary to repeat the pouring operation several times until the adhesives had become viscous enough, and were therefore not able to flow through the gaps in the moulds. Figure 3.2 shows a schematic representation of

the butt joints and Figure 3.3 shows a photograph of a butt joint together with an aluminium mould.

3.3 FRACTURE EXPERIMENTS ON DT SPECIMENS

3.3.1 Introduction

Fracture data on double-torsion joints presented in the literature has so far been produced by employing expensive equipment, such as an "Instron" tensile-testing machine. However, if the "Constant Load Method" is to be used for fracture studies (see Chapter 2), then a major requirement is to find a way of applying a contant load to a double-torsion specimen so that many specimens can be tested with experiments possibly lasting several months. Obviously it is not possible to occupy a large number of expensive tensile testing machines for such a period. The problem may be solved by designing and constructing simple constant-load test-rigs. Such test-rigs have been made for the present work and their applicability has been investigated. Another advantage of the new technique is that it can easily be used for the study of adhesive joints in hostile environments. The test equipment, designed and built for the present research, is described in detail below after a brief description of the usual constant-displacement rate tests.

3.3.2 Tests Conducted at a Constant Displacement Rate

A tensile-testing machine was used for fracture tests of bulk adhesive samples at room temperature and under dry laboratory conditions. Some compliance tests were also performed on the same machine, using bulk samples and adhesive joints under dry environmental conditions. All tests were performed at a constant cross-head speed of 0.5 mm/min.

3.3.3 Calibration of the Tensile-Testing Machine

The data concerning the fracture event of a bulk sample or of a joint were recorded by a chart recorder which was attached to the tensile-testing machine. The load cell and the chart recorder were first calibrated using the calibrating devices incorporated in the assembly. Then, the cross-head was moved slowly until the two hemispheres, situated at the end of the main shaft as Figure 3.5 shows, just touched the specimen. This was accompanied by a slight movement of the pen on the chart recorder paper. The pen was then positioned in the beginning of the chart paper, where the applied load was initially zero, and hence tests on double-torsion bulk specimens or joints could be carried out.

3.3.4 Compliance Measurements

A linear displacement transducer was fixed on to the main shaft in a vertical position so as its free end was in direct contact with the specimen near the loading point. The transducer was connected to an amplifier which was in turn connected to an X-Y plotter. The assembly was first calibrated, as described below. The compliance measurements were performed in such a way so as to enable the load and the corresponding displacement of the specimen at the loading point to be continuously monitored and recorded on the graph paper of the plotter.

3.3.5 Calibration of Transducer

The linear variable displacement transducer (LVDT) was calibrated in such a way so as to be able to detect accurately very small displacements. A standard "Instron" supermicrometer was used, as shown in Figure 3.4, in which the transducer was mounted in a horizontal position. Markings on the plotter paper were made for every 0.1 mm turn of the supermicrometer, and hence the actual displacements could be determined.

3.3.6 Compliance Tests

Rubber-modified and unmodified adhesive bulk specimens and joints were next tested in the tensile-testing machine under dry (i.e. 55% R.H.) laboratory conditions using the double-torsion test method. Cracks of different lengths were first inserted into the specimens using a saw and their lengths were measured using a travelling microscope. The X-Y plotter recorded the event from the moment the load was applied until fracture, by a crack propagating in the middle of the sample, was about to occur. At this stage, the tests were stopped, since all the data needed was already recorded in the form of graphs of load against displacement at the point of application of the load. The graphs were approximately linear for most of the loading, and the best straight lines were fitted and the slopes were measured.

3.3.7 Fracture Tests

Double-torsion bulk adhesive samples were tested in the tensile-testing machine at 25°C, 40°C, and 55°C using a heater until final failure. The fracture data were recorded on the chart recorder paper as plots of load against time for each sample.

3.3.8 Constant Load Tests

Fracture tests on rubber-modified and unmodified double-torsion adhesive joints were carried out using the constant-load test-rigs. The joints were immersed into distilled water at 25°C, 40°C, and 55°C. The main aims of the tests were firstly to obtain fracture data and secondly, to use the new test-method to assess joint durability. Compliance tests using rubber-modified and unmodified bulk adhesive samples and joints were also carried out since this information is needed, of course, to determine values of the fracture energy, G_C. The compliance tests were performed under both dry (55% R.H.) laboratory conditions and in water at the temperature of the aqueous surroundings.

3.3.9 Test Equipment

Rubber-modified and unmodified double-torsion adhesive joints were tested in distilled water at various temperatures using a simple constant-load test-rig which was specifically designed and constructed for the present research. A schematic representation of the device is shown in Figure 3.5 and consists of a shaft supported by bearings in a vertical position. The specimen was placed at the bottom of the main shaft into a brass bath and different loads were applied. Distilled water could be easily added in the "perspex" bath, which surrounds the brass bath, so that tests could be carried out in water at different temperatures. Hence, loads could be easily applied in the presence of an environment to give a "stressed-durability" test. Figure 3.6 shows the total set up for the double-torsion tests: five rigs were made and connected together using plastic piping. Therefore, by using a water pump and heater, water at a given temperature could circulate around the baths. The baths were covered with plastic films to prevent excessive heat losses.

3.3.10 Compliance Measurements

Rubber-modified and unmodified double-torsion bulk samples and adhesive joints were used in order to investigate the applicability of the constant compliance concept using the constant-load test-rig. Cracks of different lengths were introduced on the specimens using a saw and were measured using a travelling microscope. The LVDT used in the constant displacement tests was also used in the present tests, but this time it was connected to a digital amplifier. The digital reading on the amplifier displayed any change in the transducer movement in terms of change in voltage, and therefore calibration was again necessary. The transducer was mounted on to the main shaft of the test-rig in a vertical position and near to the loading point.

3.3.11 Calibration of Transducer

A standard "Instron" supermicrometer was again used where the transducer was mounted in a horizontal position. The change in voltage reading was recorded for every 0.1 mm turn of the supermicrometer several times and the average reading was taken. Hence, displacements could be accurately determined.

3.3.12 Compliance Tests

The specimen was placed into the brass bath, and the main shaft, without any load, was allowed to slide gently downwards, until the two small hemispheres at the bottom end of the shaft were in contact with the specimen. The weight of the shaft without any load was recorded, as well as the reading on the digital display of the displacement on the amplifier. Distilled water at the temperature of the environment was also added in some cases at this stage, and the reading on the digital display was found to change slightly, most probably due to the water uptake by the adhesive. The set up was therefore allowed to stabilise and loads were added after a period of about one hour and recorded. The corresponding readings of voltage on the digital display were also recorded and transformed into displacements using the results from the calibration of the transducers. The specimens were gradually loaded until final failure, and the data was plotted as a graph of load against displacement. The data points were found to be fitted by straight lines, and each slope, which corresponded to a particular value of an initial crack length of a sample, was calculated and recorded. Finally, graphs of slope against crack length were plotted for each group of samples which had different initial crack lengths, but were made from the same material, had approximately the same dimensions, and were tested under identical conditions.

3.3.13 Fracture Tests

Rubber-modified and unmodified double-torsion adhesive joints were

tested in the constant-load test-rigs. In order to be able to continuously monitor the crack growth in the adhesive layer, from the instant it first occured until final failure of the joint, a crack propagation gauge was designed. The gauge was prepared by spraying graphite on one face of each joint, of width of about 4 mm, and along the length of the adhesive layer, which was about 95 mm long on each joint. The graphite layer converts the material between the metal substrates from a non-conductive into a conductive one, and hence any change in the resistance of the gauge, which may be caused by a crack propagating along the adhesive layer, can be accurately detected by means of potentiometers connected across the gauge. The initial resistance of the graphite gauge was at about 100 Ω for every joint. Two holes of diameter 0.5 mm were drilled in one end of each joint near the graphite gauge and two electrodes were inserted. When the joint was under test, the face with the gauge was the lower face and a signal was taken from the electrodes to a potentiometer, which was built for this research to detect any crack propagation, such that the voltage output was proportional to the crack length. To examine the output characteristics of the potentiometer, different cracks were cut into the joints and the voltage across the gauge was recorded. The procedure was repeated on several joints. The output of the potentiometer was connected to a chart recorder and therefore the fracture data was immediately displayed on the chart paper. Figure 3.1 shows a schematic representation of the gauge.

The joints were placed into the brass baths and the main shaft was gently lowered, without any load, until the two hemispheres, situated at the bottom of the main shaft, were in contact with the joint, each one on either side of the adhesive layer. In order to avoid electrical contact, and therefore a shortcircuit between the joint and the rig, the metal substrates were covered with an electrical insulating tape. Distilled water was next allowed to circulate with the help of the pump and heater. When the water had reached the desired temperature, and therefore the joint was also heated to the temperature of the water, the potentiometer bridge was balanced so as the chart recorder pen was at the zero

point on the chart paper, corresponding to a voltage in the bridge of about 0.0 volts. Loads were then added gently by hand at the top of the main shaft and the bridge was rebalanced. Cohesive starter cracks were initially inserted in the joints by tapping sharp razor blades on to the adhesive layer using a hammer. However, the fracture mode was such that the artificial starter cracks did not propagate, but instead a new crack was formed at the interface which propagated through the joint and was responsible for joint failure. When a joint was fractured, the chart recorder pen moved to the other end of the chart paper, which corresponded to a voltage in the bridge of about 1.0 volts. The trace on the chart paper, Figure 3.7, was used to calculate the crack speed, as described below. The same trace was also used in order to estimate accurately the incubation time, i.e. the time taken for the chart recorder pen to start moving which corresponded to the time from the application of the load to the time at which the crack began to propagate.

In the first stages of this work, only one constant-load test-rig was built in order to investigate the applicability and reproducibility of the test. As this was successful, four more rigs were constructed and joint durability tests were performed in the five test-rigs which were connected to two chart recorders of a total capacity of five pens through five independent potentiometer bridges.

3.3.14 Crack Speed Calculations

Considering the methods of calculating the crack speed, then an average speed could be obtained from the gauge trace on the chart recorders in the following way: consider region AB in Figure 3.7:

V_A = voltage at point A

V_B = voltage at point B

t_{AB} = time for the crack to travel region AB

then

$(V_B - V_A)/t_{AB}$ is the change in voltage with time in this region of stable crack

growth.

The crack speed in this region was determined as follows:

$$d\alpha/dt = [(\alpha_f - \alpha_i)/(V_f - V_i)] \quad [(V_B - V_A)/t_{AB}]$$

where:

$d\alpha/dt$ was the speed in region AB

α_f was the final crack length (end of gauge)

α_i was the initial crack length

V_f was the final voltage when the gauge breaks (1.0 volts) and

V_i was the initial voltage across the gauge corresponding to the initial crack length(set at 0.0 volts).

3.4 FRACTURE EXPERIMENTS ON BUTT JOINTS

3.4.1 Introduction

Double-torsion joints have so far been considered in order to obtain fracture data under the application of various constant loads and in the presence of distilled water. The specimen geometry and test method allow a fracture mechanics approach to be adopted for analysing the results and this approach should give parameters indepentent of the detailed joint geometry. Havingsuccessfullyestablished the applicability and reproducibility of the new test method, the next step would be to use this method in order to predict the durability of joints of other geometries, which may fail under the application of constant loads in hostile environments. Butt joints were therefore tested in the presence of distilled water and under the application of externally applied constant loads. The specimen geometry was such, so as to allow the load to be applied in a tensile manner.

3.4.2 Test Equipment

The apparatus which was built for this part of the research programme is shown in Figure 3.8. Three rigs were made and a perspex bath surrounded the joints, so that

tests in distilled water could be carried out. Circulation of the water was achieved using a pump and heater. Timers were mounted on the rigs which enabled the fracture time to be measured and recorded.

3.4.3 Calibration

Before tests could proceed, calibration of the rigs was necessary in order to determine the tensile load applied to the joints accurately. A spring balance was therefore used, and the actual values of the tensile loads W_2 were measured and recorded which corresponded to the W_1 loads added by hand in the weight hanger. Figure 3.9 shows a schematic arrangement of the forces set up in the rig due to the external loading.

3.4.4 Fracture Tests

The equipment was now ready to be used for fracture studies of adhesively bonded tensile butt joints. The butt joints were therefore placed into the rigs, initially without any external load, and distilled water was poured into the perspex bath and circulated and heated to 25°C with the help of the pump and heater. After a time interval of one hour, which was sufficient enough for the assembly to reach steady conditions, external loads were gently added by hand in the weight hanger and the timers were set.

3.5 SCANNING ELECTRON MICROSCOPY (SEM)

In order to identify the locus of joint failure, a Cambridge Stereoscan model 250 Mk 2 scanning electron microscope (SEM) was used. Small samples were cut from the joints and were coated with a thin film of gold (100Å-300Å) using a Polaron specimen coating unit E 5000. Micrographs were taken of the pretreated mild steel surface prior to bonding and joint sections after exposure to distilled water and stress using either Ilford ortho film (50 ASA) or Polaroid type 55 land film (50 ASA).

3.6 X-RAY PHOTOELECTRON SPECTROSCOPY (XPS)

In order to identify the locus of joint failure in more detail, an x-ray photoelectron spectrometer has been used. X-ray photoelectron spectroscopy (XPS), or as it is sometimes called electron spectroscopy for chemical analysis (ESCA), is a technique which allows quantitative elemental analysis of a sample's surface. The technique involves irradiating the sample in vacuo with soft x-rays, typically AlKα, detecting the emitted core-level photoelectrons and then analysing them according to their energies. The technique is extremely sensitive as the emitted photoelectrons must reach the detector without losing any energy and so, in general, useful information can only be obtained from the outermost 100Å of a surface.

Table 3.1: List of the epoxy resins examined in the present investigation, together with the curing agents, the compositions and the cure treatments

Number	Epoxy resin	Curing Agent	Composition	Cure Schedule
1	MY750+Rubber	Piperidine	100:15:5	16 hours at 120°C
2	MY750	Piperidine	100:5	16 hours at 120°C
3	MY750	HY906+DY062	100:70:1	2 hours at 120°C
4	MY750	HY906+DY062	100:90:1	2 hours at 120°C
5	CT200+Z300	HT901	100:30:200	16 hours at 135°C
6	CT200+Z300	HT901	100:30:300	16 hours at 135°C
7	CT200	HT901	100:30	16 hours at 135°C
8	MY750	TEPA	100:10	23 hours at 23°C + 8 hours at 80°C

Table 3.2: Chemical forms of epoxy resins and hardener used in the present investigation

Epoxy Resin	Supplier	Form
MY750	Ciba Geigy plc	DGEBA(Diglycidyl ether of bisphenol A)
CT200	Ciba Geigy plc	DGEBA
Hardener		**Form**
HY906		Methylendomethy-lenetetrahydrophthalic anhydride
TEPA		Tetraethylene pentamine
HT901		Phthalic anhydride
Rubber Form: Carboxyl-terminated butadiene-acrylonitrite ("1300x8" grade from B.F.Goodrich Co.)		

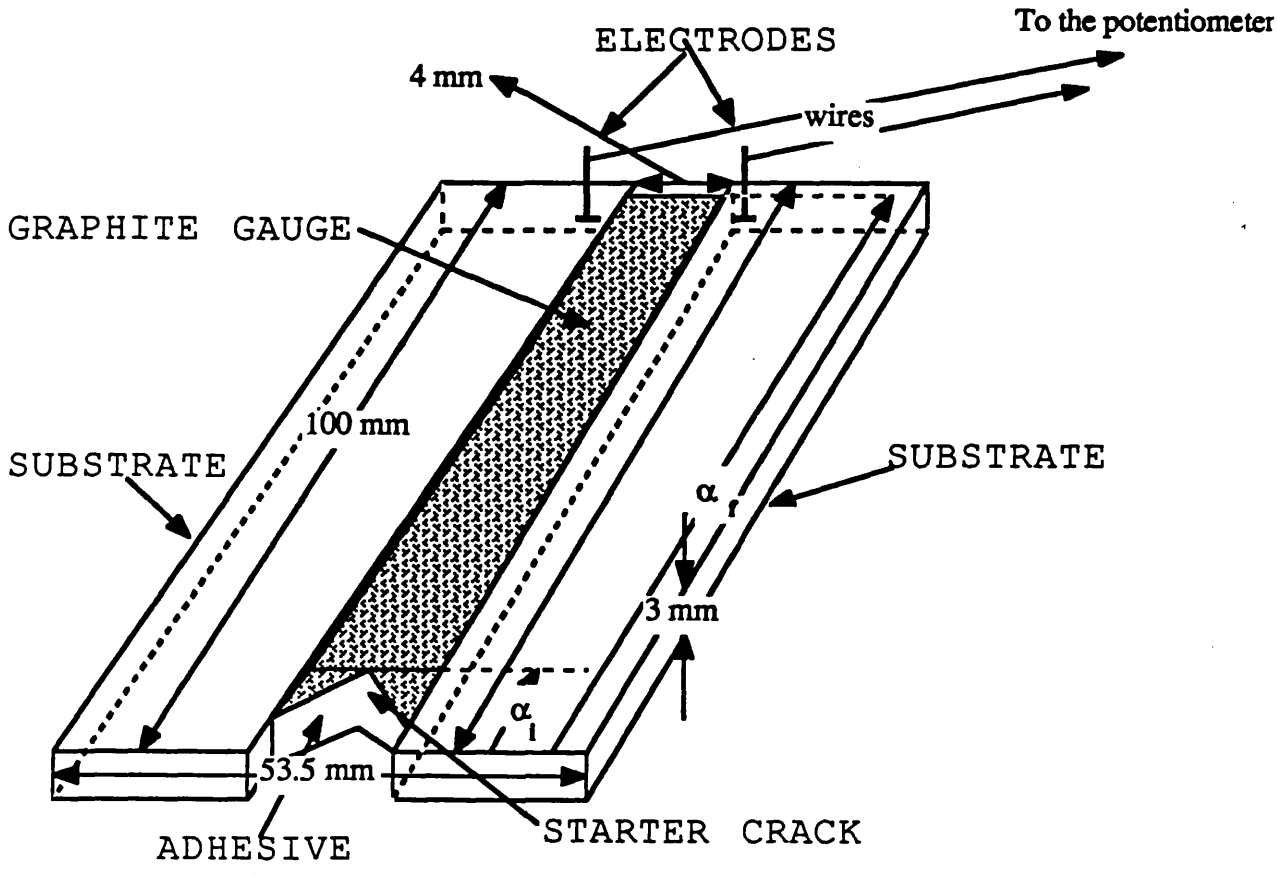


Figure3.1 : Schematic representation of the DT joint geometry and the graphite gauge (not to scale)

α_i = **initial crack length**

α_f = **final crack length (end of graphite)**

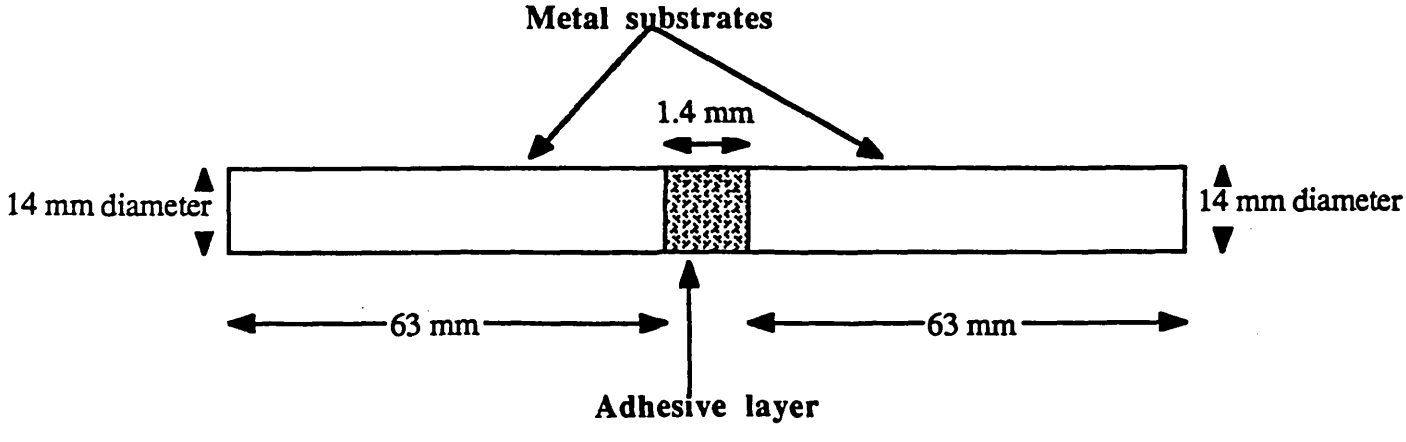


Figure 3.2: Schematic representation of a butt joint

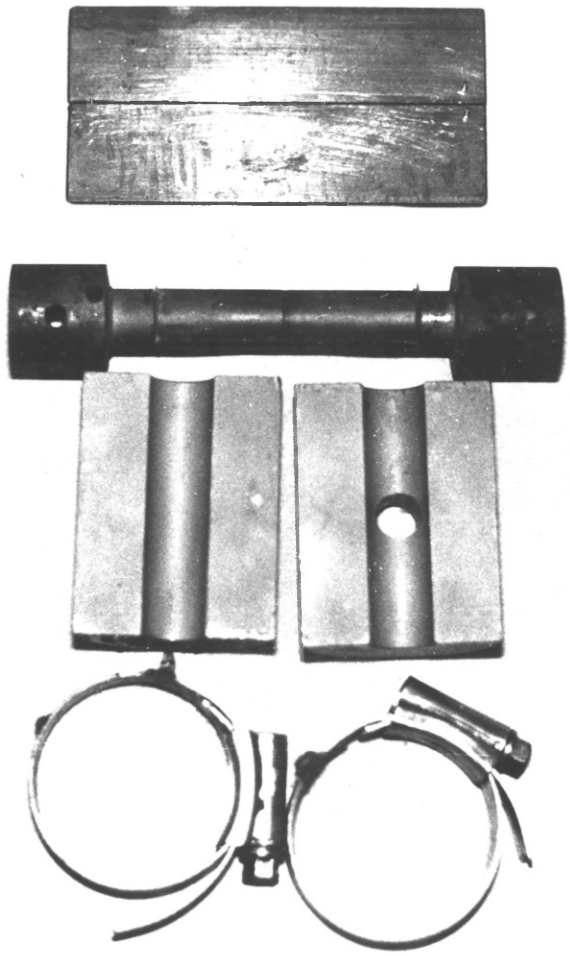


Figure 3.3: A double-torsion joint and a butt joint used in the present investigation together with an aluminium mould used for making the butt joints

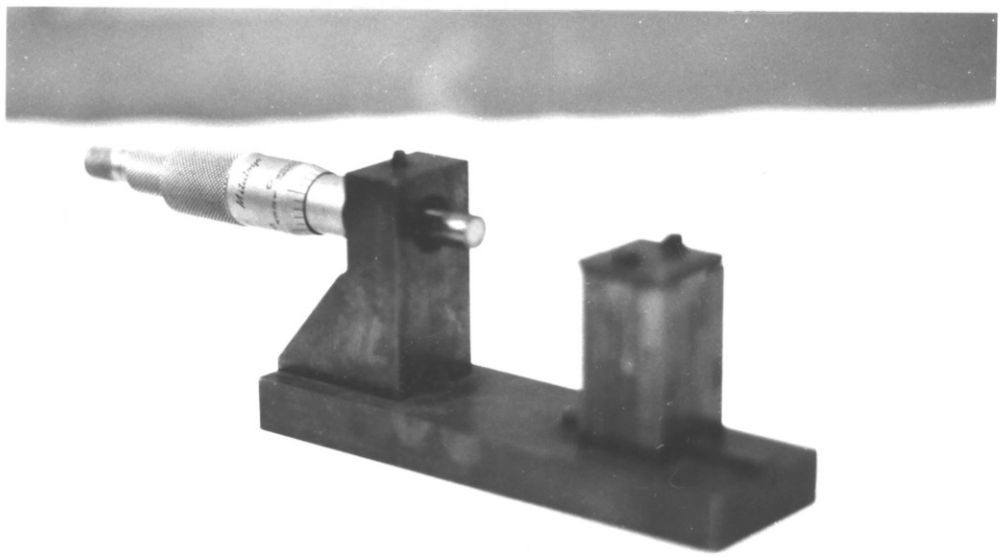


Figure 3.4: Photograph of the displacement gauge calibration arrangement

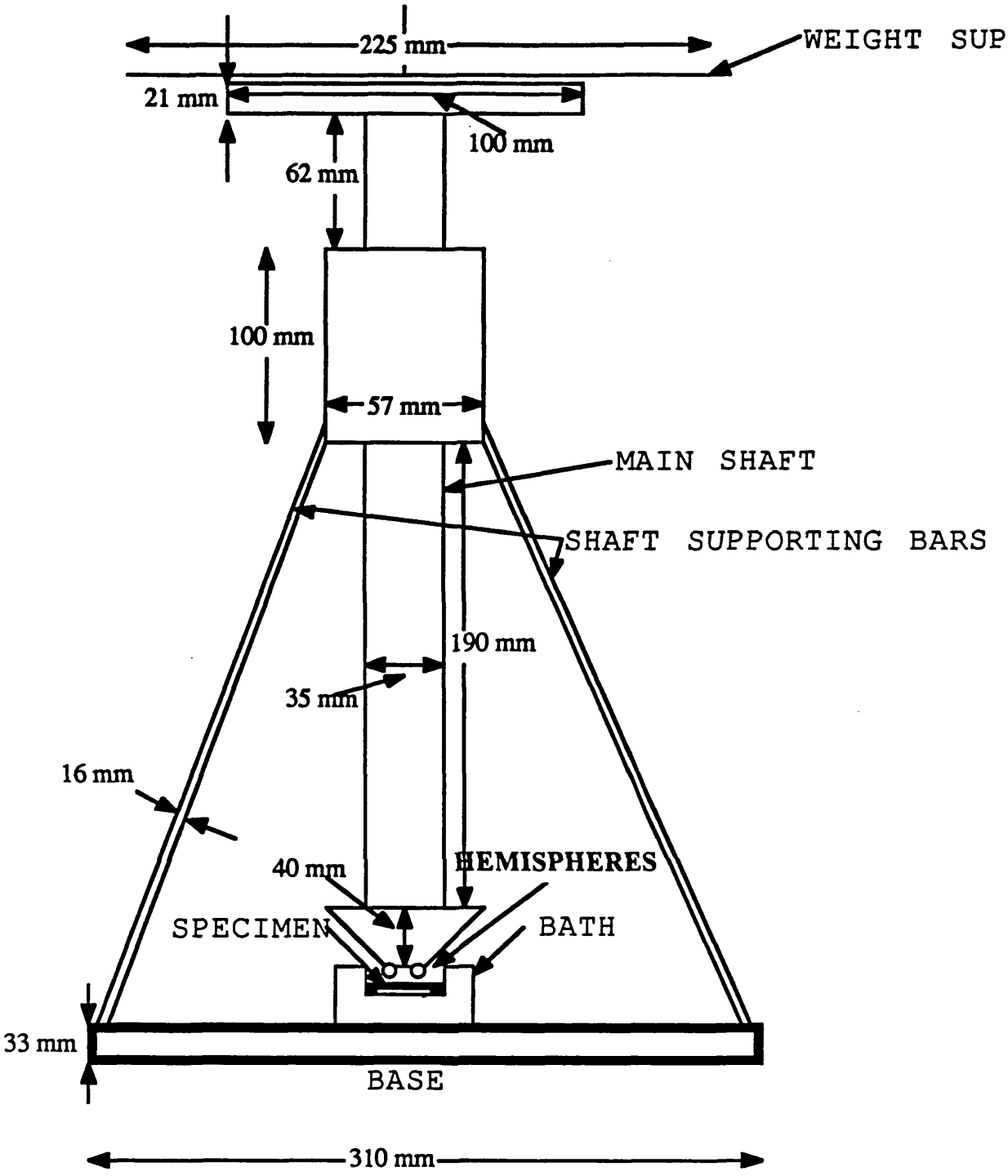


Figure 3.5: Schematic representation of the DT test device (dimensions not to scale)



Figure 3.6: The DT test devices used in the present investigation together with the heater/pump, the potentiometer, and the chart recorders. The perspex baths which contain the water are also shown

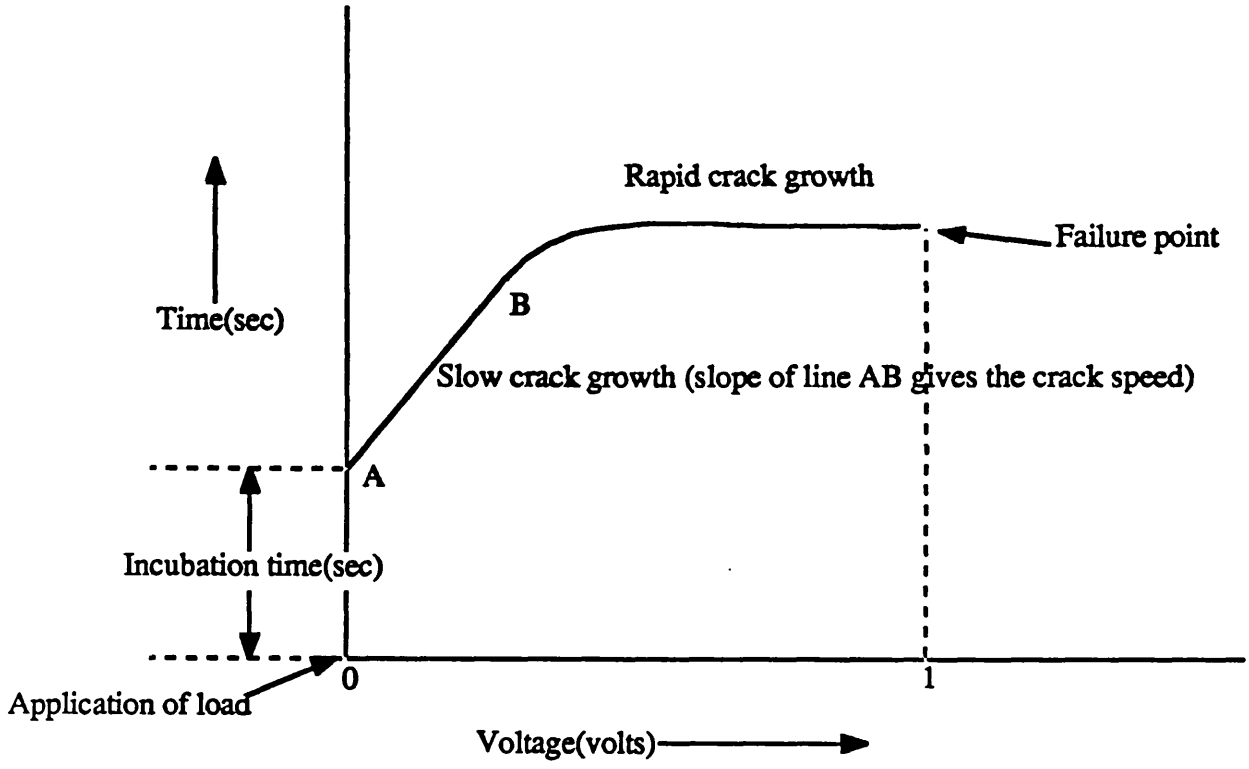


Figure 3.7: Schematic representation of a typical gauge trace on the chart recorder paper. Crack growth was monitored by a potentiometer whose voltage output was proportional to the crack length. Region AB represents slow crack growth where crack speed measurements were taken and OA is the incubation time.

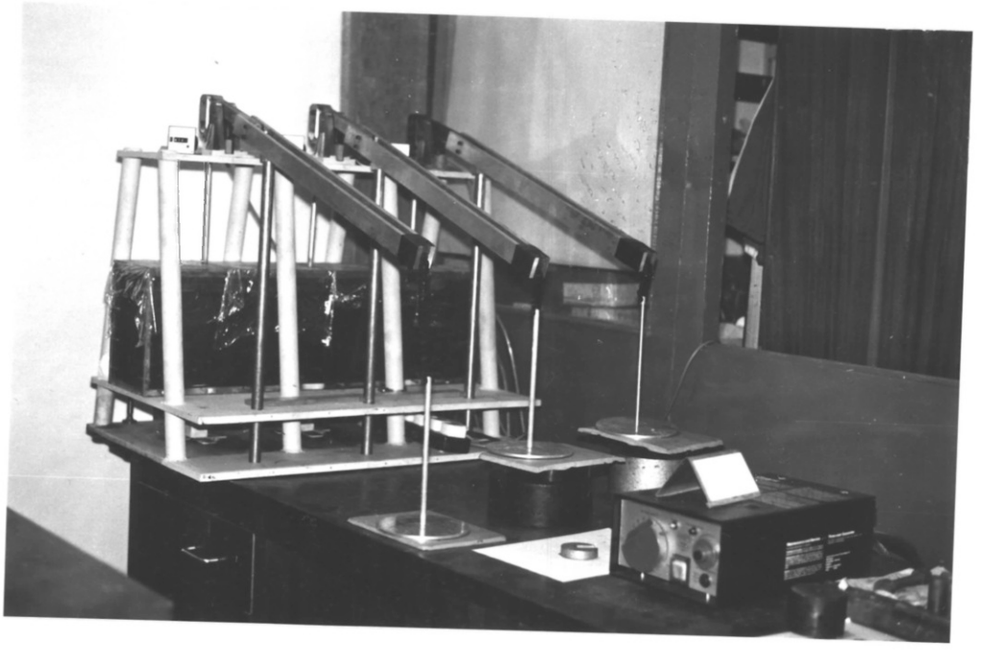


Figure 3.8: The rig used for the tests on the butt joints in the present investigation.The perspex bath containing the water is also shown as well as the heater/pump

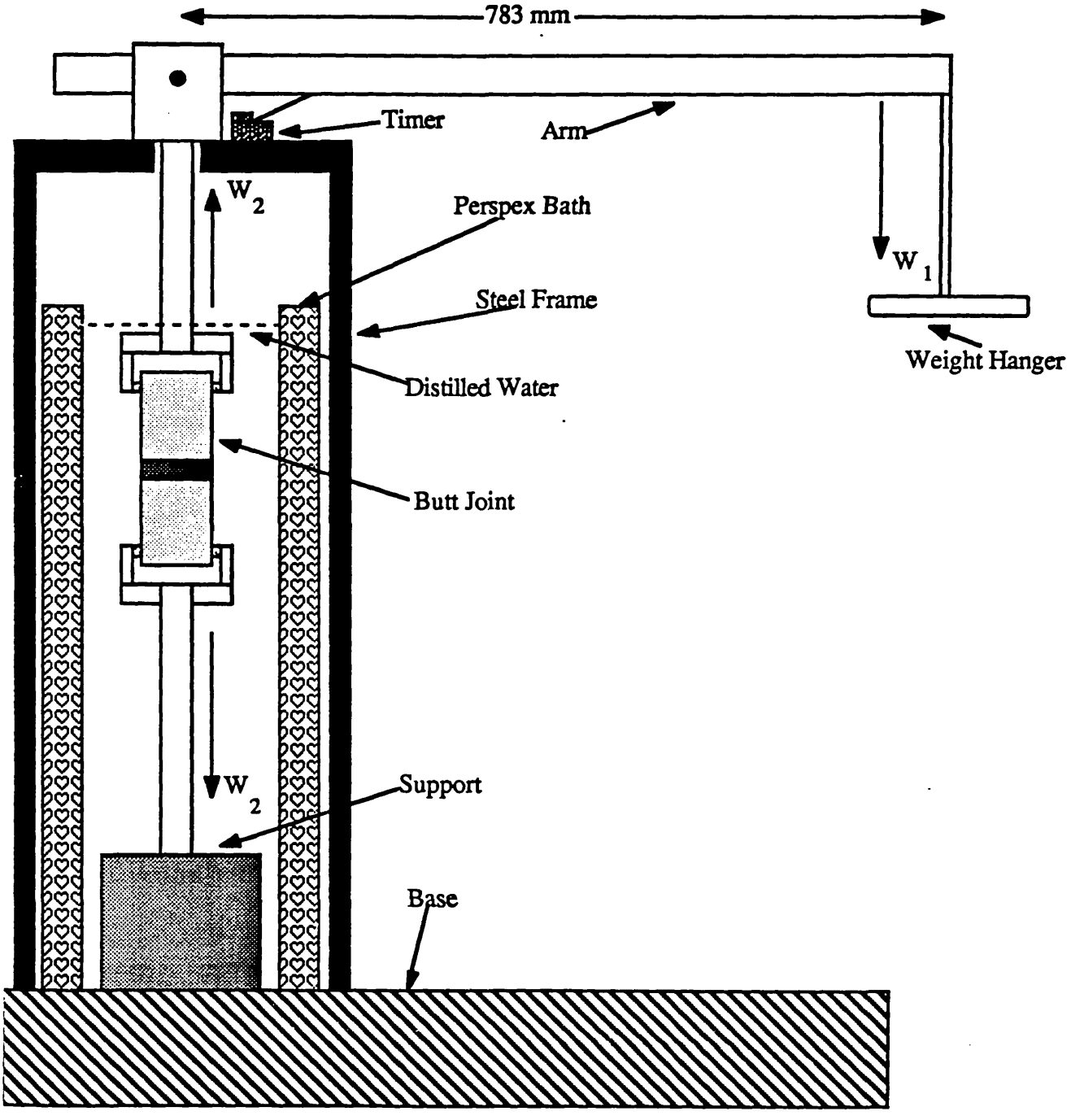


Figure 3.9: A schematic representation of the butt joint ring set up

CHAPTER 4

RESULTS AND DISCUSSIONS: FRACTURE TESTS

4.1 INTRODUCTION

In order to find an epoxide resin that would always give continuous crack propagation, bulk double-torsion specimens were first examined by conducting fracture tests at a constant rate of displacement. If such an epoxide resin system could be found then it was considered that this would make the subsequent durability experiments easier to perform and interpret. Next fracture studies on double-torsion adhesive joints were conducted by using the constant-load test-rigs. These tests were conducted under aqueous conditions, using distilled water, and at temperatures of 25°C, 40°C, and 55°C. The fracture energy and the crack speed were recorded from each fracture test. Adhesive butt joints were also tested in constant-load rigs in order to determine experimentally the fracture time, and so compare these data to theoretical predictions.

4.2 CALCULATION OF FRACTURE MECHANICS PARAMETERS

4.2.1 Introduction

It is generally accepted that engineering stuctures are most likely to fail if flaws are present in the materials. These artificial flaws, which may be induced in the material during service or from fabrication, act as stress concentrators, and therefore, a mathematical analysis of the state of stresses around the flaws could describe and identify the fracture process. This theoretical work is termed "Fracture Mechanics". The basic aim of fracture mechanics is to establish criteria that will explain the fracture process. The most well established criteria are the stress-intensity factor criterion and the energy criterion. The details of these methods were reviewed in Sections 2.1, 2.2, and 2.3 and simply the main equations will be restated here.

4.2.2 Stress-Intensity Factor Criterion

The stress-intensity factor, K, is a parameter which can be used to

describe the stress field around a flaw. When K reaches some critical value, usually denoted by K_c, then a crack may start to propagate along the material and hence fracture may begin to occur. In general, the stress-intesity factor may be calculated from the following equation:

$$K_c=Y\sigma(\alpha)^{1/2} \qquad (4.1)$$

where σ is the applied stress remote from the crack, α is the crack length, and Y is a geometry factor. In the present investigation, the equation used for calculating stress -intensity factors, using double-torsion bulk adhesive samples, was as follows:

$$K_c=Pl_m[1/(1-\upsilon)kwt^3t_n)]^{1/2} \qquad (4.2)$$

where l_m is the moment arm, υ is the Poisson's ratio, k is a parameter that depends on the dimensions of the specimens, w is the specimen width, t is the specimen thickness, and t_n is the specimen effective thickness. The k parameter depends on the ratio (w/2)/t and it was taken to be 0.2832.

4.2.3 Fracture Energy Criterion

Crack propagation may be considered to take place when the work done by an external force and the energy stored in the bulk of the material, are converted into fracture energy, G_c. The fracture energy may be related to the stress-intensity factor with the equation:

$$K_{Ic}^2=EG_c/(1-\upsilon^2) \qquad (4.3)$$

where E is the modulus of the bulk material. For DT joints with a crack at the interface, the modulus of the system should be considered, instead of the modulus of the adhesive.

However, to avoid the complications involved which arise from the arguments discussed in Chapter 3, only the fracture energy concept has been considered for fracture studies of the double-torsion adhesive joints. The equation used in the present investigation to calculate the fracture energy of linear elastic materials was:

$$G_c=(P_c^2/2t)\ (dC/d\alpha) \qquad (4.4)$$

where $dC/d\alpha$ is the change in specimen compliance with crack length α, and fracture load P_c. The value of $dC/d\alpha$ was determined experimentally, thus enabling G_c to be deduced.

4.2.4 Other Equations

The theoretical equation used for calculating specimen compliance was:

$$dC/d\alpha=[(1+\upsilon)/E]\ (2l_m^2/kwt^3) \qquad (4.5)$$

where E was the modulus of the bulk material. In the case of a joint, the modulus of the substrate was used, and k was taken to be 0.3047. The crack speed was calculated from the equation:

$$d\alpha/dt = [d\alpha/dV]\ [dV/dt] = [(\alpha_f - \alpha_i)/(V_f - V_i)]\ [dV/dt] \qquad (4.6)$$

where α_i and α_f are the initial and final crack lengths, and V_i,V_f is the initial and final voltage across the gauge respectively. The value of dV/dt was obtained from the chart recorder readings. The value of the term $(\alpha_f - \alpha_i)$ was taken to be as the actual length of the graphite gauge, and therefore, only the gauge length reading was needed in order to be able to proceed with the calculations.

4.2.5 Compliance Results

The results of the compliance tests performed using the tensile-testing machine, the constant-load test-rig, and bulk DT samples and DT adhesive joints, are presented below.

It will be recalled that the fracture energy, G_c, may be determined from the equation:

$$G_c=(P_c^2/2t)(dC/d\alpha) \qquad (4.4)$$

where $dC/d\alpha$ is change in compliance, C, with crack length α, P_c is the load at fracture, and t is the specimen thickness. However, to use this equation, the value of $dC/d\alpha$ is required. Therefore, compliance tests have been conducted, and the results of the tests are discussed below.

4.2.5.1 Bulk Material

Compliance test results performed using the tensile-testing machine at a constant displacement rate are shown in Figures 4.1 and 4.2. The theoretical values of the change in compliance with crack length were calculated from the equation:

$$dC/d\alpha=[(1+\upsilon)/E]\ (2l_m^2/kwt^3) \qquad (4.7)$$

where E is the modulus of the bulk material, see Kinloch (1985), υ is the Poisson's ratio of the adhesive, l_m is the moment arm, w is the width of the specimen, t is the specimen thickness, and k is a constant that depends on the ratio (w/2)/t, see Table 2.3. Tables 4.1 and 4.2 show the results of the compliance tests performed on the tensile testing machine and on the constant-load test-rig at 25°C. Bulk DT specimens of the same thickness, t, but different effective thicknesses, t_n, were used and the tests were performed under dry conditions. It is evident from the above equation, that the theoretical calculation of $dC/d\alpha$

takes no account for the effective thickness. Since E for the unmodified material is higher than that of the rubber-modified material, the theoretical values of $dC/d\alpha$ for the rubber-modified specimens were found to be greater than those of the unmodified specimens. The same trend was obtained from the experimental values, indicating an agreement between theory and experiment. However, the experimental values of $dC/d\alpha$ for both materials were found to be somewhat larger than the theoretical values. This may be due to the fact that the theoretical equation for calculating $dC/d\alpha$ assumes that plastic deformation of the material does not occur, which is not necessarily the situation in the present tests. Bulk specimens were tested on the constant-load rig-test, and after a period of five to ten days they were removed from the rig and examined. It was found that all specimens had suffered some degree of permanent deformation, and therefore the difference between the theoretical and experimental values may be explained in terms of the material being plastically deformed. The fact that the effective thickness is not included in the theoretical equation might also have led to some errors. However, it was considered that the errors involved were negligible because the V-grooves, which were machined on the specimens, only directed the cracks rather than played any important part in determining the compliance behaviour of the specimens.

Results from the compliance tests, performed on the constant-load rig-test, are shown in Figures 4.3 to 4.6. The tests were performed under dry conditions, and in distilled water at 25°C. In the latter case, the specimens were left into the water for some time before testing, about one hour, in order for the test conditions (for example testing temperature and graphite gauge resistance) to reach a steady-state. The experimental data obtained from the dry tests coincided with that obtained from the tests conducted in water, indicating that the total time of the compliance tests was not sufficient enough for the water at 25°C to have an effect on the static compliance behaviour of the materials. The experimental values were found to be in general a little higher in value than the theoretical ones, again possibly because plastic deformation of the material in the theoretical equation for calculating $dC/d\alpha$ is neglected.

4.2.5.2 Adhesive Joints

Compliance test results performed using either the tensile-testing machine at a constant crosshead speed of 0.5mm/min or the constant-load rig-test, are shown in Figures 4.7, 4.8, and 4.9. The results of tests performed using the rig-test, either dry or in distilled water, are shown in Figure 4.9. The specimens were left in the water baths for about one hour, so that the test conditions were steady when they were tested. As may be seen, the plot of compliance, C (=y/P), against crack length, α, gave a good linear relationship in all cases. The comparison between experimental and theoretical values is shown in Table 4.3. Again the agreement between the experimental and theoretical values is very good, being typically within $\pm 15\%$.

4.2.5.3 Conclusions

The compliance values of both bulk and adhesive joint double-torsion specimens have been measured and the relations between compliance, C, and crack length, α, were all good linear relationships, as expected from the theoretical analyses. Indeed, there is good agreement between the experimentally determined values and the theoretically calculated values. Further, in the case of the adhesive joint DT specimens exposure to distilled water has been found to have little effect on the values of $dC/d\alpha$.

4.3 FRACTURE OF BULK MATERIAL

4.3.1 Introduction

The examination of the different adhesives listed in Table 3.1 to find one that would give a continuous mode of crack propagation, revealed that no epoxide resin could satisfy this requirement. The mode of fracture was mainly stick-slip, and in some cases a combination of stick-slip and continuous crack propagation. Further, the stress-intensity factor values were found to be lower than the values reported in the literature. The results of the tests are discussed in more detail below.

4.3.2 Types of Crack Growth

The literature survey into epoxide resin fracture behaviour suggested that some epoxide resins, when tested in a tensile-testing machine at a constant cross-head speed of 0.5 mm/min and under dry laboratory conditions, may fail due to a crack propagating at a constant rate along the centre groove of the bulk double-torsion specimen. However, the bulk DT epoxide specimens used in the present study all failed by essentially stick/slip type fracture, showing the type of load against displacement curve shown in Figure 2.7 (b). Now from the literature it would have been expected that compositions numbers 1 to 8 listed in Table 3.1 would have failed by continuous, stable crack growth, Figure 2.7 (a). The reason for this difference is probably due to somewhat more crack blunting occuring in the present studies, which promotes stick/slip fracture, as discussed earlier. Small changes in the amount of hardener, curing conditions and test conditions may well lead to the different type of crack propagations observed. Such changes will slightly affect the value of the material's yield stress and this, in turn, controls the type of crack growth observed.

4.3.3 Values of Stress-Intensity Factor

Table 4.4 shows the stress-intensity factor values obtained from the tests performed on the double-torsion bulk adhesives: K_{Ic} is the stress-intensity factor for continuous crack propagation, whereas, K_{Ii} and K_{Ia} are the stress-intensity factors at initiation and arrest points respectively. These values may then be compared with the corresponding values reported in the literature, shown in Table 4.5. As it can be seen, lower values of the stress-intensity factors have been obtained in most cases in the present work than those reported in the literature. Therefore, this work confirms that continuous crack propagation in dry conditions and at room temperature is not the usual mode of crack growth, although it was considered that continuous crack growth would have been more suitable for the present work. At this point it was decided not to pursue further this search for a formulation which consistently exhibits continuous crack-growth but to use

only MY750 epoxide resin with and without rubber (i.e. epoxide resin numbers 1 and 2). These two resin formulations would allow the effect of a rubbery particulate microstructure to be studied.

4.3.4 Effect of Structure

Since the search of an adhesive formulation that would give a continuous type of crack propagation when bulk specimens are fractured under dry conditions had not been successful, the epoxide resin MY750 cured with piperidine, with and without incorporating rubber particles (epoxide resin numbers 1 and 2), was selected as the main adhesive for the investigation on the durability of adhesive joints. This choice of adhesive will allow the effect of the rubber particles to be experimentally investigated when the double-torsion adhesive joints are subjected to static loading in distilled water at different temperatures.

When bulk samples only were examined, the investigation showed that the value of the stress-intensity factor of the rubber-modified bulk adhesive (epoxide resin number 1) was higher than the values of the unmodified epoxide bulk samples (epoxide resin numbers 2,3,4,8). The unmodified MY750 epoxide resin when cured with piperidine is a brittle material, but the formulation with the added rubber cured to give a far tougher material. As shown by A.J. Kinloch et al (1986, 1985) the role of the rubber particles is to increase the extent of localised plastic deformation around the crack tip. Hence, the crack tip will be blunter at the start of crack propagation and this is reflected in a higher value of K_{Ic}, or G_{Ic}, for the rubber-modified epoxide system.

4.3.5 Summary

The search of an adhesive formulation which consistently fractured by a crack propagating at a steady rate through the material of double-torsion bulk adhesive samples when they were tested in a tensile testing machine at a constant cross-head speed of 0.5 mm/min and under dry laboratory conditions was unsuccessful. The results

showed that failure occured mainly in a stick-slip manner, i.e. the crack propagated along the specimen in a non-steady manner. The search was conducted because it was hoped that double-torsion adhesive joints would have fractured in a steady rate, like the bulk adhesives, when they were tested in moisture conditions. This would enable the fracture data, in the form of graphs of fracture energy, G_c, against crack speed and incubation time to be obtained very readily and compared to the dry behaviour of the joints. However, since the results of the tests performed using the bulk adhesive samples were not successful in this respect, it was decided for the remaining part of this work (which involved the fracture of adhesive joints in wet environments at different temperatures and under the application of static external loads) to use the unmodified and rubber-modifed epoxide resins.

The results from the tests carried out in a tensile testing machine using double-torsion bulk adhesive samples, also indicated that the rubber-modified material had a larger stress-intensity factor than the unmodified material, i.e. the epoxide resin alone. This was explained in terms of toughening mechanisms taking place within the material which produced blunting of the crack tip, and therefore an increase in the crack resistance of the rubber-modified material.

It should be noted that the main objective of the present work was to produce environmental fracture data using double-torsion adhesive joints exposed to aqueous environmental conditions at different test temperatures and under the application of external static loads, without the use of expensive equipment, such as tensile testing machines. With the choice of the above adhesive system, it was hoped that the mode of fracture would change from stick-slip in the dry tests to continuous when the joints were exposed to distilled water. This did indeed occur and hence the investigations on the double-torsion adhesive joints were successful, and the results are therefore presented and discussed below.

4.4 FRACTURE OF ADHESIVE JOINTS

4.4.1 Introduction

Fracture tests on double-torsion and butt adhesive joints under dry and environmental conditions have been conducted. The joints consisted of mild steel substrates bonded with either the unmodified or the rubber-modified epoxide adhesive. A constant-load test-rig and a tensile- testing machine have been used. The dry tests were performed in the tensile-testing machine at 25°C, 40°C, and 55°C, whereas, the constant-load test-rig was used for tests in distilled water at the same temperatures. The experimental fracture data was then used to assess the effect of the rubber particles on the double-torsion adhesive joints and to attempt to predict the fracture time of the adhesive butt joints.

4.4.2 Constant Displacement Rate Tests

The results from the tests performed under dry conditions using a tensile -testing machine at a constant cross-head speed of 0.5 mm/min are shown in Figure 4.10. The data shows the values of the adhesive fracture energy, G_c, and suggests that the fracture energy of the rubber-modified and unmodified DT joints did not significantly increase with temperature, but remained essentially constant over the temperature range of 25°C to 55°C. The data in Figure 4.10 also demonstrates that the rubber-modified joints have higher fracture toughnesses than the unmodified joints when tested under dry conditions, in agreement with the earlier discussions.

4.4.3 Effect of Test Temperature

The dry fracture energy of the double-torsion adhesive joints has been found to be independent of the test temperature according to the data in Figure 4.10. Since the glass transition temperature of the epoxide adhesive used in the present investigation is about 100°C then, it may be expected that, an increase in temperature from 25°C to 55°C should not significantly affect the properties of the double-torsion adhesive joints. The

data in Figure 4.10 has therefore been found to confirm this.

4.4.4 Effect of Structure

The data in Figure 4.10 clearly demonstrates the effect of the rubber particles on the adhesive, since the unmodified adhesive joints were found to have lower values of the fracture energy, G_c, than the rubber-modified joints.

4.4.5 Constant Load Tests

Rubber-modified and unmodified double-torsion adhesive joints were tested in distilled water at 25°C, 40°C, and 55°C, using the constant-load rigs. Different loads were applied to the specimens and the data from the experimental work are shown in Figures 4.11 to 4.26. The data in these Figures are presented as plots in logarithmic form of the joint fracture energy, G_c, against crack speed, $d\alpha/dt$, or incubation time. Interfacial failure, as assessed by visual examination, was observed to occur in all the joints tested.

It should be noted that the test reveals the presence of an incubation time, during which a new, apparently interfacial, crack growth developed. The rate of growth of this newly formed crack could be readily distinguished and measured.

4.4.5.1 Effect of Environment

Visual examination of the fracture surfaces of the double-torsion joints exposed to distilled water at 25°C, 40°C, and 55°C, and to externally applied stresses, showed that failure was always very close to the substrate surface. The same failure path was observed with the double-torsion joints fractured under dry conditions at 25°C, 40°C, and 55°C, in the tensile-testing machine. These results therefore indicate that the substrate/ adhesive interface was the weakest region in all the double-torsion joints tested, and that the water first attacked this region rather than the adhesive itself.

4.4.5.2 Incubation Time

Figures 4.11 to 4.16 display the fracture data collected from the tests performed using the double-torsion joints at various temperatures, as logarithmic plots of the fracture energy, G_c, against incubation time. Incubation time has been defined as the time interval from the moment of application of the load to a double-torsion joint immersed in distilled water until the moment when a crack starts to propagate along the interface leading to the fracture of the joint. The data was fitted by straight lines indicating that a linear relationship exists between the fracture energy and the incubation time on logarithmic scales. The very low scatter obtained from these experiments is particularly noteworthy.

Figure 4.17 shows a comparison of the fracture energy, G_c, against incubation time data between the unmodified double-torsion joints immersed in distilled water at 25°C, 40°C, and 55°C. The data in this Figure suggests that the incubation time of the joints increased as the temperature of the distilled water was increased. The durability of the unmodified double-torsion adhesive joints has therefore been found to increase with increasing the temperature of the distilled water from 25°C to 55°C.

Figure 4.18 shows a comparison of the fracture energy against incubation time data between the rubber-modified double-torsion joints immersed in distilled water at 25°C, 40°C, and 55°C. The data suggests that, raising the temperature of the distilled water from 25°C to 40°C had no effect on the incubation time. However, as the temperature was increased to 55°C, the incubation time was found to decrease. This may suggest that exposure of the rubber-modified double-torsion adhesive joints to distilled water at 55°C reduces the durability of the joints.

4.4.5.3 Crack Speed

Figures 4.19 to 4.24 display the fracture data collected from the tests performed using the double-torsion joints at various temperatures, as logarithmic plots of the fracture energy, G_c, against crack speed. The data could be fitted by straight lines

indicating that the fracture energy was linearly related to crack speed on logarithmic scales. The data in these Figures also suggests that, the crack speed of the rubber-modified and unmodified double-torsion adhesive joints increased as the applied fracture energy, G_c, was increased in value.

Figure 4.25 shows a comparison of the fracture energy against crack speed data for the rubber-modified double-torsion adhesive joints immersed in distilled water at 25°C, 40°C, and 55°C. The data suggests that the crack speed decreased with increasing test temperature. The same phenomenon was observed with the unmodified double-torsion joints, as Figure 4.26 shows: the crack growth was found to decrease as the temperature of the distilled water was increased.

4.4.5.4 Effect of Structure

In order to assess the effect of the rubber particles on the performance of the double-torsion adhesive joints used in the present investigation Figures 4.27 to 4.32 have been plotted. These Figures show the variation of the normalised fracture energy of the double-torsion adhesive joints, G_c(in water)/ G_c(dry), with logarithmic crack speed, $\dot{\alpha}$, or logarithmic incubation time.

The data in Figures 4.27 to 4.29 indicates, when compared on a normalised basis, that the unmodified double-torsion adhesive joints were more resistant to crack propagation than the rubber-modified joints when they were exposed to distilled water at 25°C, 40°C, and 55°C, and subjected to external applied stresses. At 55°C, the unmodified double-torsion adhesive joints were found to become much more tougher in resisting crack propagation than the rubber-modified joints at the same temperature.

The data in Figures 4.30 to 4.32 indicates that the unmodified double-torsion adhesive joints were more durable than the rubber-modified joints when they were exposed to distilled water at 25°C, 40°C, and 55°C, and subjected to external stresses. At 55°C, the durability of the unmodified double-torsion joints was found to be far higher than that of the rubber-modified joints at the same temperature.

4.4.5.5 Conclusions

The rubber-modified double-torsion adhesive joints have been found to have higher fracture energies than those of the unmodified joints when they were tested in the tensile-testing machine under dry conditions at 25°C, 40°C, and 55°C. It was therefore suggested that the rubber particles had increased the dry toughness of the adhesive of the DT joints. The dry fracture energy of the DT joints was found to be independent of the test temperature for both types of joints examined.

The toughness of the rubber-modified and unmodified double-torsion adhesive joints exposed to distilled water at 25°C, 40°C, and 55°C, was found to increase with increasing the test temperature. A comparison between the two types of joints used, has shown that, the unmodified double-torsion joints were tougher than the rubber-modified joints at the above temperatures. The difference in joint toughness was found to be largest at 55°C. The incubation time of the rubber-modified double-torsion adhesive joints has been found to decrease with increasing the test temperature. For the unmodified double-torsion joints, an increase in incubation time with temperature has been observed. A comparison between the two types of adhesive joints used, has shown that, the unmodified double- torsion joints were more durable than the rubber-modified joints with increasing the test temperature. The difference in joint durability was found to be larger at 55°C.

4.5 ADHESIVE BUTT JOINT TESTS

Rubber-modified and unmodified adhesive butt joints have been fractured in distilled water at 25°C and under the application of external loads. The results of the tests are discussed below.

4.5.1 Introduction

The new test method for assessing the durability and obtaining fracture data of double-torsion (DT) adhesive joints exposed to moisture and stresses has been

found to be reproducible and therefore applicable to life prediction studies. The next step is to attempt to predict the service life of adhesive joints using the fracture data obtained from this new test method. Therefore, adhesive butt joints have been tested under the application of stresses and moisture exposure, and the results of the fracture tests are discussed below.

4.5.2 Rubber-modified Epoxide Data

The data collected from the tests performed using the rubber-modified butt adhesive joints in distilled water at 25°C is shown in Figure 4.33. This Figure displays the fracture data as a plot of the butt joint tensile stress against the measured fracture time. The data suggests that there may be a value of tensile stress beyond which no fracture of the rubber-modified butt joints can occur. This will be discussed later in Chapter 7.

4.5.3 Unmodified Epoxide Data

The data collected from the tests performed using the unmodified butt adhesive joints in distilled water at 25°C is shown in Figure 4.34. This Figure displays the fracture data as a plot of the butt joint tensile stress against the fracture time. The same suggestion as before can be made, that there may be a value of tensile stress beyond which no fracture of the unmodified butt adhesive joints can occur.

4.5.4 Comparison of Butt Joints Fracture Data

A comparison between the data in Figures 4.33 and 4.34 is shown in Figure 4.35. The data in this Figure suggests that the unmodified butt adhesive joints were more durable than the rubber-modified joints.

4.5.5 Butt Joints Fracture Surface

Figure 4.36 shows a schematic representation of the fracture surfaces of

a typical butt adhesive joint tested in distilled water at 25°C and under the application of external stresses. Two regions can be visually distinguished: an interfacial region and a region of cohesive-in-adhesive failure. The failure path was very close to the substrate surface in the apparently interfacial region and this process might have been accompanied by a slow crack growth.

4.6 Conclusions

The new test method involving using double-torsion (DT) adhesive joints to assess the durability of joints exposed to distilled water has been very successful. From the stressed DT joint tests in distilled water at different temperatures two separate processes have been identified. Firstly, an incubation time, which is the time taken for a new apparently interfacial crack to develop, may be measured. Secondly, the subsequent rate of growth of this new interfacial crack may be measured. Such measurements have been undertaken for both an unmodified and rubber-modified epoxide adhesives as a function of test temperature of the aqueous environment.

Also, adhesive butt joints have been tested and data of applied tensile stress against time-to-failure measured.

The next Chapter will consider the diffusion of water into the adhesives used for the above work. Chapter 6 will then discuss the locus of failure and Chapter 7 will suggest mechanisms and mechanics of environmental failure.

Table 4.1: Comparison between theoretical and experimental values of dC/dα from tests performed using unmodified and rubber-modified bulk double-torsion (DT) samples on a tensile-testing machine at a cross-head speed of 0.5 mm/min and under dry conditions. The theoretical values of dC/dα were calculated from the equation:

$dC/d\alpha=[(1+\upsilon)/E]\ (2l_m^2/kwt^3)$

where E is the modulus of the bulk material, υ is the Poisson's ratio, l_m is the moment arm, w is the width of the DT specimens, t is the specimen thickness, and k is a constant that depends on the ratio (w/2)/t.

Material	Theoretical(dC/dα)	Experimental(dC/dα)	Effective thickness
Unmodified	$0.133x10^{-3}N^{-1}$	$0.156x10^{-3}N^{-1}$	3.36 mm
Rubber-modified	$0.157x10^{-3}N^{-1}$	$0.1725x10^{-3}N^{-1}$	3.18 mm

Table 4.2: Comparison between theoretical and experimental values of dC/dα from tests performed using unmodified and rubber-modified bulk double-torsion (DT) samples on the constant-load rig-test and under dry and wet, i.e. in distilled water at 25°C, conditions. The theoretical values of dC/dα were calculated from the equation:

$dC/d\alpha=[(1+\upsilon)/E]\ (2l_m^2/kwt^3)$

where E is the modulus of the bulk material, υ is the Poisson's ratio, l_m is the moment arm, w is the width of the DT specimens, t is the specimen thickness, and k is a constant that depends on the ratio (w/2)/t.

Material	Theoretical(dC/dα)	Experimental(dC/dα)	Effective thickness
Unmodified	$0.133x10^{-3}N^{-1}$	$0.134x10^{-3}N^{-1}$	3.00 mm
Rubber-modified	$0.157x10^{-3}N^{-1}$	$0.135x10^{-3}N^{-1}$	3.00 mm
Unmodified	$0.133x10^{-3}N^{-1}$	$0.195x10^{-3}N^{-1}$	2.10 mm
Rubber-modified	$0.157x10^{-3}N^{-1}$	$0.166x10^{-3}N^{-1}$(Dry)	2.30 mm

Table 4.3: Comparison between theoretical and experimental values of dC/dα from tests performed using unmodified and rubber-modified double-torsion (DT) joints on the constant-load rig-test and on the tensile-testing machine, and under dry and wet, i.e. in distilled water at 25°C, conditions. The theoretical values of dC/dα were calculated from the equation:

$dC/d\alpha=[(1+\upsilon)/E_S]\ (2l_m^2/kwt^3)$

where E_S is the modulus of the substrate material, υ is the Poisson's ratio, l_m is the moment arm, w is the width of the DT specimens, t is the specimen thickness, and k is a constant that depends on the ratio (w/2)/t.

Material	Theoretical(dC/dα)	Experimental(dC/dα)	Layer thickness
Unmodified	$0.015x10^{-3}N^{-1}$	$0.021x10^{-3}N^{-1}$(Dry)	3.00 mm
Rubber-modified	$0.015x10^{-3}N^{-1}$	$0.0156x10^{-3}N^{-1}$(Dry)	3.00 mm
Rubber-modified	$0.015x10^{-3}N^{-1}$	$0.0187x10^{-3}N^{-1}$(Wet)	3.00 mm
Rubber-modified	$0.015x10^{-3}N^{-1}$	$0.0174x10^{-3}N^{-1}$(Dry)	3.00 mm

Table 4.4: Fracture behaviour of epoxide resins studied in the present investigation. The tests on the bulk samples were performed using a tensile-testing machine at a crosshead speed of 0.5 mm/min under dry laboratory conditions. K_{Ii}, K_{Ia}, and K_I are the critical stress intensity factors at initiation and arest points and for continuous crack propagation respectively. Values of the critical stress intensity factor were calculated using the equation:

$K^2_{IC}=P^2_C\, l^2_m\, [1/(1-\upsilon)kwt^3 t_n]$

where the symbols are explained in the text (the epoxide resin numbers are listed in Table 3.1).

Number	Fracture mode	$K_I(MNm^{-3/2})$	$K_{Ii}(MNm^{-3/2})$	$K_{Ia}(MNm^{-3/2})$
1	stick-slip/continuous	2.10	0.80	2.00
2		Rapid Failure		
3	stick-slip	1.20	0.70	
4	stick-slip	0.74	0.68	
5	stick-slip/continuous	2.17	1.86	2.00
6	stick-slip/continuous	2.67	2.48	2.30
7		Rapid Failure		
8	stick-slip	0.98	0.82	

Table 4.5: Fracture behaviour of epoxy resins reported in the literature.

Number	Fracture mode	Reference	$K_{IC}(MNm^{-3/2})$
1	continuous	(1)	2.24
2	continuous	(1)	0.73
3	continuous	(2)	-
4	continuous	(2)	-
5	continuous	(3)	2.78 (in distilled water)
6	continuous	(3)	-
7	continuous	(3)	-
8	continuous	(4)	0.48

Notes:

(a) Reference numbers: (1) A.J.Kinloch, D.Maxwell and R.J.Young (1985)

(2) D.C.Phillips and J.M.Scott (1974)

(3) R.J.Young and P.W.R.Beaumont (1975)

(4) R.A.Gledhill and A.J.Kinloch, S.Yamini and R.J.Young (1978)

(b) "-" Values of K_{Ic} not reported in literature

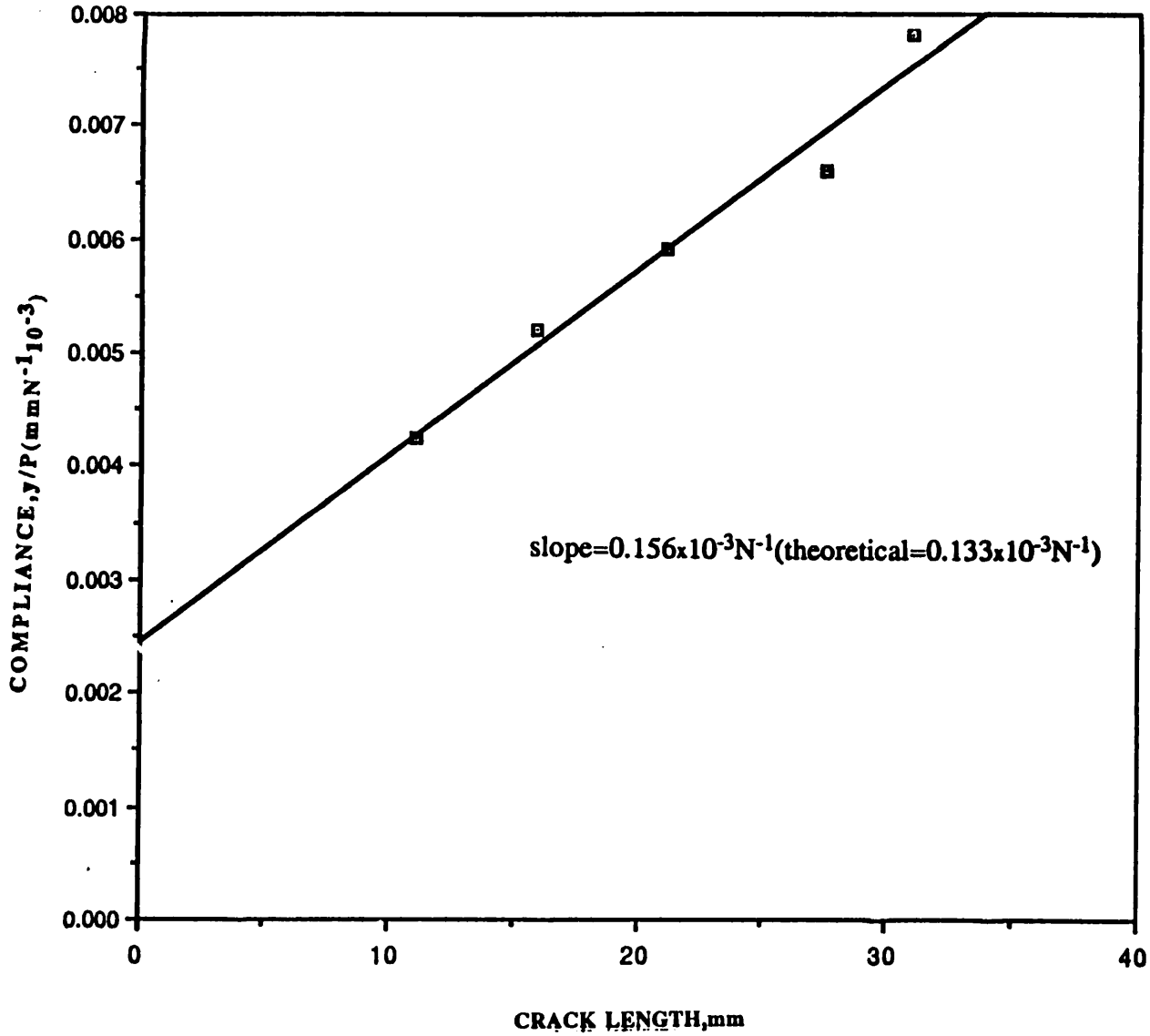


Figure 4.1: Compliance test results performed on the tensile-testing machine using unmodified epoxy resin bulk specimens of effective thickness t_n=3.36 mm. The tests were performed under dry laboratory conditions:

y=specimen displacement

P=instantaneous load

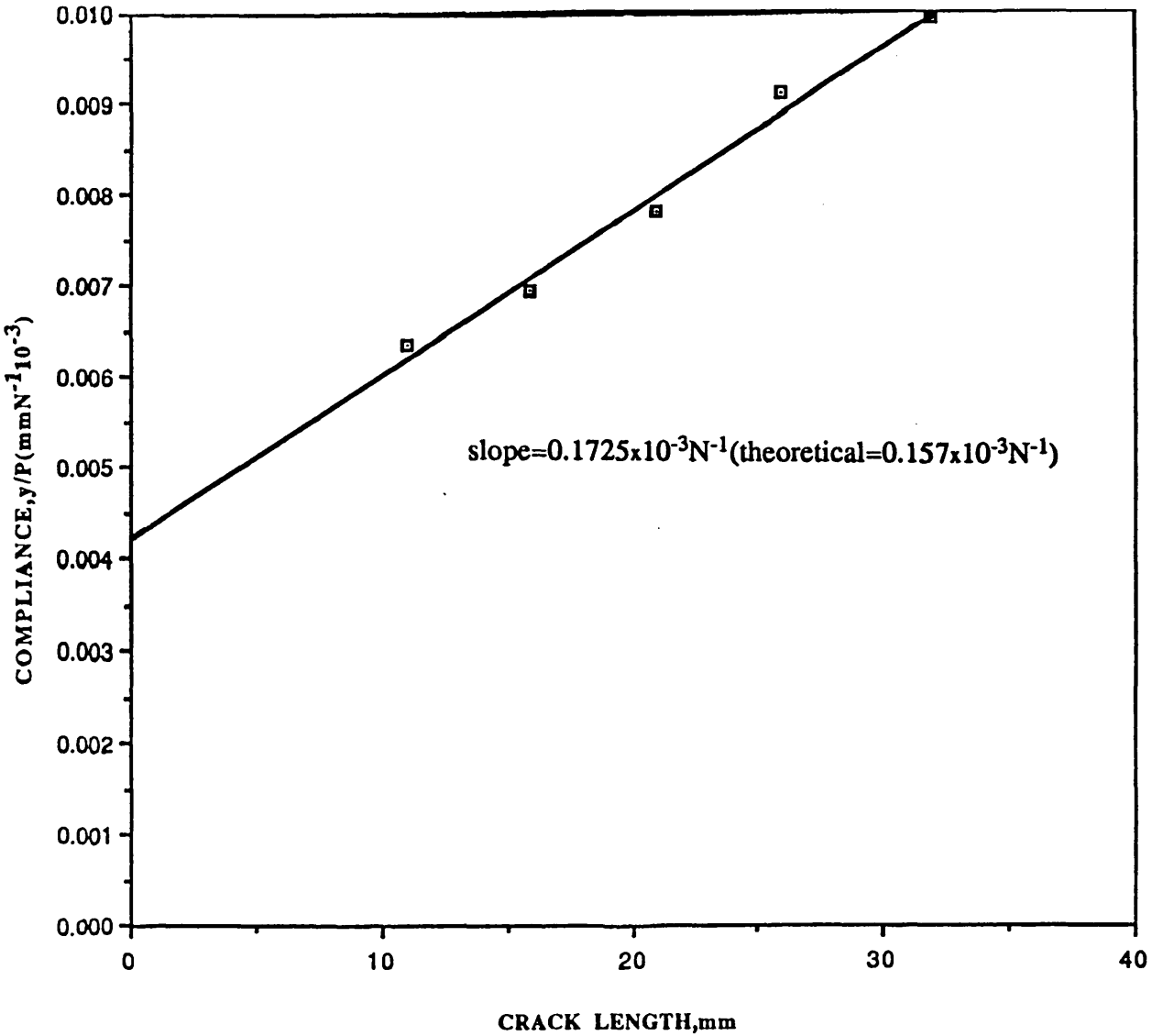


Figure 4.2: Compliance test results performed on the tensile-testing machine using rubber modified epoxy resin bulk specimens of effective thickness t_n=3.18 mm. The tests were performed under dry laboratory conditions:

y=specimen displacement

P=instantaneous load

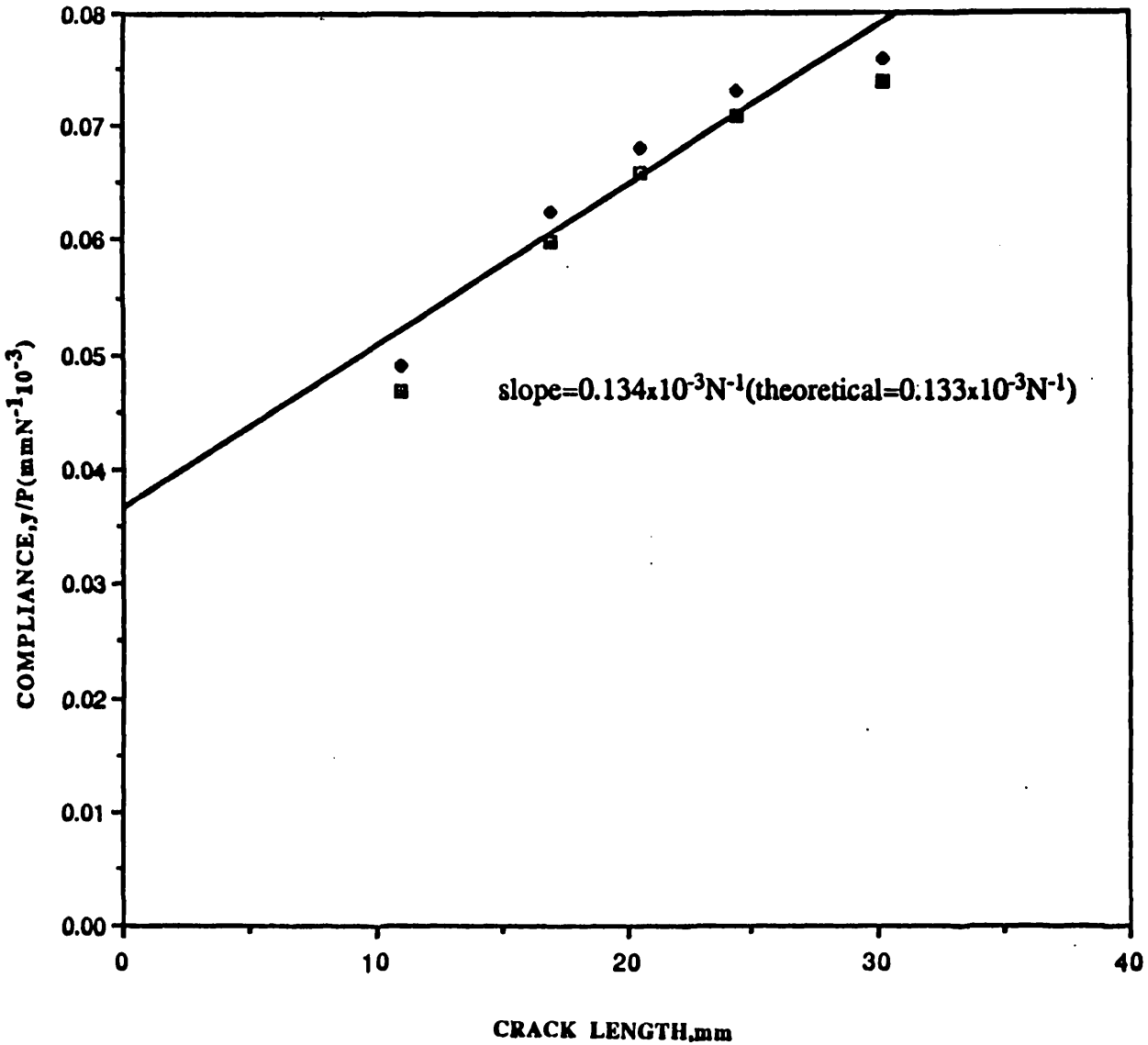


Figure 4.3: Compliance test results performed on the constant-load test-rig using unmodified epoxy resin bulk specimens of effective thickness t_n=3.00 mm. The tests were performed under dry (white points) and wet (i.e. in distilled water at room temperature) conditions (black points):

y=specimen displacement

P=instantaneous load

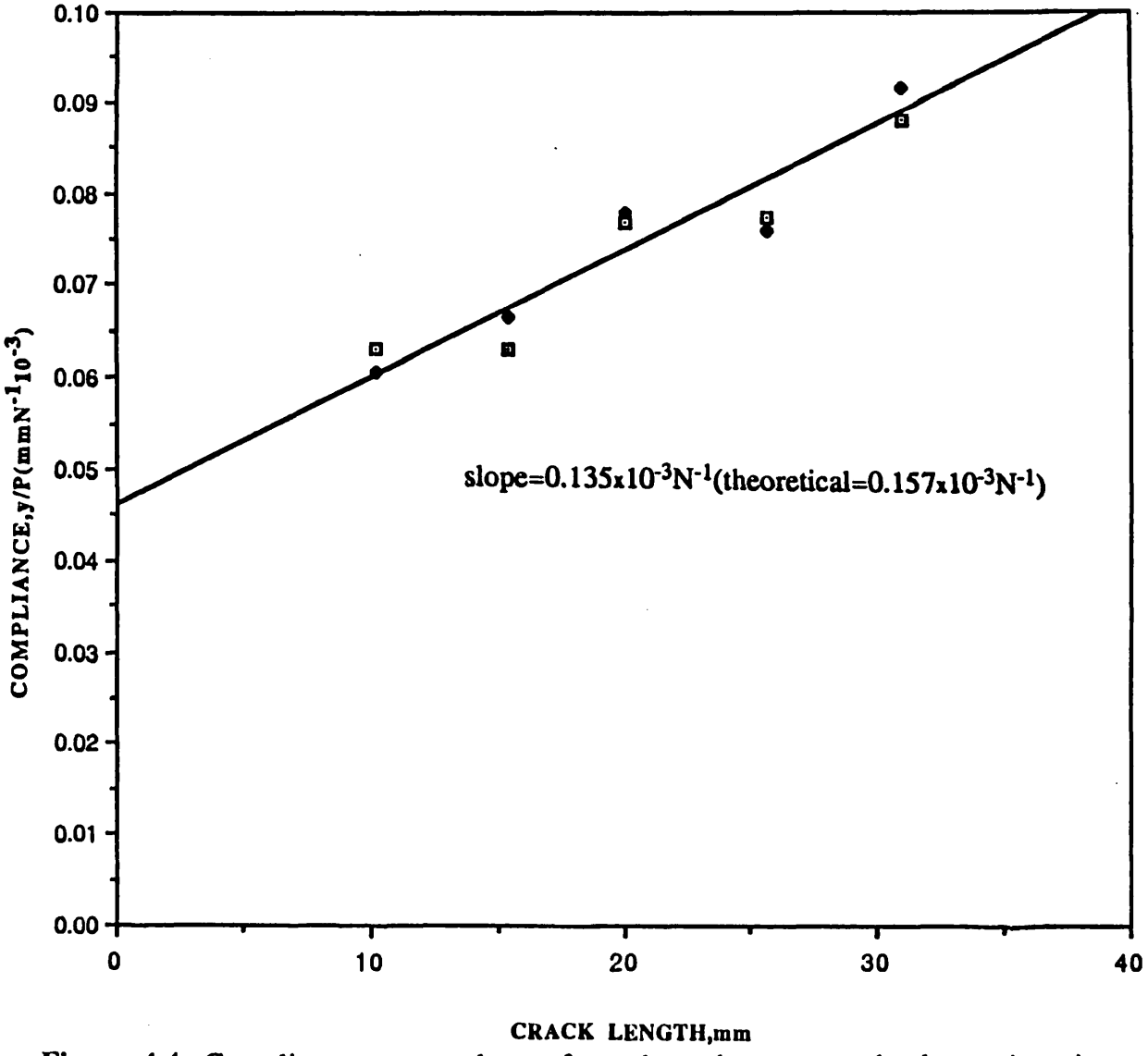


Figure 4.4: Compliance test results performed on the constant-load test-rig using rubber modified epoxy resin bulk specimens of effective thickness t_n=3.00 mm. The tests were performed under dry (white points) and wet (i.e. in distilled water at room temperature) conditions (black points):

y=specimen displacement

P=instantaneous load

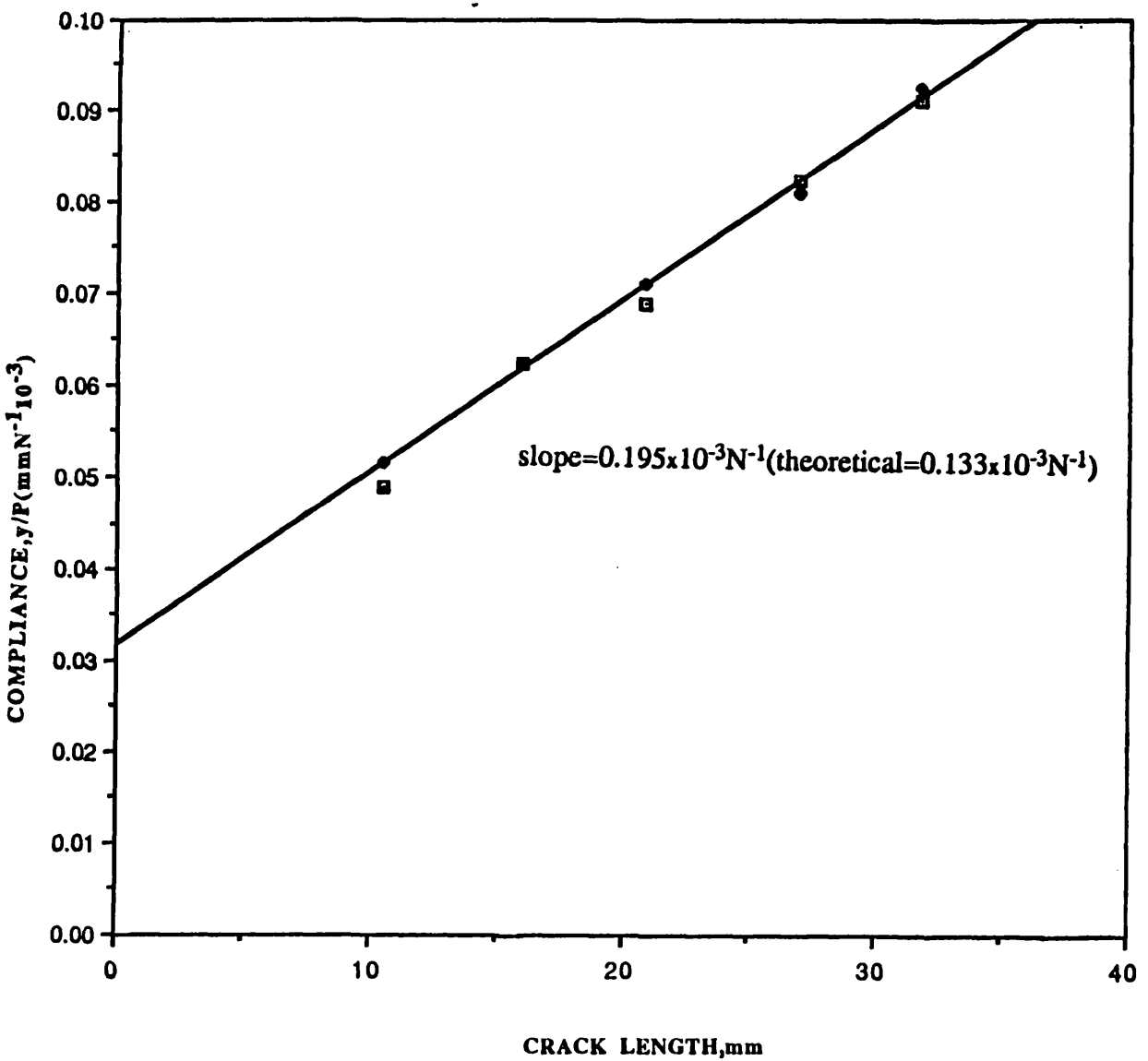


Figure 4.5: Compliance test results performed on the constant-load test-rig using unmodified epoxy resin bulk specimens of effective thickness t_n=2.10 mm. The tests were performed under dry (white points) and wet (i.e. in distilled water at room temperature) conditions (black points):

y=specimen displacement

P=instantaneous load

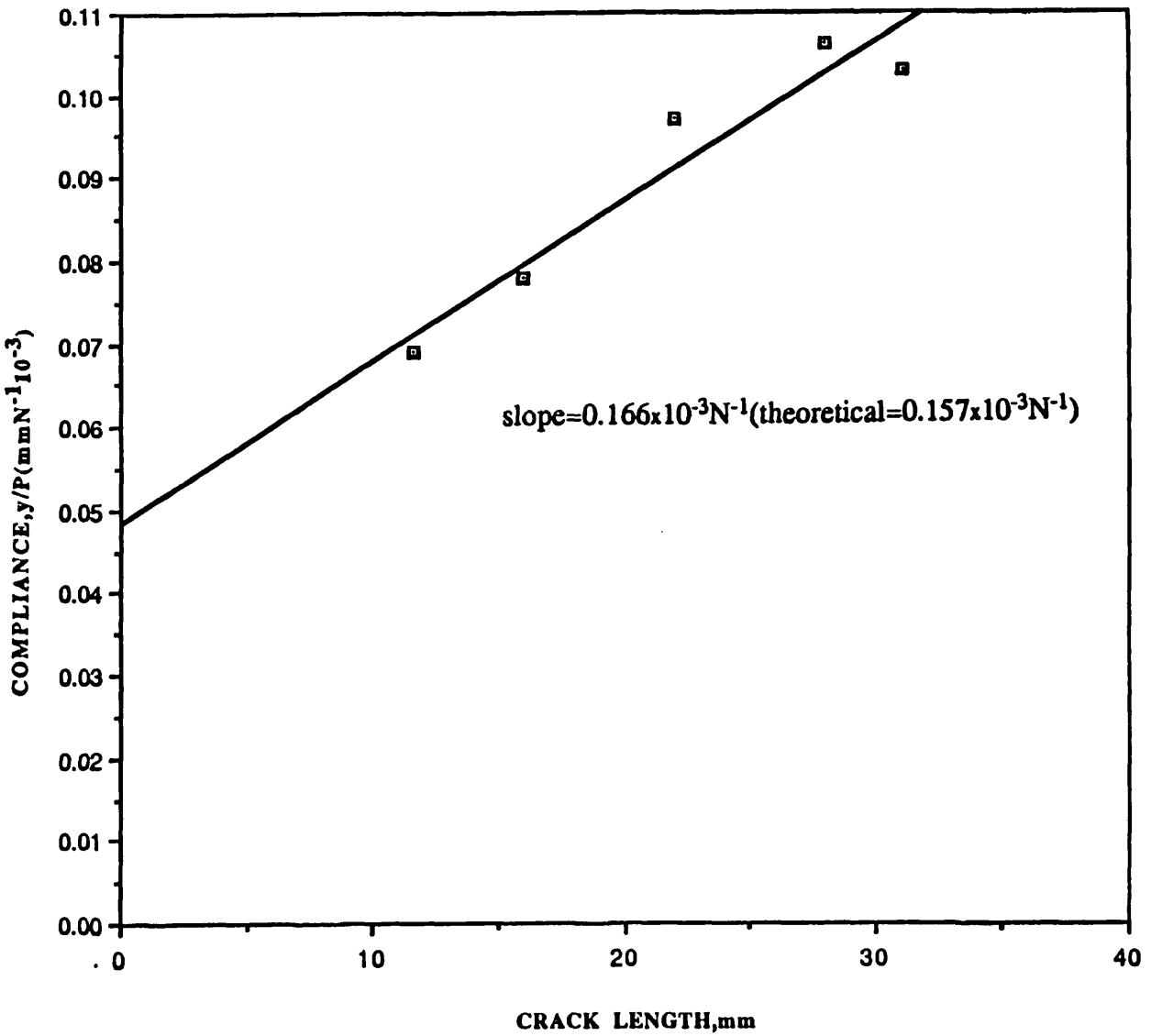


Figure 4.6: Compliance test results performed on the constant-load test-rig using rubber modified epoxy resin bulk specimens of effective thickness t_n=2.30 mm. The tests were performed under dry laboratory conditions:

y=specimen displacement

P=instantaneous load

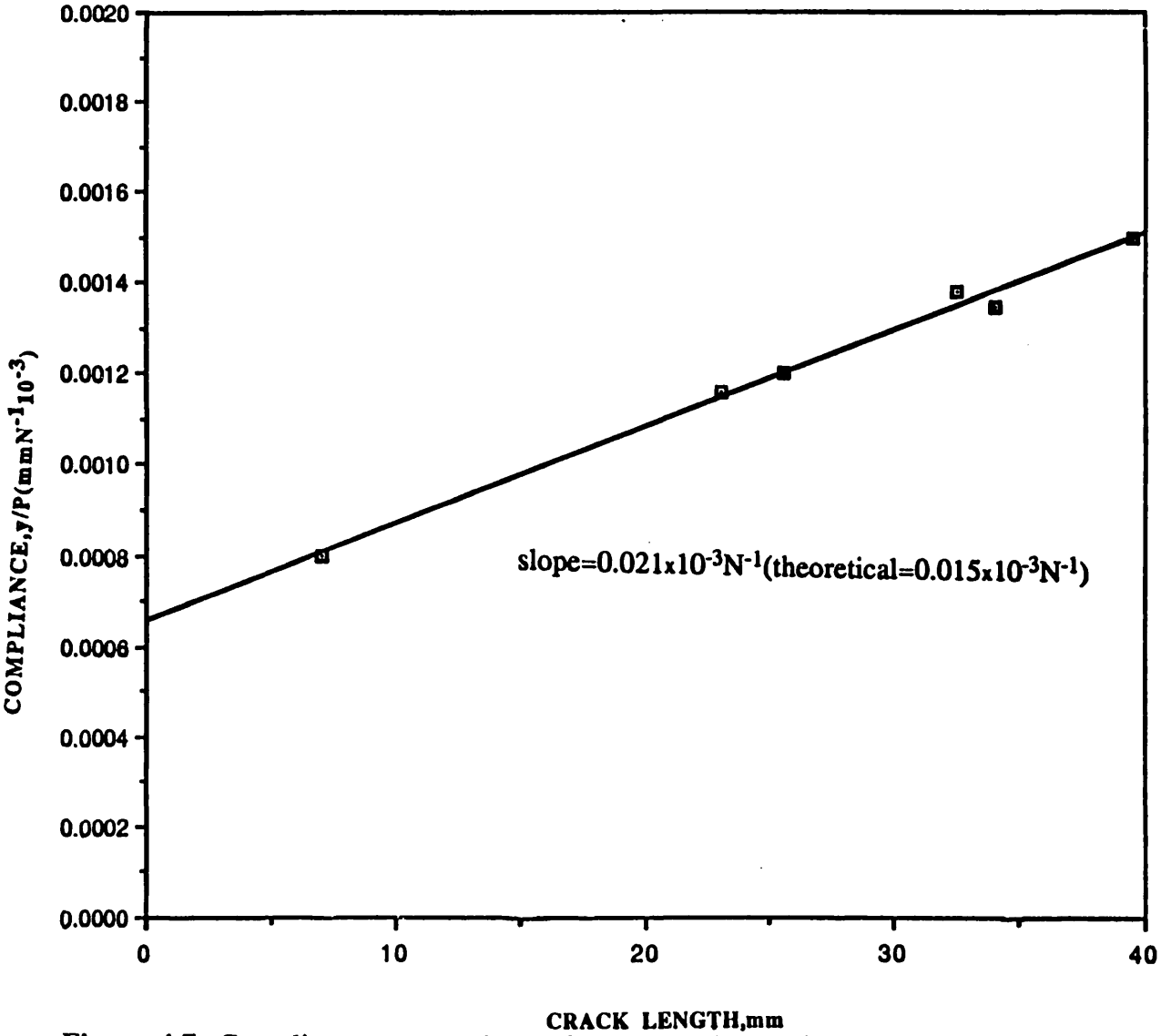


Figure 4.7: Compliance test results performed on the tensile-testing machine using rubber modified epoxy resin DT joints of thickness t=3.00 mm. The tests were performed under dry laboratory conditions:

y=specimen displacement

P=instantaneous load

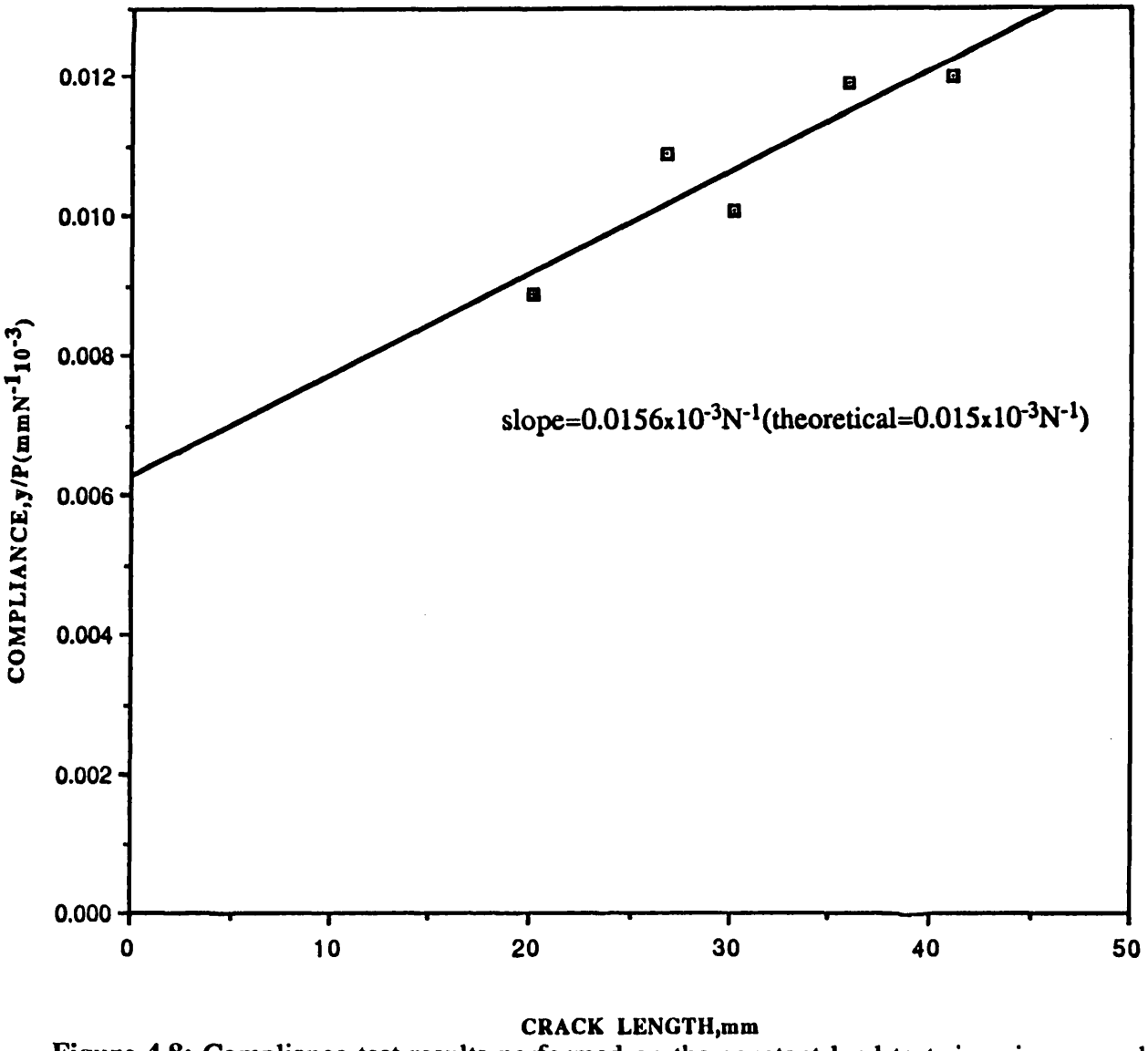


Figure 4.8: Compliance test results performed on the constant-load test-rig using unmodified epoxy resin DT joints of thickness t=3.00 mm. The tests were performed under dry laboratory conditions:

y=specimen displacement

P=instantaneous load

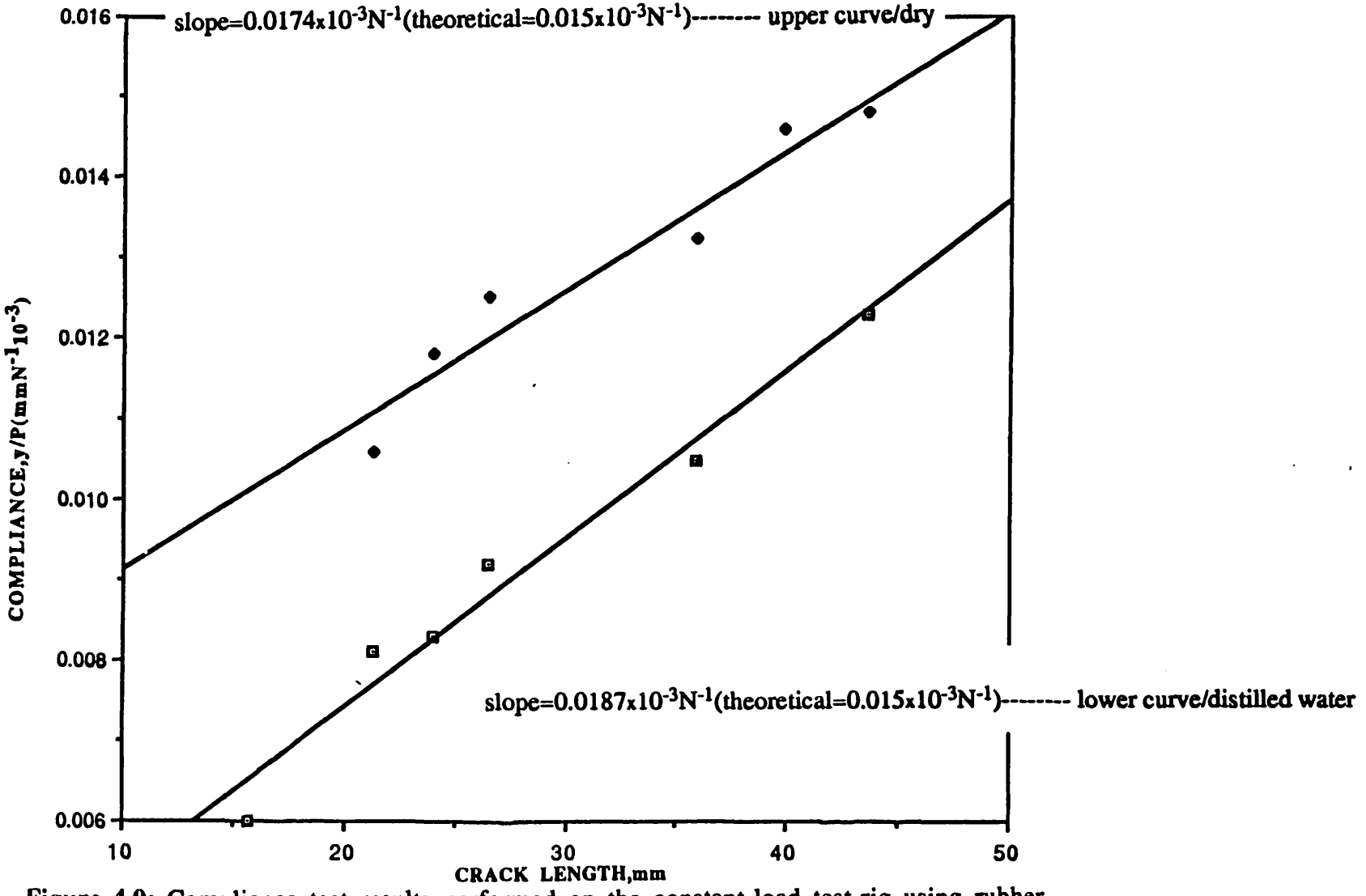


Figure 4.9: Compliance test results performed on the constant-load test-rig using rubber modified epoxy resin DT joints of thickness t=3.00 mm. The tests were performed under dry (upper curve) and wet (i.e. in distilled water at room temperature) conditions (lower curve).

y=specimen displacement

P=instantaneous load

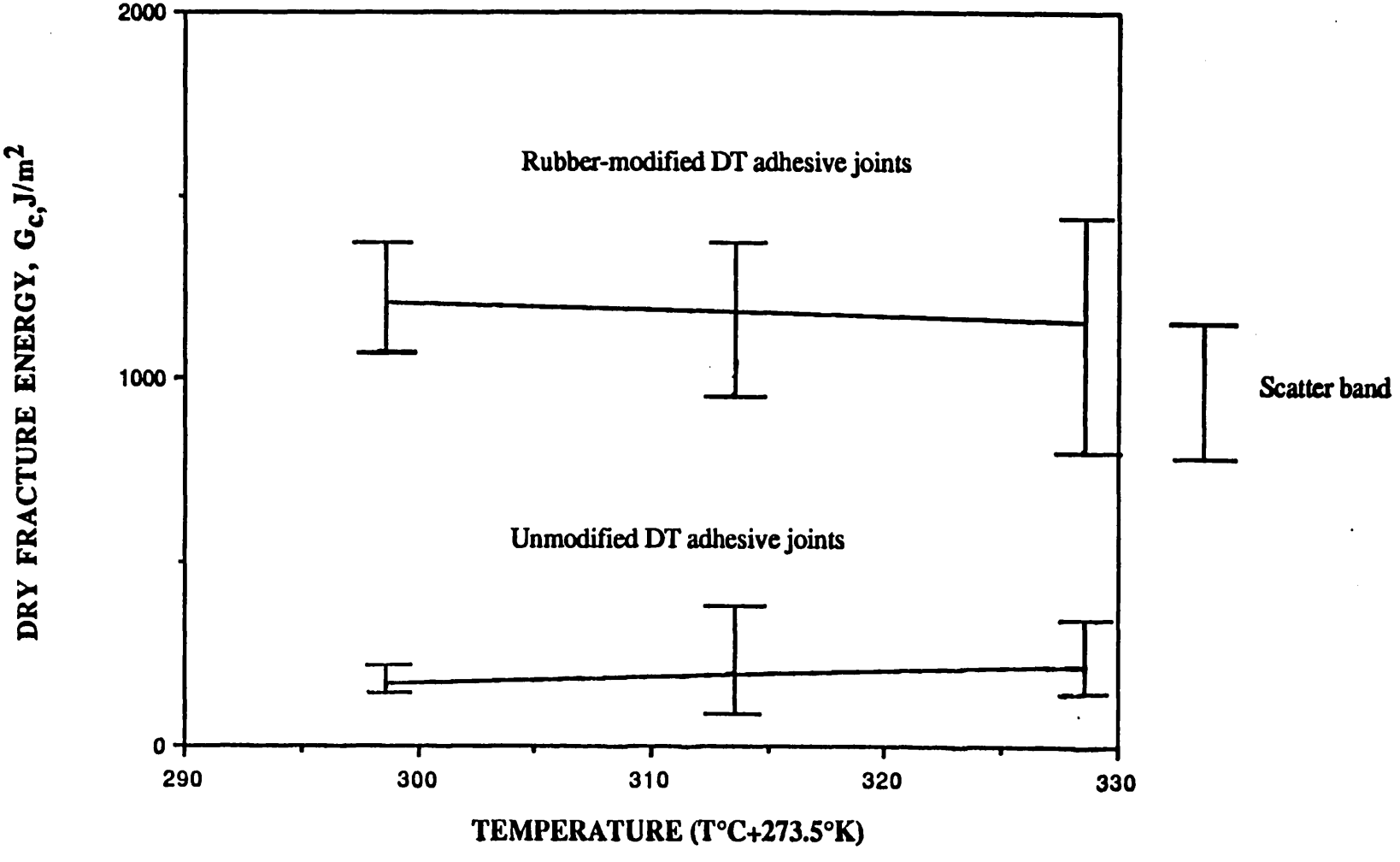


Figure 4.10: Comparison of the variation of the dry fracture energy with test temperature between the rubber-modified and unmodified double-torsion adhesive joints.

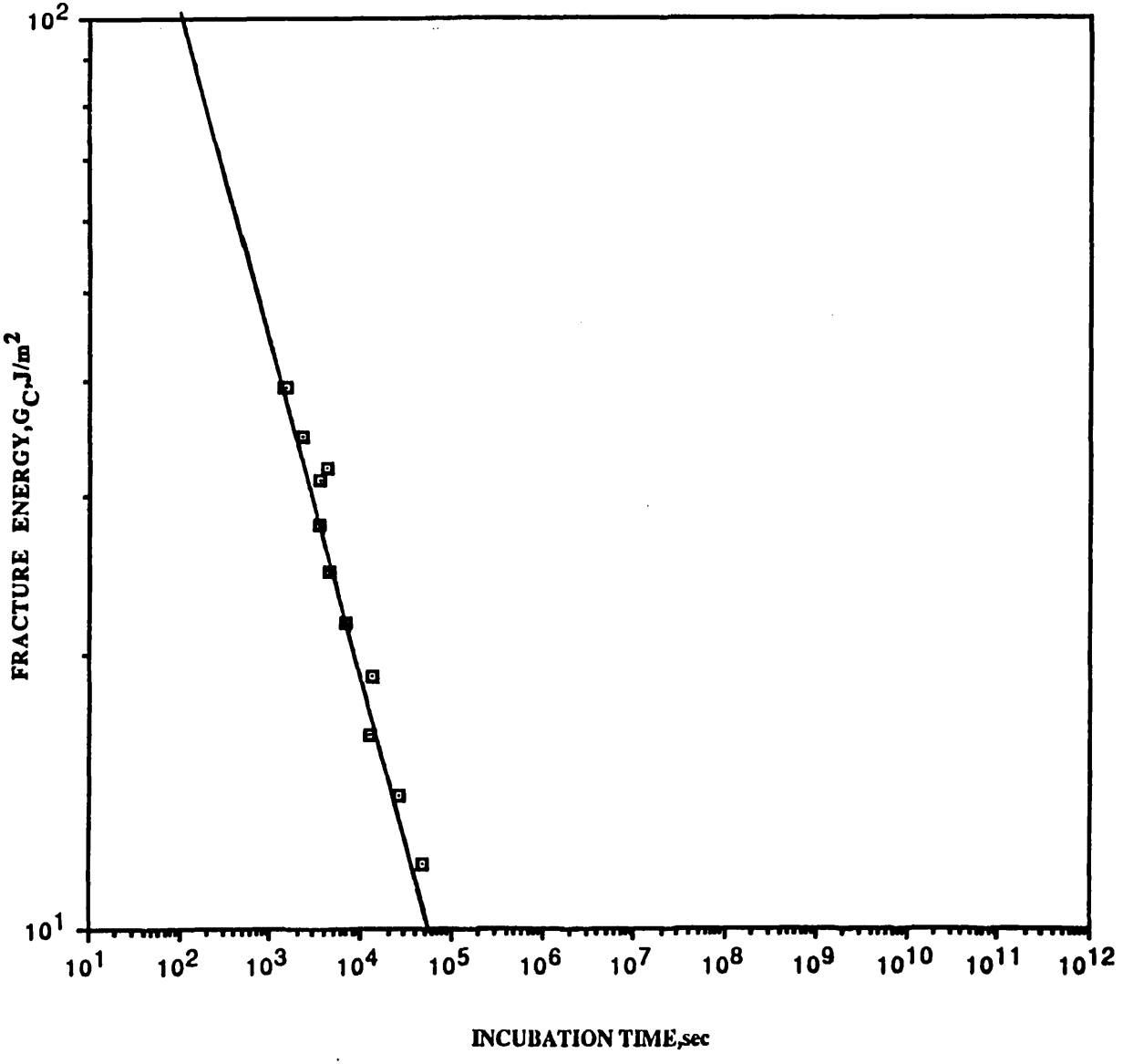


Figure 4.11: Fracture energy, G_c, against incubation time data plotted in logarithmic form for the unmodified double-torsion joints exposed to water at 25°C and subjected to various loads

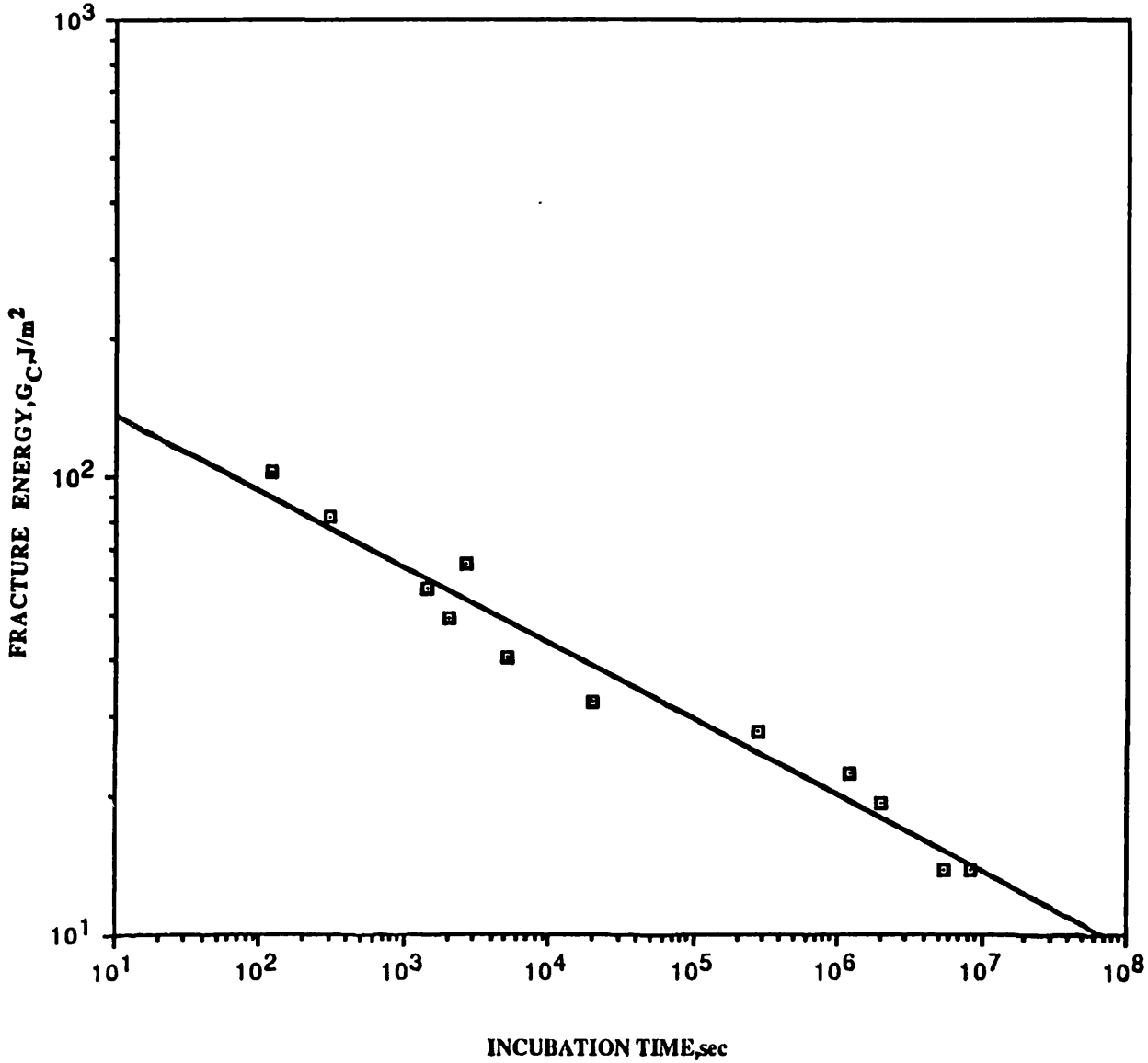


Figure 4.12: Fracture energy, G_c, against incubation time data plotted in logarithmic form for the unmodified double-torsion joints exposed to water at 40°C and subjected to various loads

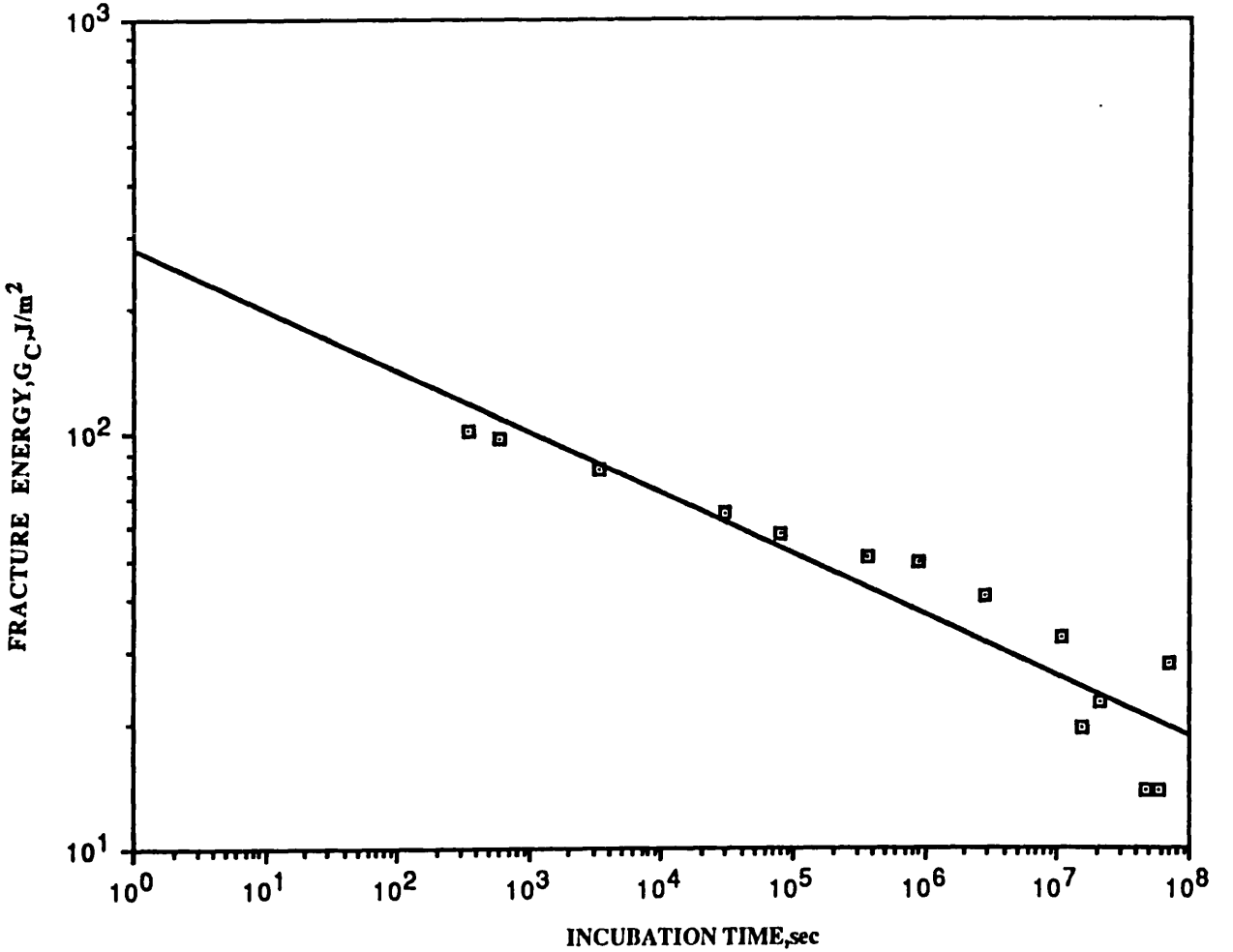


Figure 4.13: Fracture energy, G_c, against incubation time data plotted in logarithmic form for the unmodified double-torsion joints exposed to water at 55°C and subjected to various loads

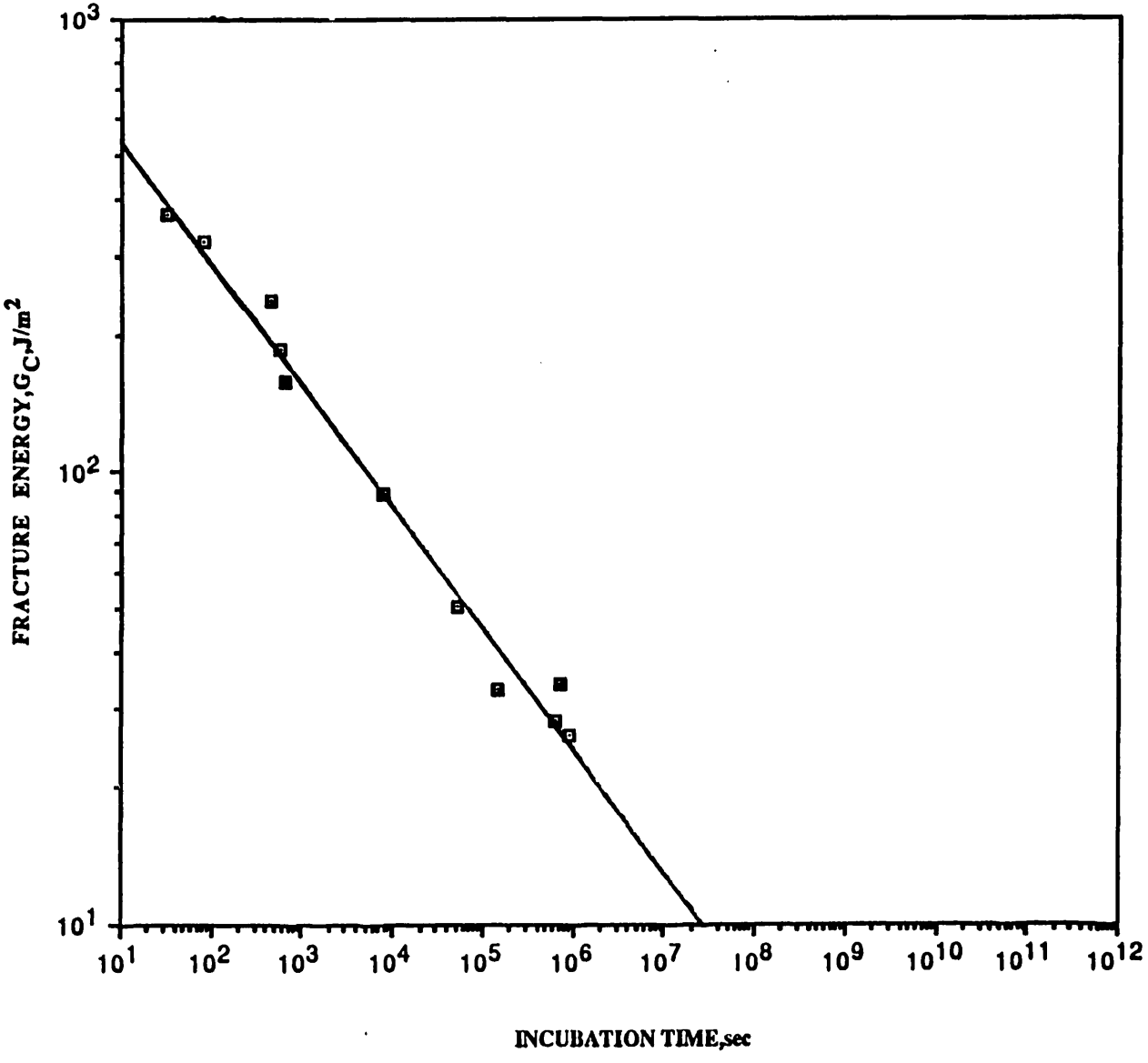


Figure 4.14: Fracture energy, G_c, against incubation time data plotted in logarithmic form for the rubber-modified double-torsion joints exposed to water at 25°C and subjected to various loads

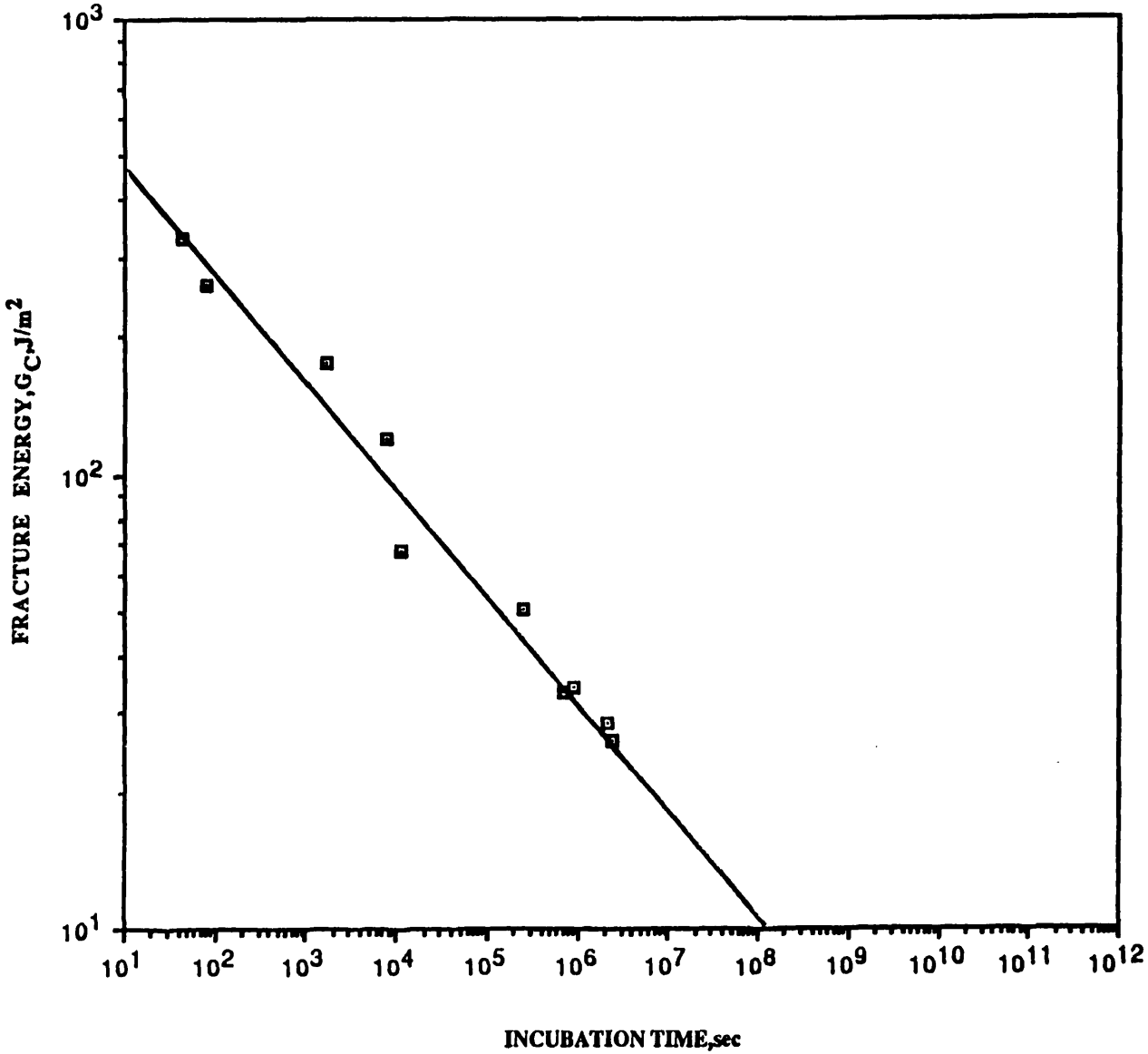


Figure 4.15: Fracture energy, G_C, against incubation time data plotted in logarithmic form for the rubber-modified double-torsion joints exposed to water at 40°C and subjected to various loads

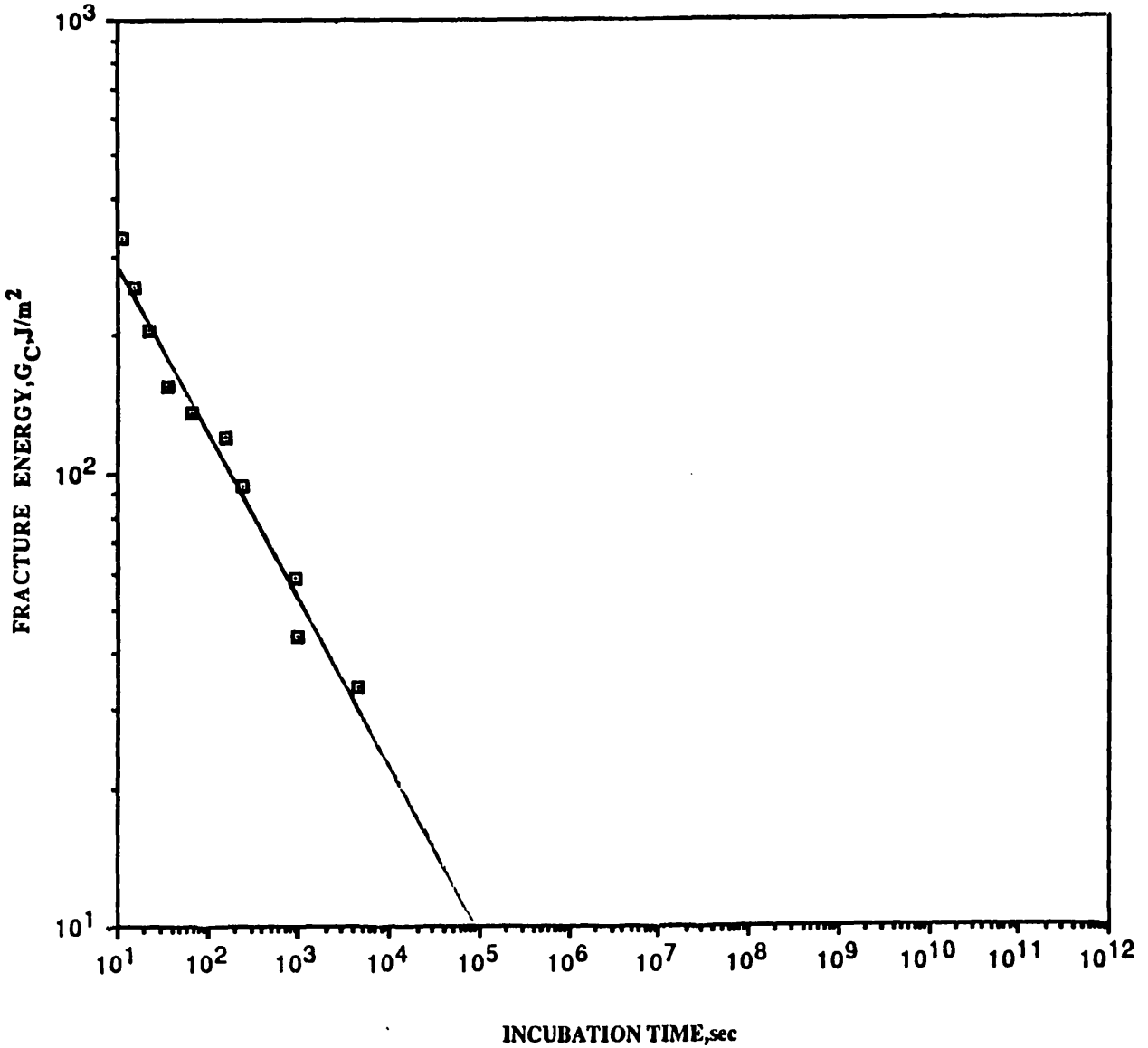


Figure 4.16: Fracture energy, G_c, against incubation time data plotted in logarithmic form for the rubber-modified double-torsion joints exposed to water at 55°C and subjected to various loads

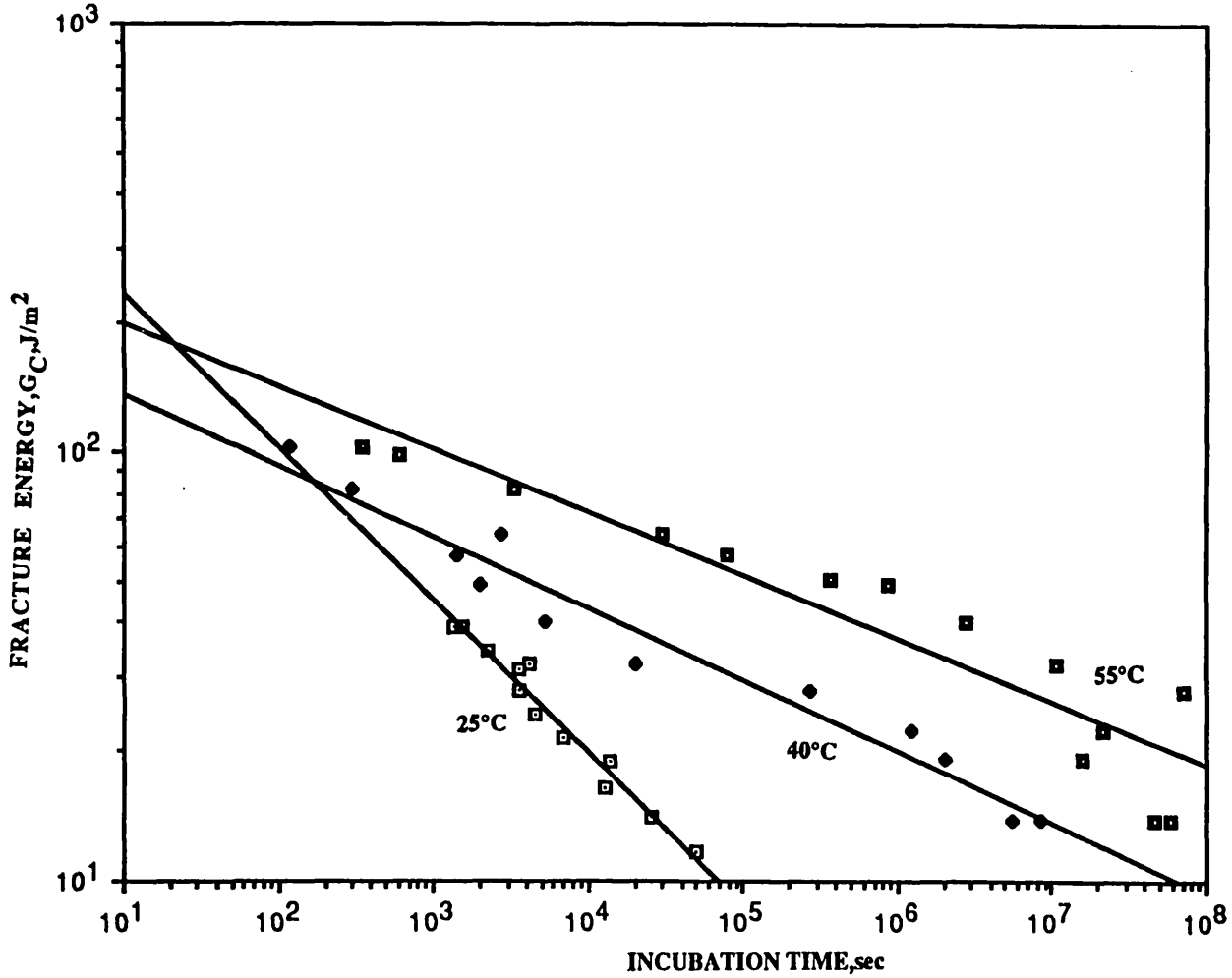


Figure 4.17: Comparison of fracture energy, G_C, against incubation time data between unmodified double-torsion joints immersed in water at 25°C, 40°C, and 55°C and subjected to various loads

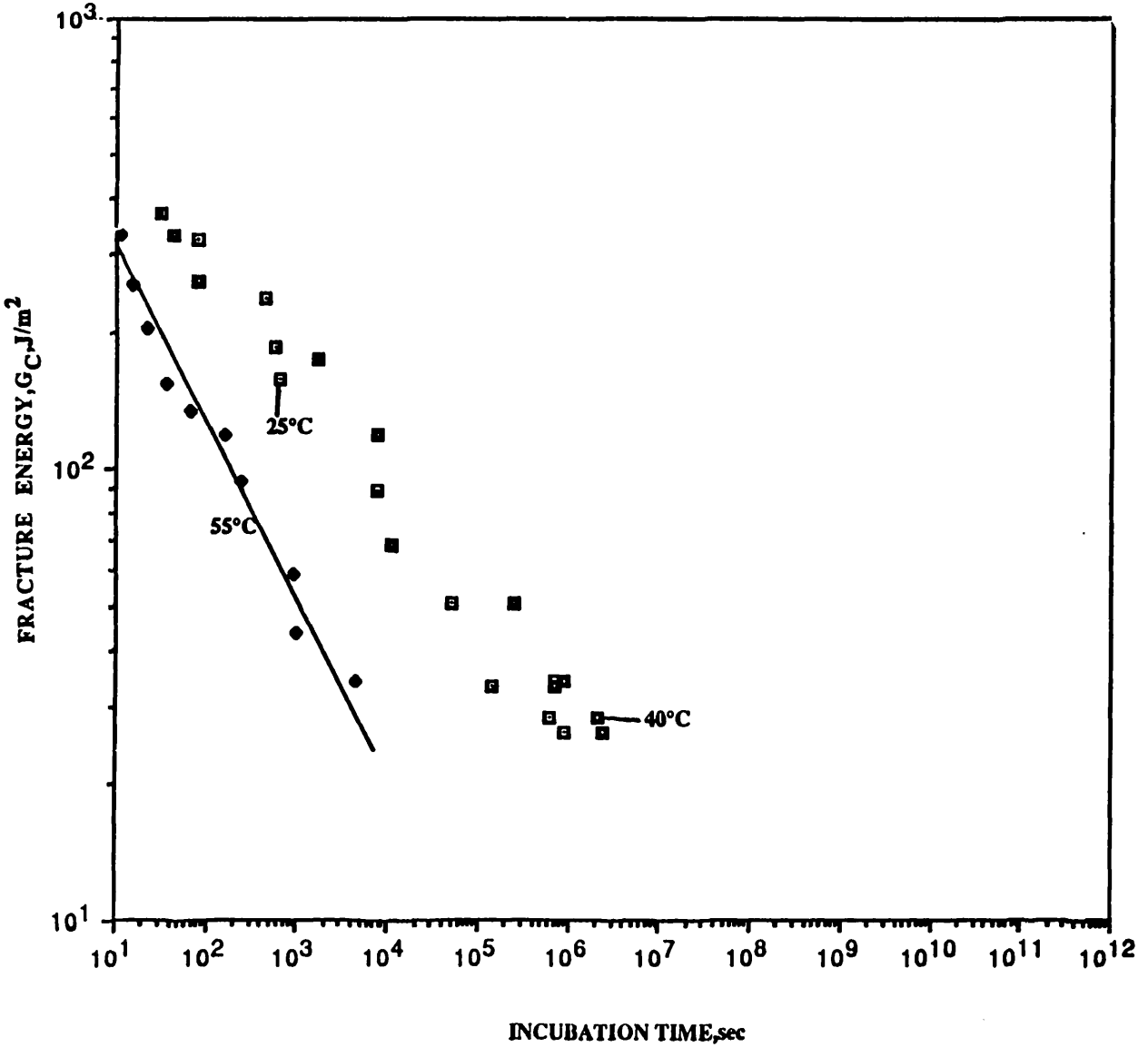


Figure 4.18: Comparison of fracture energy, G_C, against incubation time data between rubber-modified double-torsion joints immersed in water at 25°C, 40°C, and 55°C and subjected to various loads

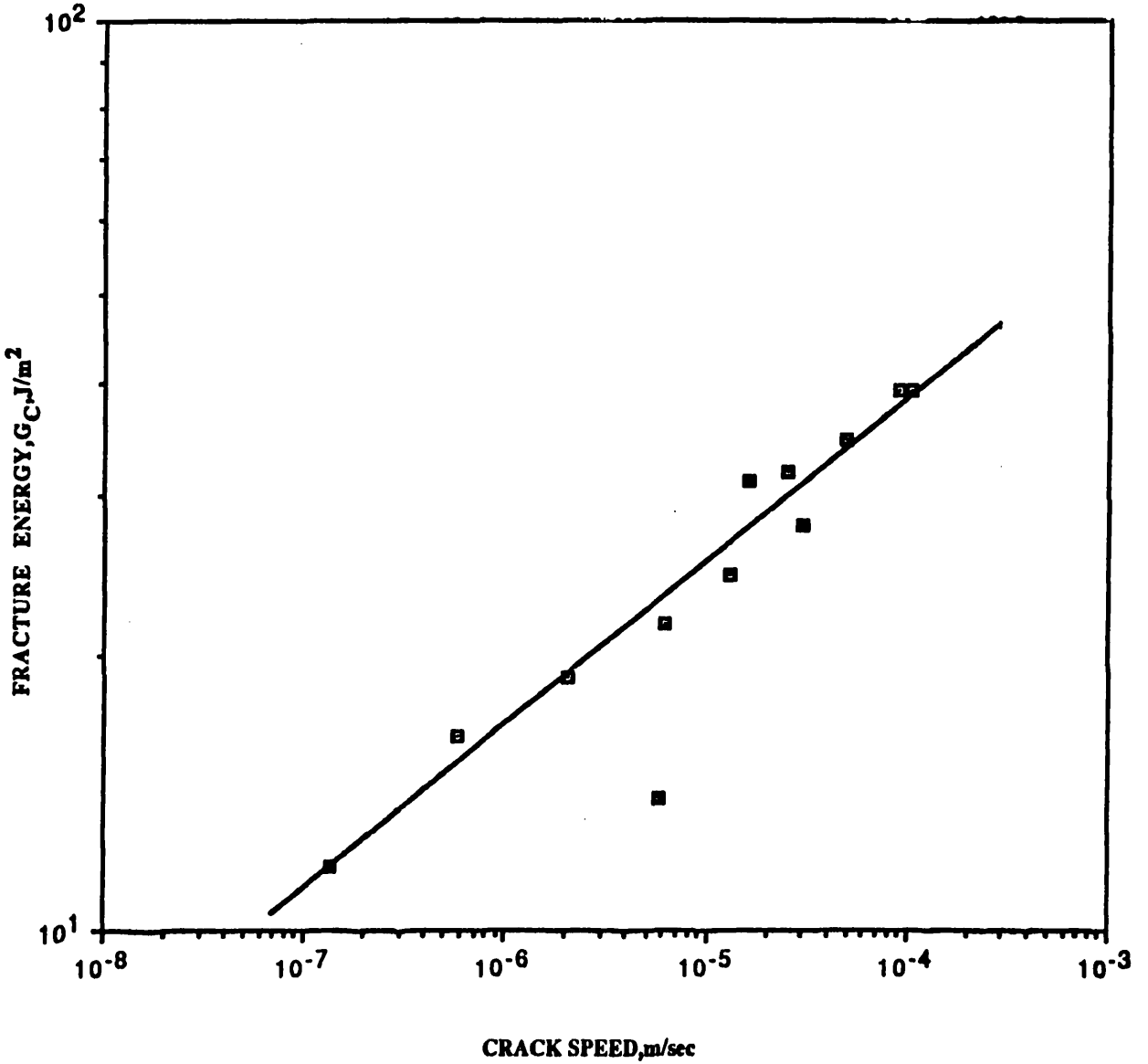


Figure 4.19: Fracture energy, G_c, against crack speed data, plotted in logarithmic form, for unmodified double-torsion joints exposed to water at 25°C and subjected to various loads

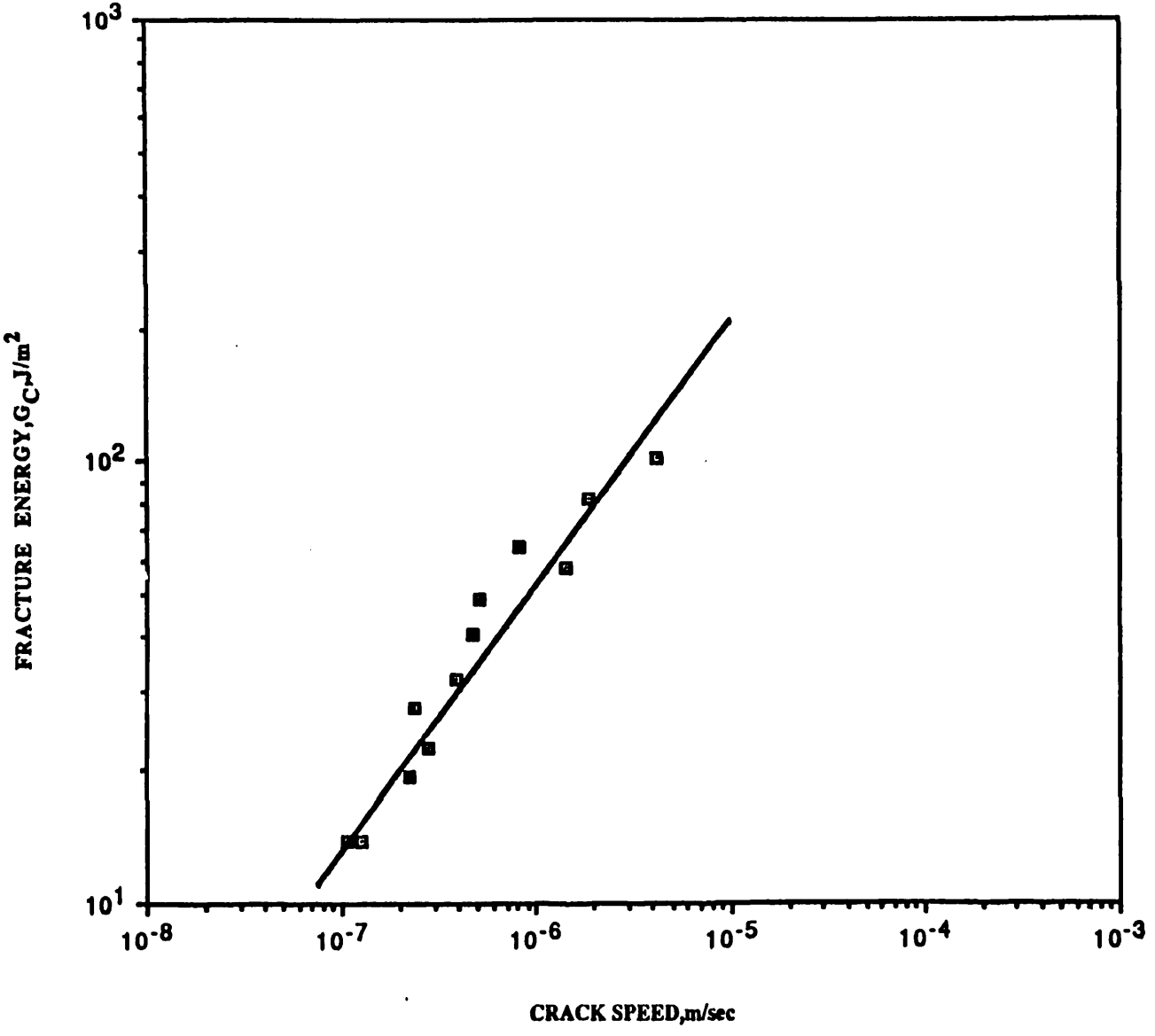


Figure 4.20: Fracture energy, G_C, against crack speed data, plotted in logarithmic form, for unmodified double-torsion joints exposed to water at 40°C and subjected to various loads

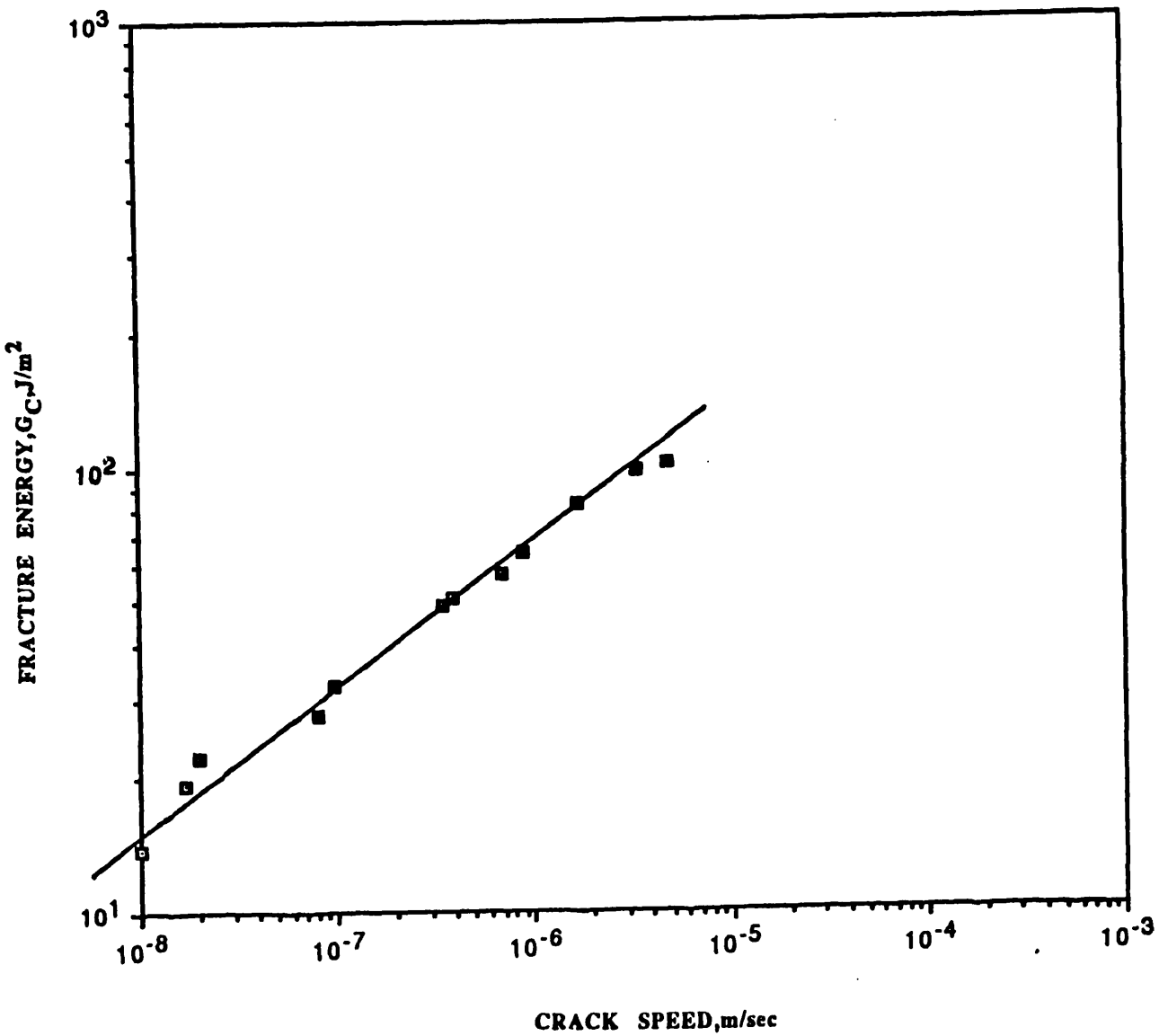


Figure 4.21: Fracture energy, G_c, against crack speed data, plotted in logarithmic form, for unmodified double-torsion joints exposed to water at 55°C and subjected to various loads

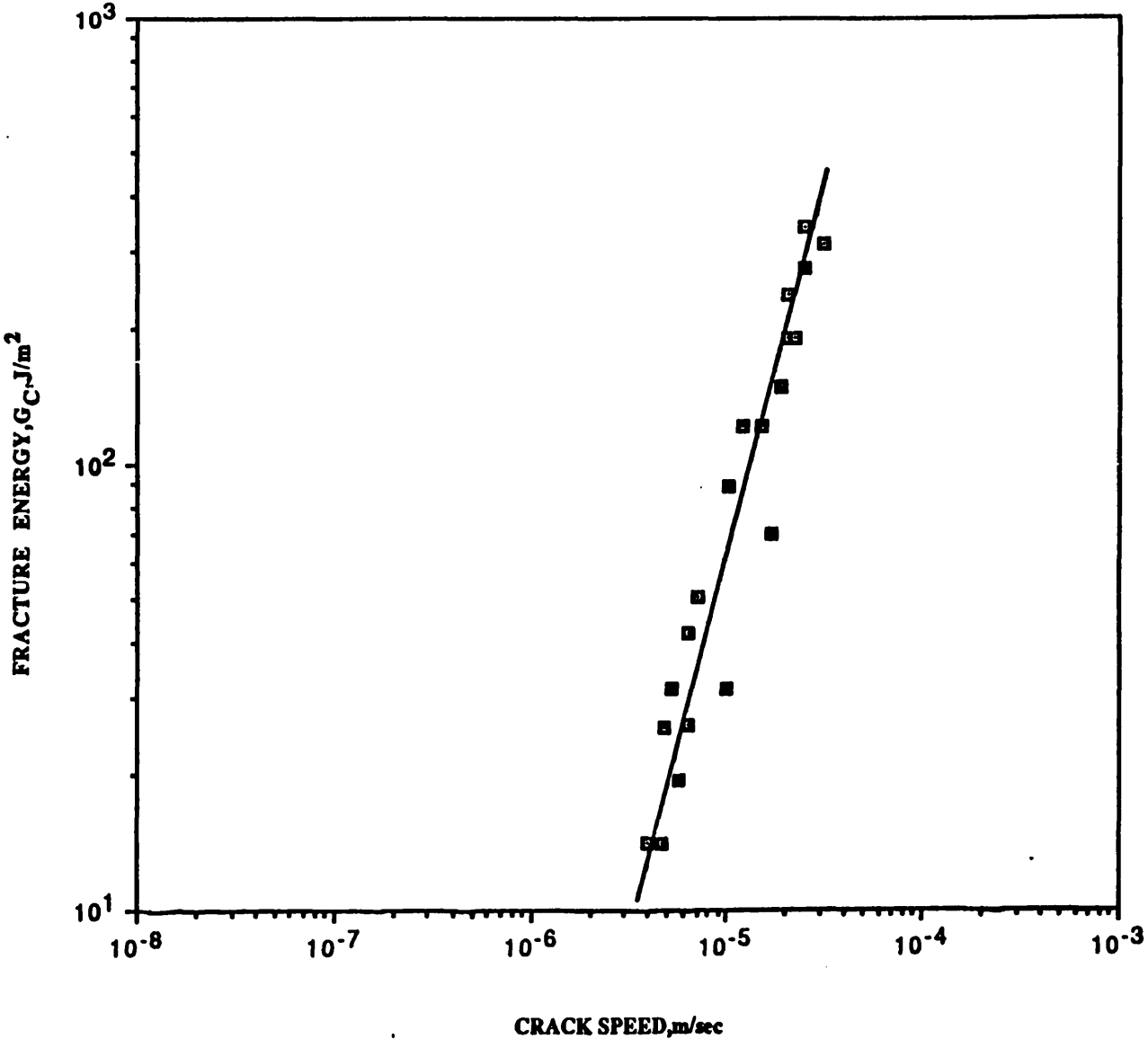


Figure 4.22: Fracture energy, G_C, against crack speed data, plotted in logarithmic form, for rubber-modified double-torsion joints exposed to water at 25°C and subjected to various loads

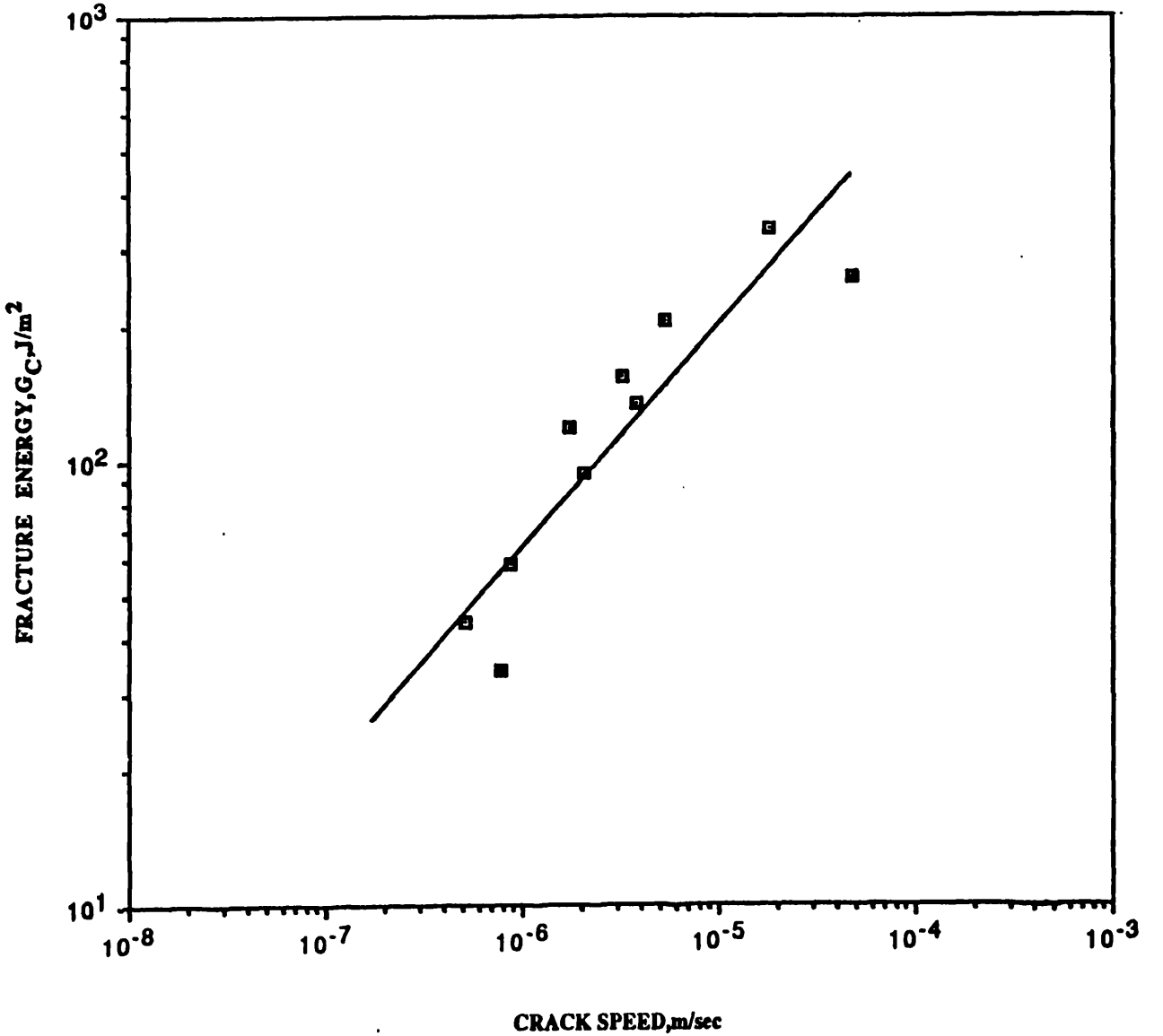


Figure 4.23: Fracture energy, G_C, against crack speed data, plotted in logarithmic form, for rubber-modified double-torsion joints exposed to water at 40°C and subjected to various loads

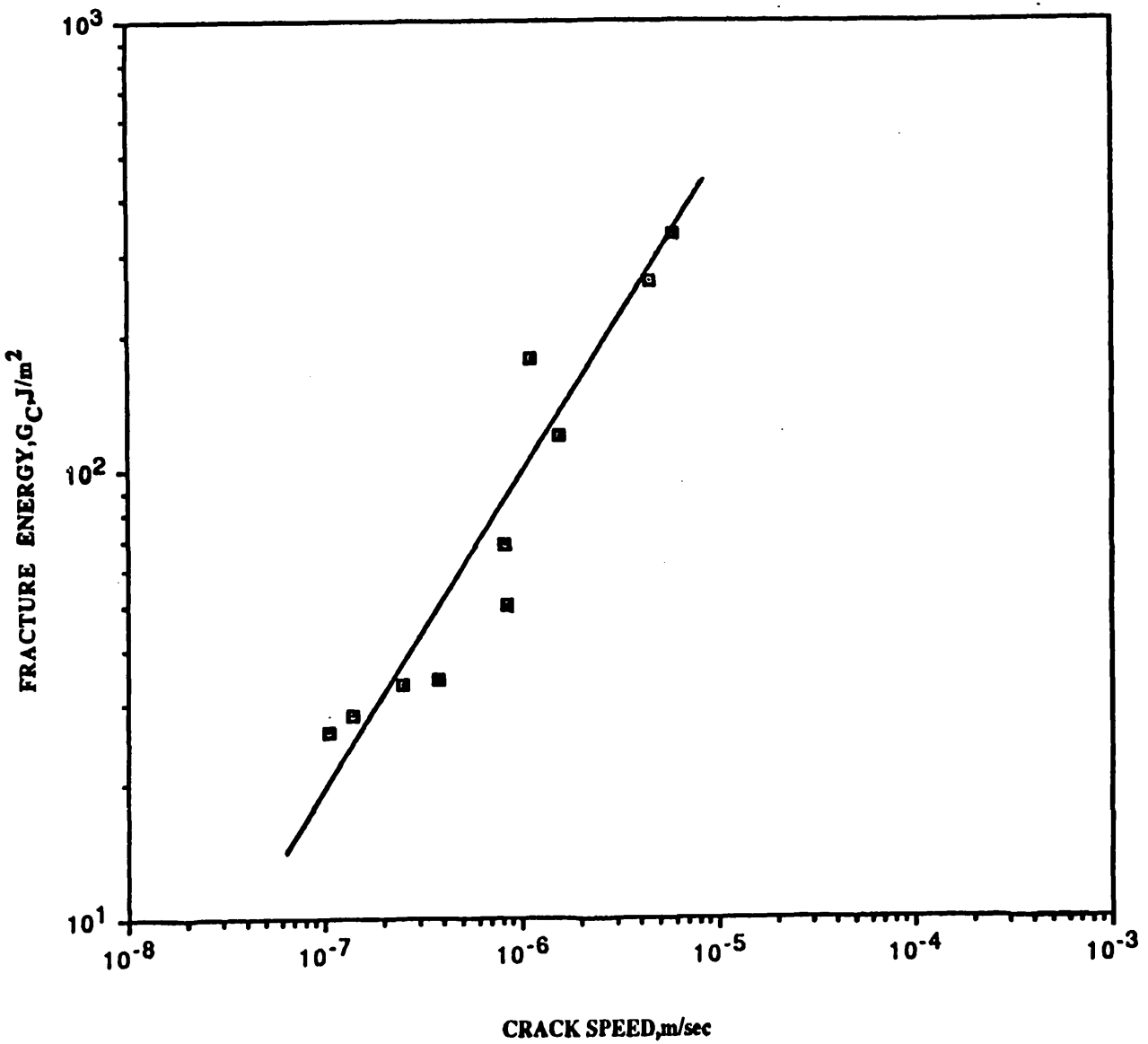


Figure 4.24: Fracture energy, G_C, against crack speed data, plotted in logarithmic form, for rubber-modified double-torsion joints exposed to water at 55°C and subjected to various loads

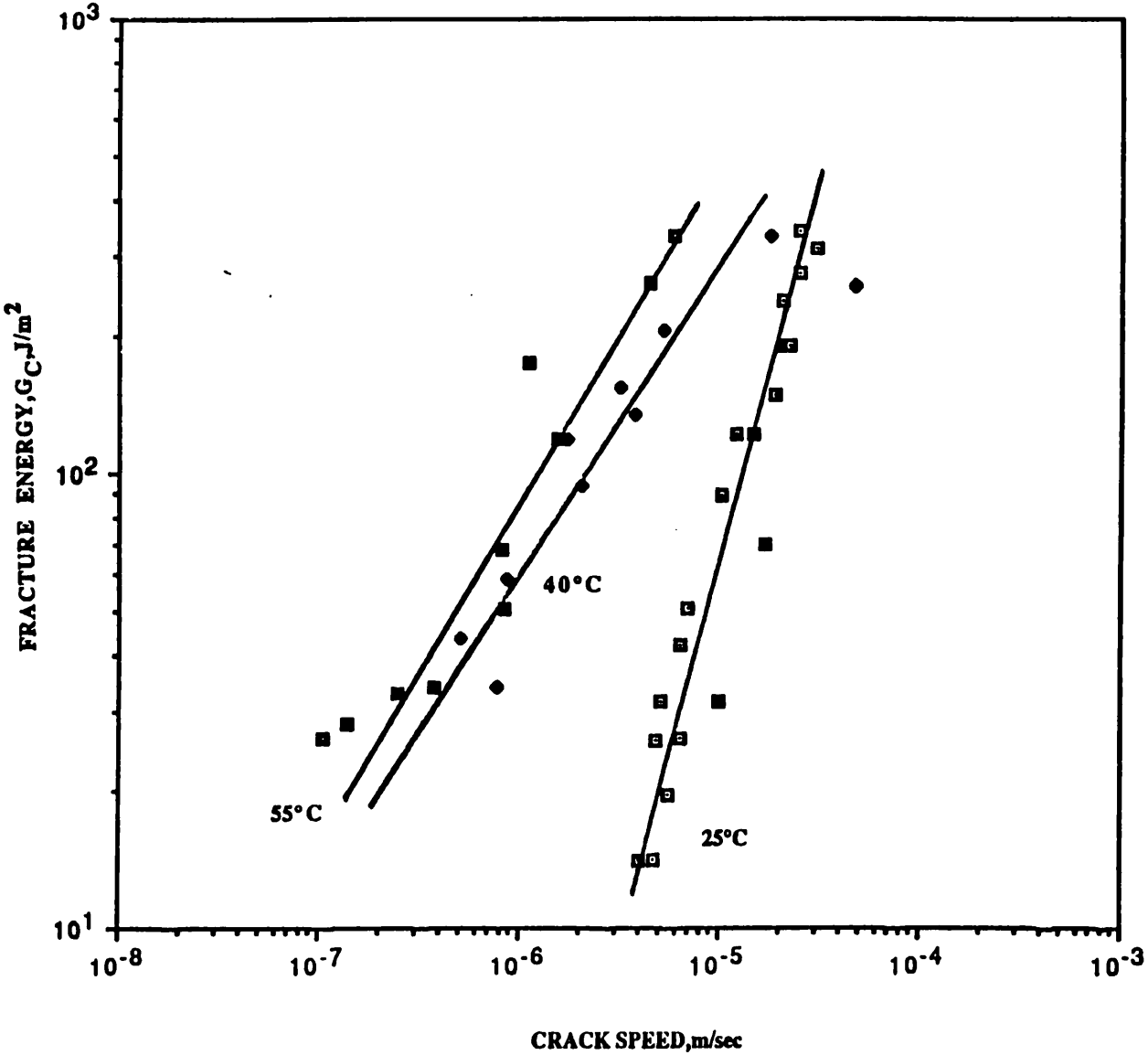


Figure 4.25: Comparison of fracture energy, G_c, against crack speed data between rubber-modified double-torsion joints immersed in water at 25°C, 40°C, and 55°C and subjected to various loads

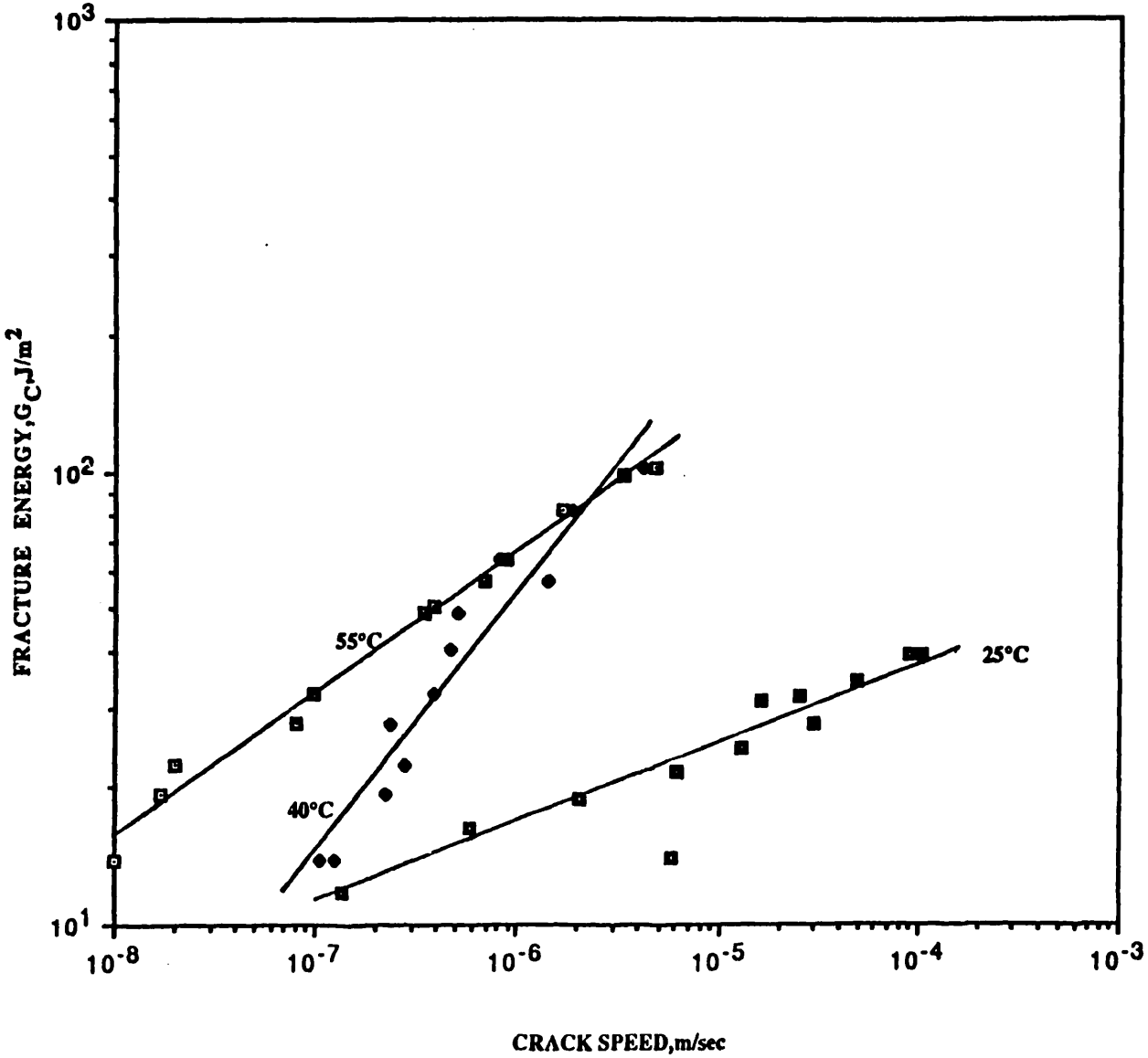


Figure 4.26: Comparison of fracture energy, G_c, against crack speed data between unmodified double-torsion joints exposed to water at 25°C, 40°C, and 55°C and subjected to various loads

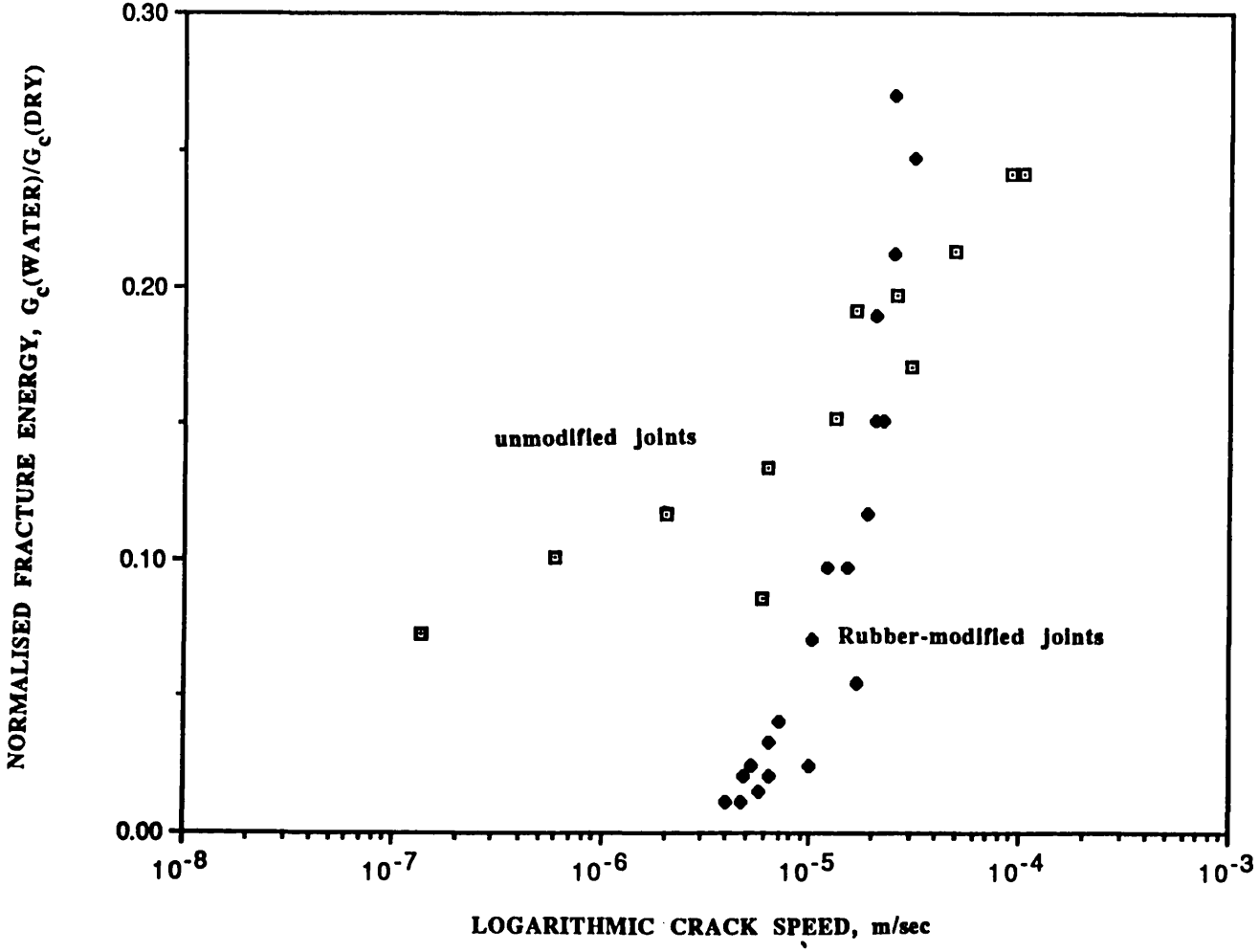


Figure 4.27: Comparison of the variation of the normalised fracture energy, G_c(water)/G_c(dry), with the logarithmic crack speed between the rubber-modified and unmodified double-torsion adhesive joints exposed to distilled water at 25°C.

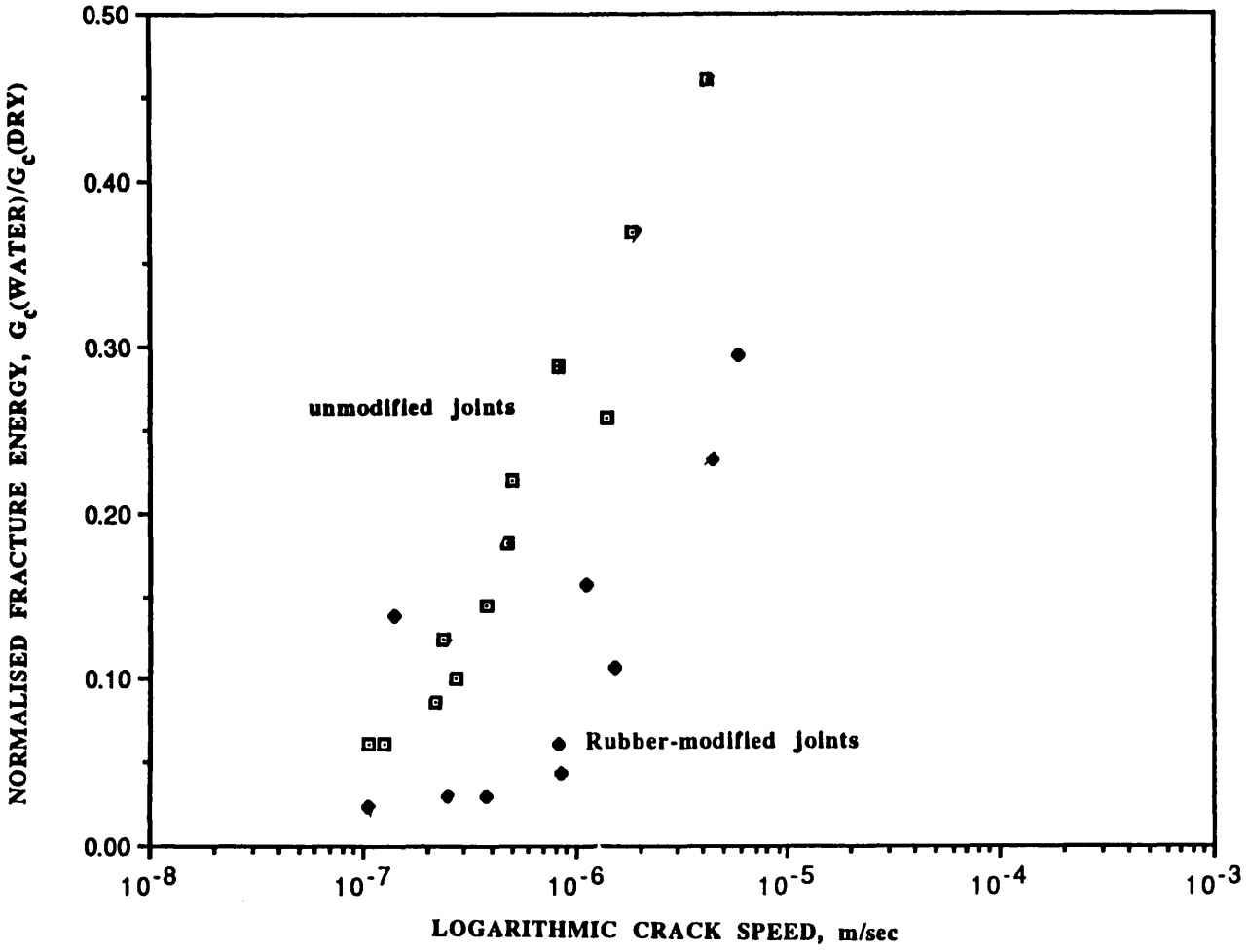


Figure 4.28: Comparison of the variation of the normalised fracture energy, G_c(water)/G_c(dry), with the logarithmic crack speed between the rubber-modified and unmodified double-torsion adhesive joints exposed to distilled water at 40°C.

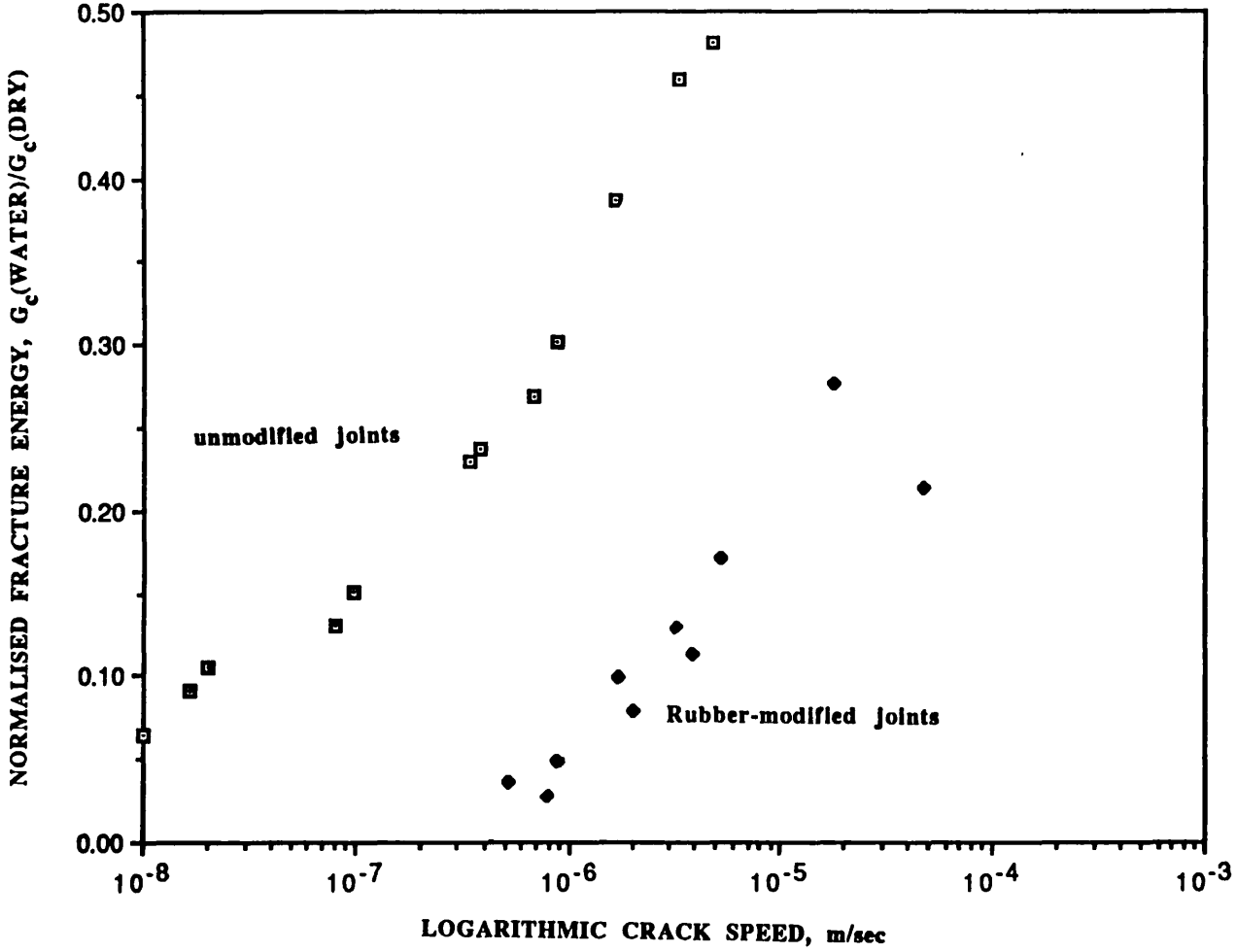


Figure 4.29: Comparison of the variation of the normalised fracture energy, G_c(water)/G_c(dry), with the logarithmic crack speed between the rubber-modified and unmodified double-torsion adhesive joints exposed to distilled water at 55°C.

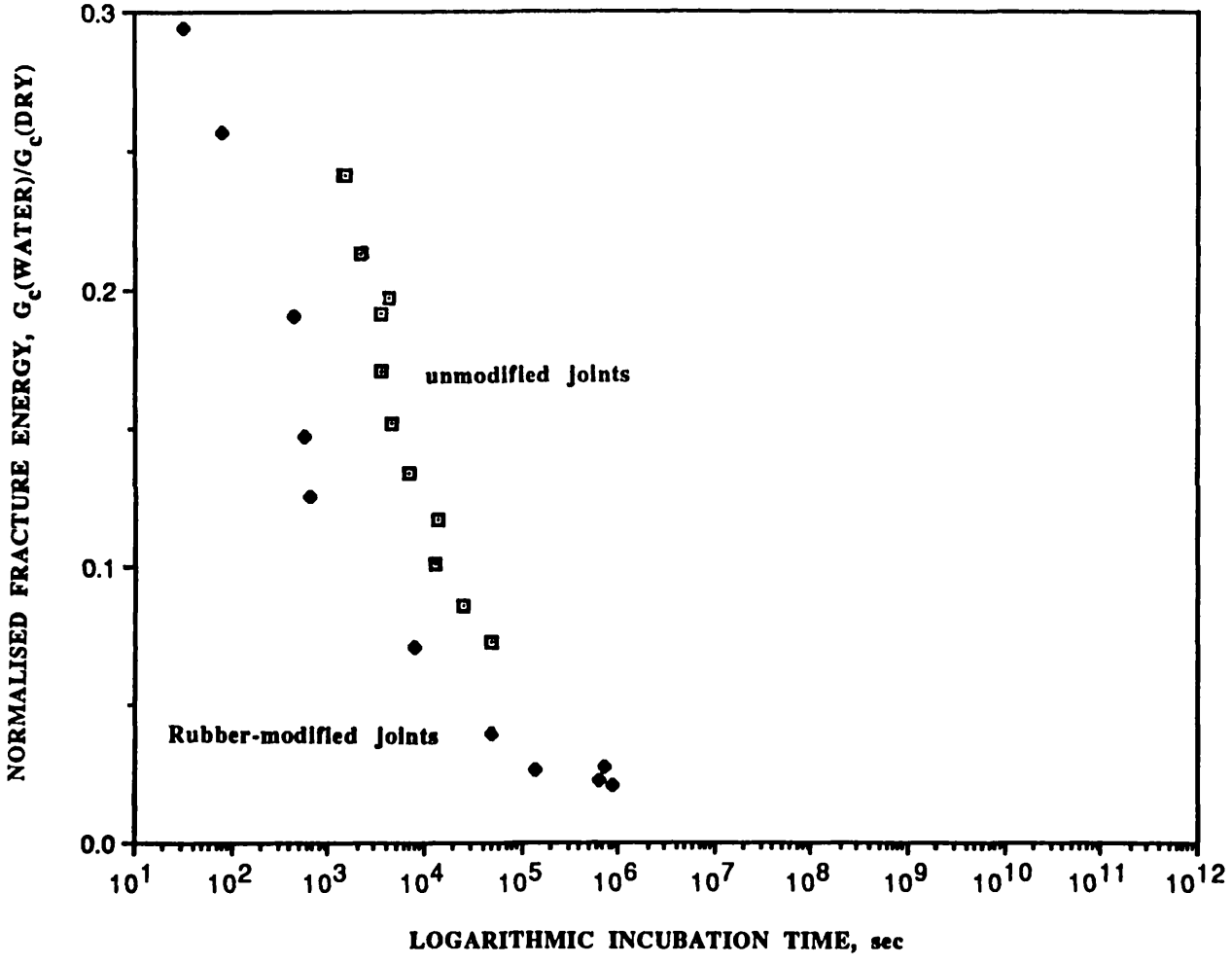


Figure 4.30: Comparison of the variation of the normalised fracture energy, G_c(water)/G_c(dry), with the logarithmic incubation time between the rubber-modified and unmodified double-torsion adhesive joints exposed to distilled water at 25°C.

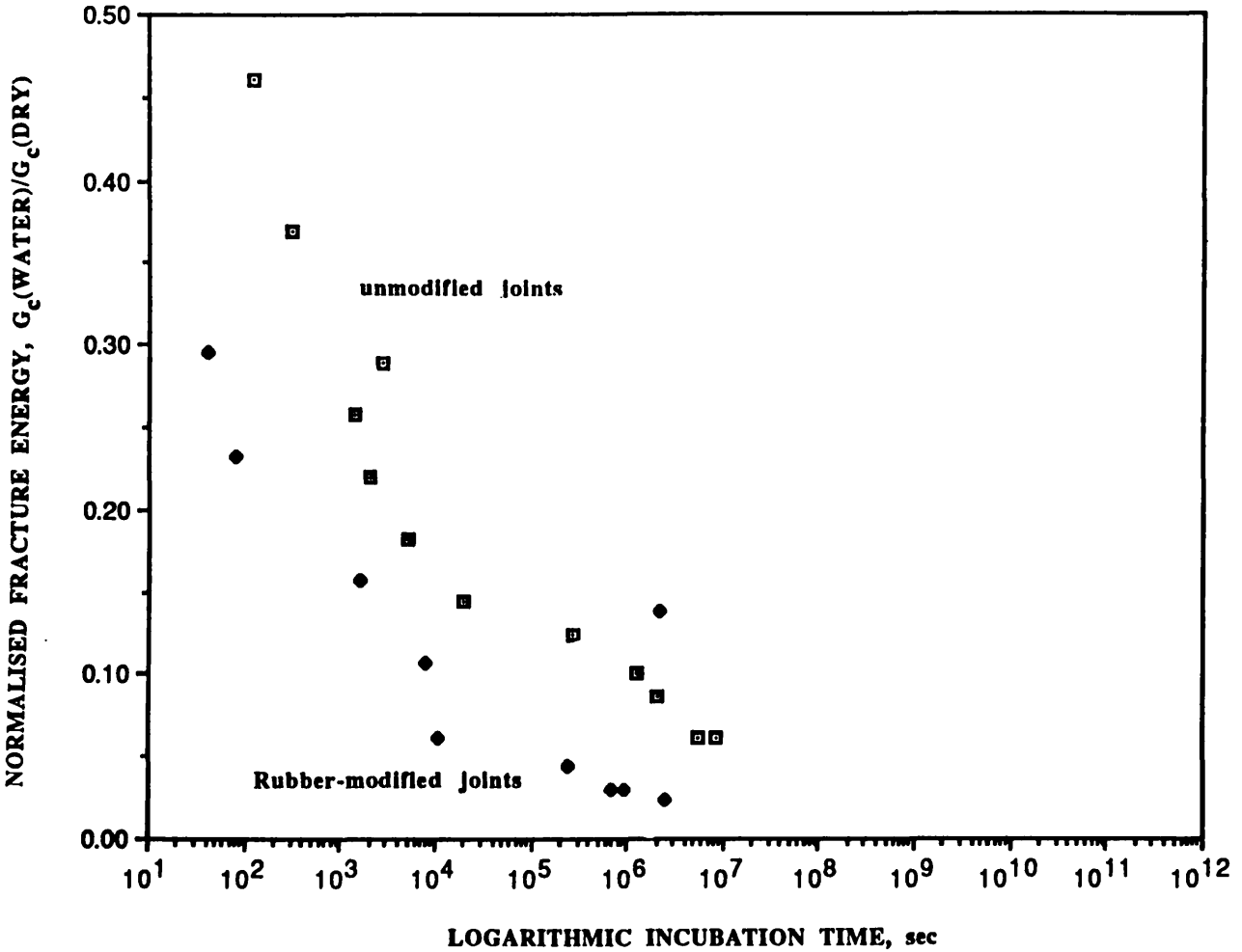


Figure 4.31: Comparison of the variation of the normalised fracture energy, G_c(water)/G_c(dry), with the logarithmic incubation time between the rubber-modified and unmodified double-torsion adhesive joints exposed to distilled water at 40°C.

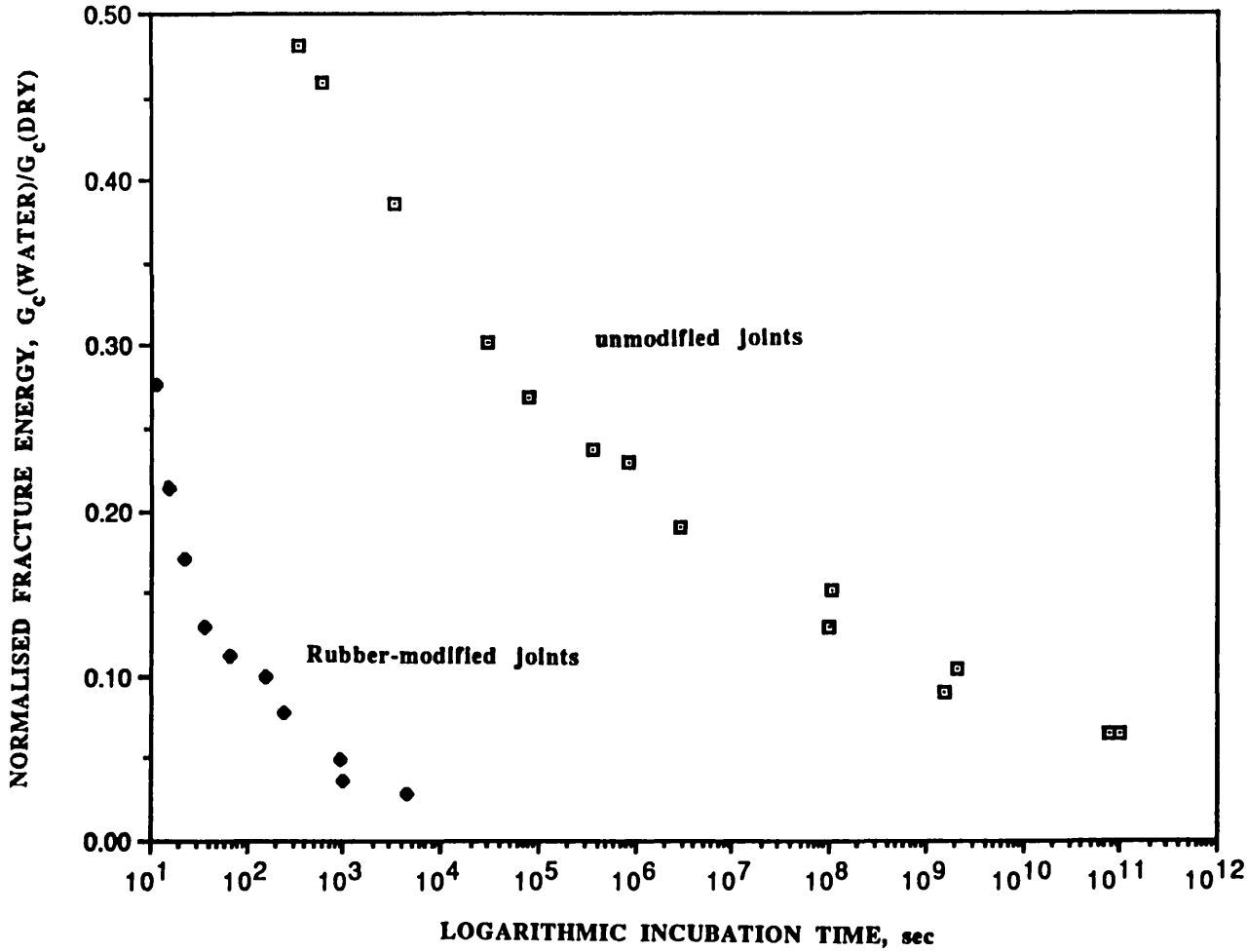


Figure 4.32: Comparison of the variation of the normalised fracture energy, G_c(water)/G_c(dry), with the logarithmic incubation time between the rubber-modified and unmodified double-torsion adhesive joints exposed to distilled water at 55°C.

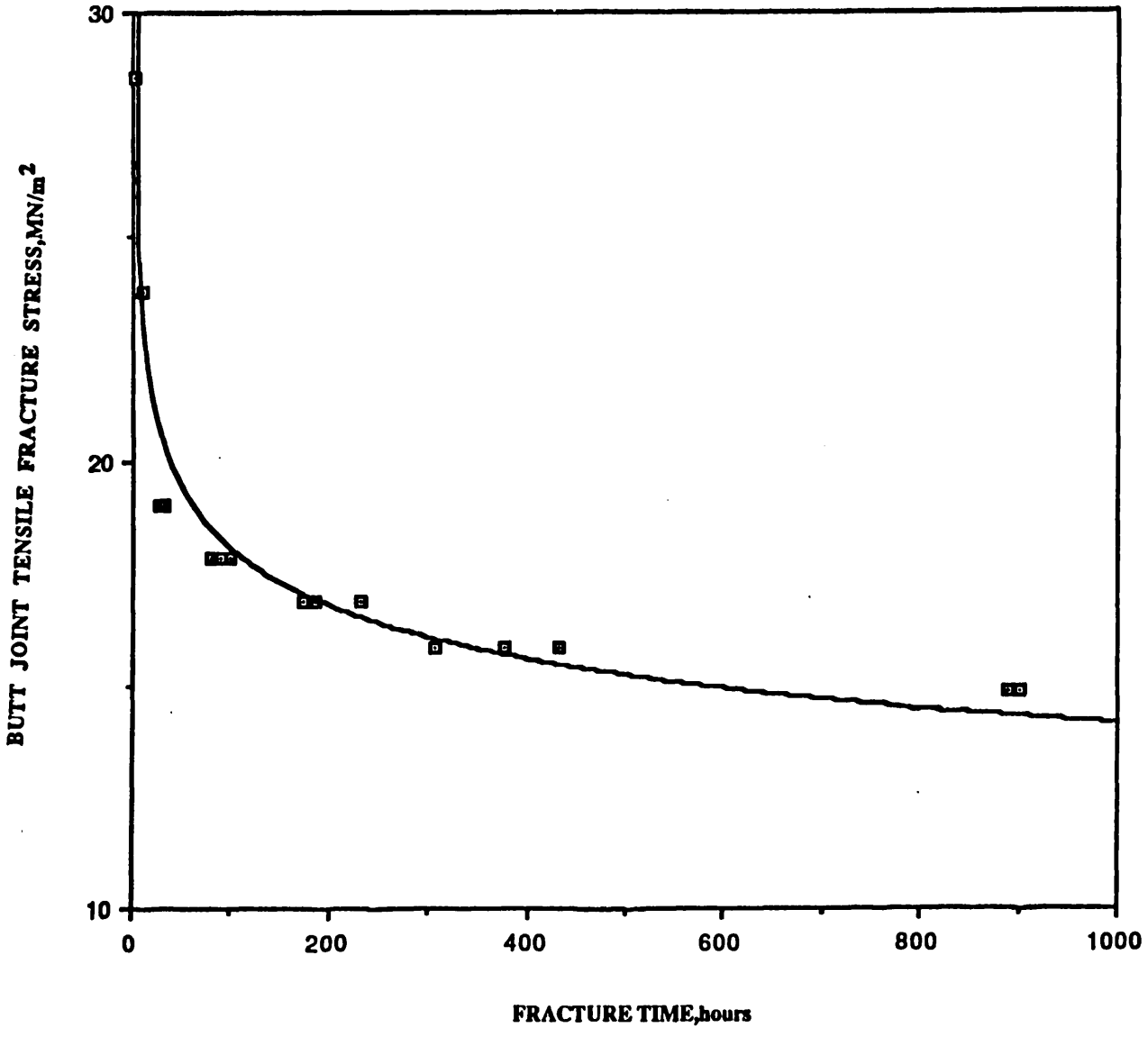


Figure 4.33: Fracture data obtained from the tests using rubber-modified butt joints in distilled water at 25°C and subjected to various static loads.

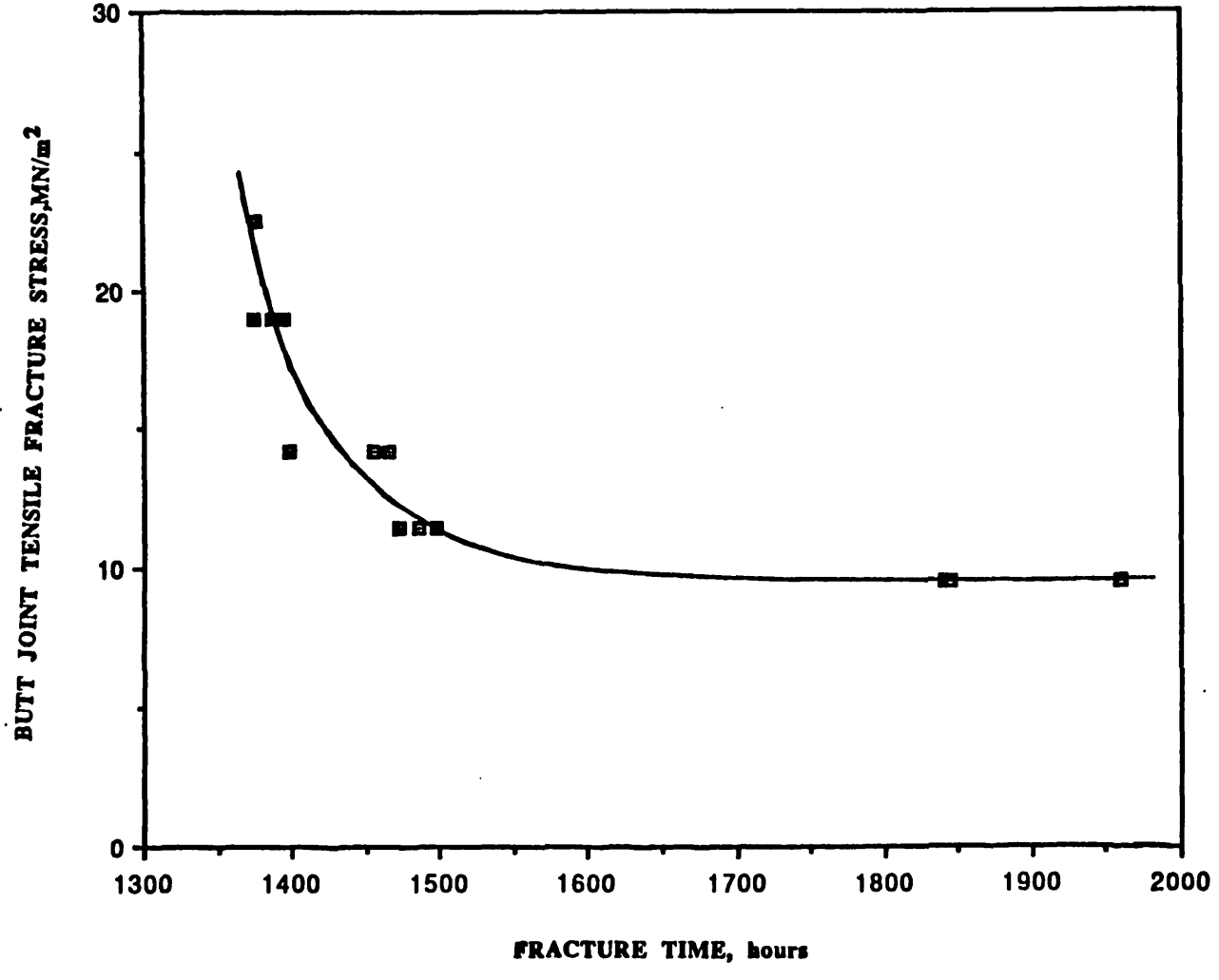


Figure 4.34: Fracture data obtained from the tests using unmodified butt joints in distilled water at 25°C and subjected to various static loads.

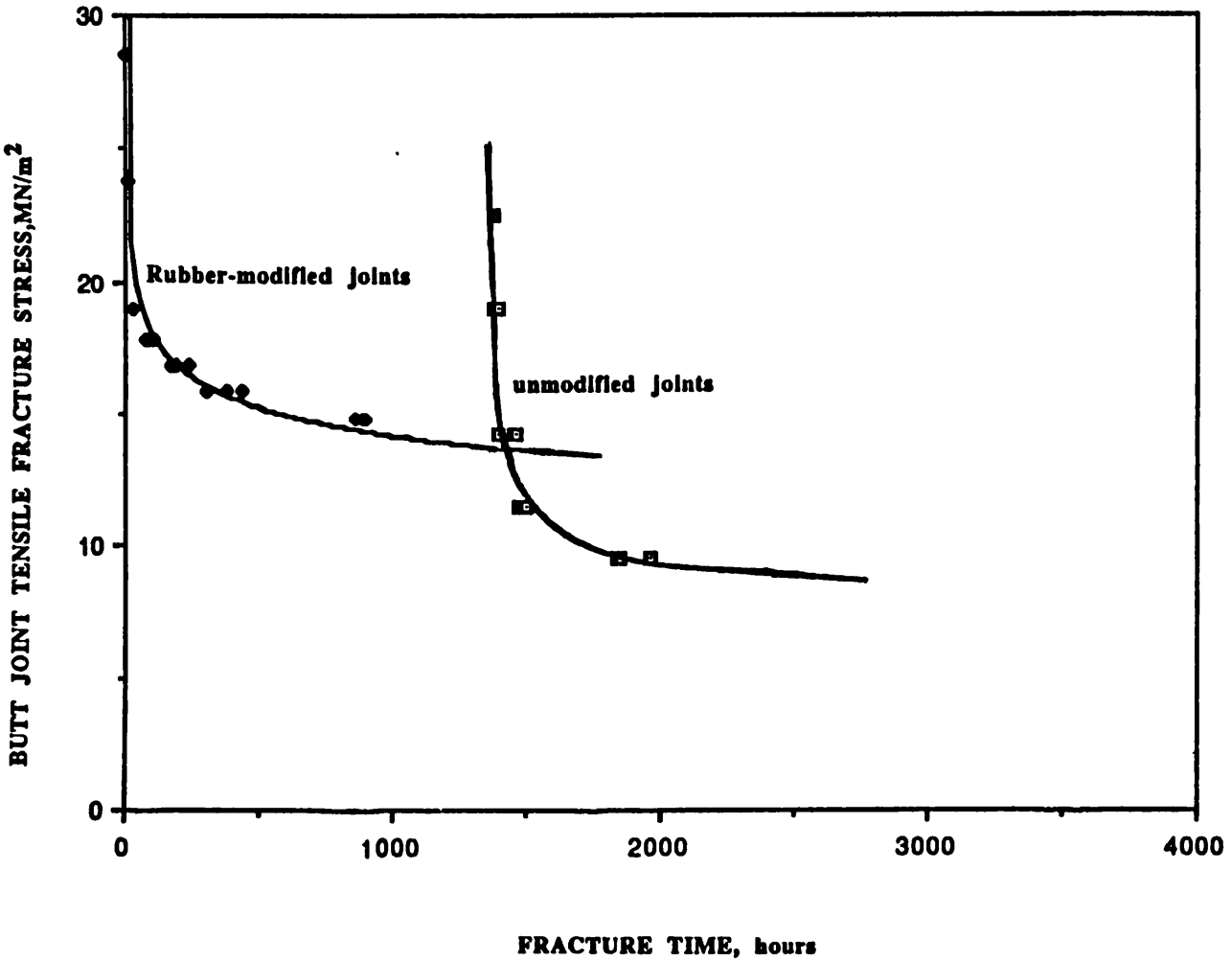


Figure 4.35: Comparison between the fracture data obtained from the tests using rubber-modified and unmodofied butt adhesive joints in distilled water at 25°C and subjected to various static loads.

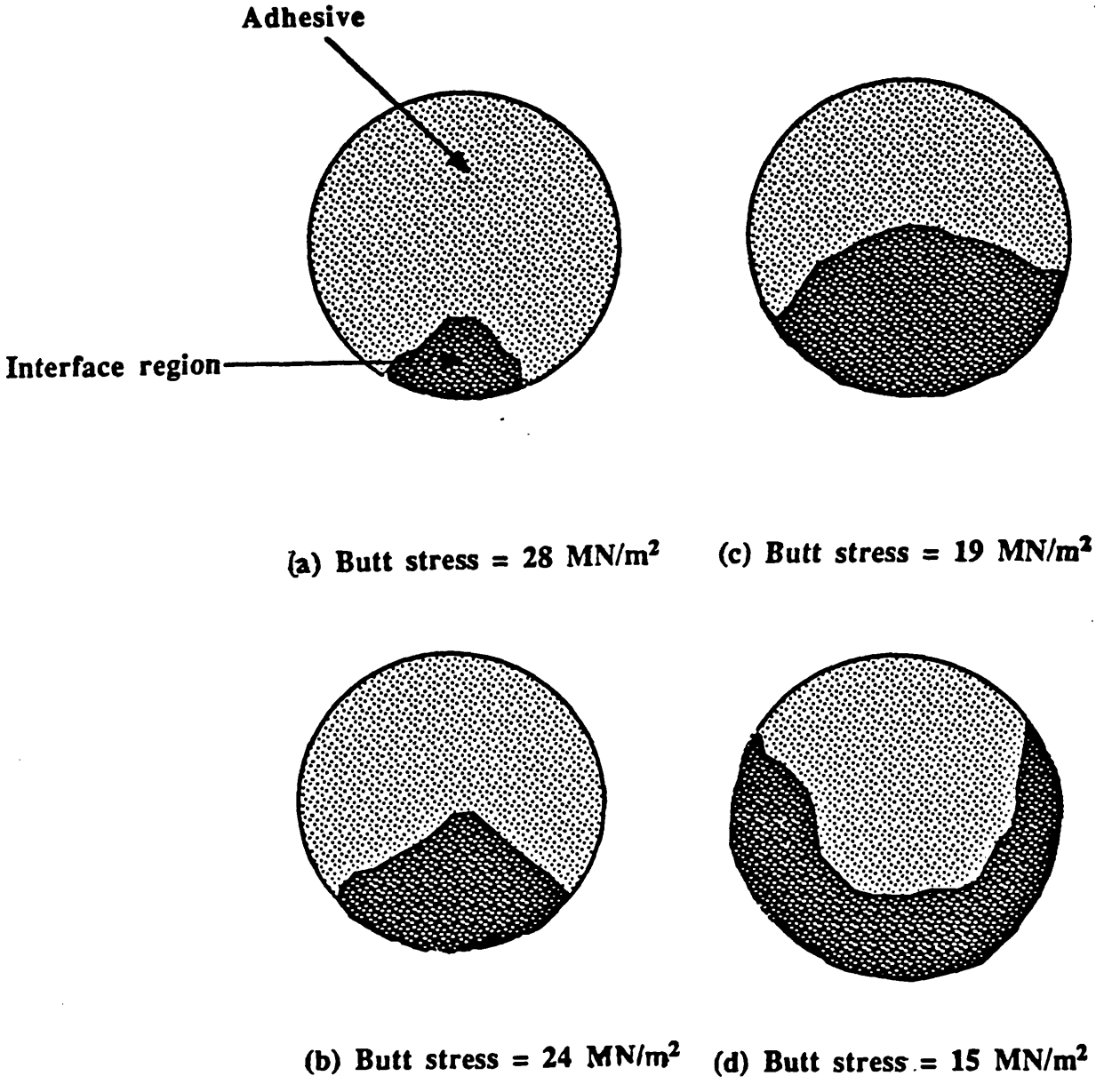


Figure 4.36: Schematic representation of typical fracture surfaces of butt adhesive joints studied in the present investgation subjected to various static loads in distilled water at 25°C.

CHAPTER 5

RESULTS AND DISCUSSIONS: DIFFUSION OF WATER STUDIES

5.1 INTRODUCTION

It is evident from the work described in the previous chapter that adhesive joints suffer a considerable loss of strength when they are exposed to moisture. Several factors have been suggested to be involved in the environmental attack mechanisms. For example, R.A. Gledhill et al (1980) suggested that , the accumulation of a critical concentration of water in the adhesive/metal substrate regions of the bonded component may be responsible for the loss in joint strength. Further, R.A. Gledhill et al (1980) have also suggested that the rate of attaining this critical concentration may be governed by the rate of water diffusion through the adhesive. The rate of water diffusion was found to be accelerated when the temperature of the water was increased.

It was therefore thought to be necessary to examine the diffusion properties of the rubber-modified and unmodified adhesive systems used in the present work, in order to identify in more detail the manner by which the concentration and the rate of water ingress affect the observed losses in joint strength.

5.2 WATER UPTAKE DATA

The diffusion data collected from the tests performed using the bulk adhesive samples is shown in Figures 5.1 to 5.6 in the form of plots of the per cent change in the weight of the specimens, $(W_t-W_o)/W_o$ %, where W_t is the weight of the sample at time t_d and W_o the initial weight, against $t_d^{1/2}/t$, where t_d is the time of exposure to distilled water at different temperatures and t is the thickness of the samples. The results shown for any material/temperature are from four replicate tests and, as may be seen, there is very little experimental scatter. The sorption curves obtained in this study were initially linear and therefore the sorption process was assumed to be Fickian up to $(W_t-W_o)/W_o$ =0.5 for the unmodified adhesive at 25°C and $(W_t-W_o)/W_o$=0.7 for the rubber-modified adhesive at the same temperature. As the temperature of the distilled

water was increased, the value of the parameter $(W_t-W_0)/W_0$ up to which the sorption process was Fickian also increased. The values were found to be 0.7 and 1.2 for the unmodified material at 40°C and 55°C respectivelly, and 0.8 and 1.6 for the rubber-modified material approximately. The linear parts of the graphs in Figures 5.1, 5.2, 5.3, and 5.4 were found to be followed by a non-linear transition zone leading to an equilibrium plateau region. The same phenomenon was observed with the data in Figures 5.5 and 5.6, i.e. for the rubber-modified material at 40°C and 55°C respectively, but this time a second slow uptake step was evident which eventually led to equilibrium. This step was found to occur after about 75.5 days when the material had been exposed to distilled water at 40°C, and after 74.5 days for exposure to distilled water at 55°C, i.e. the same time period in both cases. The second water uptake process when the material had been exposed to distilled water at 55°C, was found to occur at a faster rate than that at 40°C. The duration of the second uptake process was found to be approximately the same at the two temperatures, 69.5 days for the material exposed to 40°C and 62 days for exposure at 55°C.

Previous work by J. Comyn and his coworkers (1980) involving epoxide adhesives, reached similar conclusions, namely, that the epoxide resins examined exhibited Fickian diffusion and in most cases a water uptake equilibrium had been attained, thus confirming the results of the present investigation. A second slow water uptake step has also been found by the same investigators for a commercial liquid resin consisting largely of the diglycidyl ether of bisphenol A cured with DDM hardener (4,4'-diaminodiphenyl methane) and exposed to distilled water at 100°C. In the present studies the fact that only the rubber-modified adhesive shows this second slow water uptake step points to the presence of the second phase rubber particles as being responsible for this observation.

5.3 CALCULATIONS OF DIFFUSION AND SOLUBILITY COEFFICIENTS

5.3.1 Equations

The concentration of water at time t_d, C_t, in the bulk material may be related to the concentration at equilibrium, C_∞, with the equation for a Fickian process by:

$$C_t/C_\infty=1-(4/\pi)\sum\{(-1)^n/(2n+1)\}\exp\{-D(2n+1)^2\pi^2t_d/t^2\}\cos\{(2n+1)\pi x/t\} \qquad (5.1)$$

where t is the depth of the layer, x is the depth from the layer's boundary given by $0\geq x\geq t/2$ and assuming that the initial concentration of water in the layer is zero. Integrating the above equation to give the total water content gives:

$$(W_t-W_o)/W_o=(4D^{1/2}t_d^{1/2})/(t\pi^{1/2}/2)=(4D^{1/2}/\pi^{1/2})(2t_d^{1/2}/t) \qquad (5.2)$$

The slope of the linear part of the data in Figures 5.1 to 5.6 therefore gives the value of the coefficient of diffusion since:

$$\text{slope of line}= 4D^{1/2}/\pi^{1/2} \qquad (5.3)$$

5.3.2 Values of Diffusion and Solubility Coefficients

The values of the water concentration at equilibrium, C_∞, were estimated from the Figures 5.1 to 5.6 by determining the equilibrium plateau of each material. For the unmodified material at 25°C, C_∞ was found to be about 0.905 %W/W and for the rubber-modified at the same temperature was about 1.142 %W/W. The value of C_∞ increased with increasing the temperature of the distilled water for both rubber-modifed and unmodified materials. For the unmodified material, C_∞ increased from 1.450 %W/W at 40°C to 1.720 %W/W at 55°C, and for the rubber-modified material, the increase was

estimated to be 1.700 %W/W at 40°C to 3.340 %W/W at 55°C. Thus the solubility of distilled water in the adhesive systems examined has been found to depend on temperature. Previous similar work by J. Comyn et al (1980, 1987) has found that the solubility of water in some epoxides was independent of the temperature of the water and that water solubilities might have increased or decreased.

Table 5.1 shows the values of the diffusion coefficients and equilibrium uptake levels of distilled water in the epoxide resins investigated at different temperatures. In all cases the coefficient of diffusion has been found to increase with increasing temperature. Similar results have been obtained by J. Comyn et al (1980, 1987) and they concluded that the diffusion process in the epoxide resins may be an activated-rate process. However, the increase in the diffusion coefficient in the rubber-modified material has been found to be higher than that in the unmodified material, probably due to the existence of the secondary rubbery phase. The effect of the rubber particles on the properties of the epoxide resin may therefore be to increase the amount of water uptake by the material.

Figures 5.7 and 5.8 show the variation of the diffusion coefficient of the unmodified and rubber-modified materials with immersion temperature of the distilled water. The data in these Figures has been plotted as lnD against 1/T, where T was the temperature in degrees Kelvin. The diffusion coefficient D, according to J. Crank et al (1968) and J. Crank (1956), may be related to the activation energy for diffusion, E_D, and to the temperature, T, with the equation:

$$D=D_0 \exp(-E_D/RT) \qquad (5.4)$$

where D_0 is a constant and R is the gas constant, R=8.31 J K^{-1} mol^{-1}. The slope of the lines in Figures 5.7 and 5.8 may therefore be given by:

$$\text{slope of line} = E_D/R \qquad (5.5)$$

and hence, values for the activation energies for diffusion for the two materials under investigation may be calculated. For the unmodified material E_D was found to be 77 kJ/mol, and for the rubber-modified material an activation energy of 92.2 kJ/mol was estimated. It can be seen that the activation energy for the rubber-modified material was found to be greater than that of the unmodified material. J. Comyn and his coworkers (1987) found that the activation energies of most epoxides examined in their studies were of a similar order of magnitude of around 70 kJ/mol. Figure 5.9 shows a comparison between the data in Figures 5.8 and 5.7. It can be seen that the slope of the line for the rubber-modified material is greater than that of the unmodified material, indicating that the sorption process in the unmodified adhesive may be accelerated with the introduction of the secondary rubbery phase.

5.3.3 Water Ingress into Joints

The experimentally measured diffusion coefficient may be used to calculate the concentration of water at any point within a joint, and also to estimate the total amount of water absorbed at any time. The glue line of the double-torsion joints may be regarded as an infinitely long rectangle of thickness t. Figure 5.10(a) shows a proposed model for the double-torsion joint glue line coordinate system. Water may enter from x and y directions as shown. No water may penetrate through the metallic substrates. It may also be assumed that, since t is much less than the length l of the glue line, one dimensional water penetration takes place in the x-direction. Figure 5.10(b) shows a proposed model for the butt joint glue line coordinate system. Water may enter from the x direction only as shown. No water may penetrate through the metallic substrates. The solution to Fick's second law of diffusion for sorption by a semi-infinite area in an infinite bath, according to J. Crank (1956) and J. Crank et al (1968), may be taken to be given by the equation:

$$C_t/C_\infty=1-(4/\pi)\sum\{(-1)^n/(2n+1)\}\exp\{-D(2n+1)^2\pi^2t_d/t^2\}\cos\{(2n+1)\pi x/t\} \qquad (5.6)$$

where t was the length of the adhesive layer that the water has to penetrate, x is the depth from the layer's boundary given by $0\leq x\leq t/2$ and assuming that the initial concentration of water in the layer is zero. C_t is the concentration of water within the adhesive layer at time t_d and C_∞ is the concentration at saturation point. The above equation may be assumed to be valid for the double-torsion joints. A computer programme was writen to solve equation (5.6) where n was allowed to take the values of 0, 1, 2, 3...etc, until the difference between successive terms was less than 10^{-5}. The results are shown in Figures 5.11 and 5.12 for the unmodified and rubber-modifed DT adhesive joints at 25°C and in Figures 5.13 and 5.14 for a temperature of 40°C and in Figures 5.15 and 5.16 for 55°C. These Figures show the variation of the concentration of water into the DT adhesive joint, C_t, with distance into the joint from the centre of the adhesive layer to the edge at different time intervals. It can be seen that, as the immersion time increases, the concentration of water into the adhesive layer of the joints also increases. Figures 5.17, 5.18, and 5.19 show a comparison between the unmodified and rubber-modified DT adhesive joints at 25°C, 40°C, and 55°C respectively. These Figures suggest that the rubber-modified DT adhesive joints adsorbed water at faster rates than the unmodified joints for the same immersion times.

Turning to the butt joints, then the appropriate equation for water diffusing into a cylindrical adhesive layer, Figure 5.10(b), may be given by, Crank (1973):

$$C_t/C_\infty=1-(2/r)[\sum(1/r_n)\{J_o(xr_n)/J_1(rr_n)\}\exp(-Dr_n^2t_d)] + (2/r^2)\sum\exp(-Dr_n^2t_d)\{J_o(xr_n)/J_1^2(rr_n)\}\int xf(x)J_o(xr_n)dx \qquad (5.7)$$

where r is the radius of the cylindrical adhesive layer, x is the distance into the layer, and $J_o(x)$ and $J_1(x)$ are the Bessel functions of zero and first order respectively. The

boundary conditions for equation (5.7) require the initial concentration of water to be zero at the surface where x=r at time $t_d \geq 0$, and at distance defined as $0<x<r$ the concentration is a function of distance x, i.e:

$$C = 0 \quad \text{at} \quad x = r \quad \text{and} \quad t_d \geq 0 \tag{5.8}$$

$$C = f(x) \quad \text{for} \quad 0<x<r \quad \text{at} \quad t_d = 0 \tag{5.9}$$

Now these equations may be used (J. Crank, 1973) to model the concentration, C_t, at any time, t_d, into the cylindrical adhesive layer of the butt joint. Figures 5.20 and 5.21 show some typical results obtained at 25°C for the unmodified and rubber-modified butt adhesive joints respectively. These Figures show the variation of the concentration of water into the butt adhesive joint, C_t, with distance into the joint from the centre of the adhesive layer to the edge at different time intervals. It can be seen that, as the immersion time increases, the concentration of water into the cylindrical adhesive layer of the butt joints also increases.

5.4 SUMMARY

A method for studying water uptake by epoxide resins has been described and used for an unmodified epoxide resin and for a rubber-modified epoxide resin in order to examine the effect of the rubber particles on the epoxide material. The method, which has been well established by J. Comyn et al (1987, 1980), involved immersion of bulk samples of the adhesives in distilled liquid water with periodic removal for weighing. The epoxide resins examined in this investigation exhibited Fickian diffusion and a water equilibrium value was attained, as reported by J. Comyn et al (1987, 1980). The activation energies for diffusion were estimated and it has been suggested that the possible effect of the rubber particles on the epoxide material is to increase the rate of water uptake. Finally,diffusion models for double-torsion and butt adhesive joints have been described and used to model the penetration of water into the adhesive layer.

Table 5.1: Diffusion coefficients and equilibrium uptake levels of distilled water at different temperatures in the adhesives examined in the present investigation

Adhesive	Temperature	Diffusion coefficient	Equilibrium concentration
	(°C)	($D/10^{-7}$ mm^2/sec)	(C_∞% W/W)
unmodified	25	1.00	0.905
	40	1.96	1.450
	55	17.67	1.720
rubber-modified	25	1.03	1.142
	40	7.85	1.700
	55	31.42	3.340

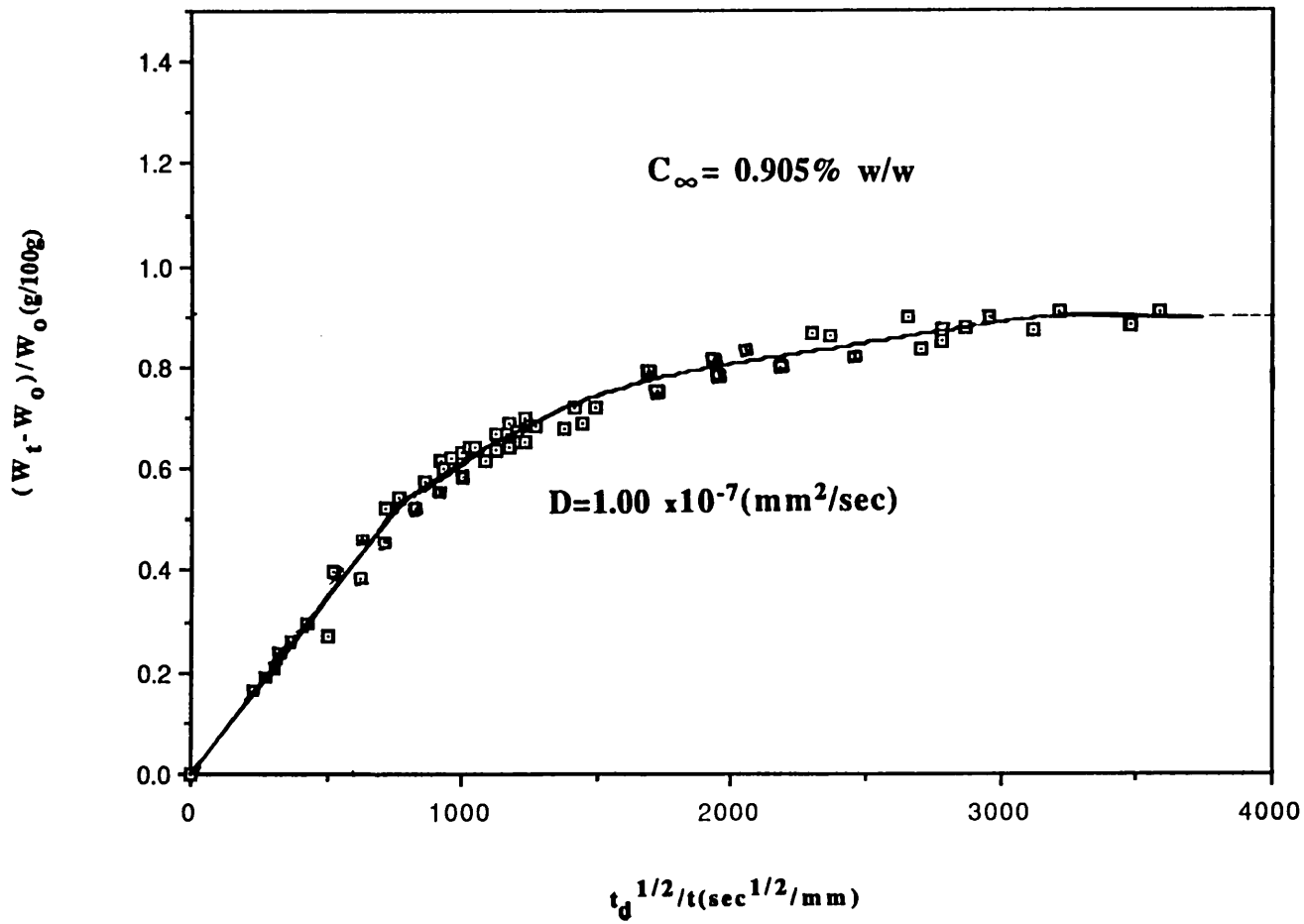


Figure 5.1: Water uptake $(W_t-W_0)/W_0$ % plotted against $(time)^{1/2}/(thickness)$ for unmodified bulk adhesive specimens immersed in distilled water at 25C, where t is the sample thickness and t_d the time (points shown are from four replicates)

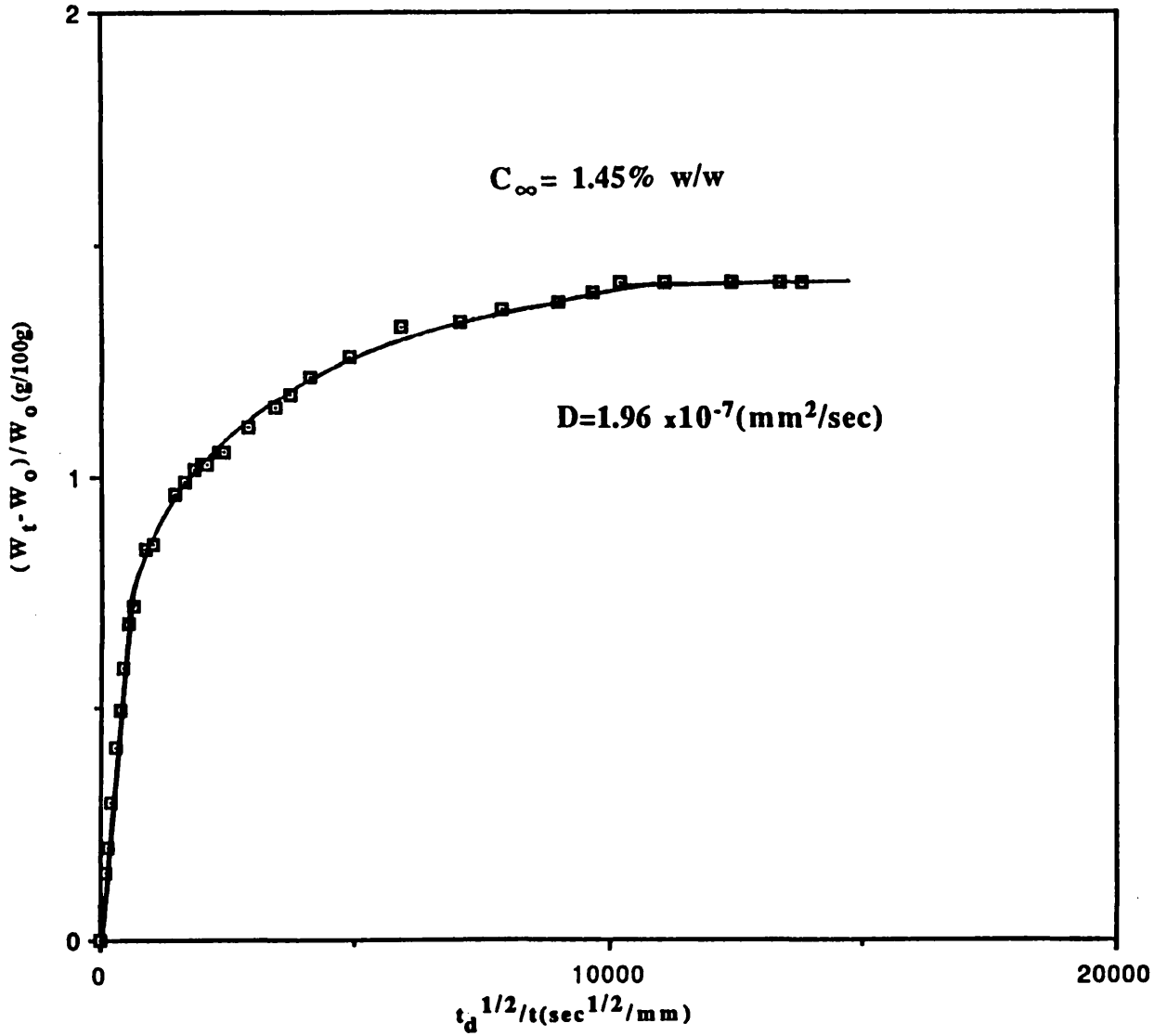


Figure 5.2: Water uptake $(W_t-W_0)/W_0$ % plotted against $(\text{time})^{1/2}/(\text{thickness})$ for unmodified bulk adhesive specimens immersed in distilled water at 40°C, where t is the sample thickness and t_d the time

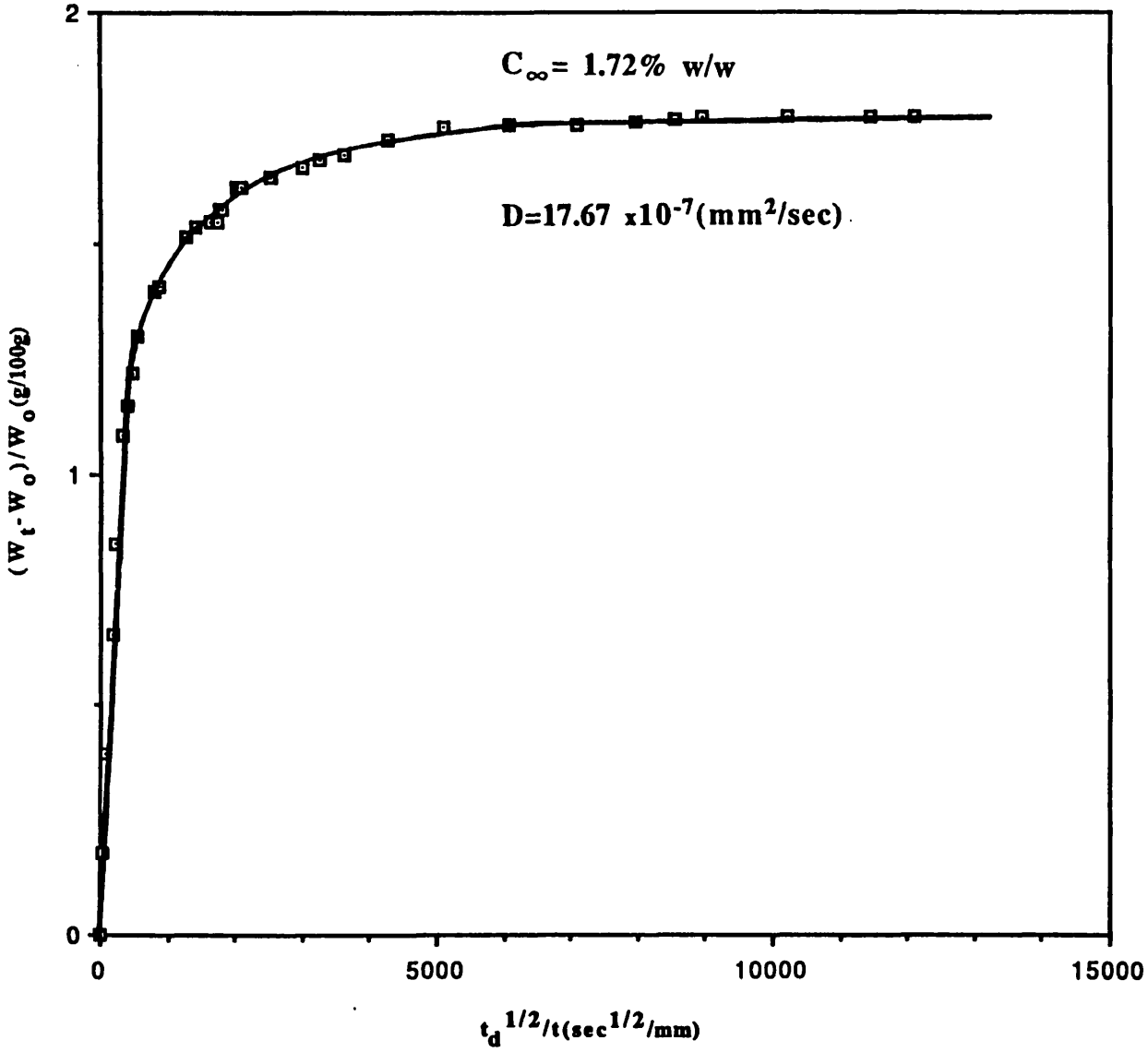


Figure 5.3: Water uptake $(W_t-W_o)/W_o$ % plotted against $(time)^{1/2}/(thickness)$ for unmodified bulk adhesive specimens immersed in distilled water at 55°C, where t is the sample thickness and t_d the time

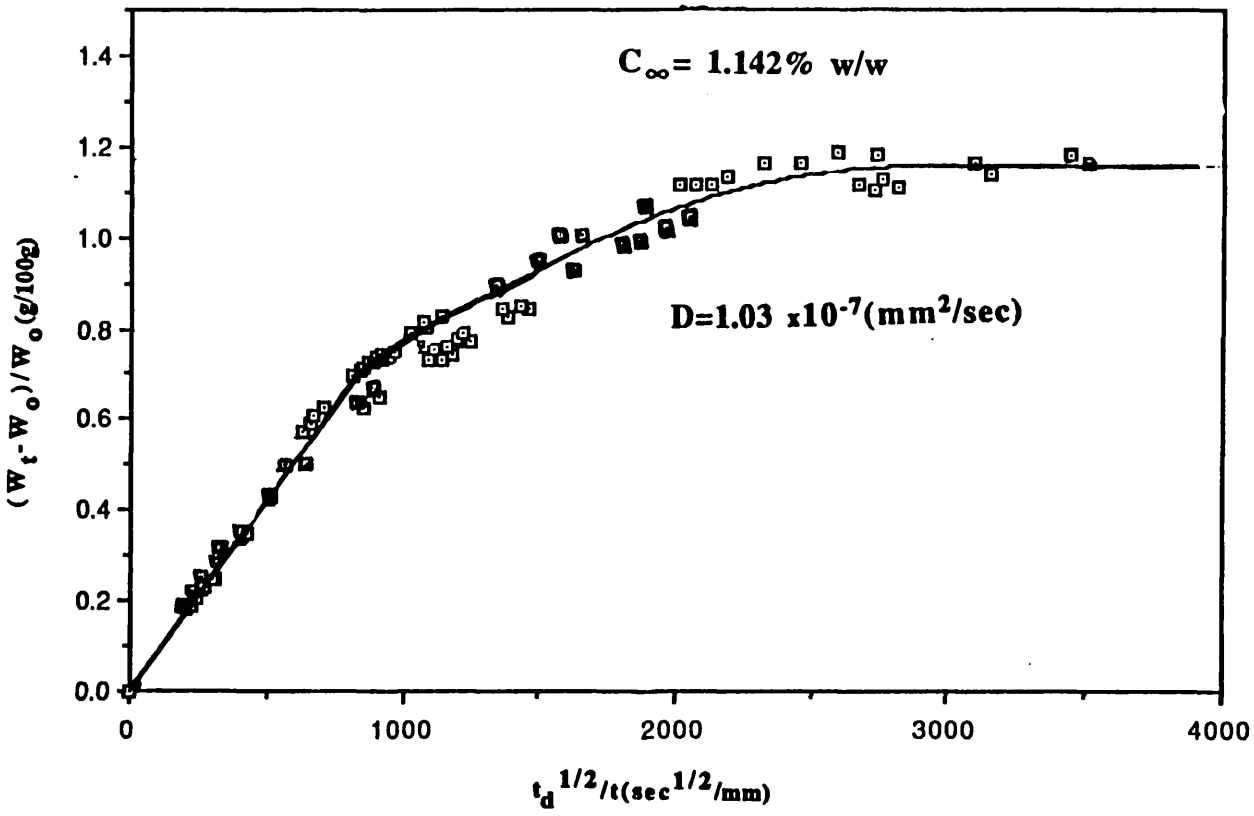


Figure 5.4: Water uptake $(W_t-W_0)/W_0$ % plotted against $(time)^{1/2}/(thickness)$ for rubber-modified bulk adhesive specimens immersed in distilled water at 25°C, where t is the sample thickness and t_d the time

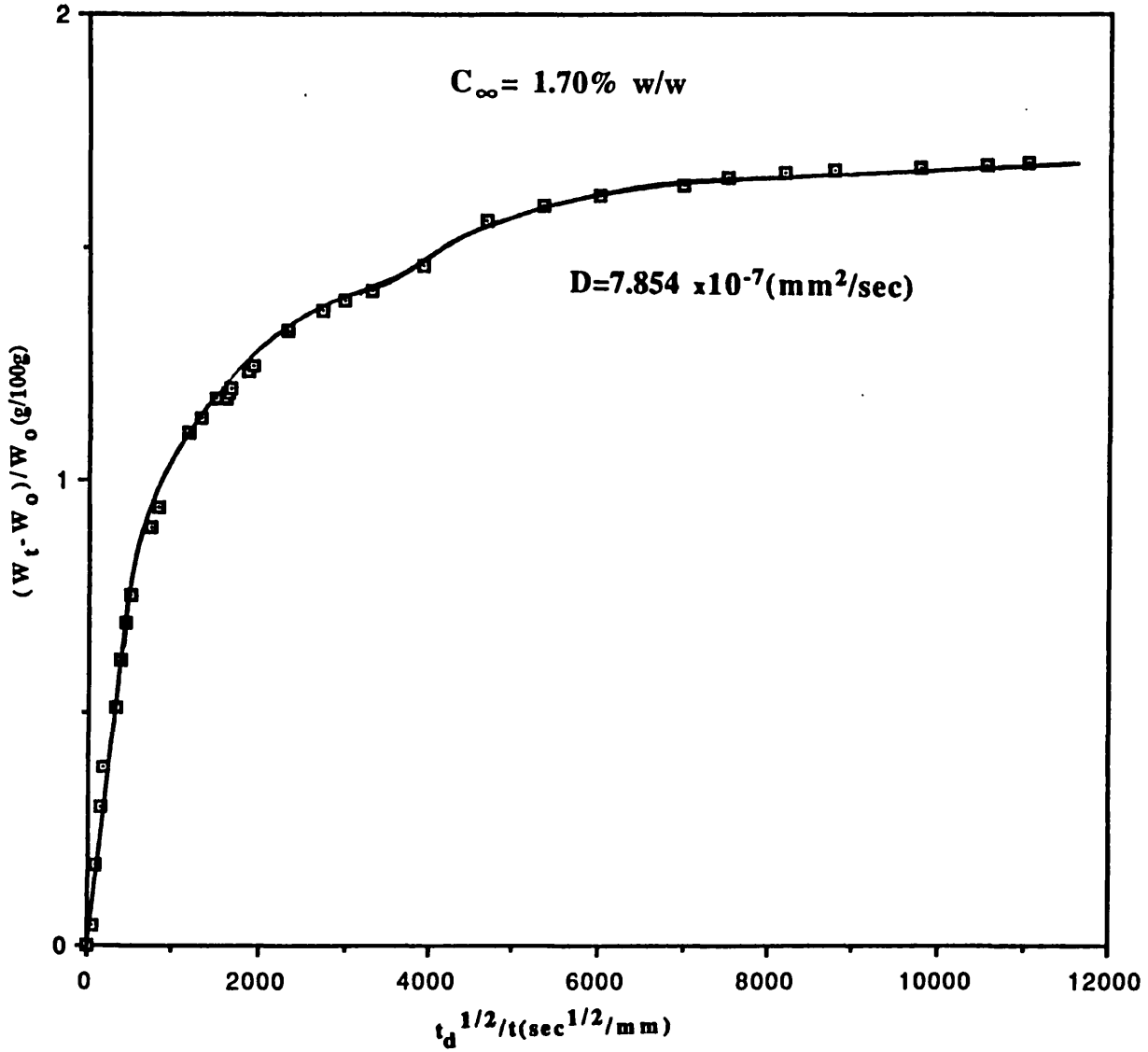


Figure 5.5: Water uptake $(W_t-W_0)/W_0$ % plotted against $(time)^{1/2}/(thickness)$ for rubber-modified bulk adhesive specimens immersed in distilled water at 40°C, where t is the sample thickness and t_d the time

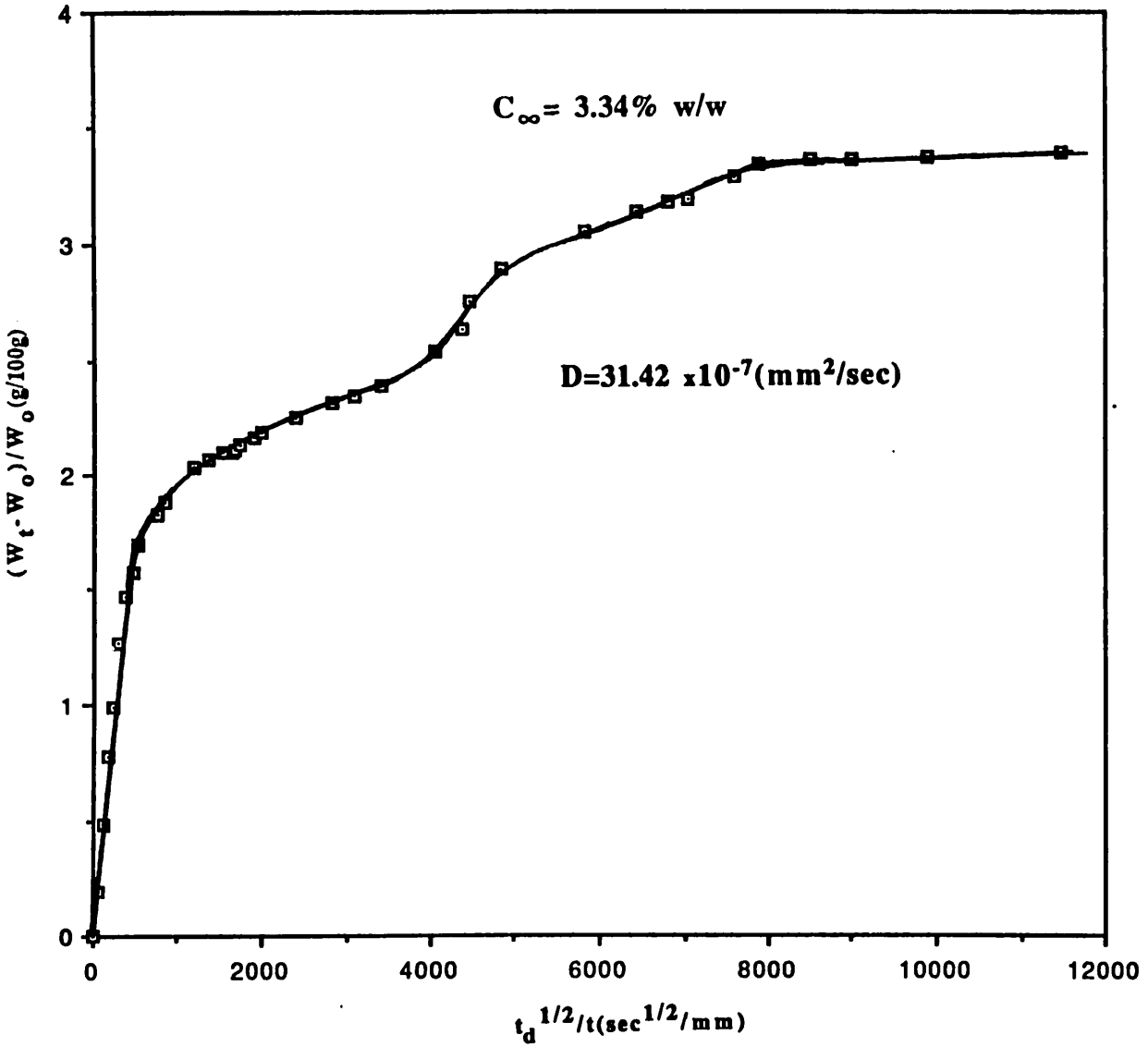


Figure 5.6: Water uptake $(W_t-W_0)/W_0$ % plotted against $(\text{time})^{1/2}/(\text{thickness})$ for rubber-modified bulk adhesive specimens immersed in distilled water at 55°C, where t is the sample thickness and t_d the time

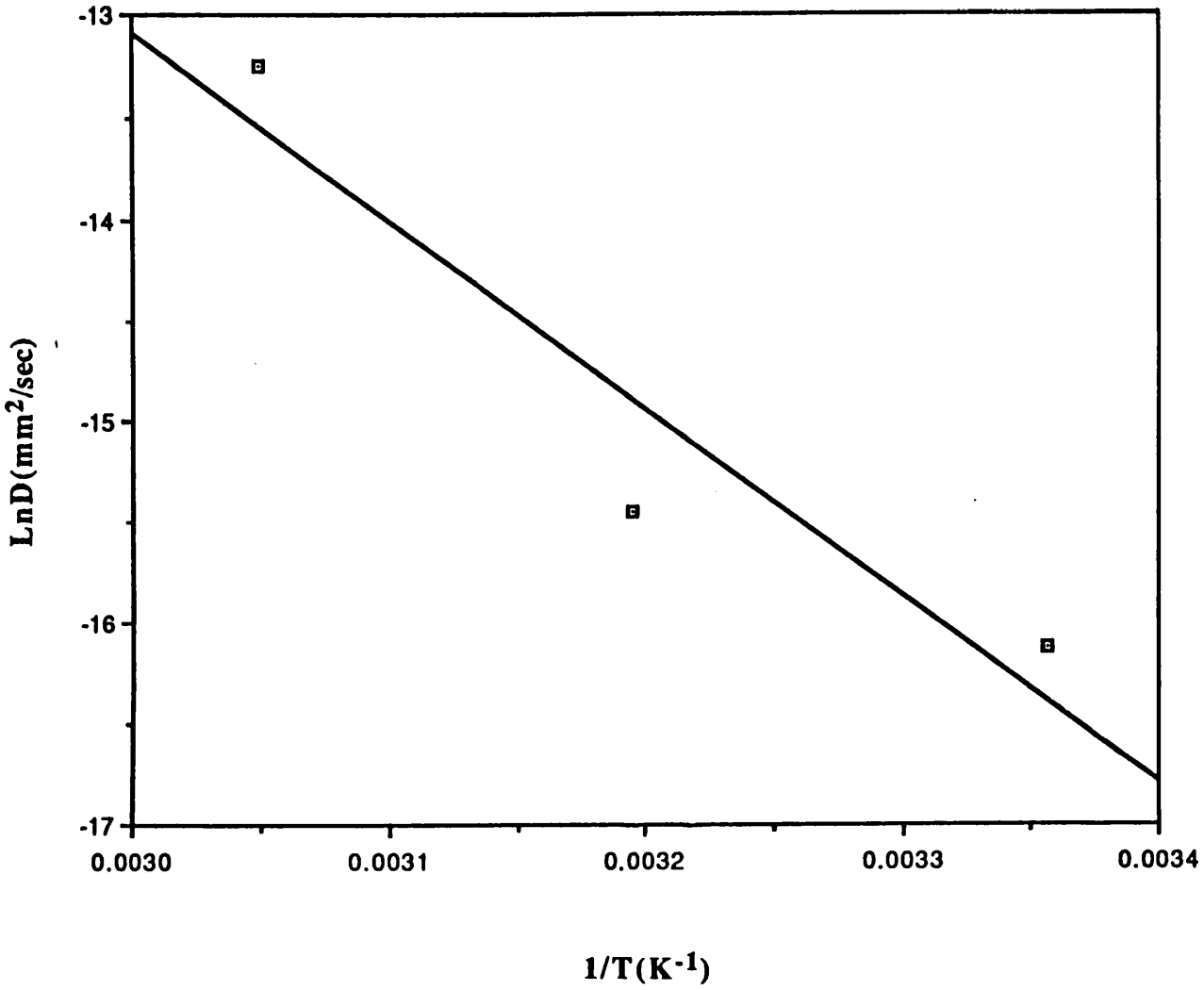


Figure5.7: Plot of the natural logarithm of the diffusion coefficient, lnD, against the reciprocal of the temperature in degrees Kelvin, 1/T, for the unmodified material.

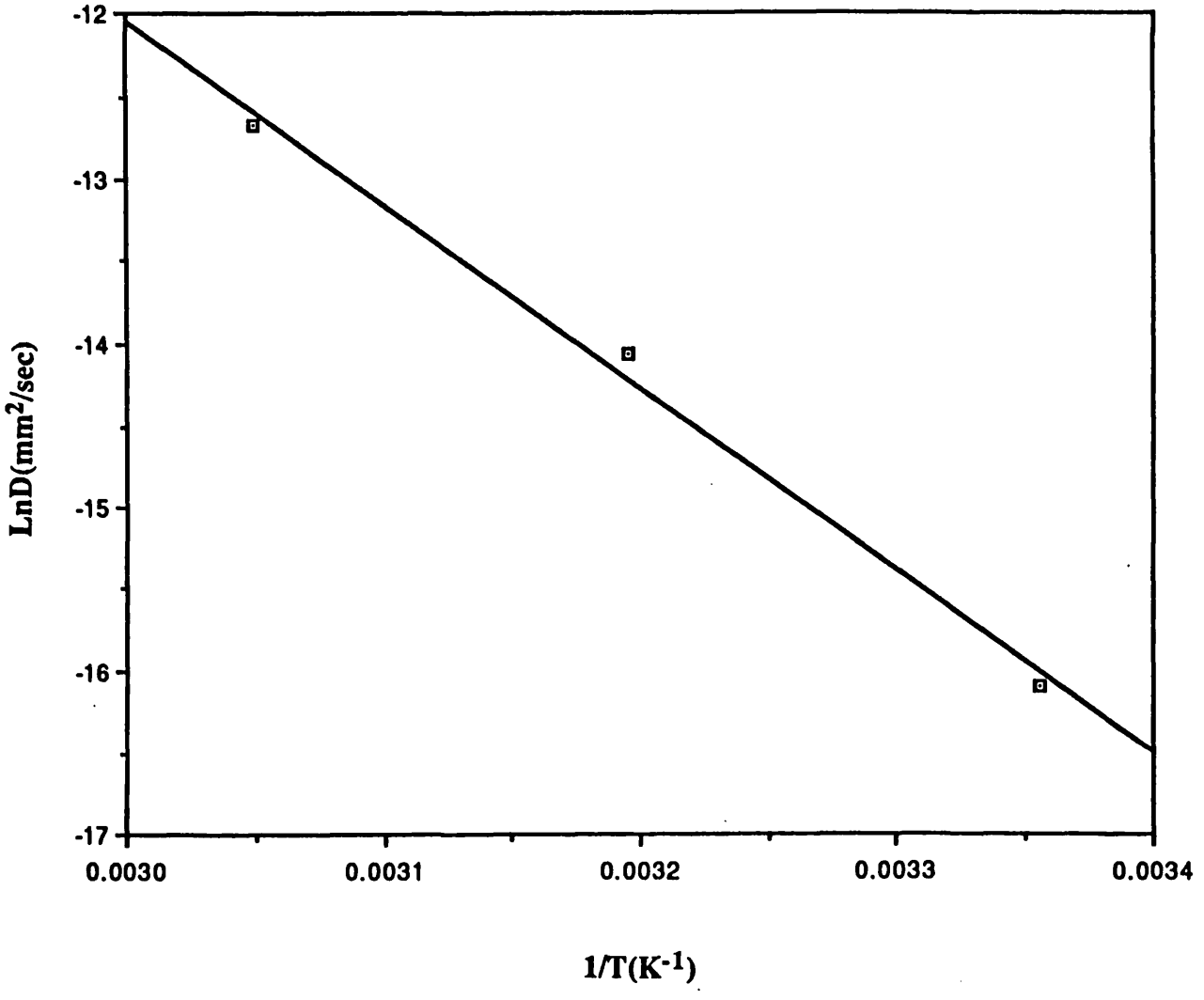


Figure5.8: Plot of the natural logarithm of the diffusion coefficient, lnD, against the reciprocal of the temperature in degrees Kelvin, 1/T, for the rubber-modified material.

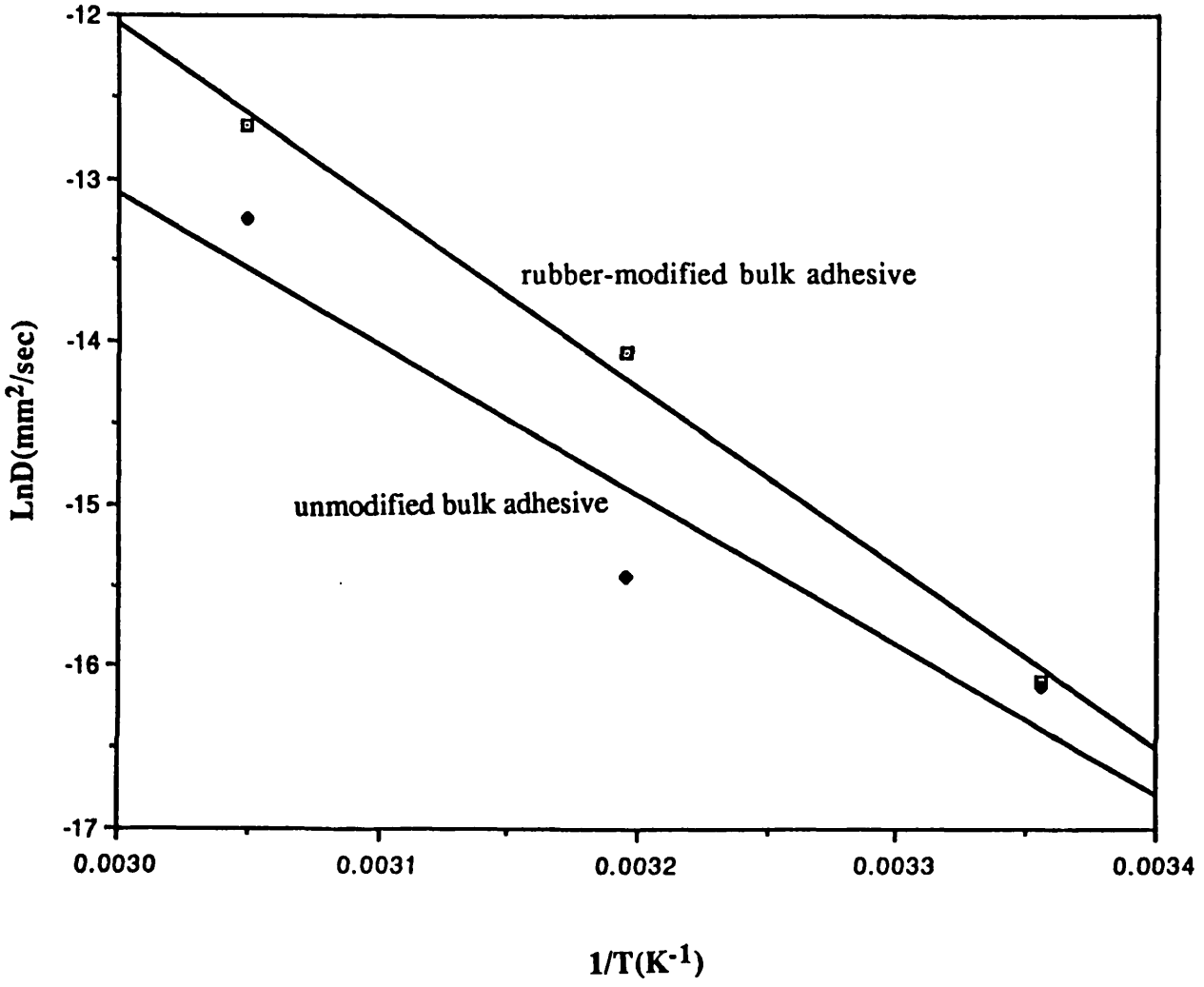


Figure5.9: A comparison between the data obtained in Figures 5.7 and 5.8 for the adhesives studied in the present investigation

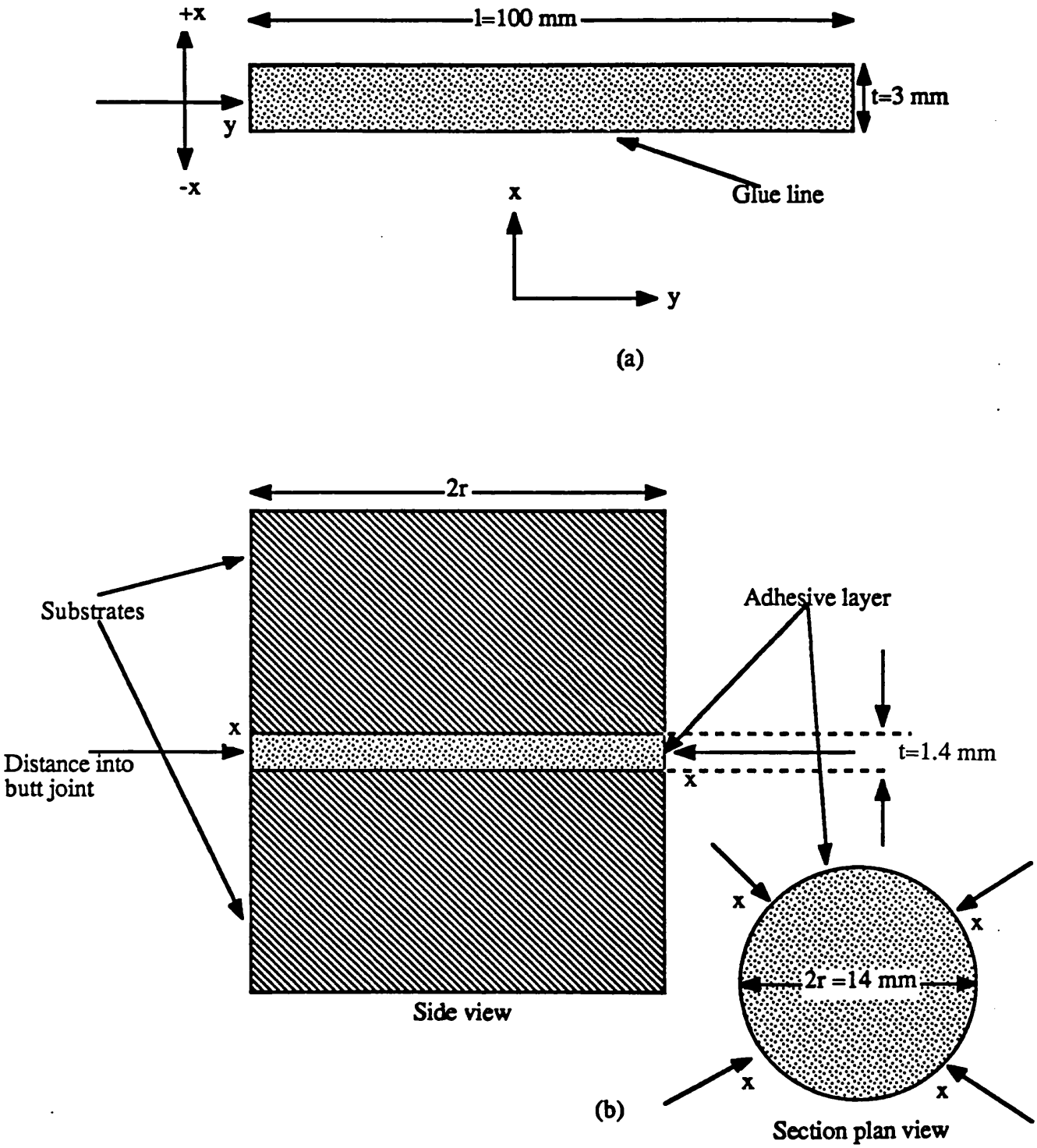


Figure 5.10: Proposed diffusion models in the adhesive layer for the double-torsion (a) and butt (b) adhesive joints studied in the present investigation

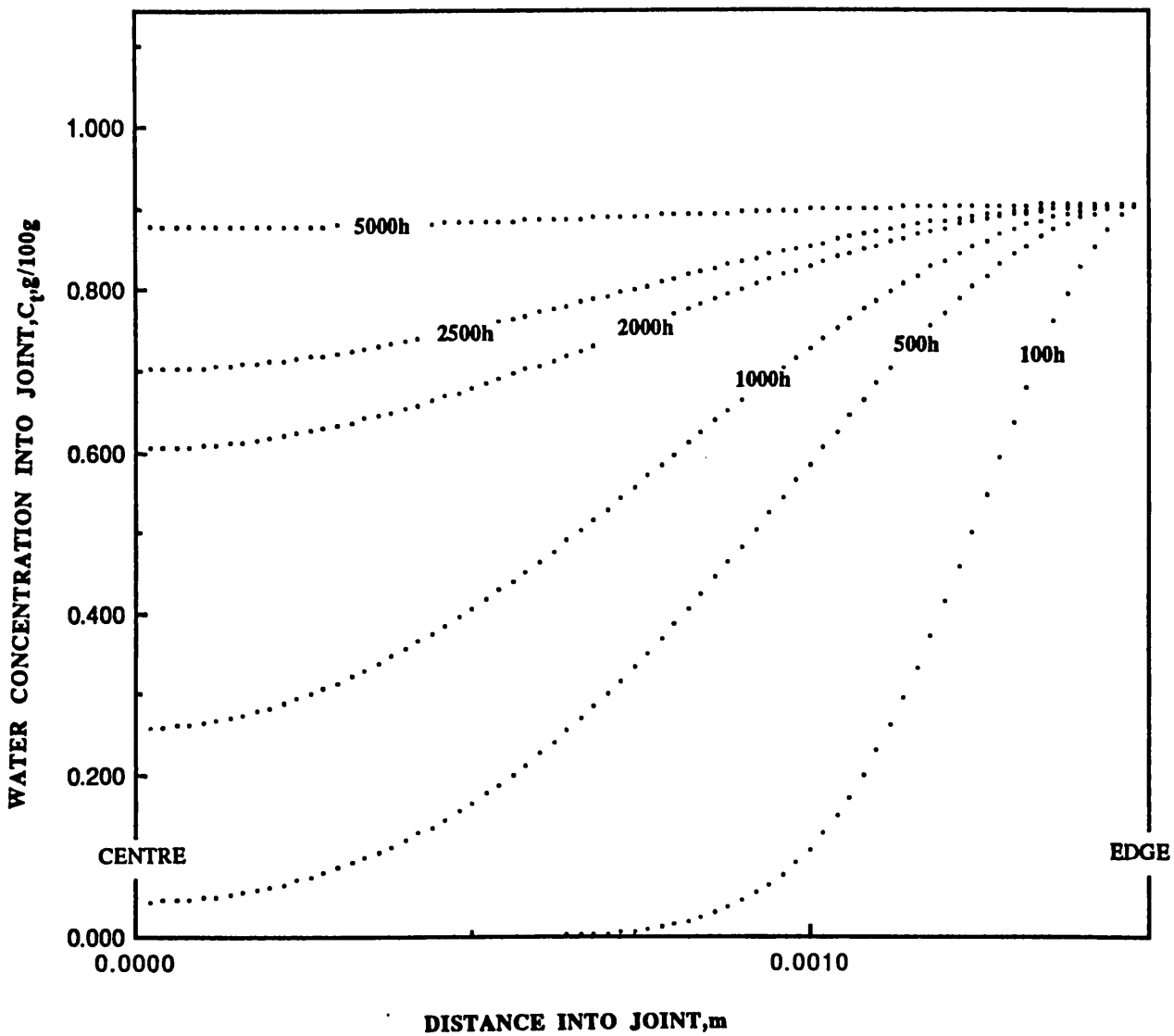


Figure 5.11: Water concentration, C_t, in adhesive layer as a function of time, t_d, and penetration depth, x, for unmodified DT adhesive joints immersed in distilled water at 25°C

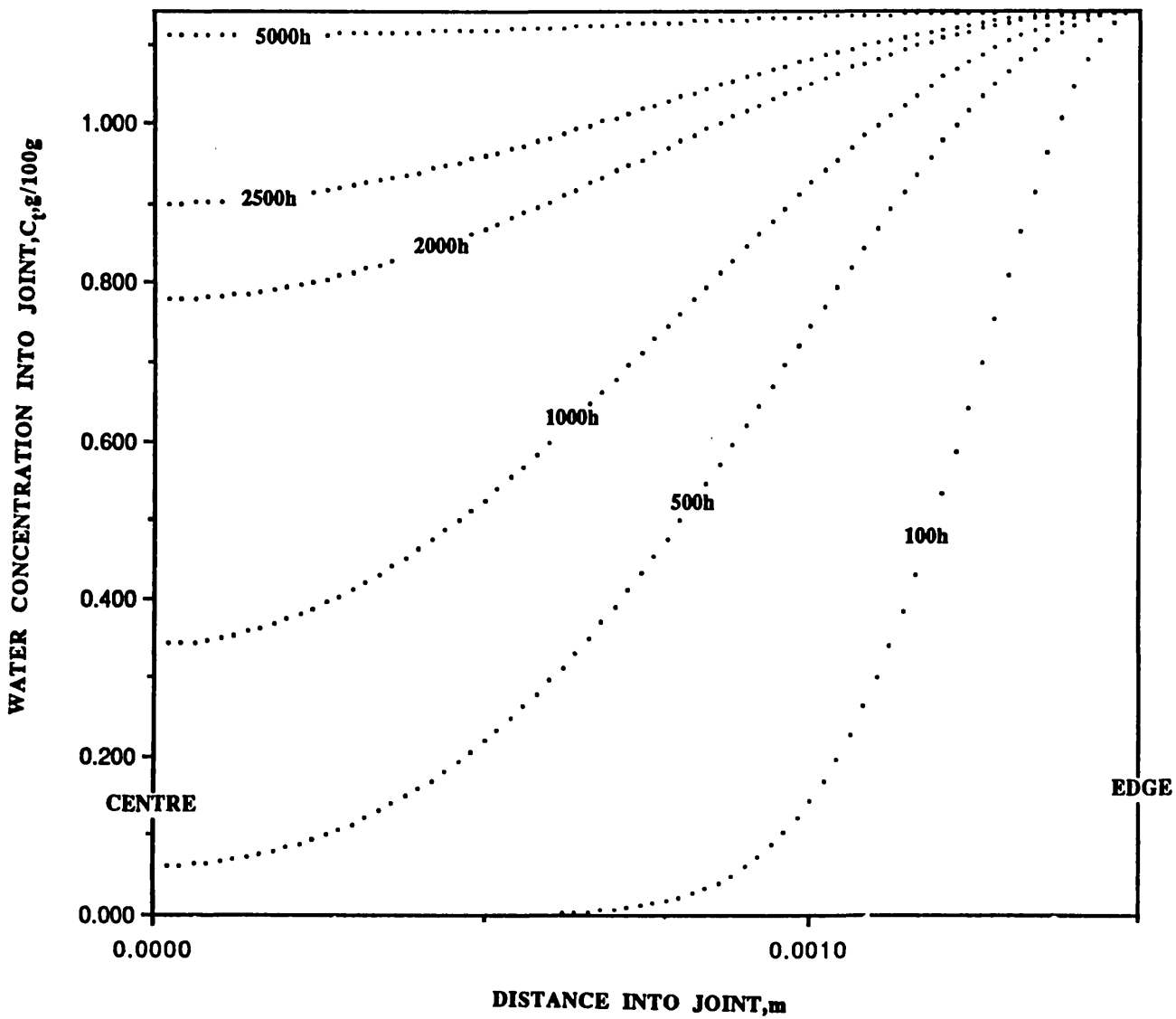


Figure 5.12: Water concentration, C_t, in adhesive layer as a function of time, t_d, and penetration depth, x, for rubber-modified DT adhesive joints immersed in distilled water at 25°C

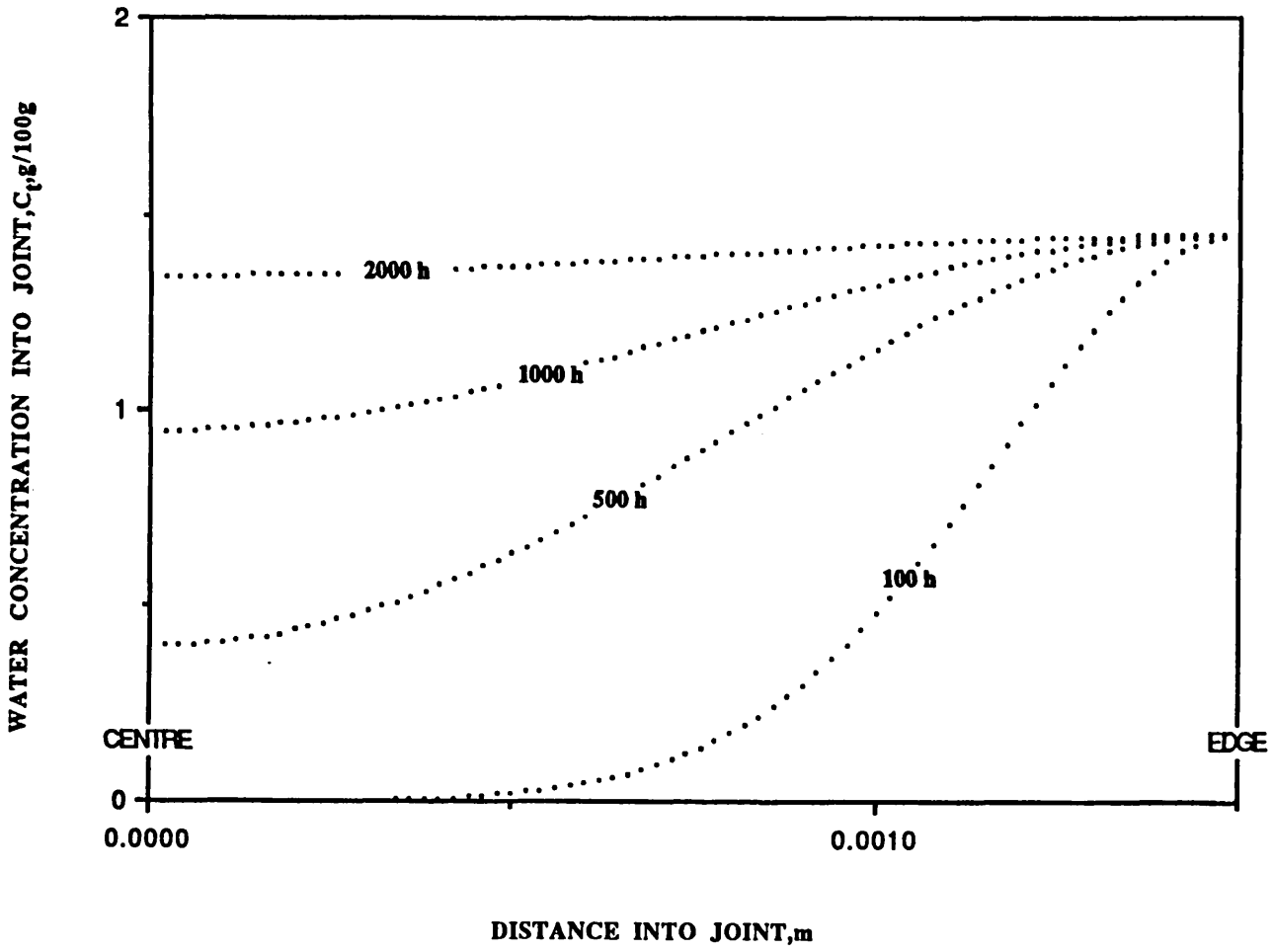


Figure 5.13: Water concentration, C_t, in adhesive layer as a function of time, t_d, and penetration depth, x, for unmodified DT adhesive joints immersed in distilled water at 40°C

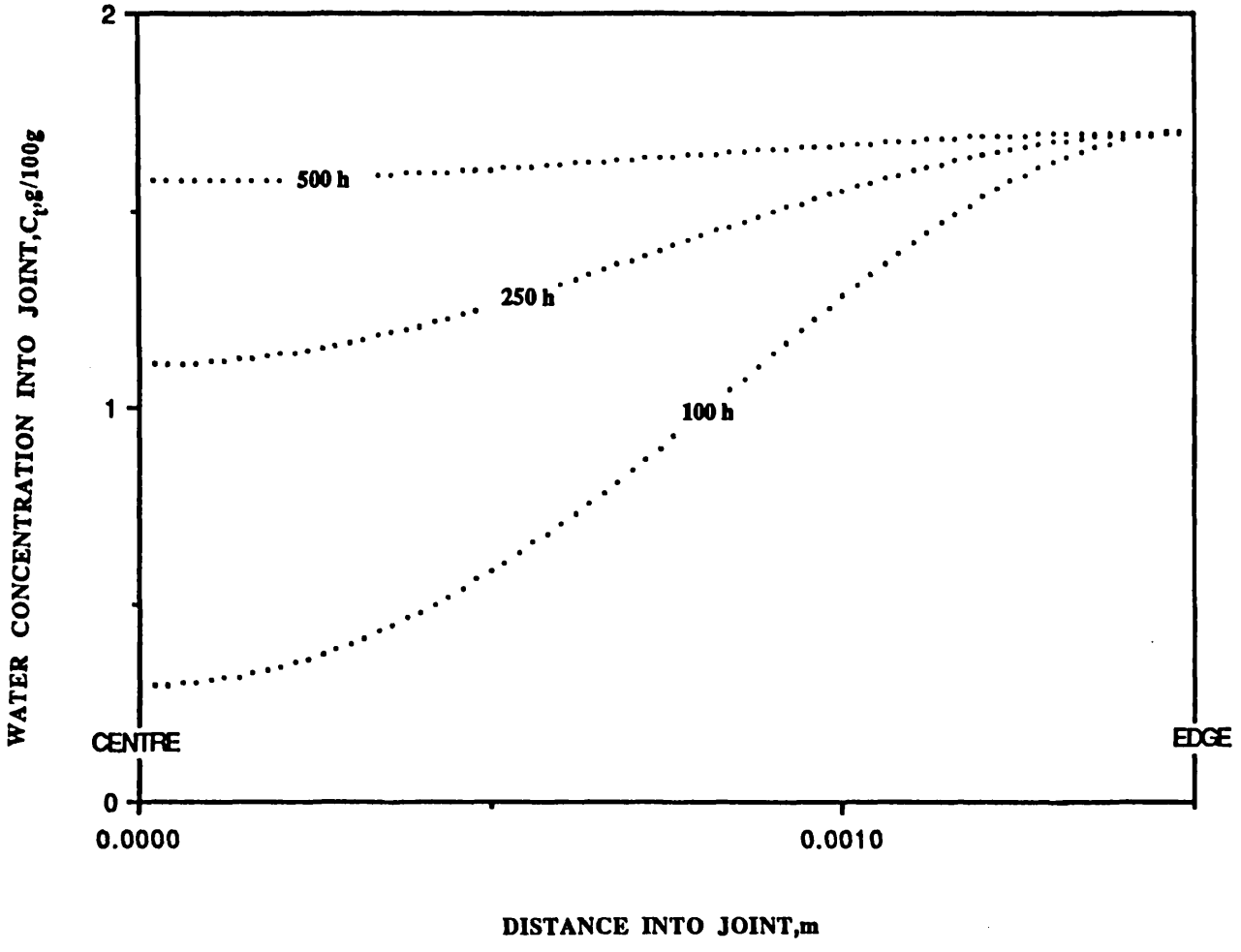


Figure 5.14: Water concentration, C_t, in adhesive layer as a function of time, t_d, and penetration depth, x for rubber-modified DT adhesive joints immersed in distilled water at 40°C

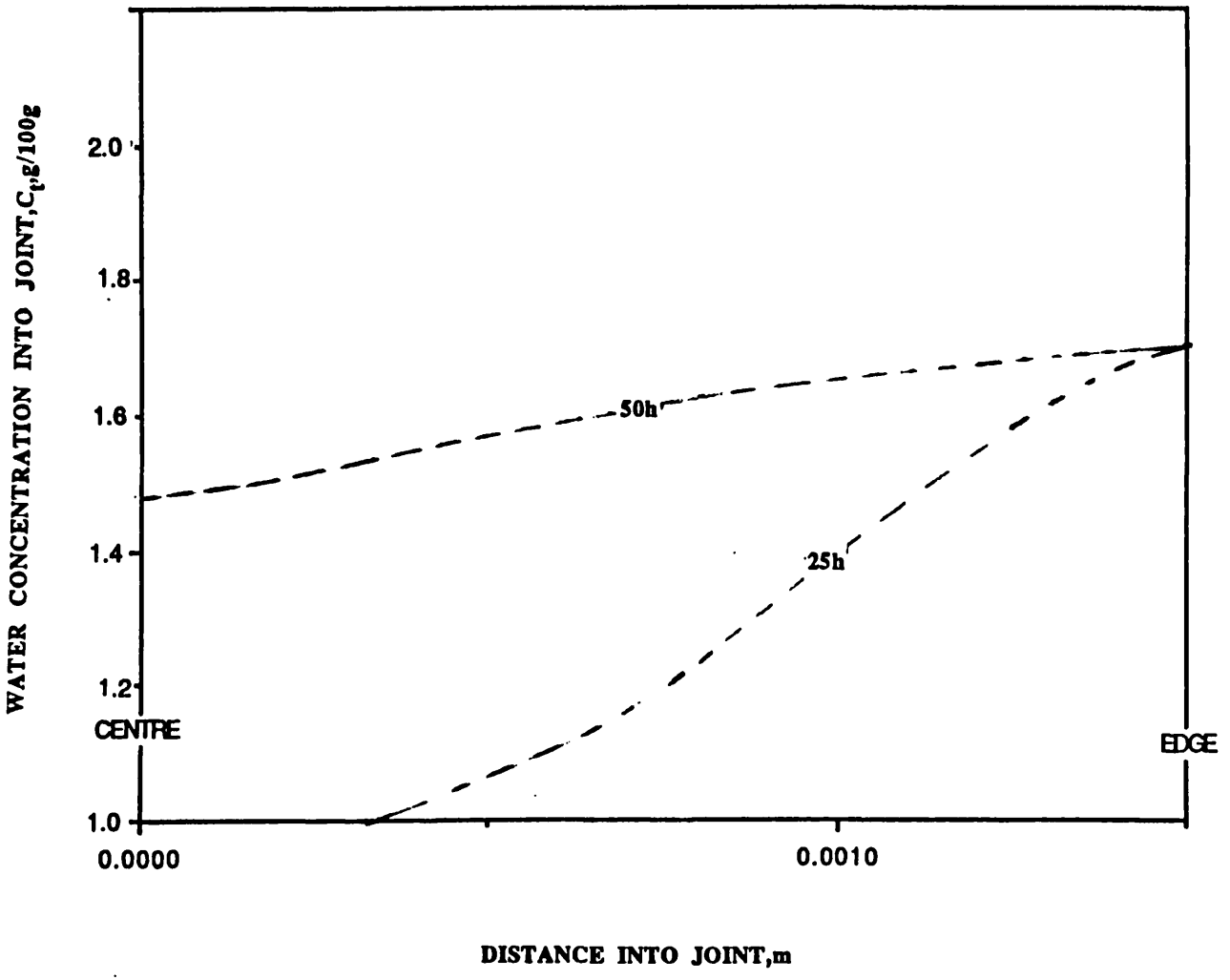


Figure 5.15: Water concentration, C_t, in adhesive layer as a function of time, t_d, and penetration depth, x, for unmodified DT adhesive joints immersed in distilled water at 55°C

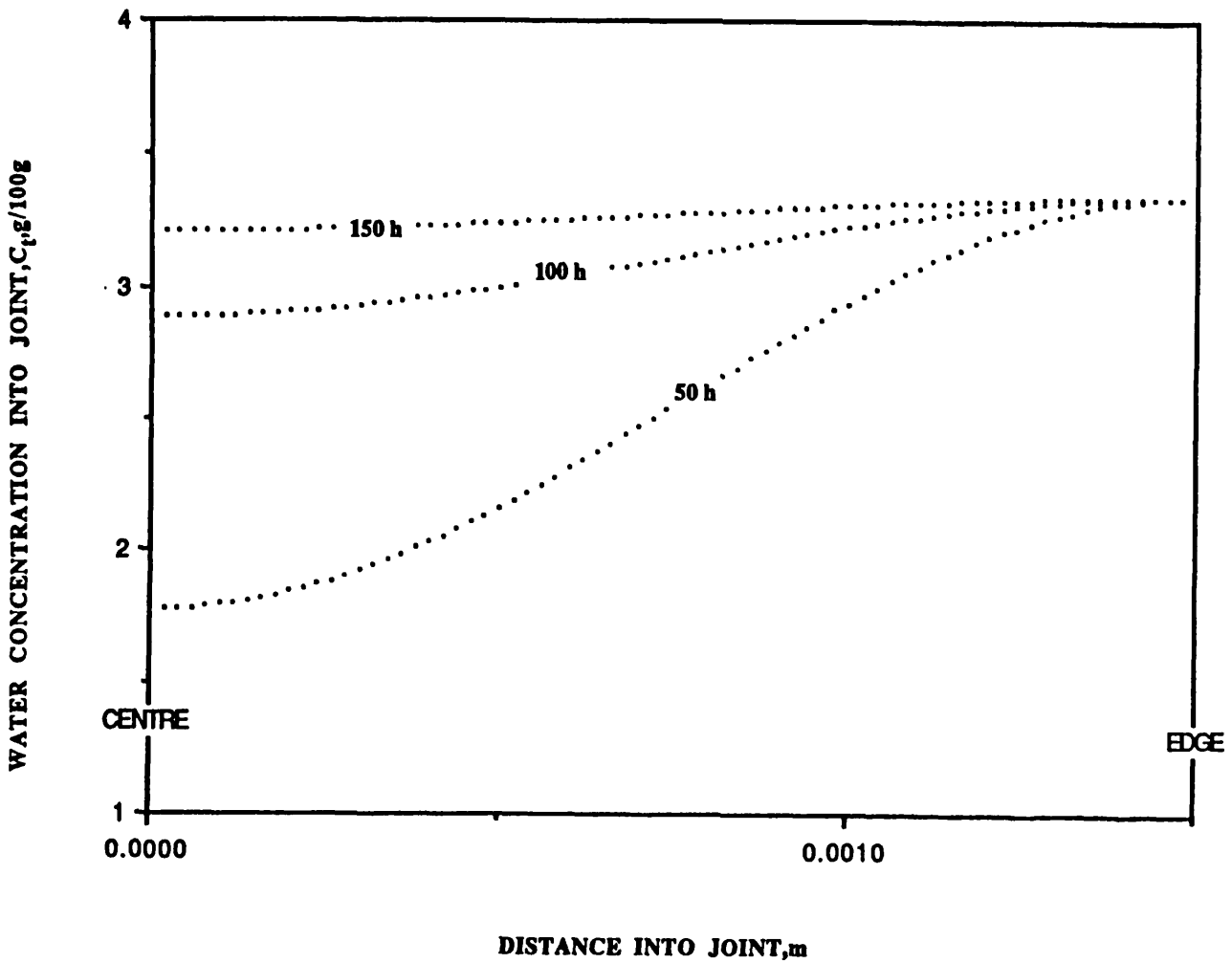


Figure 5.16: Water concentration, C_t, in adhesive layer as a function of time, t_d, and penetration depth, x, for rubber-modified DT adhesive joints immersed in distilled water at 55°C

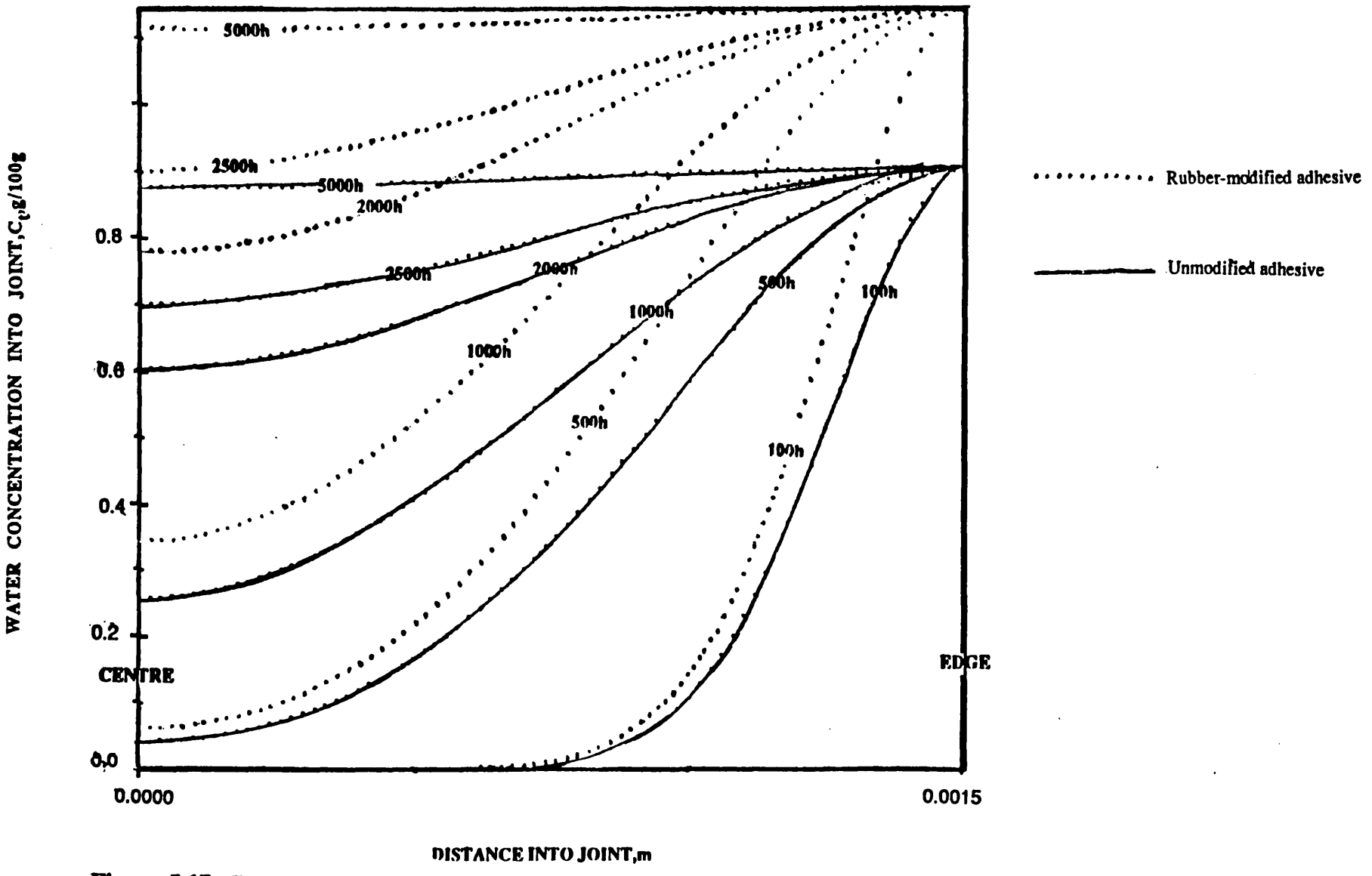


Figure 5.17: Comparison of water concentration in adhesive layer, C_t, as a function of time ,t_d, and penetration depth, x, between rubber-modified and unmodified DT adhesive joints immersed in distilled water at 25°C

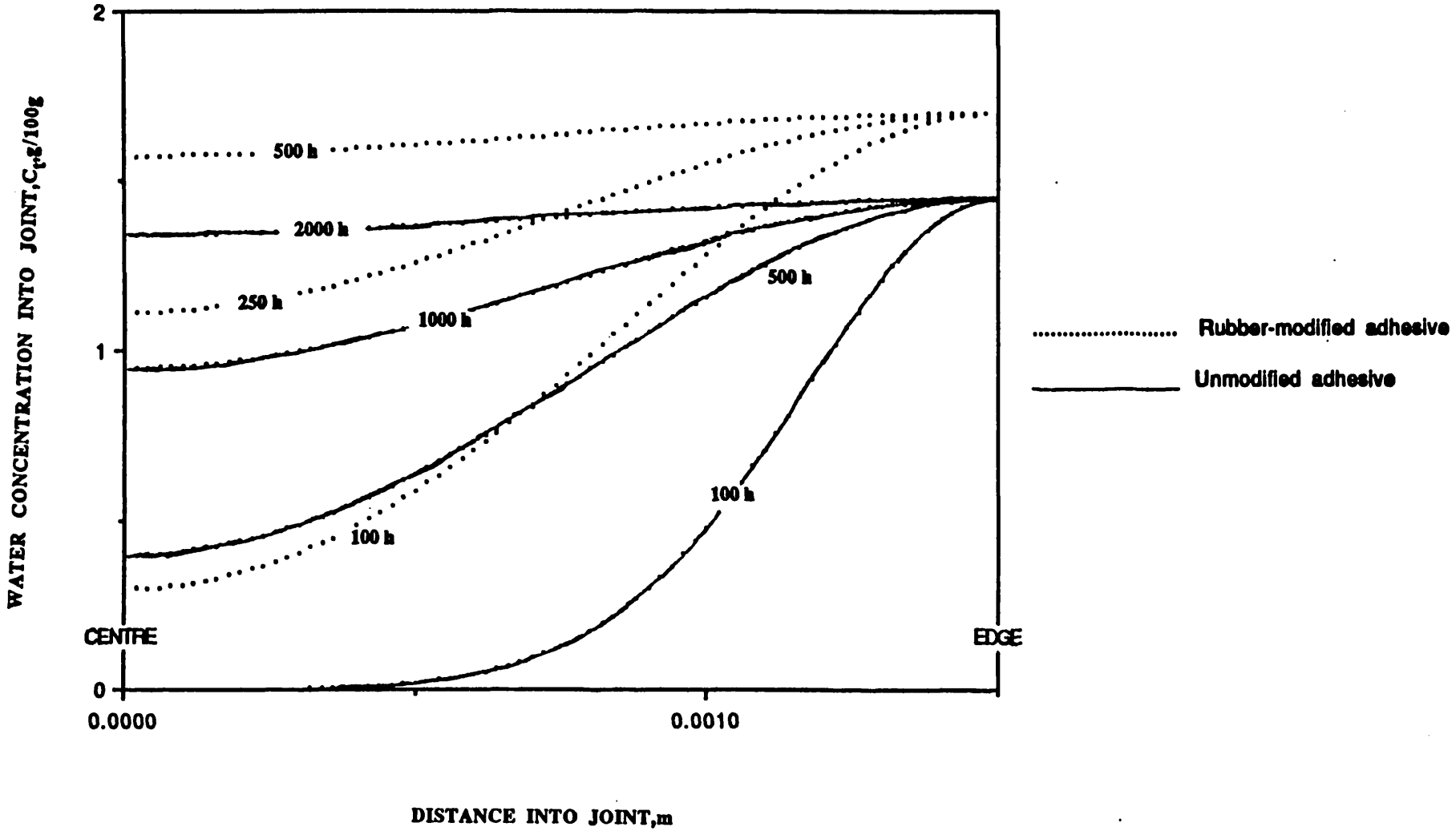


Figure 5.18: Comparison of water concentration in adhesive layer, C_t, as a function of time ,t_d, and penetration depth, x, between rubber-modified and unmodified DT adhesive joints immersed in distilled water at 40°C

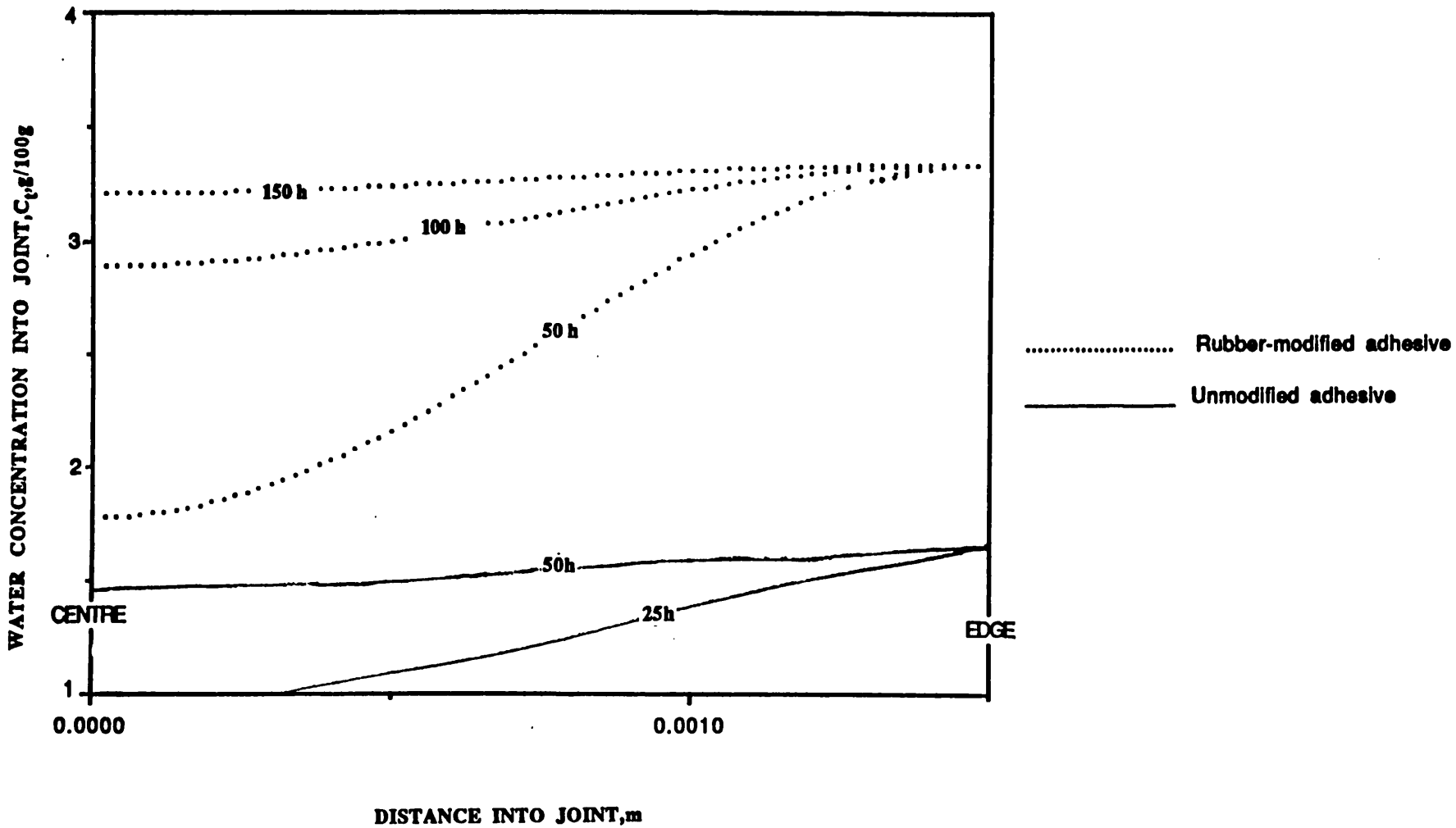


Figure 5.19: Comparison of water concentration in adhesive layer, C_t, as a function of time ,t_d, and penetration depth, x, between rubber-modified and unmodified DT adhesive joints immersed in distilled water at 55°C

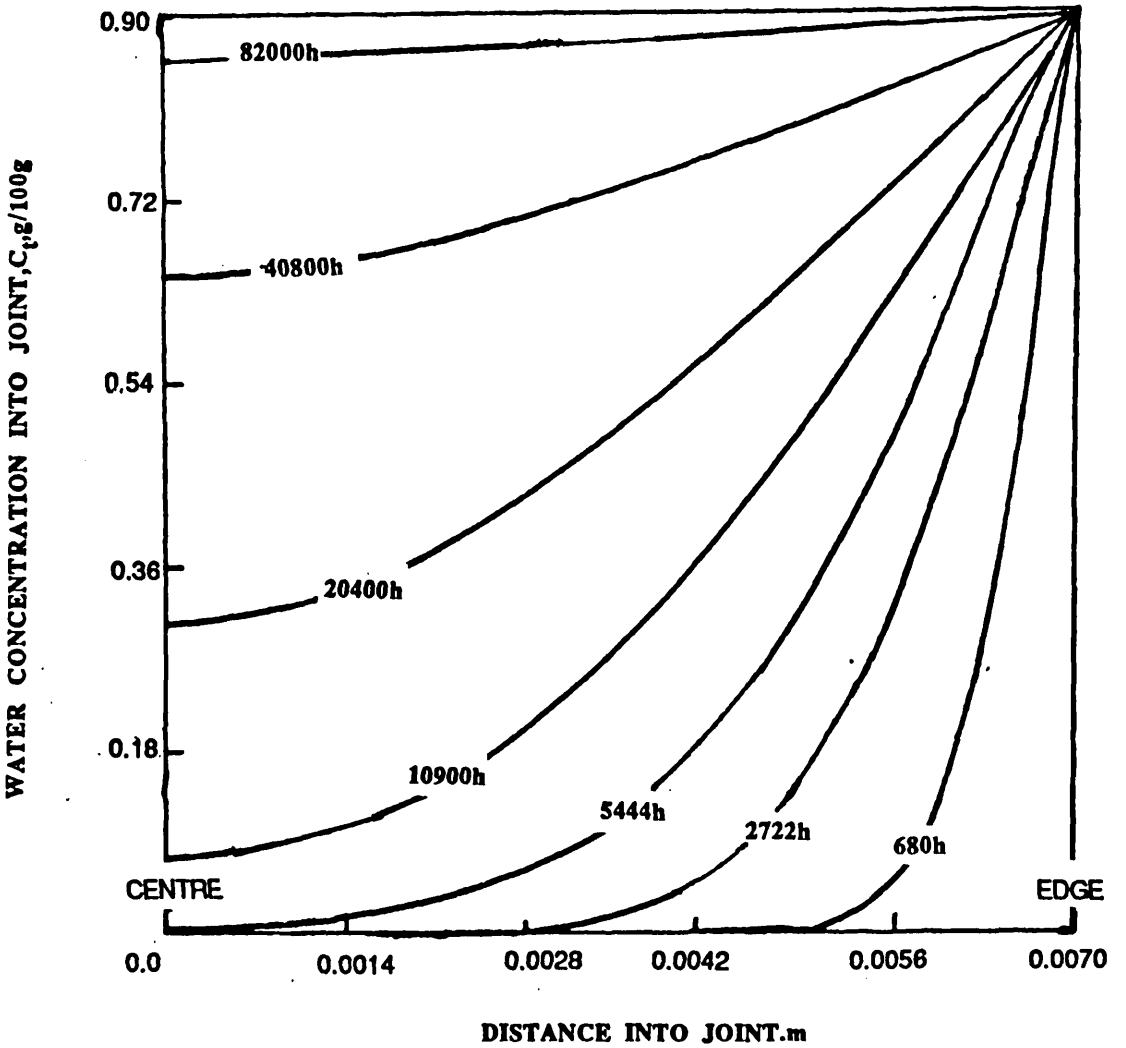


Figure 5.20: Water concentration, C_t, in a cylindrical adhesive layer as a function of time, t_d, and penetration depth, x, for unmodified butt adhesive joints immersed in distilled water at 25°C

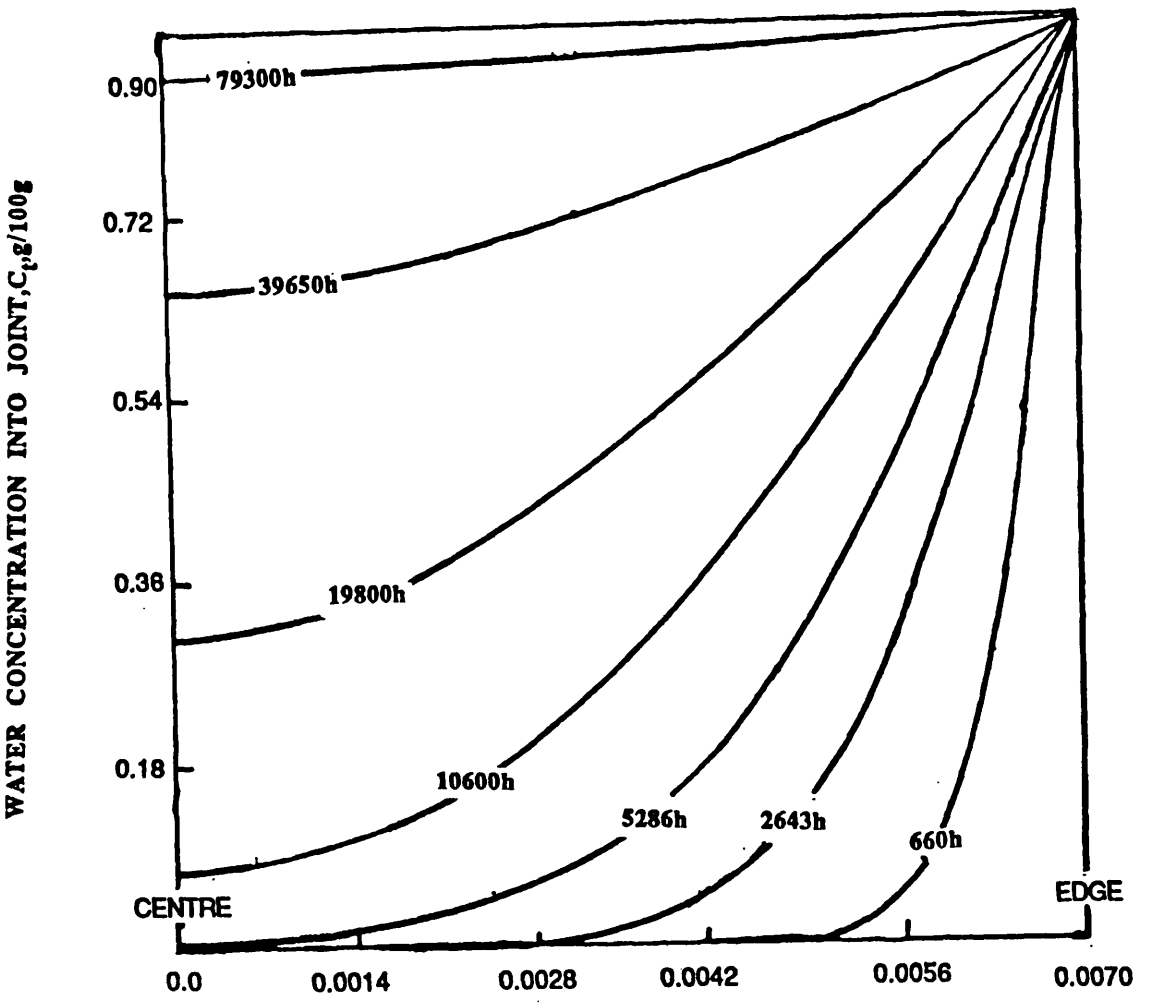


Figure 5.21: Water concentration, C_t, in a cylindrical adhesive layer as a function of time, t_d, and penetration depth, x, for rubber-modified butt adhesive joints immersed in distilled water at 25°C

CHAPTER 6

RESULTS AND DISCUSSIONS: LOCUS OF JOINT FAILURE STUDIES

6.1 INTRODUCTION

To assist in interpreting the mechanisms of environmental attack it is necessary to determine the locus of joint failure. Therefore, modern surface-sensitive analytical techniques such as scanning electron microscopy (SEM) and X-ray photoelectron spectroscopy (XPS) have been employed. The present Chapter will discuss the results and conclusions of the data obtained from these experimental methods.

6.2 VISUAL EXAMINATION OF THE FRACTURE SURFACES OF DOUBLE-TORSION (DT) JOINTS

Figure 6.1 shows a schematic representation of one side of a DT fracture surface and is representative of both joints tested "dry" and those which have been tested in water. On the upper region ("Region A") of the surface there was clearly a strip of cohesive-in-adhesive failure completely along the joint. This is where compressive stresses act upon the DT specimen whilst it is being tested. These turn from compressive to tensile as the crack grows, as the neutral axis along the specimen moves upwards as the crack propagates (P.S. Leevers (1982), and P.S. Leevers and J.G. Williams (1985)). Along the lower region ("Region B") of the DT specimen there appeared to be interfacial failure. The lower region of the DT specimen is subjected to tensile stresses during testing. In the following Section the results obtained from the scanning electron microscope will be considered and micrographs from "Region A" and "Region B" will be shown. The latter region, where high tensile stresses act, is the region of most interest.

6.3 SCANNING ELECTRON MICROSCOPY OF THE FAILED DT JOINTS

6.3.1 Introduction

The results of the scanning electron microscopy studies are shown in

Figures 6.2 to 6.7. Various samples were examined using the SEM and the locus of failure was found not to vary significantly from sample to sample, i.e., the locus of joint failure was the same at all temperatures and loads considered. This observation leads to the suggestion that the locus of failure is determined by the properties of the materials forming the bond, the detailed substrate pretreatment, and by the presence of the hostile environment, i.e. distilled water. Thus, the application of external stresses and an increase in the temperature of the water may change the rate of the environmental failure process, but not the locus of joint failure.

6.3.2 Prior to Environmental Attack

Figure 6.2 shows the mild-steel substrate prior to bonding. The angular features of the grit-blasted surface are clearly visible.

Figure 6.3 shows micrographs of an unmodified DT joint. Figures 6.3 (a) and 6.3 (b) show "Region A" and the cohesive-in-adhesive failure in the upper part of the specimen may be clearly seen. In the more important lower part ("Region B"), where the tensile forces act, it appears that interfacial failure at the adhesive/oxide interface has occurred, but with isolated areas of cohesive-in-adhesive failure leaving behind patches of retained adhesive. Figure 6.4 shows "Region B" at a higher magnification and appears identical to Figure 6.2 (b). This confirms that interfacial failure occurs in much of "Region B".

A similar picture emerges for the rubber-modified DT joints. Figure 6.5 shows that in "Region A" cohesive-in-adhesive failure occurs but in "Region B" it is a mixture of interfacial and cohesive-in-adhesive fracture, see Figure 6.5 (a). In Figure 6.5 (b) an area of cohesive-in-adhesive fracture from "Region B" is shown at higher magnification and the rubber particles may be clearly seen in the fracture surface of the rubber-modified adhesive.

6.3.3 After Environmental Attack

Figure 6.6 shows the fracture surface of a rubber-modified DT joint after exposure to water at 55°C. This micrograph is mainly of "Region A" but in the lower part of the specimen ("Region B") a mixture of interfacial failure and isolated patches of cohesive-in-adhesive failure are clearly visible. It is difficult to make a quantitative judgement as to the amount of interfacial failure that has occurred, but by comparing Figures 6.5 (a) and 6.6 it does seem that exposure to water has increased the amount of interfacial failure. Higher-magnifications micrographs of "Region B" in these joints are given in Figures 6.7. The areas of metal oxide, where interfacial failure has occurred, and patches of adhesive, where cohesive-in-adhesive failure has occurred, are both clearly visible. The latter, of course, having the distinctive rubber particles present. Thus, the micrographs in Figure 6.7 confirm that interfacial failure has mainly occurred, with a few isolated patches of cohesive-in-adhesive fracture. The other joints tested using unmodified adhesive, at different loads and temperatures, all showed the same locus of failure as described above.

6.4 X-RAY PHOTOELECTRON SPECTROSCOPY RESULTS

6.4.1 XPS Results of Metal Surface Prior to Bonding and Bulk Adhesives

XPS results from tests performed using a metal surface prior to bonding are shown in Figure 6.8. The metal surface was first grit-blasted and then degreased in a solvent. This Figure shows the spectrum as a plot of the electron binding energy against counts per second (electrons detected per second), obtained from the substrate surface. Peaks at about 710 eV, 540 eV, and 285eV were detected indicating the existence of iron (Fe), oxygen (O), and carbon (C) respectively . The oxygen peak was formed due to the metal oxide, or hydroxide, or carbon-oxygen (C-O) species. The carbon peak was strong indicating the presence of a high level of contamination. The rise in the background in the Fe peak indicates a continuous layer of oxide, i.e. no pinholes.

XPS results from tests performed using the bulk unmodified adhesive

and rubber-modified adhesive samples are shown in Figures 6.9 and 6.10 respectively as plots of electron binding energy against counts per second. The samples were cut from plates of the adhesives so that fresh adhesive surfaces were examined. The bulk adhesive spectra show that strong peaks at about 285eV and 540eV were detected in both the unmodified and rubber-modified adhesives which are characteristic of carbon and oxygen respectively. Weaker peaks at 400eV, 850eV, 210eV, and 485eV were also detected, but these peaks were much weaker compared to the carbon and oxygen peaks. However, a difference between the two spectra in Figures 6.9 and 6.10 is the detection of silicon, Si, in the rubber-modified adhesive, at about 100 and 150eV. The silicon may therefore be associated with the rubber, i.e. as an additive used in the preparation of the rubber.

6.4.2 XPS Results of Unmodified DT Joints

The XPS spectra of all double-torsion joints examined were found to be similar, and therefore, only some typical results will be discussed. The XPS spectra of an unmodified double-torsion joint exposed to distilled water at 40°C is shown in Figures 6.11 and 6.12 as plots of the binding energy against counts. Figure 6.11 shows the spectra obtained from the substrate surface where failure was cohesive-in-the-adhesive (see Figure 6.1, "Region A"). Carbon and oxygen peaks were visible on the adhesive surface. Silicon peaks were also detectable at about 100 and 150eV. Figure 6.12 shows the spectra obtained from the substrate surface where failure was visually mainly interfacial ("Region B"). Carbon, oxygen, iron and silicon peaks were detected.

From Figures 6.8 and 6.12 it appears that the mainly interfacial region of the fracture surface of the DT joint has a strong concentration of iron, arising from the oxide layer. However, the iron peak is weaker than for the substrate surface prior to bonding (Figure 6.8) and this, together with the relatively strong carbon and oxygen signals, confirms the locus of failure concluded from the scanning electron microscopy results. This was that fracture of the joint in this region ("RegionB") occurred by interfacial failure at the adhesive/oxide interface but with isolated patches of cohesive-

in-adhesive fracture leading to areas of retained adhesive.

Considering other possibilities, then there was no evidence of iron retained on the opposite fracture surface ("Region B"). It is therefore unlikely to have been fracture in the oxide layer itself. Another possibility is that a thin layer of adhesive of a few nanometers at most, covers the iron oxide surface. However, this is considered unlikely bearing in mind the relatively strong iron signal (Figure 6.12). Finally, from the results discussed in Section 6.4.1, the presence of silicon on all the failure surfaces of the unmodified joints is surprising. One possible explanation may be that silicon containing compounds have been leached from the silicone-based sealant used to seal the water baths, resulting in silicon contamination of the surfaces after failure.

6.4.3 XPS Results of Rubber-modified DT Joints

Figures 6.13 and 6.14 show the XPS spectra obtained from the tests performed using the rubber-modified double-torsion failure surfaces exposed to distilled water at 55°C. The data is identical to that discussed above, and hence the locus of failure in "Region B" is again interpreted to be mainly interfacial at the adhesive/oxide interface with isolated patches of cohesive-in-adhesive failure.

6.4.4 XPS Results of Unmodified Butt Joints

Figures 6.15 and 6.16 show the spectra obtained from the XPS tests performed using unmodified butt joint fracture surfaces which were exposed to distilled water at 25°C. The spectra in these Figures are again presented as plots of binding energy against counts per second. Figure 6.15 shows the spectrum obtained from the surface where failure was cohesive-in-the-adhesive. Strong carbon and oxygen peaks are recorded. Silicon peaks were also detected, possibly as a result of contamination. Figure 6.16 shows the spectrum obtained from the surface where failure was visually mainly interfacial. Carbon, oxygen, silicon and iron peaks were detected. This again suggests that a mixture of cohesive-in-adhesive and interfacial failure occurred.

6.4.5 XPS Results of Rubber-modified Butt Joints

Figures 6.17 and 6.18 show the spectra obtained from the rubber-modified butt joint failure surfaces. The joint was exposed to distilled water at 25°C and similar results to the unmodified butt joint were obtained.

6.5 CONCLUSIONS

From the studies on the locus of failure of the joints the following conclusions may be reached:

1. For the double-torsion (DT) joints in the upper region of the specimen, where compressive stresses act during testing, the locus of failure is always by cohesive-in-the adhesive fracture.

2. In the more important lower region, where tensile stresses act, the locus of failure before environmental attack appears to be via failure largely at the adhesive/oxide interface, with patches of cohesive-in-adhesive fracture.

3. In the lower region of the DT joints after environmental attack the locus of failure is very similar to that described above but it appears that there is more adhesive/oxide failure and less cohesive-in-adhesive failure. Although it is difficult to quantify this statement.

4. In the butt joints, after exposure to distilled water, failure occurred increasingly by interfacial failure at the adhesive/oxide interface.

5. The type of adhesive, load or test temperature has no effect on the locus of failure in the presence of water. Thus, these factors appear not to affect the mechanism of water attack, but merely to change the kinetics of environmental attack.

6. The feature that in the DT joints the upper region fails by cohesive-in-adhesive fracture, even after long exposure to water at 55°C, suggests that compressive stresses inhibit the mechanism of environmental attack, or the rate at which such attack occurs.

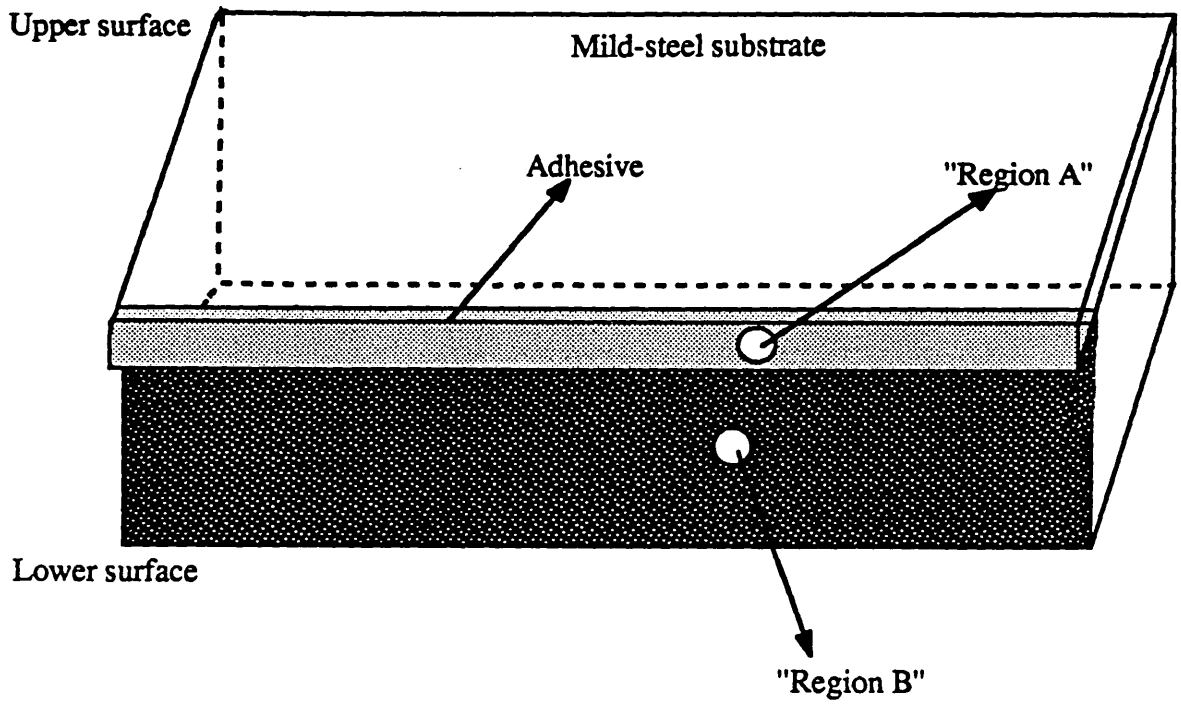
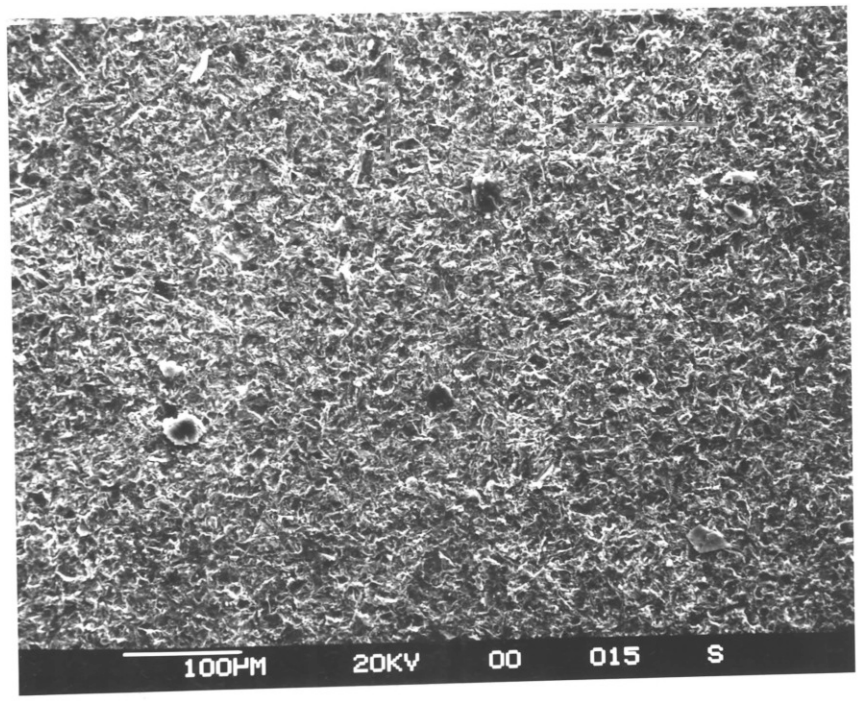
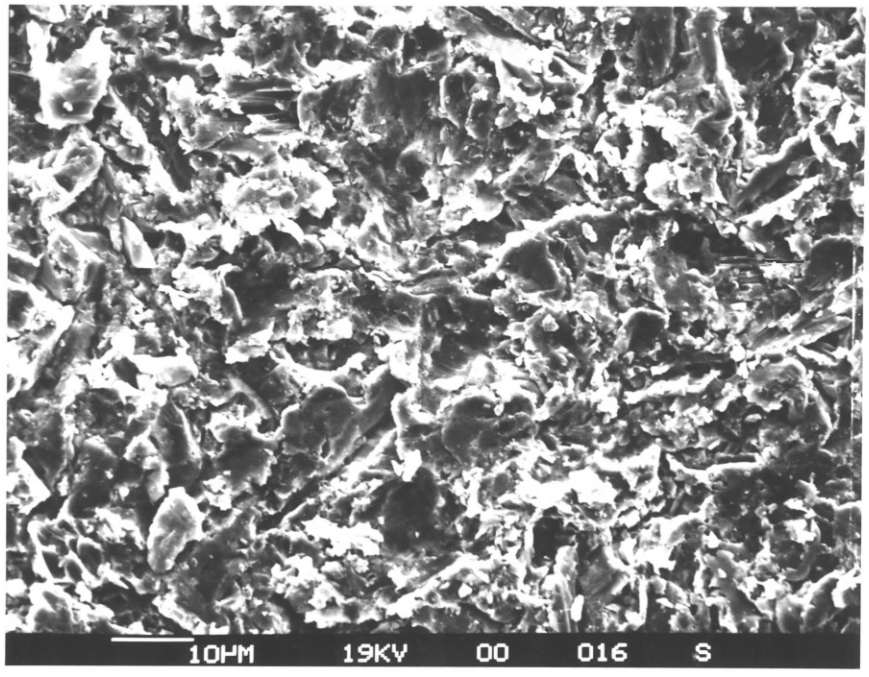


Figure 6.1: Schematic representation of a typical DT fracture surface.

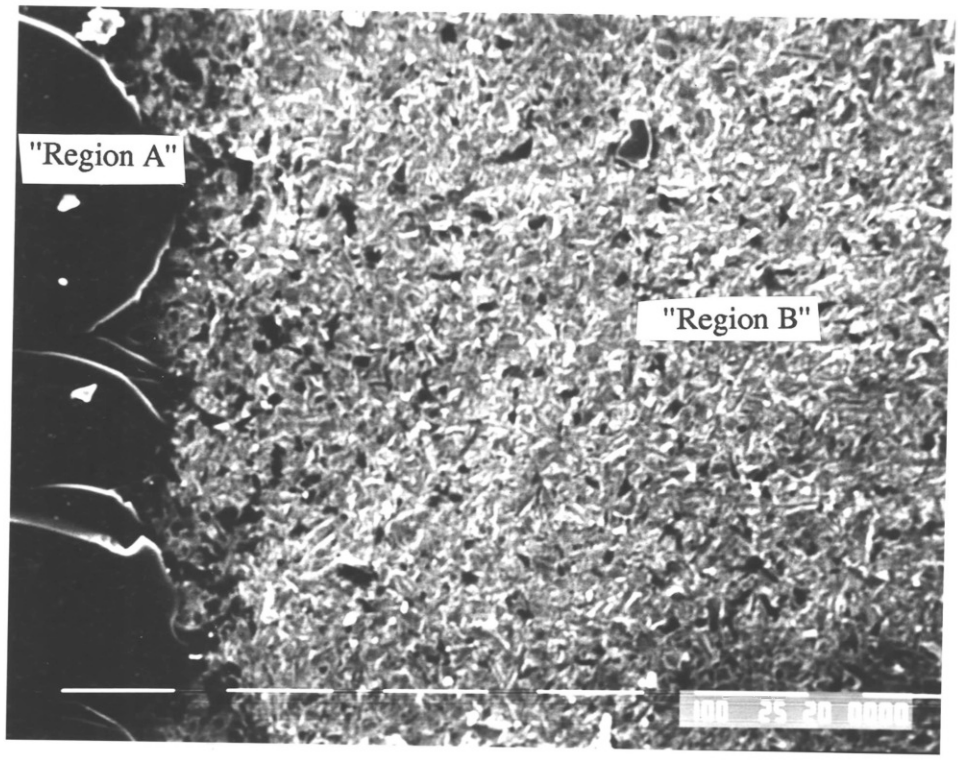


(a)

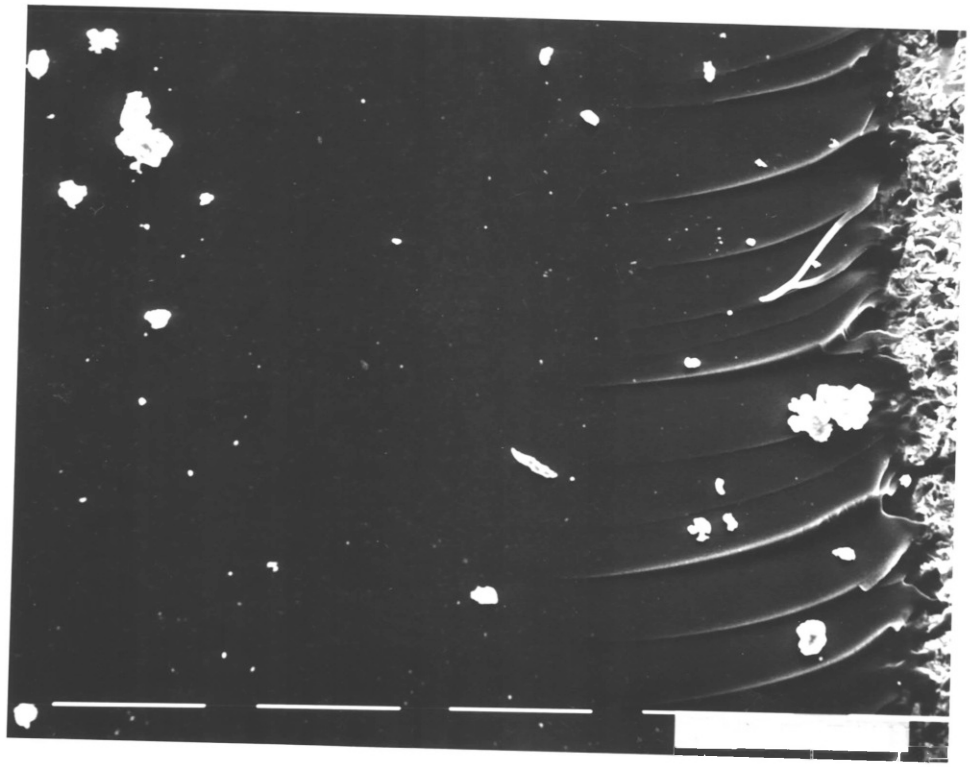


(b)

Figure 6.2: SEM photographs of the substrate surface prior to bonding, at magnifications x 150 (a) and x 1,000 (b) respectively.



(a) "Region A"/"Region B"

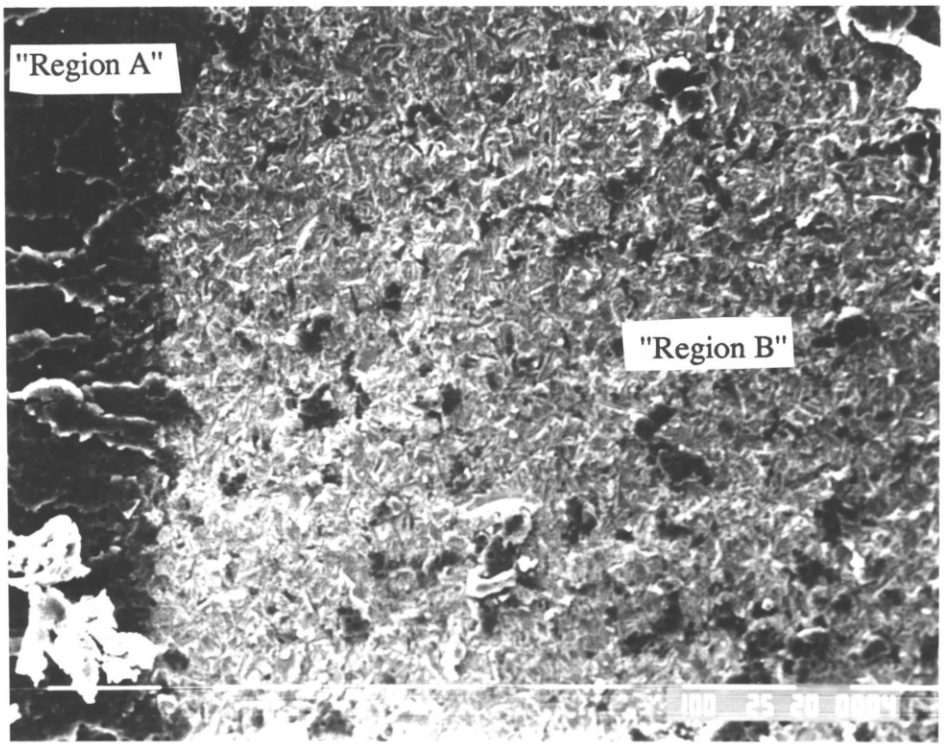


(b) "Region A"

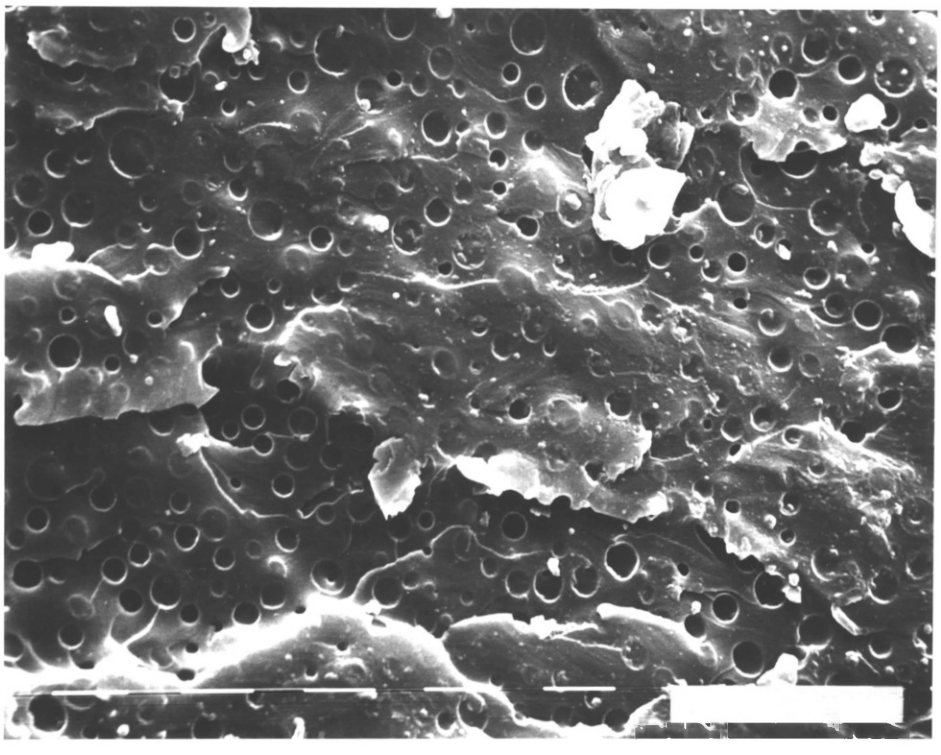
Figure 6.3: SEM photographs of the fracture surface of an unmodified DT joint (tested "dry") at magnifications x 150 (a) and x 200 (b) respectively.



Figure 6.4: SEM photograph of the fracture surface of an unmodified DT joint (tested "dry") at magnifications x 1,000 ("Region B").



(a) "Region A"/"Region B"



(b) Cohesive-in-adhesive part of "Region B"

Figure 6.5: SEM photographs of the fracture surface of a rubber-modified DT joint (tested "dry") at magnifications x 100 (a) and 1,000 (b).

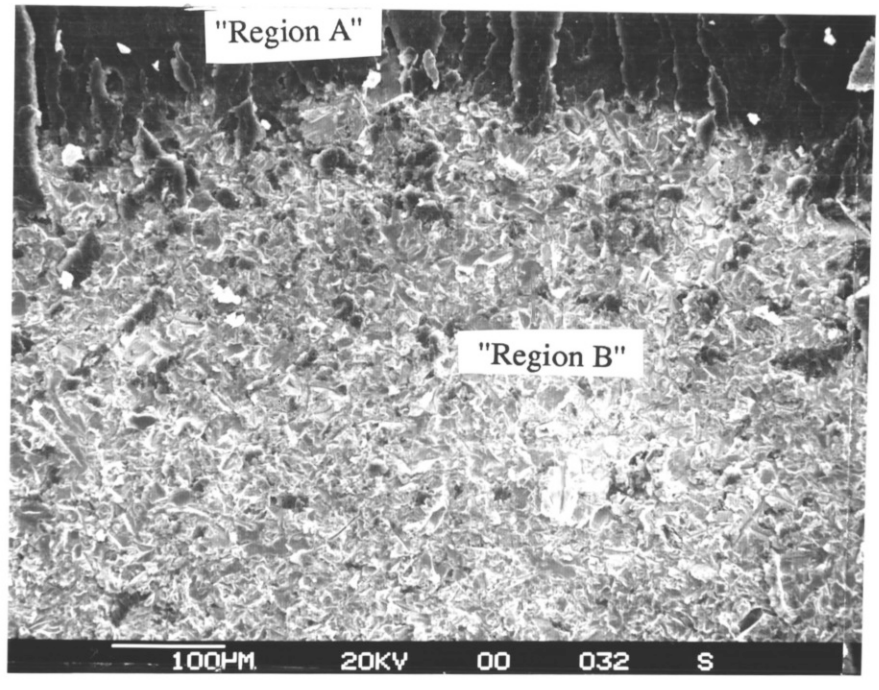
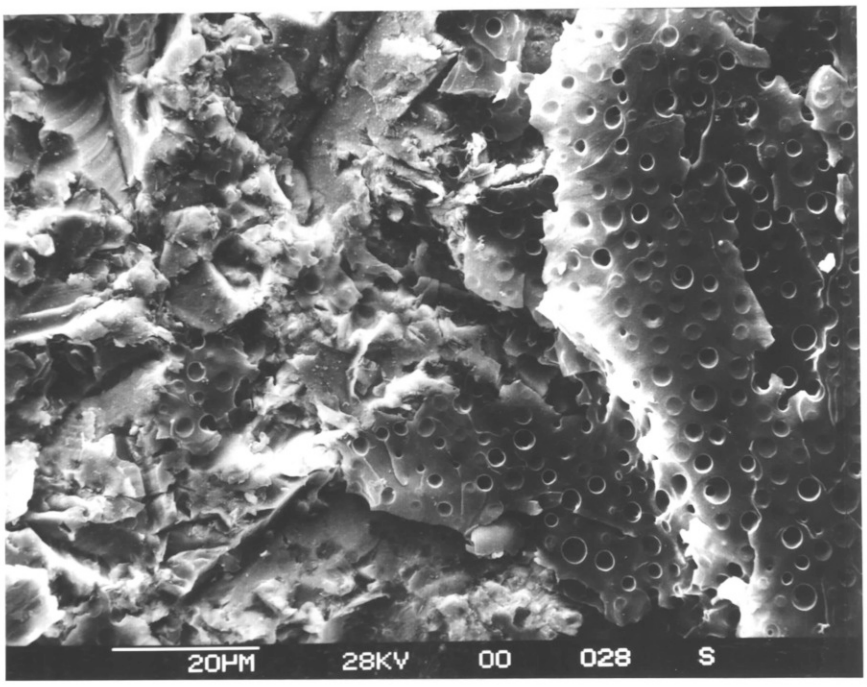
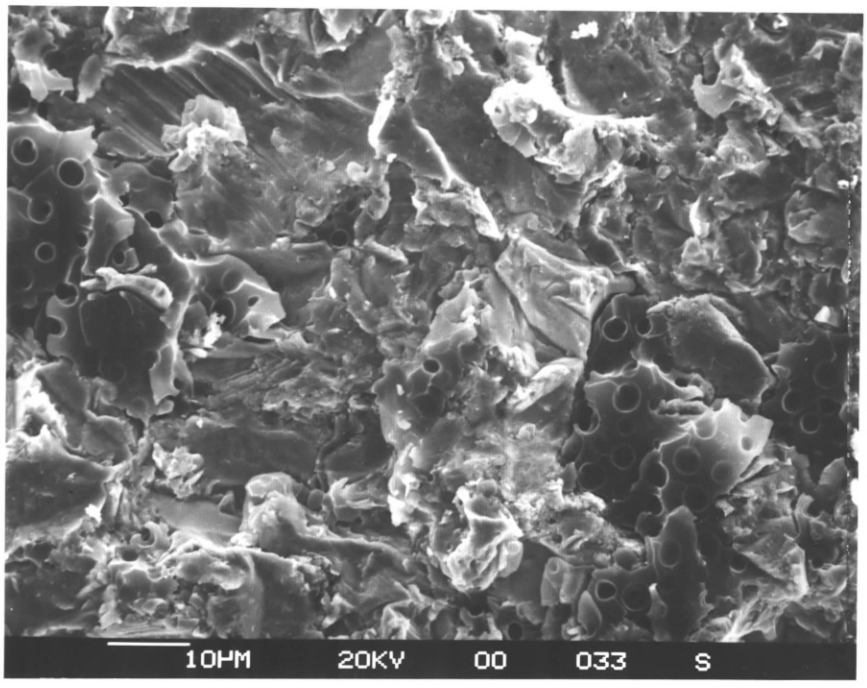


Figure 6.6: SEM fracture surface of a rubber-modified DT joint after exposure to water at 55°C at magnification x 150 ("Region A"/"Region B").



(a)



(b)

Figure 6.7: SEM fracture surface of a rubber-modified DT joint after exposure to water at 40°C, (a), and 55°C, (b), at magnification x1,000 ("Region B").

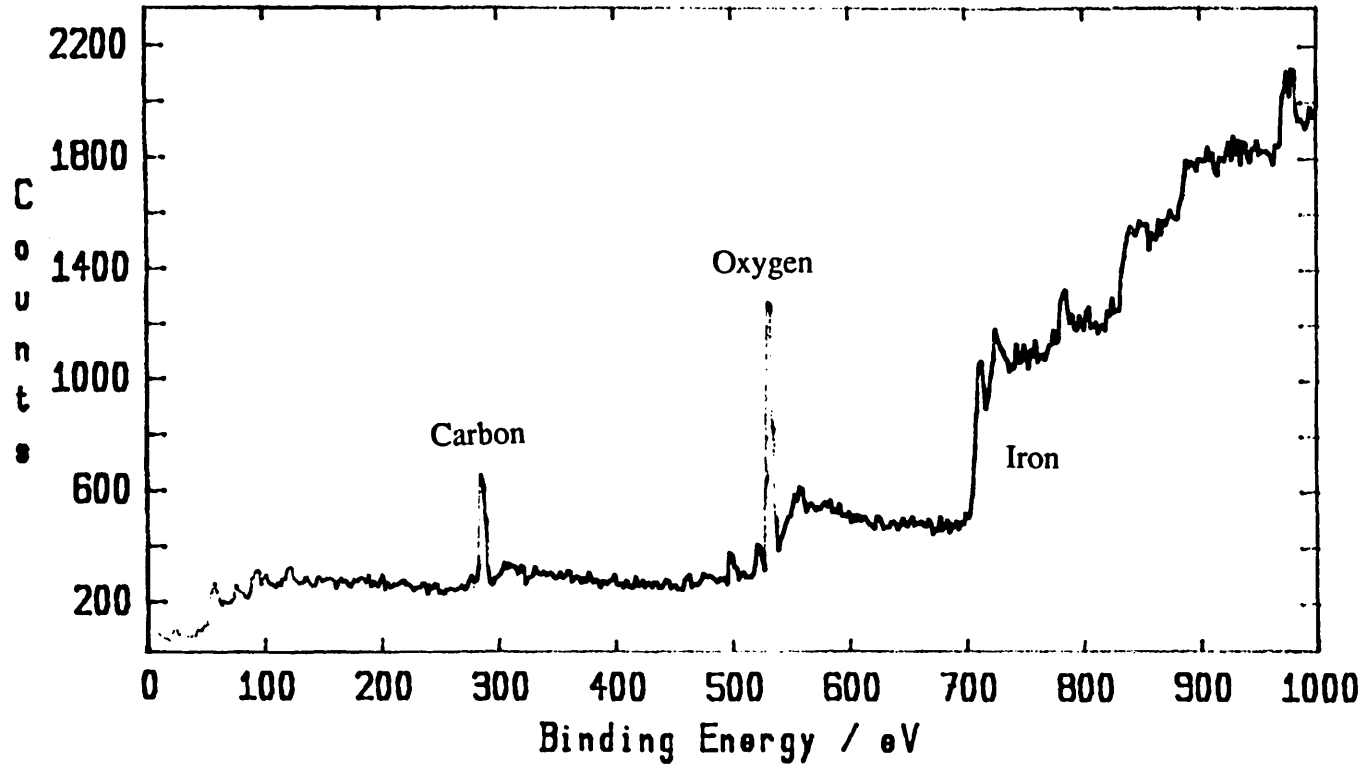


Figure 6.8: XPS results from tests performed using a mild-steel substrate surface prior to bonding.

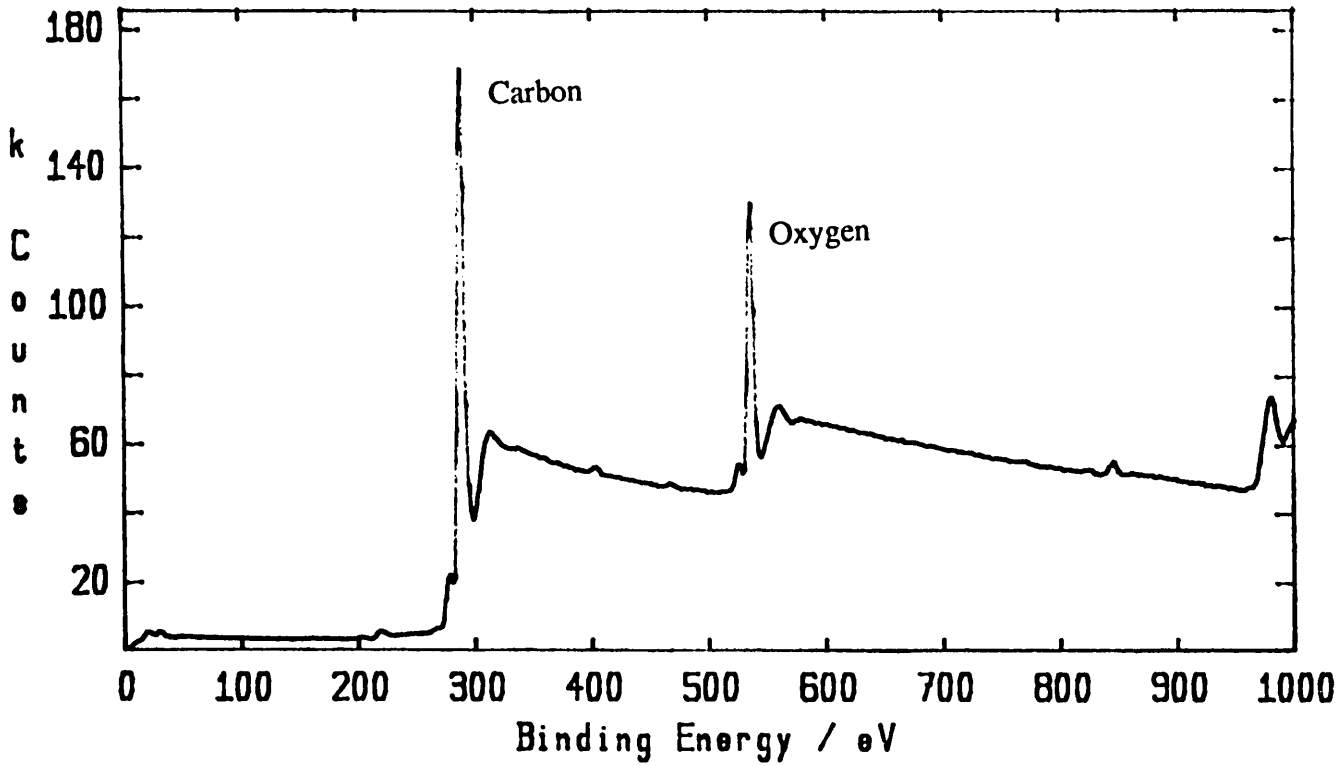


Figure 6.9: XPS results from tests performed using bulk unmodified adhesive samples.

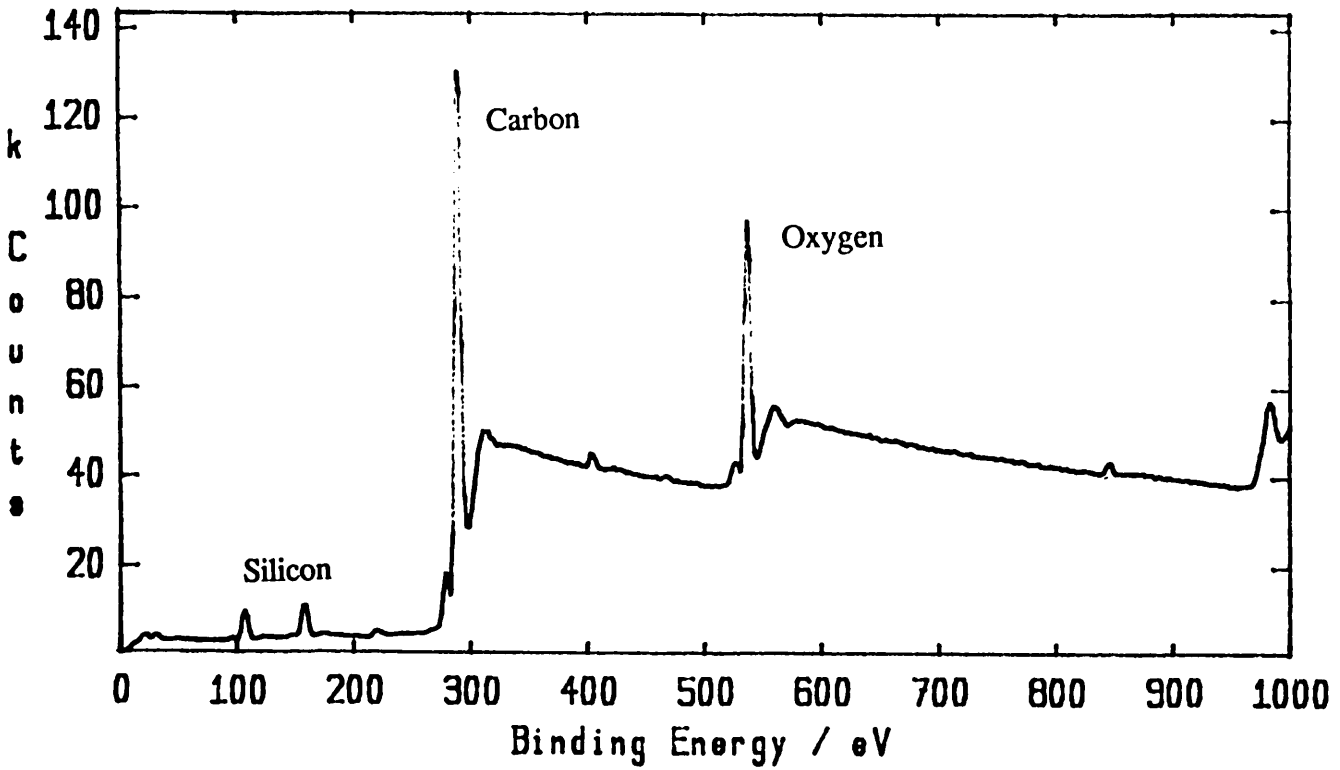


Figure 6.10: XPS results from tests performed using bulk rubber-modified adhesive samples.

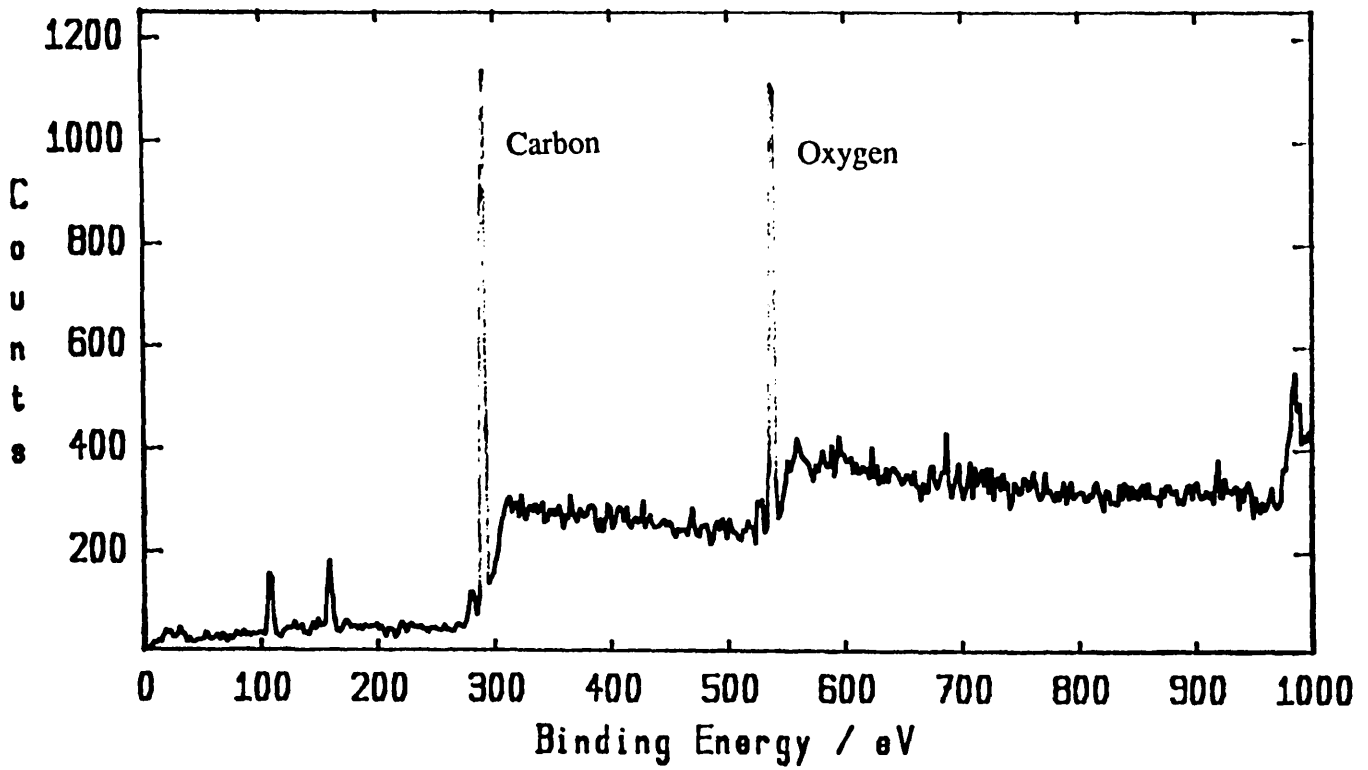


Figure 6.11: XPS spectra of an unmodified double-torsion adhesive joint after exposure to distilled water at 40°C and failure. The spectra was obtained from the surface where failure was cohesive-in-adhesive ("Region A").

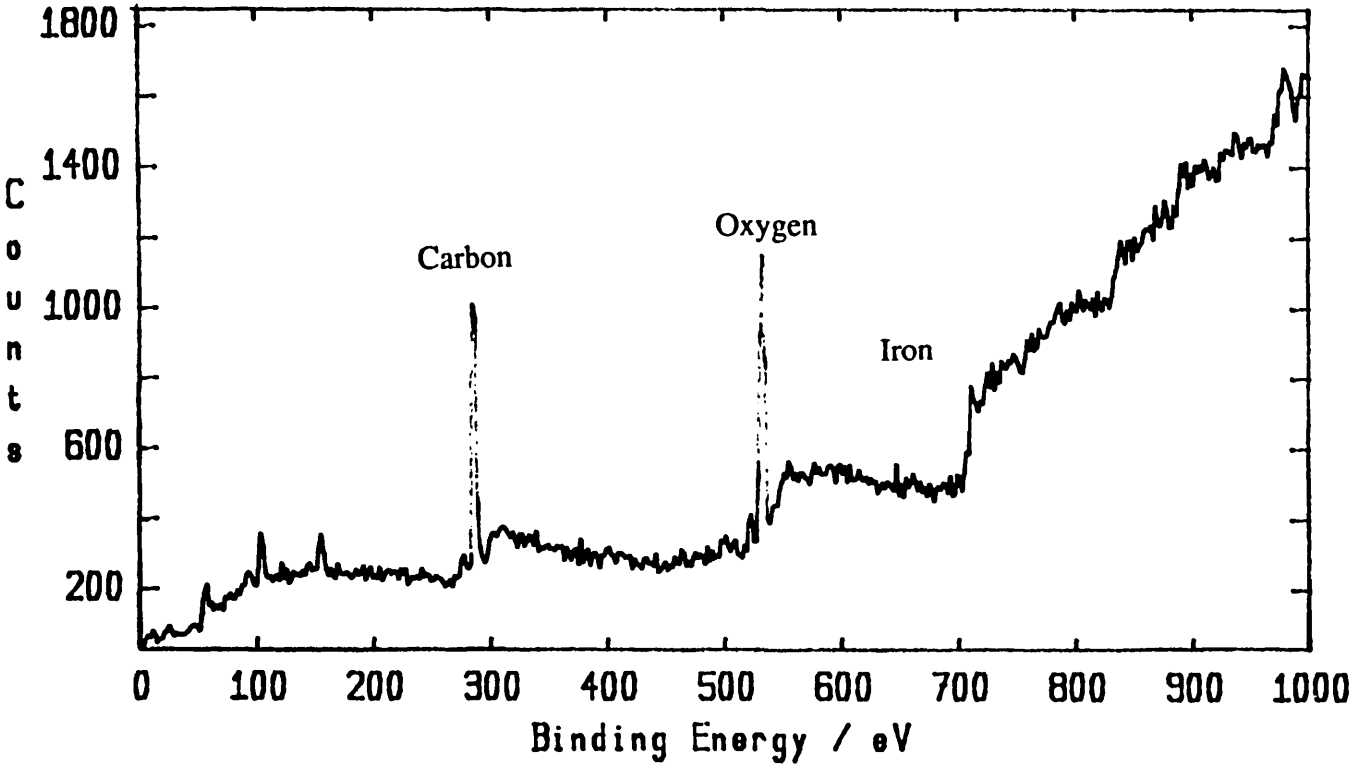


Figure 6.12: XPS spectra of an unmodified double-torsion adhesive joint after exposure to distilled water at 40°C and failure. The spectra was obtained from the surface where failure was visually mainly interfacial ("Region B").

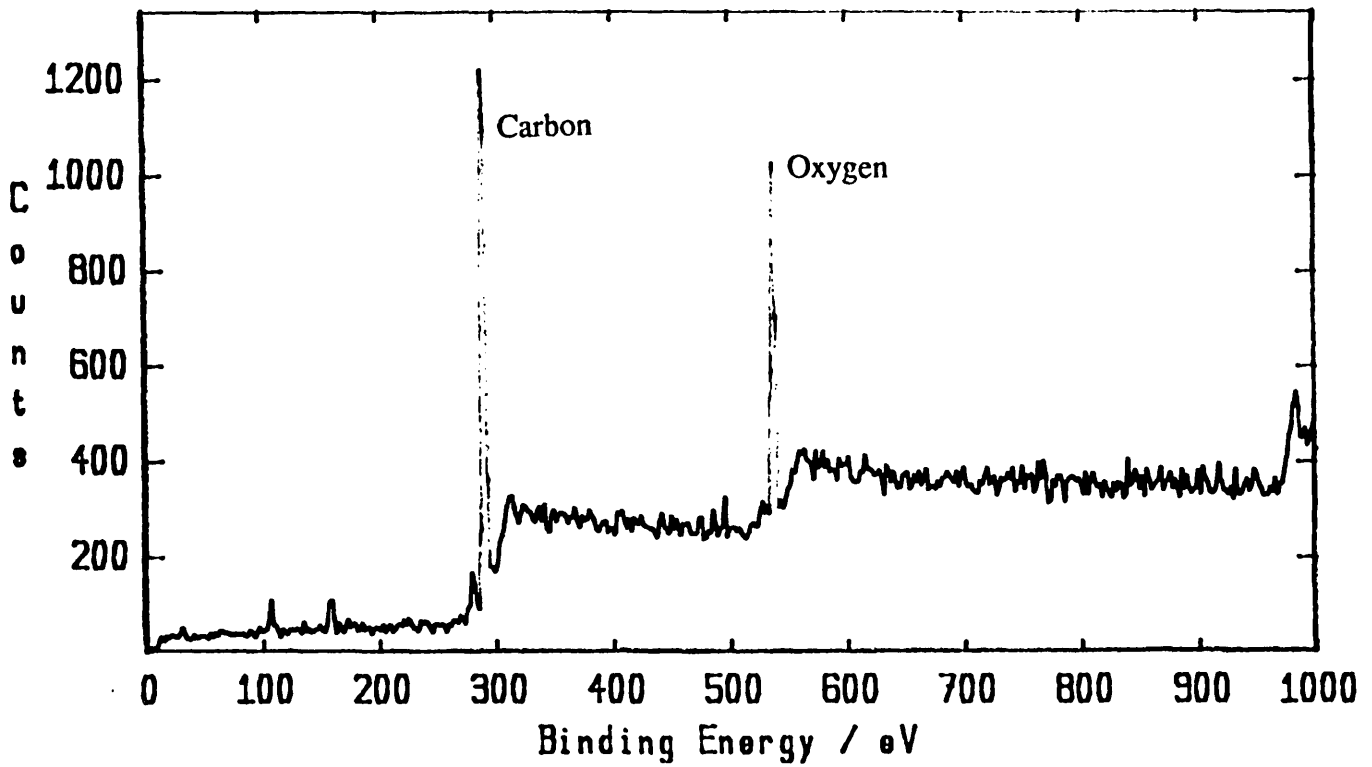


Figure 6.13: XPS spectra of a rubber-modified double-torsion adhesive joint after exposure to distilled water at 55°C and failure. The spectra was obtained from the surface where failure was cohesive-in-adhesive ("Region A").

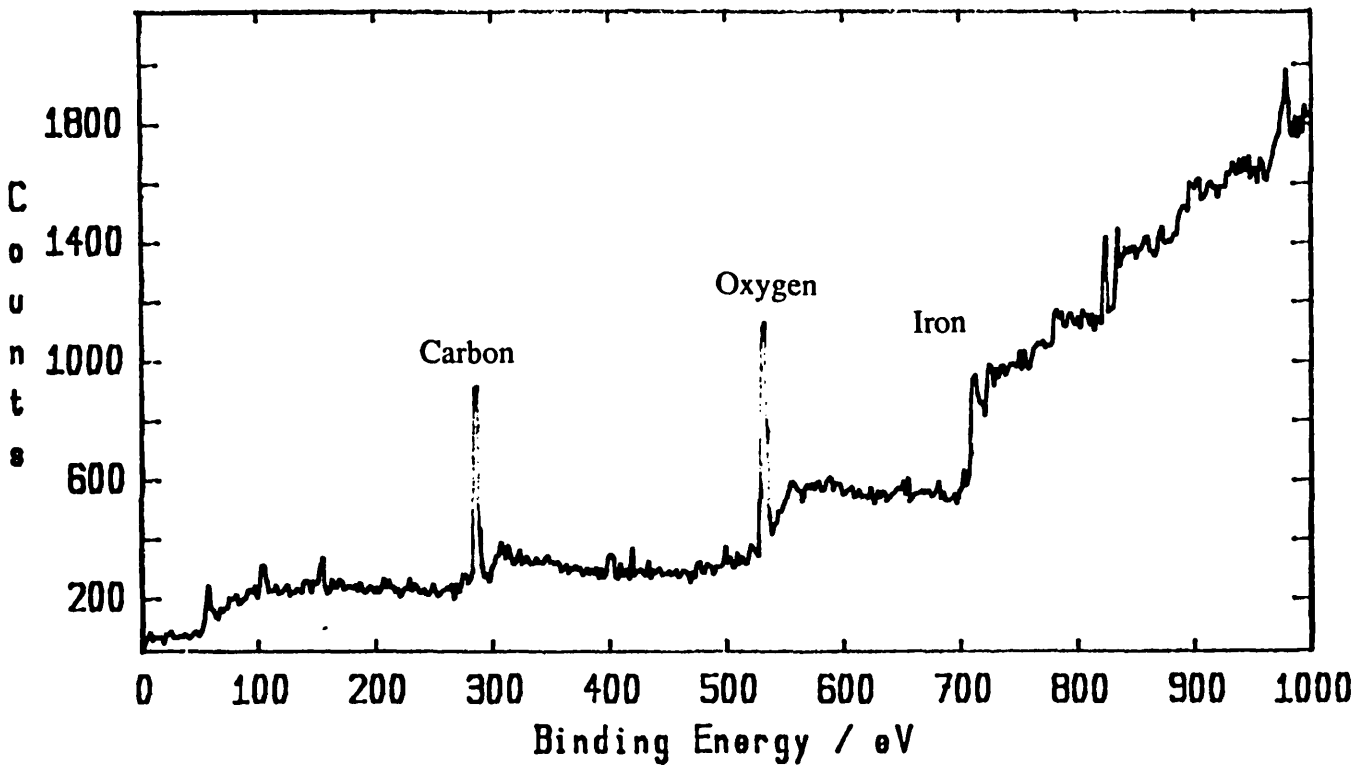


Figure 6.14: XPS spectra of a rubber-modified double-torsion adhesive joint after exposure to distilled water at 55°C and failure. The spectra was obtained from the surface where failure was visually mainly interfacial ("Region B").

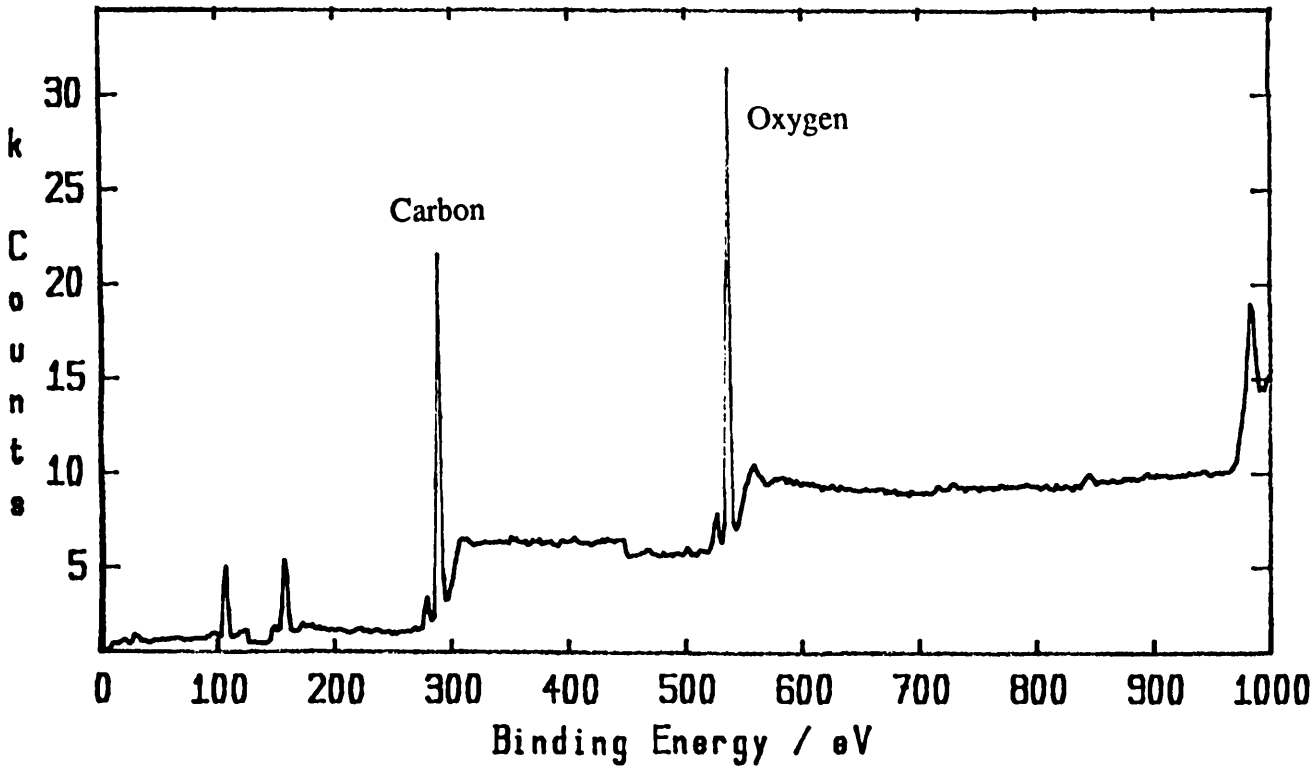


Figure 6.15: XPS spectra of an unmodified butt adhesive joint after exposure to distilled water at 25°C and failure. The spectra was obtained from the surface where failure was cohesive-in-adhesive.

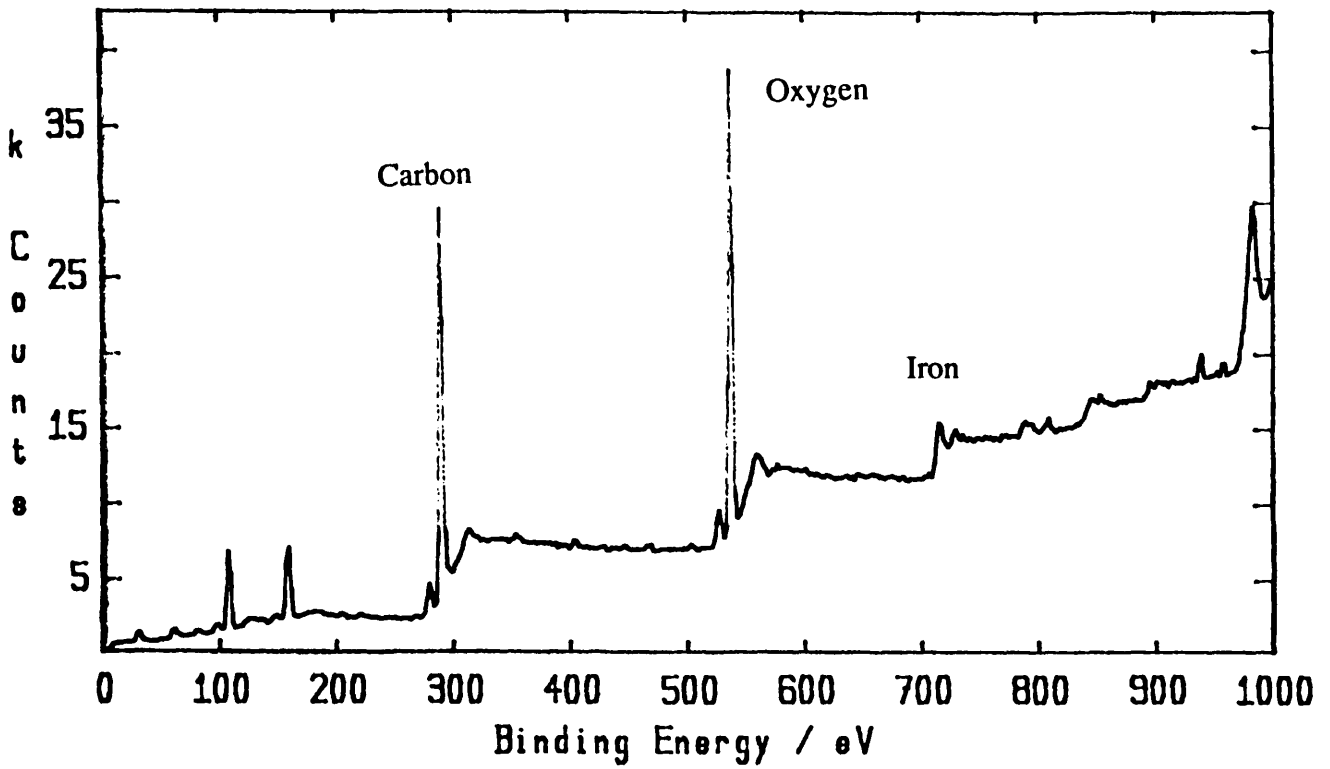


Figure 6.16: XPS spectra of an unmodified butt adhesive joint after exposure to distilled water at 25°C and failure. The spectra was obtained from the surface where failure was visually interfacial.

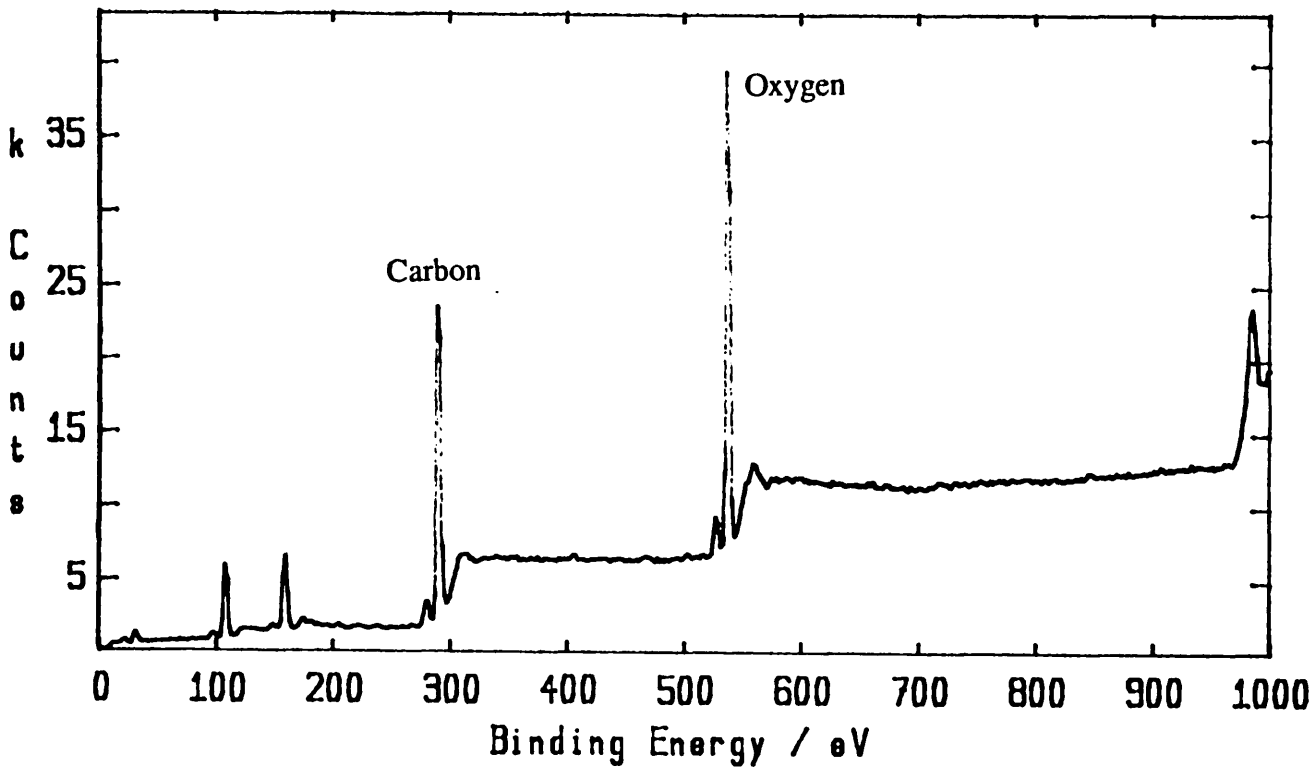


Figure 6.17: XPS spectra of a rubber-modified butt adhesive joint after exposure to distilled water at 25°C and failure. The spectra was obtained from the surface where failure was cohesive-in-adhesive.

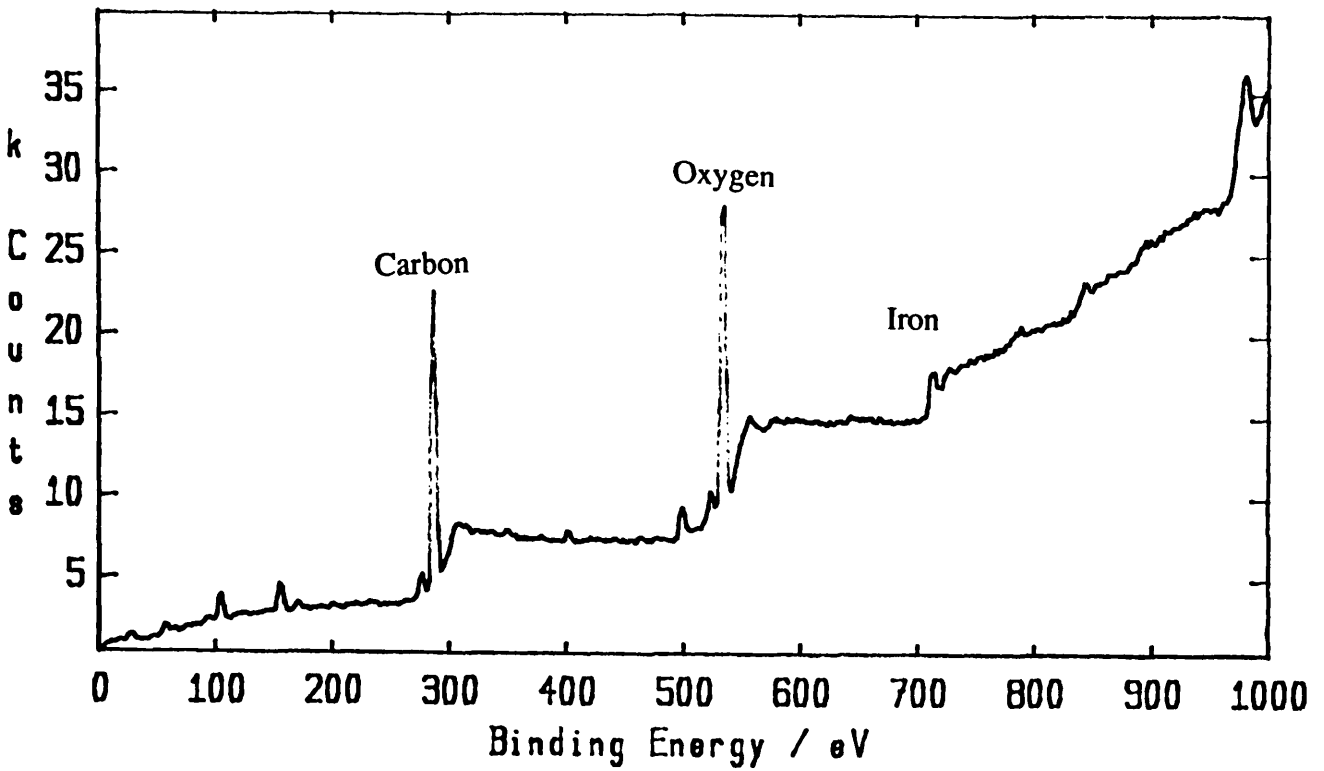


Figure 6.18: XPS spectra of a rubber-modified butt adhesive joint after exposure to distilled water at 25°C and failure. The spectra was obtained from the surface where failure was visually interfacial.

CHAPTER 7

MECHANISMS AND MECHANICS OF ENVIRONMENTAL FAILURE

7.1 INTRODUCTION

The new test method for obtaining information about the fracture behaviour of double-torsion adhesive joints in aqueous conditions, described in Chapter 3, has been shown to give reproducible results. The next step is to use these data to identify the mechanisms of environmental failure and to attempt to develop a mathematical model for life predictions of the butt joints when exposed to distilled water at 25°C and under the application of static stresses. These aspects are discussed in the present Chapter.

7.2 MECHANISMS OF FAILURE

7.2.1 Thermodynamic Work of Adhesion

In order to understand the mechanisms of environmental failure of the adhesive joints studied in the present investigation, the thermodynamic work of adhesion, W_A, required to separate unit area of two phases forming an interface was considered. The thermodynamic work of adhesion is given from the equation (R.A. Gledhill and A.J. Kinloch, 1974):

$$W_A=\gamma_x+\gamma_y-\gamma_{xy} \qquad (7.1)$$

where γ_x and γ_y are the surface free energies of two phases x and y in contact and γ_{xy} is the interfacial free energy. If a liquid is present, then the work of adhesion may be written as W_{AL}, and given from the equation (R.A. Gledhill and A.J. Kinloch, 1974):

$$W_{AL}=\gamma_{xL}+\gamma_{yL}-\gamma_{xy} \qquad (7.2)$$

where γ_{xL} and γ_{yL} are the surface energies of the phases x and y in contact with the

liquid. Calculating the terms W_A and W_{AL}, allows predictions about the environmental stability of the adhesive/metal substrate oxide to be made; where the metal substrate is, say, the x phase, the adhesive the y phase, and the water the L phase. For a typical organic adhesive/metal-oxide interface, the work of adhesion under dry conditions, W_A, usually has a large positive value, indicating thermodynamic stability of the interface. However, in the presence of water the thermodynamic work of adhesion, W_{AL}, takes a negative value, indicating that an unstable interface has been created as a result of water ingressing at the interface. The interfacial free energy, γ_{xy}, may be given from the equation (R.A. Gledhill and A.J. Kinloch, 1974):

$$\gamma_{xy} = \gamma_x + \gamma_y - 2\{(\gamma^D_x \gamma^D_x)^{1/2} + (\gamma^P_x \gamma^P_x)^{1/2}\} \quad (7.3)$$

where γ^D and γ^P the dispersion and polar free force components of the total surface free energy γ, where γ is given by the equation:

$$\gamma = \gamma^D + \gamma^P \quad (7.4)$$

Therefore equations (1) and (2) now become:

$$W_A = 2\{(\gamma^D_x \gamma^D_x)^{1/2} + (\gamma^P_x \gamma^P_x)^{1/2}\} \quad (7.5)$$

and

$$W_{AL} = 2\{\gamma_L - (\gamma^D_x \gamma^D_L)^{1/2} - (\gamma^P_x \gamma^P_L)^{1/2} - (\gamma^D_y \gamma^D_L)^{1/2} - (\gamma^P_y \gamma^P_L)^{1/2} + (\gamma^D_x \gamma^D_y)^{1/2} + (\gamma^P_x \gamma^P_y)^{1/2}\} \quad (7.6)$$

where γ_L is the total surface free energy of water given by:

$$\gamma_L = \gamma^D_L + \gamma^P_L \qquad (7.7)$$

In the case of an epoxide adhesive joint exposed to water where we may let the x phase be the metal substrate (now termed "S") and the adhesive the y phase (now termed "A"), the values of W_A and W_{AL} may be estimated if the surface free energies can be calculated. R.A. Gledhill and A.J. Kinloch (1974), have calculated the values of γ_L, γ^D_L and γ^P_L of water and the values of γ^D_S, γ^P_S of the metal substrate, mild steel, and γ^D_A and γ^P_A of the epoxide adhesive, as shown in Table 7.1. The values of W_A and W_{AL} were found to be +291 mJ/m^2 and -255 mJ/m^2 respectively, i.e. a change from a positive to a negative value. The positive value of the thermodynamic work of adhesion may indicate thermodynamic stability at the interface, whereas the negative value may indicate that an unstable interface was created as a result of water ingressing at the interface. It may be argued that, this large change from a positive to a negative work of adhesion provide a driving force for the water to displace the adhesive on the substrate surface. Hence, an increasing amount of interfacial failure along the adhesive/metal-oxide interface would be expected as water entered into the joint (via diffusion through the adhesive, see Chapter 5). In fact, this change in the locus of failure was observed in all double-torsion and butt adhesive joints studied in the present investigation (see Chapter 6). Hence, it can be concluded that the locus of failure of the present adhesive joints can be successfully understood from the thermodynamic work of adhesion, where the mechanism of environmental attack is that of the water displacing the adhesive bonded to the metal substrate via rupture of the secondary bonds (van der Waals bonds) across the adhesive/metal-oxide interface.

7.2.2 Kinetics of Failure

7.2.2.1 Critical Water Concentration

The data in Figures 4.17 and 4.18 shows that the crack developed and

started to grow in the double-torsion adhesive joints in a matter of few minutes to few hours. Now the data in Figures 5.11 and 5.12 shows that the unmodified adhesive and the rubber-modified adhesive become saturated after an immersion period of about 5,000 hours. This reveals that the complete thickness of the adhesive layer did not become saturated before crack growth started to occur in the double -torsion joints. Thus the concentration of water in the adhesive layer in the DT adhesive joints for sufficient water to be present to give debonding was far less than C_∞, the concentration at equilibrium. Similar arguments can be made for the butt joints by considering Figures 4.35, 5.20 and 5.21. In this case, the time period for complete saturation of the adhesives is around 80,000 hours. The present work therefore agrees with the concept of critical level of water developed and proposed by R.A. Gledhill, A.J. Kinloch and S.J. Shaw (1980), and D.M. Brewis, J. Comyn, and S.T. Tredwell (1987), and D.M. Brewis, J. Comyn, and J.L. Tegg (1980). Details of the theoretical model developed by these investigators can be found in Chapter 2. The value of the critical concentration of water for crack growth to start to occur cannot be calculated from the current experimental data until the role of applied stress in accelerating environmental failure is understood (see 7.2.3).

7.2.2.2 Effect of Temperature

In some instances it has been shown that the incubation time, t_{inc}, (or the crack speed, $d\alpha/dt$) may be related to the temperature, T, by an equation of the general form (A.J. Kinloch and R.J. Young, 1983, S.M. Wiederhorn et al, 1980, 1982):

$$t_{inc} = t_o \exp[(\Delta H - v^* G_c)/RT] \qquad (7.8)$$

where t_o and v^* are constants, ΔH is the activation energy, G_c is the applied fracture energy, and R is the gas constant. Equation (7.8) assumes that the fracture process of the DT joints is an "activated rate process". To explain the term "activated rate process" consider Figure 7.1 in which the energetics of the process are represented schematically.

An activation energy, ΔH, is then needed for this process to start, i.e. to go from the stable state A (no crack growth) to the state B (crack growth initiation). The activation energy is usually independent of the temperature of the environment, and one would expect, for an activated process, incubation time to decrease and the crack speed to increase with increasing temperature. S.M. Wiederhorn et al (1980) used the above equation to fit successfully the experimental crack growth data obtained during their investigation on environmental crack growth in ceramic materials. Their data showed that the crack speed increased as the temperature of the water was increased, at a given value of G_c.

In the present investigation the use of equation (7.8) was initially considered in order to understand and predict the data given in Figures 4.11 to 4.26. However, the data in Figures 4.11 to 4.26 show that the incubation time increased and the crack speed generally decreased upon increasing the water-bath temperature. Hence, the theory of S.M. Wiederhorn et al (1980) is not valid in the present investigation, since the activation energy concept, and in particular the activation energy for water diffusion in the adhesives (Section 5.3.2) cannot be used to predict temperature effects. The data in Figures 4.11 to 4.26 suggest that a second major effect occurred during the fracture process of the double-torsion adhesive joints. Namely, it is possible that plasticization of the adhesives and crack tip blunting may explain the data shown in these Figures (see Section 7.2.3).

7.2.3 Effect of Applied Stress

The data in Figures 4.11 to 4.26 suggest that, for a given temperature, then the incubation time decreased and the crack speed increased when the applied fracture energy, G_c, of the double-torsion adhesive joints was raised. However, as the temperature of the distilled water was increased the incubation time did not decrease, as it would be expected from equation (7.8) for an "activated rate process", but actually increased in the case of the unmodified double-torsion adhesive joints (Figure 4.17). For

the rubber-modified adhesive joints the incubation time did not vary when the temperature of the distilled water was increased from 25°C to 40°C. A decrease in the incubation time was only observed in the case of the rubber-modified adhesive joints exposed to distilled water at 55°C. These experimental results suggest that a crack blunting mechanism had occurred during the tests.

The phenomenon of crack tip blunting occurring in long-term stressed experiments, and especially when water is present, is well established. R.A. Gledhill, A.J. Kinloch and S.J. Shaw (1979), observed an increase in the fracture energy needed to initiate crack propagation after loading adhesive joints compared to the fracture energy measured prior to subjecting the joints to static testing. It was also observed that the time that the joint was subjected to a statically applied load increased the value of the fracture energy which was subsequently measured. It was suggested that this rise in the fracture energy, and the delay in static failure, was due to crack tip blunting as a result of the formation of a plastic zone ahead of the crack tip. Hence, this mechanism was considered to be responsible for delaying the static fatigue failure of the adhesive joints examined. The same phenomenon was observed again recently by R.J. Davies and A.J. Kinloch (1988). Crack tip blunting occurred in adhesive joints subjected to long-term testing in the presence of distilled water. This phenomenon greatly delayed the environmental failure of the joints. The problem was overcome in the tests by increasing the applied loads in a stepwise fashion (the load at eventual failure of the joint in the water environment being considerably greater than the load initially required to fail the joint before crack tip blunting occurred).

Therefore, in the present investigation crack tip blunting probably occurred in the double-torsion adhesive joints. Since the yield stress of epoxide adhesives decreases as water is absorbed, and as the test temperature increases, this effect would be further enhanced by the presence of water (due to plasticisation) and by higher temperatures (due to viscoelasticity). Hence, the durability of the joints would tend to increase as the temperature of the distilled water is increased. In the case of the rubber-modified

adhesive, then for joints exposed to water at 25°C and 40°C, no change in the incubation time was observed, indicating that the same extent of plasticity and crack blunting had most probably occurred in the joints. However, at 55°C the incubation time of the joints was found to decrease with increasing the fracture energy, indicating that crack tip blunting had less effect on the durability of these joints. Crack tip blunting was also most probably the cause of the decrease in the crack speeds observed in all double-torsion joints tested.

Crack blunting therefore reduces the stress concentration field around the crack tip, and hence the rate of local interfacial debonding due to stress-assisted water attack is lowered, thereby increasing the durability of the double-torsion joints observed in the present investigation. This crack tip blunting mechanism therefore tends to increase the observed durability of the joints, whilst the water-attack mechanism discussed in Section 7.2.1 tends to decrease the durability of the joints.

7.2.4 Lower Bound Values of Fracture Energy

The data in Figures 4.11 to 4.26 suggests that there is no minimum value of the applied fracture energy, G_c, below which slow crack growth (and hence fracture) in the DT adhesive joints studied in the present investigation might not occur. To establish whether there is a very low "lower bound" value of G_c, then static tests over very long periods should be conducted in order to determine this value. The lower bound theory (S. Mostovoy and E.J. Ripling, 1969, B.W. Cherry and K.W. Thomson, 1977, 1980) suggests that rupture of the secondary forces acting across the interface of the double-torsion adhesive joints, due to water ingress, would not occur unless the applied fracture energy exceeds a minimum value. However, no evidence for the existence of a "lower bound" value of G_c was seen in the present studies.

7.3 PREDICTION OF ENVIRONMENTAL ATTACK

7.3.1 Introduction

An attempt has been made to predict the butt joint fracture data obtained in Figures 4.33 and 4.34 from the fracture data obtained from the experiments conducted using the double-torsion joints. In general, the total butt joint fracture time, t_f, may be taken from the equation:

$$t_f = t_{inc} + t_{sc} \tag{7.9}$$

where t_{inc} and t_{sc} are the incubation time and the time needed for continuous crack propagation of the butt joint respectively. Therefore, theoretical calculations of the two terms in the right hand side of equation (7.9) would allow the total butt joint fracture time to be estimated, and hence compared to the experimental values.

7.3.2 Incubation time

It is generally accepted that engineering components always contain flaws from fabrication or induced during in-service loading. These flaws act as stress concentrators and may contribute to the variation in the properties of the material. In the present investigation is assumed that such a flaw of length α_o exists in the epoxide layer of the unmodified and rubber-modified butt adhesive joints prior to static loading. Then, α_o can be found from the equation:

$$\alpha_o = E_a G_c / Q^2 \sigma_{fa}^2 \tag{7.10}$$

where E_a is the modulus of the epoxide adhesive, G_c is the dry fracture energy of the double-torsion adhesive joints, Q is the geometry factor ($Q^2=\pi$), and σ_{fa} is the dry fracture stress of the adhesive. Values of the dry butt stress for the unmodified and rubber-modified adhesive joints were taken to be 65 MN/m^2 and 50 MN/m^2 for the

unmodified and rubber-modified adhesives respectively from the work of A.F. Yee and R.A. Pearson (1986). Taking the value of E_a to be 3.3 GPa and 2.8 GPa for the unmodified and rubber-modified materials respectively from the work of A.J. Kinloch et al, (1985), and the values of G_c from Figure 4.10, the values of α_o calculated for the adhesive in the unmodified and rubber-modified butt joints were 4.04 x 10^{-5} m and 4.49 x 10^{-4} m respectively. Having found α_o, values of the fracture energy, G_c, applied to butt joints, for a given applied stress level can be estimated using the equation:

$$G_c = Q^2 \sigma_f^2 \alpha_o / E_a \qquad (7.11)$$

where G_c is now the value for the "wet" butt joint fracture energy, σ_f is the tensile stress applied to butt joint and Q=1.1. Values of the fracture energies applied to the butt joints which were subjected to a constant stress, σ_f, whilst being immersed in water are shown in Table 7.2, together with the applied fracture stresses, σ_f, and the theoretical predictions for the incubation times, t_{inc}. These predictions were made using the data in Figures 4.11 and 4.14 where the data may be fitted to:

$$G_c = (\text{constant})\, t_{inc}^{-z} \qquad (7.12)$$

where z is the slope of the line and the constant is the intercept on the fracture energy axis. The values of the constant and the slope are shown in Table 7.3. Using equation (7.12) values of the incubation time, t_{inc}, can be found from the corresponding estimated values of G_c (equation 7.11).

7.3.3 Crack Growth Stage

A mathematical equation for the calculation of the time for slow crack growth term in equation (7.9), t_{sc}, may be derived by considering the data in Figures 4.19 and 4.22. This data may be fitted into an equation of the form:

$$G_c = A\,\alpha^n \tag{7.13}$$

where A is a constant, n is the slope of the line and α is the crack speed ($\alpha = d\alpha/dt$). Equation (7.13) becomes:

$$t_{sc} = \int_{\alpha_o}^{\alpha_f} A^{1/n}/G^{1/n}_c \, d\alpha \tag{7.14}$$

where α_f is the final crack length. But, since G_c can be expressed by the equation $G_c = Q^2\,\sigma_f^2\,\alpha/E_a$, where Q=1.1, then equation (7.14) may become:

$$t_{sc} = \int_{\alpha_o}^{\alpha_f} A^{1/n}/(\,Q^2\,\sigma^2_f\,\alpha/E_a\,)^{1/n}\,d\alpha$$

$$= E_a^{1/n}\,A^{1/n}/\,Q^{2/n}\,\sigma^{2/n}_f \int_{\alpha_o}^{\alpha_f} \alpha^{-1/n} d\alpha$$

$$= \{\,E_a^{1/n}\,A^{1/n}/\,Q^{2/n}\,\sigma^{2/n}_f\,\}\{\,n/(n-1)\}\,[\,\alpha_f^{(n-1)/n} - \alpha_o^{(n-1)/n}] \tag{7.15}$$

If n is small then $\alpha_f >> \alpha_o$, then equation (7.15) becomes:

$$t_{sc} = \{\,E_a^{1/n}\,A^{1/n}/\,Q^{2/n}\,\sigma^{2/n}_f\,\}\{\,n/(1-n)\}\,[\alpha_o^{(n-1)/n}] \tag{7.16}$$

If n is not small then:

$$t_{sc} = \{\,E_a^{1/n}\,A^{1/n}/\,Q^{2/n}\,\sigma^{2/n}_f\,\}\{\,n/(1-n)\}\,[\,\alpha_o^{(n-1)/n} - \alpha_f^{(n-1)/n}] \tag{7.17}$$

Hence, the time for slow crack propagation in the adhesive butt joints

can be calculated from equations (7.16) or (7.17). Equation (7.16) can be used for the unmodified butt adhesive joints since n was found to be small. For the rubber-modified butt joints, where n was not small, equation (7.17) can be used to calculate t_{sc}. However, in this case $t_{sc} << t_{inc}$, and therefore calculations to find t_{sc} were not necessary. The values of the constant A and the slope n are shown in Table 7.4 and these values were calculated from Figures 4.19 and 4.22. Finally, Table 7.5 shows the values of the applied butt joint stress, σ_f, and the theoretically calculated values for the incubation time, t_{inc}, the time for slow crack growth, t_{sc}, and the total time, t_f.

7.3.4 Comparison of Theoretical and Experimental Approaches

A comparison between the experimental and theoretical butt joint fracture data is shown in Figures 7.2 and 7.3 for the unmodified and rubber-modified joints respectively. These Figures display the data as plots of the butt joint applied tensile stress, σ_f, against the logarithmic fracture time, t_f. The points in these Figures are experimental measurements and the curves are the theoretical predictions. From the data shown in Figure 7.2 it can be seen that the theoretical predictions for the unmodified butt joints do not agree with the experimental measurements. This is considered to be due to the very marked effects of crack tip blunting, as described previously, for the unmodified adhesive. However, the agreement between the theoretical and experimental measurements was found to be far better in the case of the rubber-modified butt joints, as the data in Figure 7.3 demonstrate. This, again, is to be expected as there is a lower degree of crack tip blunting in the rubber-modified epoxy. This is in agreement with previous work (R.A. Gledhill et all, 1979,) where they found that it was the more brittle adhesives (e.g. the unmodified epoxide) which underwent the greatest crack tip blunting effects. The model proposed in the present Section does not take crack tip blunting effect into account. However, the above model has never previously been applied to the failure of adhesive joints and the reasonable agreement between theory and experiment for the rubber- modified adhesive joints is very encouraging. Obviously, the next step should be

to incorporate crack tip blunting effects into the model.

7.4 CONCLUSIONS

The following conclusions may be made:

1. The mechanism of water attack appears to be via the diffusion of water through the adhesive at the interface. The water then ruptures the secondary bonds acting across the adhesive/metal oxide interface.

2. The above mechanism may be explained by considering the thermodynamic work of adhesion. In the presence of water the value of the thermodynamic work of adhesion changes from a positive to a negative value, indicating that the interface is unstable and will debond when water is present.

3. The above mechanism accounts for the observations in Chapter 6 of an increasing amount of interfacial failure occurring after the joints had been exposed to water.

4. From comparing the environmental fracture data (Chapter 4) and the diffusion data (Chapter 5) it is evident that the water concentration in the adhesive layer does not have to reach equilibrium, i.e. saturation, for environmental attack to occur.

5. There is no evidence for a "lower bound" value of the adhesive fracture energy, below which environmental failure does not occur.

6. An "activation energy" approach to understanding and predicting the effect of temperature on the rate of environmental attack is unsuccessful due to crack tip blunting occurring in the DT specimens. The effect of crack tip blunting is to lower the stress concentration at the crack tip and so decrease the stresses acting on the interface. This lowers the rate of environmental attack upon the joint.

7. Thus, the water attack mechanism is a "weakening" mechanism, but crack tip blunting is a "strengthening" mechanism.

8. A model has been proposed for predicting the lifetime of the adhesive butt joints when exposed to water, using data obtained from the DT joint experiments. This is the first time such a model has been applied to adhesive joints.

9. The model is not successful for the unmodified epoxide joints due to excessive crack tip blunting occurring.

10. However, for the rubber-modified joints, when crack tip blunting effect are not so severe, then the model is reasonably successful and experimental and theoretical results are in reasonable agreement.

Table 7.1: Surface free energies of water and dispersion and polar force components of the epoxide adhesive and the ferric oxide:

Phase	Surface free energy (mJ/m^2)								
	γ^D_L	γ^P_L	γ_L	γ^D_S	γ^P_S	γ_S	γ^D_A	γ^P_A	γ_A
Water	22.0	50.2	72.2	-	-	-	-	-	-
Ferric Oxide	-	-	-	41.2	5.0	46.2	-	-	-
Epoxide adhesive	-	-	-	-	-	-	107	1250	1357

Table 7.2: Theoretical values of the fracture stress, σ_f,MN/m^2, the energy applied, G_c, J/m^2, and the incubation time, t_{inc}, hours:

Unmodified butt adhesive joints			Rubber-modified butt adhesive joints		
σ_f	G_c	t_{inc}	σ_f	G_c	t_{inc}
25	8.42	133	25	110	2.8
20	5.39	555	20	70.6	5.5
15	3.03	2,222	15	39.7	55.5
10	1.35	22,222	10	17.6	1,389

Table 7.3: Values of the constant, J/m^2, and the slope z, $Jm^{-2}sec^{-1}$, from the data in Figures 4.11 and 4.14 obtained using equation 7.12:

Unmodified DT joints		Rubber-modified DT joints	
Constant	n	Constant	n
536.9	-1.34×10^{-5}	992.8	-4.90×10^{-8}

Table 7.4: Values of the constant A, J/m^2, and the slope n, $Jm^{-3}sec$, obtained from Figures 4.19 and 4.22 respectively:

Unmodified DT adhesive joints		Rubber-modified DT adhesive joints	
A	n	A	n
224.9	0.191	2.52	1.521

Table 7.5: Time to failure predictions for the adhesive butt joints. The time for slow crack growth t_{sc}, hours, for the rubber-modified butt adhesive joints was very small and therefore neglected, and t_{sc} for the unmodified butt adhesive joints was calculated from the equation:

$$t_{sc} = \{ E_a^{1/n} A^{1/n} / Q^{2/n} \sigma_f^{2/n} \} \{ n/(1-n) \} [\alpha_o^{(n-1)/n}] \qquad \text{(Equation 7.16)}$$

where the σ_f values are in MN/m^2.

Unmodified butt adhesive joints				Rubber-modified butt adhesive joints		
σ_f	t_{inc}	t_{sc}	t_f	σ_f	t_{inc}	t_f
25	133	0.05	133.05	25	2.8	2.8
20	555	0.5	555.5	20	5.5	5.5
15	2,222	9.91	2231.91	15	55.5	55.5
10	22,222	692.2	22914.2	10	1,389	1,389

(where times are in seconds)

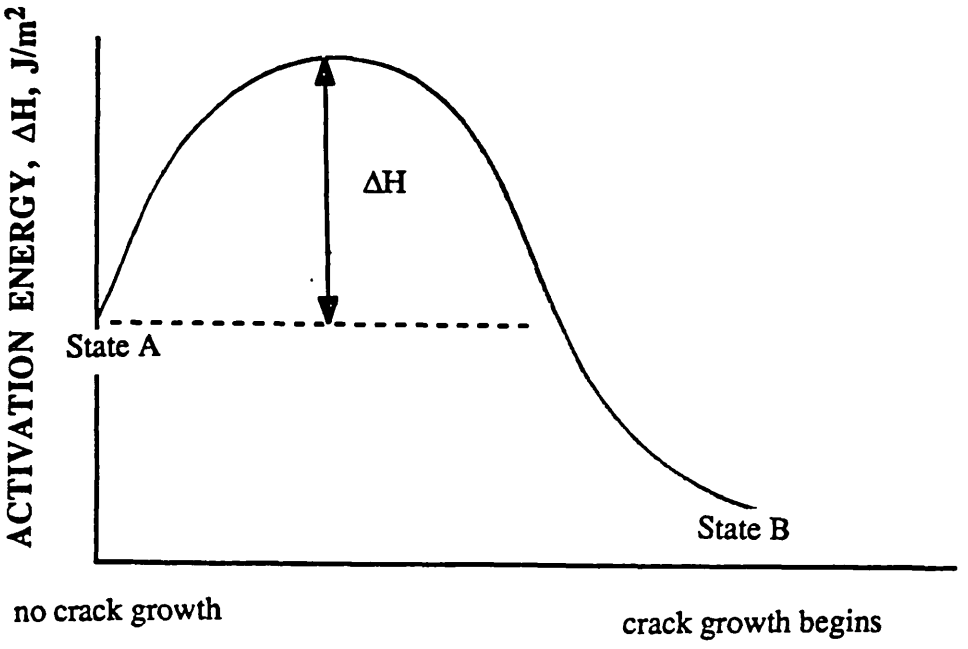


Figure 7.1: Schematic representation of the activation energy, ΔH, needed for crack propagation to start. In state A no crack propagation occurs, and in state B crack propagation, and therefore rupture of bonds, initiates.

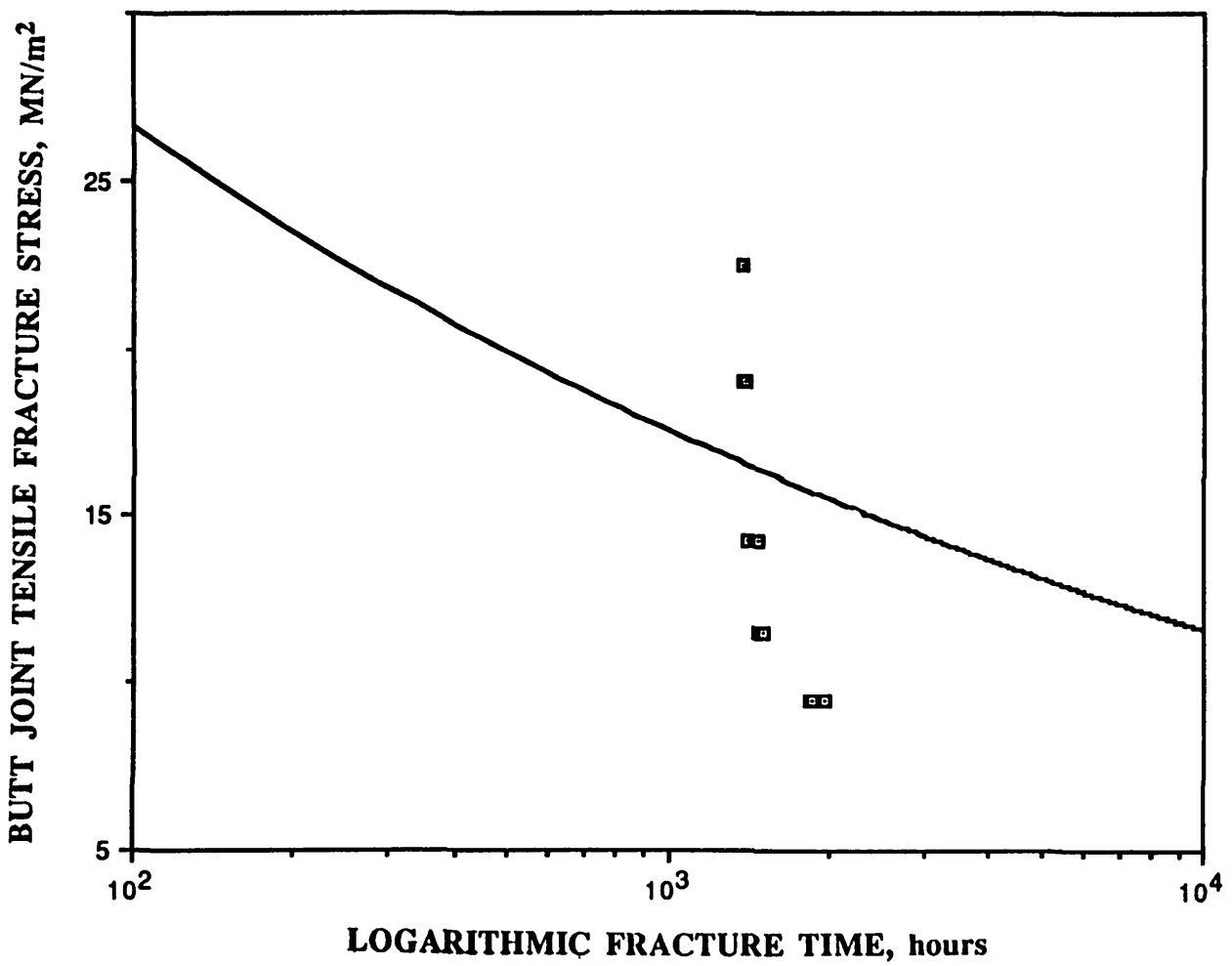


Figure 7.2: Butt adhesive joints fracture stress, σ_f, versus logarithmic fracture time, t_f. The data was obtained for unmodified joints exposed to distilled water at 25°C. Points are experimental measurements and the solid curves are the theoretical predictions.

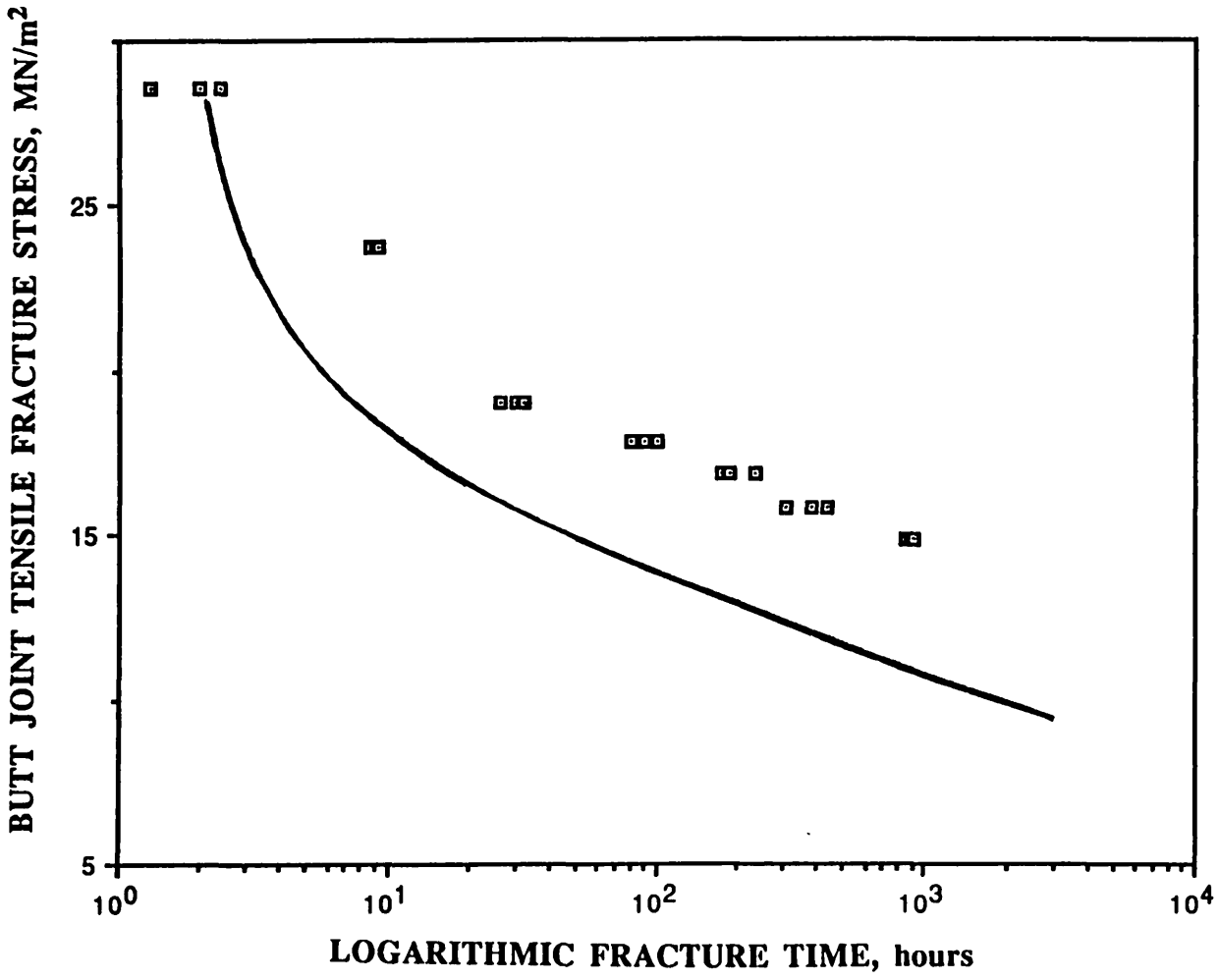


Figure 7.3: Butt adhesive joints fracture stress, σ_f, versus logarithmic fracture time, t_f. The data was obtained for rubber-modified joints exposed to distilled water at 25°C. Points are experimental measurements and the solid curves are the theoretical predictions.

CHAPTER 8

MAIN CONCLUSIONS

The main conclusions from the present studies are:

1. It was initially considered that an adhesive formulation which failed via a crack propagating in a stable, steady manner could be the most suitable for the present study. However, the search for an adhesive formulation which consistently fractured by a crack propagating in a steady, controlled rate was unsuccessful. All the formulations examined by testing fracture mechanics specimens at a constant displacement rate showed that, before exposure to an aqueous environment, the crack propagated in a stick/slip, unstable manner.

2. Therefore, twe model adhesive formulations were selected for the work. One was a simple unmodified epoxide whilst the other was a rubber-modified epoxide. The latter possessed the higher value of fracture energy, G_{Ic}, and stress-intensity factor, K_{Ic}, and this may be explained in terms of additional toughening mechanisms which occur at the crack tip. These produce blunting of the crack tip and therefore increase the crack resistance of the rubber-toughened epoxide. Having characterised the fracture of these adhesives prior to environmental exposure, the next step was to examine the durability of these adhesives bonding mild steel substrates and exposed to distilled water at various temperatures.

3. To examine the durability of the adhesive joints a novel test method has been developed. The basic idea was to develop a simple, inexpensive durability test which uses stress and temperature to accelerate the environmental attack mechanism. The new test method involves using double-torsion (DT) adhesive joint specimens, loaded via a simple constant-load apparatus.

4. The experimental compliances of such DT joints have been measured and found to agree extremely well with the theoretical values. These values of specimen compliance have been used to calculate the fracture energy, G_c, of the joints.

5. This new test method has been shown to give reliable and reproducible fracture data

when DT joints are tested in aqueous environments. Two separate failure processes have been identified. Firstly, an incubation time, defined as the time taken for a new interfacial crack to initiate at the adhesive/oxide interface. Secondly, the subsequent steady growth of this interfacial crack along the adhesive/oxide interface. Hence, plots of the values of G_c versus the incubation time and G_c versus the rate of crack growth may be obtained. The incubation time decreases, and the subsequent rate of crack growth increases, as the value of G_c is increased.

6. A complicating factor in the above experiments was that, whilst the joint was weakened by environmental attack at the adhesive/oxide interface, the effect of the applied load and presence of water was to cause crack tip blunting. This reduces the stress concentration in the joint and therefore acts to increase the durability of the joint. The effect was particularly marked in the more brittle unmodified adhesive, and so this adhesive appeared to be more durable than the rubber-modified epoxide on the basis of the current tests.

7. To identify in more detail the manner by which the concentration of water and the rate of water ingress into the adhesive joints affect the observed losses in joint strength, the water absorption properties of the rubber-modified and unmodified materials were examined. It was found that the epoxide adhesives exhibited Fickian diffusion. A diffusion coefficient and a water equilibrium value were measured for each epoxide. From the calculated activation energies for diffusion it has been suggested that the possible effect of the rubber particles on the epoxide material is to increase the rate of water uptake. From these studies it has also been suggested that saturation of the adhesive layer in the joints is not a necessary requirement for environmental attack to occur. A far lower concentration of water than the equilibrium (i.e. saturation) level is necessary to induce environmental attack.

8. The locus of joint failure was studied using scanning electron microscopy and X-ray photoelectron spectroscopy. For the double-torsion adhesive joints two different regions were recorded. In the upper region, where compressive stresses initially act during

testing, the locus of failure was via cohesive fracture in the adhesive. In the most important lower region of the specimen, where tensile stresses act, the locus of failure was mainly interfacial at the adhesive/oxide interface. The extent of interfacial failure increased after environmental attack by water. The feature of the upper region always failing by cohesive-in-adhesive fracture suggested that compressive stresses inhibit the mechanism of environmental attack. The type of adhesive, load, or test temperature had no effect on the locus of failure in the presence of water. It was concluded that these factors appeared not to affect the mechanisms of water attack, but merely changed the kinetics of environmental attack.

9. The thermodynamic work of adhesion for the adhesive/oxide interface in water is negative in value. This suggests that the mechanism of water attack is by the water rupturing the interfacial secondary (van der Waal's) bonds and so displacing the adhesive from the steel substrate surface.

10. The fracture mechanics data measured from the DT joint specimens have been used to attempt to predict the lifetimes of butt joints exposed to distilled water and simultaneously subjected to various levels of applied stress. A novel model has been proposed and, in the absence of extensive crack tip blunting, is moderately successful in predicting the lifetimes of the butt joints.

CHAPTER 9

SUGGESTIONS FOR FURTHER WORK

The following are considered to be areas where further research work would be of considerable advantage in developing an understanding of the mechanics and mechanisms of the environmental failure of adhesive joints using a fracture mechanics approach:

1. Using the new test method developed in the present work to investigate parameters such as the effect of type of substrate, substrate pretreatments, and the effect of applying an electropotential across the DT adhesive joints.

2. Further, investigations to determine whether there is a "lower bound" value of the applied fracture energy for the DT joints below which no crack growth is observed.

3. Improving the new life prediction theory to account for the phenomenon of crack tip blunting which occurred during environmental testing.

4. Studies on the effect of relative humidity (i.e. water concentration) on the relations between G_c and incubation time, and G_c and crack growth rate. These studies should enable the critical concentration for interfacial attack to be identified. This information can then be used to introduce the diffusion data into the life prediction theory, and so predict the time to failure for joints from the diffusion data and fracture mechanics data combined.

REFERENCES

E.H.ANDREWS and A.J.KINLOCH, "Mechanics of Adhesive Failure I", *Proc.Roy.Soc.*, **A332**, 1973, 385.

C.B.BUCKNALL, "Toughened Plastics", Applied Science, London, 1977.

W.D.BASCOM, S.T.GADOMSKI, C.M.HENDERSON and R.L.JONES, "Fracture Markings on Stress-corroded Epoxy/aluminium Butt Joints", *J. Adhesion* , **8**, 1977, 213.

P.W.R.BEAUMONT and R.J.YOUNG,(a), "Failure processes in a silica particle-filled epoxy resin composite", *Journal of Materials Science*, **10**, 1975, 1343.

P.W.R.BEAUMONT and R.J.YOUNG,(b), "Crack Propagation in Polymethylmethacrylate and Time to Failure Predictions", *Journal of Materials Science*, **10**, 1975, 1334.

P.W.BEAUMONT and R.J.YOUNG, "Effect of Composition upon the Fracture of Silica particle-filled Epoxy Resin Composites", *Journal of Materials Science*, **12**, 1977, 684.

J.BOERIO and D.J.ONDRUS, "X-Ray Photoelectrom Spectroscopy of the Fracture Surfaces of Iron/epoxy and Titanium/epoxy Adhesive Joints", *J.Adhesion*, **22**, 1987, 1.

D.M.BREWIS, J.COMYN and S.T.TREDWELL, "Diffusion of Water in Some Modified Phenolic Adhesives", *Int. J. Adhesion and Adhesives*, **7(1)**, 1987, 30.

D.M.BREWIS, J.COMYN, R.J.A.SHALASH and J.L.TEGG, "Interaction of Water with Some Epoxide Adhesives", Polymer, **21**, 1980, 357.

D.M.BREWIS, J.COMYN, and J.L.TEGG, "The Durability of Some Epoxide Adhesive-bonded Joints on Exposure to Moist Warm Air", *Int. J. Adhesion Adhesives* , **1**, 1980, 35.

D.BRIGGS, D.M.BREWIS, and M.D.KONIECZHO, "X-ray Photoelectron Spectroscopy Studies of Polymer Surfaces", *J.Material Science*, **11**, 1976, 1270.

D.BROEK, "Elementary Engineering Fracture Mechanics", Noordoff, 1974, Leyden.

R.I.BUTT and J.L.COTTER, "The Effect of High Humidity on the Dynamic Mechanical Properties and Thermal Transitions of an Epoxy-polyamide Adhesive", *J. Adhesion* , **8**, 1976, 11.

H.S.CARSLAW, and J.C.JAEGER, "Conduction of Heat in Solids", Oxford Univ. Press, London, 1959.

J.COMYN, "Structural Adhesives: Developments in Resins and Primers" (Edited by A.J.KINLOCH), Applied Science Pub., London, 1986, 269.

J.CRANK, and G.S.PARK, "Diffusion in Polymers", Academic Press, London, 1968, 16.

J.CRANK, "The Mathematics of Diffusion", Oxford Univ. Press, London, 1956, 241.

R.J.DAVIES, and A.J.KINLOCH, "The Surface Characterisation and Adhesive Bonding of Aluminium", *Adhesion*, **13**, (Edited by K.W.ALLEN), Elsevier Applied Science, London, 1989, (to be published).

B.V.DERYAGUIN, N.A.KROTOVA, V.V.KARASSEV, Y.M.KIRILLORA, and I.N.ALEINIKOVA, "Proceedings of the 2nd International Congress on Surface Activity - III", Butterworths, London, 1957, 417.

B.V.DERYAGUIN, and V.P.SMILGA, "Adhesion Fundamentals and Practice", Mclaren and Son, London, 1969, 152.

B.V.DERYAGIN, "Problems of Adhesion", *Research* , **8**, 1955, 70.

A.G.EVANS, "A method for evaluating the time dependent failure characteristics of brittle materials and its application to polycrystalline alumina", *Journal of Materials Science*, **7**, 1972, 1137.

J.R.EVANS and D.E.PACKHAM, "Adhesion of Polyethylene to Copper", *Adhesion* , **1**, (Edited by K.W.ALLEN), Applied Science Pub., London, 1977, 297.

J.R.EVANS and D.E.PACKHAM, "Adhesion of Polyethylene to Copper: Reactions between Copper Oxides and the Polymer", *J.Adhesion* , **9**, 1978, 267.

J.R.EVANS and D.E.PACKHAM, "Adhesion of Polyethylene to Copper: Importance of Substrate Topography", *J.Adhesion* , **10**, 1979, 39.

A.G.EVANS "A Simple Method for Evaluating Slow Crack Growth in Brittle Materials", *Int. Journ. of Fracture*, **9**, 1973, 267.

R.H.FRENCH and RISHI RAJ, "Use of the Double-Torsion Method to Study Crack Propagation in an Adhesive Layer", *Journal of Testing and Evaluation*, **7**(3), 1979, 160.

M.GETTINGS, F.S.BAKER, and A.J.KINLOCH, "Use of Auger and X-ray Photoelectron Spectroscopy to Study the Locus of Failure of Structural Adhesive Joints", *J. Applied Polymer Science*, **21**, 1977, 2375.

M.GETTINGS, and A.J.KINLOCH, "Surface Analysis of Polysiloxane/metal Oxide Interfaces", *J.Material Science*, **12**, 1977, 2511.

M.GETTINGS, and A.J.KINLOCH, "Surface Characterization and Adhesive Bonding of Stainless Steels - The Steel/adhesive Interface", *Surf.Interf.Anal.*, **6**, 1979, 40.

R.A.GLEDHILL, A.J.KINLOCH, and S.J.SHAW, "A Model for Predicting Joint Durability", *J. Adhesion* , **11**, 1980, 3.

R.A.GLEDHILL, and A.J.KINLOCH, "Environmental Failure of Structural Adhesive Joints", *J. Adhesion* , **6**, 1974, 315.

R.A.GLEDHILL and A.J.KINLOCH S.YAMINI and R.J.YOUNG, "Relationship Between Mechanical Properties and Crack Propagation in Epoxy Resin Adhesives", Polymer, **19**, 1978, 574.

R.A.GLEDHILL, A.J.KINLOCH, and S.J.SHAW, "A Self-toughening Mechanism in Epoxide Resins", *J. Materials Science*, **14**, 1979, 1769 (Letters).

A.A.GRIFFITH, "The Phenomena of Rupture and Flow in Solids", *Phil.Trans.Roy.Soc.*, **221 A**, 1920, 163.

GRAFT VON H.HARRACH, and B.N.CHAPMAN, "Change Effects in Thin Film Adhesion", Thin Solid Films, **13**, 1972, 157.

P.J.HINE, S.EL.MUDDARRIS, and D.E.PACKHAM, "Surface Pretreatment of Zinc and its Adhesion to Epoxy Resins", *J.Adhesion*, **47**, 1984, 207

J.R.HUNTSBERGER, "The Nature of Adhesion", *Adhesives Age* , **13 (11)**, 1970, 43.

G.R.IRWIN, "Fracture Strength of Relatively Brittle Structures and Materials", Journal of The Franklin Institute, **290 (6)**, 1970, 513.

J.N.ISRAELACHVILI, and D.TABOR, "The Measurement of Van der Waals' Forces in the Range 1.5 to 130 nm", *Proc.Roy.Soc.*, **A331**, 1972, 19.

C.W.JENNINGS, "Surface Roughness and Bond Strength of Adhesives", *J.Adhesion* , **4**, 1972, 25.

K.L.JOHNSON, K.KENDALL and A.D.ROBERTS, "Surface Energy and the Contact of Elastic Solids", *Pro.Roy.Soc.*, **A324**, 1971, 301.

C.KERR, N.C.MACDONALD, and S.ORMAN, "Effect of Certain Hostile Environments on Adhesive Joints", *J. Appl. Chem.*, **17**, 1967, 62.

J.A.KIES and A.B.J.CLARK, Proceedings of the Second International Conference on Fracture, Brighton, 1969, paper 42.

A.J.KINLOCH, "Structural Adhesives: Developments in Resins and Primers" (Edited by A.J.KINLOCH), Applied Science Pub., London, 1986, 127.

A.J.KINLOCH, L.S.WELCH, and H.E.BISHOP, "The Locus of Environmental Crack Growth in Bonded Aluminium Alloy Joints", *J. Adhesion*, **16**, 1984, 165.

A.J.KINLOCH, R.J.YOUNG, "Structural Adhesives- Developments in Resins and and Primers", Applied Science, London, 1986.

A.J.KINLOCH, S.J.SHAW, D.A.TOD, and D.L.HUNSTON, "Deformation and Fracture Behaviour of a Rubber - toughened Epoxy: 1. Microstructure and Fracture Studies", *Polymer*, **24**, 1983, 1341.

A.J.KINLOCH, S.J.SHAW, and D.L.HUNSTON, "Deformation and Fracture Behaviour of a Rubber-toughened Epoxy: 2. Failure Criteria", *Polymer*, **24**, 1983, 1355.

A.J.KINLOCH, and R.J.YOUNG, "Fracture Behaviour of Polymers", Applied Science Pub., London, 1983.

A.J.KINLOCH, D.MAXWELL and R.J.YOUNG, (a) "Micromechanisms of Crack Propagation in Hybrid-Particulate Composites", *Journal of Materials Science*, **4**, 1985,1276 (Letters).

A.J.KINLOCH, D.L.MAXWELL and R.J.YOUNG, (b) "The Fracture of Hybrid-particulate Composites", *Journal of Materials Science*, **20**, 1985, 4169.

K.K.KNOCK, M.C.LOCKE, "Proceedings of the 159th Meeting of the American and Electrochemical Society", 1981, Mineapolis.

J.F.KNOTT, "Fundamentals of Fracture Mechanics", Guildford, 1974, Butterworths.

H.LEE, and K.NEVILLE, "Epoxy Resins", McGraw-Hill, London, 1967.

P.S.LEEVERS, "Crack-front Shape Effects in the Double-Torsion Test", *Journal of Materials Science* , **17**, 1982, 2469.

P.S.LEEVERS and J.G.WILLIAMS, "Material and Geometry Effect on Crack Shape in Double-Torsion Testing", *Journal of Materials Science*, **20**, 1985, 77.

A.C.MOLONEY, H.H.KAUSCH and H.R.STIEGER, "The Use of the Double-Torsion Test Geometry to Study the Fracture of Adhesive Joints", *Journal of Materials Science*, **3**, 1984, 776 (Letters).

K.NAKAMURA, T.MARUNO, and S.SASAKI, "Theory for the Decay of the Wet Shear Strength of Adhesion and its Application to Metal/epoxy/metal Joints", *Int.J.Adhesion and Adhesives*, **7(2)**, 1987, 97.

K.NAKAMURA, T.UEDA, S.HOSONO, andT.MARUNO, "Theoretical Analysis for the Decay of Shear Strength of Adhesion in Metal/epoxy/metal Joints in Aqueous Environment", *Int.J.Adhesion and Adhesives*, **7(4)**, 1987, 209.

E.OROWAN, "The Physical Basis of Adhesion", Journal of The Franklin Institute, **290 (6)**, 1970, 493.

D.C.PHILLIPS and J.M.SCOTT "Determination of the (K,V) Diagrams of Epoxide Resins", *Journal of Materials Science*, **9**, 1974, 1202 (Letters).

D.E.PACKHAM, "Developments in Adhesives-2", (Edited by A.J. KINLOCH), Applied Science Pub., London, 1981, 315.

D.E.PACKHAM, "Adhesion Aspects of Polymeric Coatings", (Edited by K. L.MITTA), Plenum, New York, 1983, 19.

A.D.ROBERTS, "Nature of Adhesive Forces in Rubber Friction", *Adhesion*, **1**, (Edited by K.W.ALLEN), Applied Science Publishers, London, 1977, 207.

I.SKEIST, "Handbook of Adhesives", 2nd edition, van Nostrand Reinhold Co, New York, 1977.

S.M.SKINNER, R.L.SAVAGE, and J.E.RUTZLER, "Electrical Phenomena in Adhesion", *J.Applied Physics*, **24**, 1953, 439.

A.STEVENSON, "On the Durability of Rubber/metal Bonds in Seawater", *Int.J.Adhesion and Adhesives*, **5** (2), 1985, 81.

D.TABOR, F.R.S., and R.H.S.WINTERTON, "The Direct Measurement of Normal and Retarded Van der Waals'Forces", *Proc.Roy.Soc.*, **A312**, 1969, 435.

R.M.VASENIN, (a) "Adhesion of High Polymers. Part II: Predicting Adhesion", *Adhesives Age* , **8** (6), 1965, 30.

R.M.VASENIN, (b) "Adhesion of High Polymers. Introductory Comments", *Adhesives Age* , **8** (5), 1965, 18.

S.S.VOYUTSKII, "Adhesion and Autohesion of Polyners", *Adhesive Age* , **5** (4), 1962, 30.

S.S.VOYUTSKII, YU.I.MARKIN, V.M.GORCHAKOVA, and V.E.GUL, "Adhesion of Polymers to Metals", *Adhesives Age* , **8 (11)**, 1965, 24.

S.S.VOYUTSKII, "Comment on Diffusion Theory", *J.Adhesion*, **3**, 1971, 69.

W.C.WAKE, "Adhesion and the Formulation of Adhesives", Applied Science Pub., London, 1982, 267.

S.M.WIEDERHORN, E.R.FULLER Jr, and R.THOMSON, "Micromechanisms of Crack Growth in Ceramics and Glasses in Corrosive Environments", Metal Science, 1980, 450.

S.M.WIEDERHORN, S.W.FREIMAN, E.R.FULLER Jr, and C.J.SIMMONS, "Effects of Water and other Dielectrics on Crack Growth", *Journal of Materials Science*, **17**, 1982, 3460.

J.G.WILLIAMS, "Fracture Mechanics of Polymers", John Wiley, London, 1984, 58.

J.G.WILLIAMS, "Fracture Mechanics of Polymers", Ellis Horwood, Chichester, 1987.

A.F.YEE, R.A.PEARSON, "Toughening Mechanisms in Elastomer-modified Epoxies, Part 1: Mechanical Studies", *J. Materials Science*, **21**, 1986, 2462.

APPENDICES

APPENDIX 1

Derivation of Fracture Energy Equation

Linear-elastic fracture-mechanics (LEFM) is strictly applicable to those materials which obey Hooke's Law. Brittle materials, such as epoxy resins, exhibit inelastic deformation around the crack tip, but such deformations are confined to the immediate vicinity of the tip. LEFM can therefore be applied to such materials and a typical linear load versus deflection curve is shown schematically in Figure A_1.

If U_1 and U_2 are the elastic energies stored in the material during loading and unloading, then:

$$U_1 = 1/2(P\delta) \quad (1)$$

and

$$U_2 = (1/2)(P + dP)(\delta + d\delta) \quad (2)$$

where P is the load and δ is the deflection.

The change in stored energy is:

$$dU = U_2 - U_1 \quad (3)$$

The shaded area represents the external work done, and if F is the external force, then:

$$dF = PdP + 1/2dPd\delta$$

$$= (P + 1/2dP)d\delta \quad (4)$$

Therefore:

$$d(F - U) = (1/2)(Pd\delta - \delta dP) \quad (5)$$

Since G_c represents the change in energy due to the external work done and the energy stored in the material per unit thickness of the material per unit crack length, then:

$$G_c = d(F - U)/bd\alpha = (1/2t)(Pd\delta/d\alpha - \delta dP/d\alpha) \quad (6)$$

where t is the thickness of the material and α the crack length.

If the compliance of the material is considered (reciprocal of stiffness) which is defined as:

$$C = \delta/P \quad (7)$$

where C is the specimen compliance, then:

$$d\delta = PdC + CdP \quad (8)$$

Hence:

$$G_c = (P_c^2/2t)(dC/d\alpha) \quad (9)$$

where P_c represents the load at fracture.

APPENDIX 2

Derivation of Equation for Theoretical Compliance

If it is assumed that there is a constant angle of twist $d\phi/dx$ from the loading point to the crack tip of the DT bulk specimen, then:

$$d\phi/dx = - [2(1 + \upsilon)/E] [1/k(w/2)t^3] M \quad (1)$$

where M is the applied moment given by:

$$M = Pl_m/2 \quad (2)$$

and k is a constant that depends on the ratio (w/2), E and υ are the elastic modulus and Poisson's ratio of the material respectively, and P is the applied load. Therefore:

$$d\phi/dx = - [(1 + \upsilon)/E] [Pl_m/k(w/2)t^3] \quad (3)$$

Integrating the above equation from the loading point (at $x = 0$, where $\phi = \phi_o$) to the crack tip (at $x = \alpha$ where $\phi = \phi_\alpha$), gives :

$$\phi_\alpha - \phi_o = - [(1 + \upsilon)/E] [Pl_m/k(w/2)t^3] \alpha \quad (4)$$

It is sufficient to assume the ligament $(1-\alpha)$ to have a torsional compliance C_ϕ, to the moment transmitted by each beam, which is finite but independent of α. Then:

$$\phi_\alpha = (Pl_m/2) C_\phi \quad (5)$$

Therefore:

$$\phi_o = (Pl_m/2) C_\phi + [(1+\upsilon) Pl_m/Ek (w/2) t^3] \alpha + \text{constant} \quad (6)$$

or multiplying by l_m/P:

$$l_m\phi_o/P = l_m^2 C_\phi/2 + [(1+\upsilon) l_m^2/Ek (w/2) t^3] \alpha + \text{constant} \quad (7)$$

Since $y = l_m \phi_o$, (y is the displacement), then converting to linear load-point compliance C, C = y/P, where C is the compliance, gives:

$$C = l_m^2 C_\phi/2 + [(1+\upsilon) l_m^2/Ek (w/2) t^3] \alpha + \text{constant} \quad (8)$$

Now the product $l_m^2 C_\phi/2$ is constant since $C\phi$ in practice seems to remain constant until $(1-\alpha)$ is reduced to about (w/2), rising rapidly thereafter. Therefore can have:

$$C = \text{constant} + [(1+\upsilon) l_m^2/Ek (w/2) t^3] \alpha \quad (9)$$

Hence, differentiating the above equation, the expression for the theoretical compliance becomes:

$$dC/da = ((1+\upsilon)/E) (2l_m^2/k\, w\, t^3) \quad (10)$$

APPENDIX 3

Derivation of Stress Intensity Factor Equation used in the Present Research.

1.Bulk Fracture

For the bulk material and for plane-strain conditions, K_{Ic} and G_{Ic} are related with the equation:

$$K_{Ic}^2 = EG_{Ic} (1-\upsilon^2) \quad (1)$$

Therefore, combining the equations of the compliance and the fracture energy with the above equation , gives:

$$K_{Ic}^2 = P_c^2 l_m^2 [1/(1-\upsilon) kwt^3 t_n] \quad (2)$$

2.Joint Fracture

In a joint, both moduli of the system should be considered. If fracture occurs within the adhesive layer and E_s and E_a are the moduli of the substrate and the adhesive, then for a thin adhesive layer:

$$K_{Ic}^2 = P_c^2 l_m^2 [1/(1-\upsilon) kwt^3 t_n] (E_a/E_s) \quad (3)$$

If interfacial fracture occurs, then it is better to measure only G_c to avoid any complications involving E.

APPENDIX 4

Electrical Circuit Operation

IC_2 (Figure A_2) keeps the voltage across the gauge constant at 0.1 volts. IC_3 and its associated resistors form a differential amplifier whose output is 10 (V_Y-V_X). V_Y is held constant at 0.2 volts by the buffer stage IC_1. Initially R_G is adjusted until it is equal to R_g, so that V_X = 0.2 volts and V_{OUT} = 0.0, as detected by LED driver IC_4. As R_g increases, the current through it falls, the voltage across R_G falls as V_G= 0.1(R_G/R_g) so that V_X= 0.1(1+(R_G/R_g) and V_{OUT} rises as (1-(R_G/R_g)). When the gauge breaks, V_{OUT} = 1.0.

APPENDIX 5

Computer program for calculating the concentration of water into the adhesive layer of the double-torsion adhesive joints

```
5 REM ************INITIAL CONDITION***************
10 DIM A(300),XX(200),AA(200),X(200),CN(300),CT(300)
20 LET D=3.142E-12
30 LET CA=3.34
35 INPUT "INPUT TIME=";TT
40 LET T=3600*TT
100 X(1)=0
110 FOR I=1 TO 200
120 X(I+1)=X(I)+.00002
130 IF X(I+1)>.0015 THEN GOTO 150
140 NEXT I
150 NN=I
300 PRINT:PRINT"CT     X"
302 M=0
310 FOR I=1 TO NN
315 M=M+1
316 TOT=0
320 FOR N=0 TO M
321 L=.0015
322 B=((-1)^N)/(2*N+1)
323 E=EXP(((-D)*((2*N+1)^2)*(3.14^2)*T)/(4*(L^2)))
324 F=COS(((2*N+1)*3.14*X(I))/(2*L))
325 TOT=TOT+B*E*F
328 NEXT N
330 LET CN=CA*(1-((4/3.14)*TOT))
```

```
342 IF M=1 THEN K=CN
350 IF ABS(CT-K) <=.00001 THEN GOTO 370
351 K=CT
355 GOTO 315
370 S=M
375 A(I)=CT
376 XX(I)=X(I)/.0015
377 AA(I)=A(I)/3.34
380 PRINT USING"   ##.##^^^^------        ##.##^^^^";A(I);X(I)
390 NEXT I

7200 REM ******* TRANSFER DATA FOR MAKING GRAPH *******
7210 CLS:PRINT"YOUR DATA HAS BEEN STORED IN THE CLIPBOARD"
:PRINT:PRINT
7220 PRINT "CHANGE DISK. INSERT THE --Cricket Graph-- DISK" :PRINT
7230 INPUT "Press Return key to contimue?",DUM$
7240 OPEN "CLIP:" FOR OUTPUT AS #2
7260 FOR I=1 TO NN
7270 WRITE#2,A(I);X(I) :NEXT I
7350 CLOSE #2
7360 STOP
```

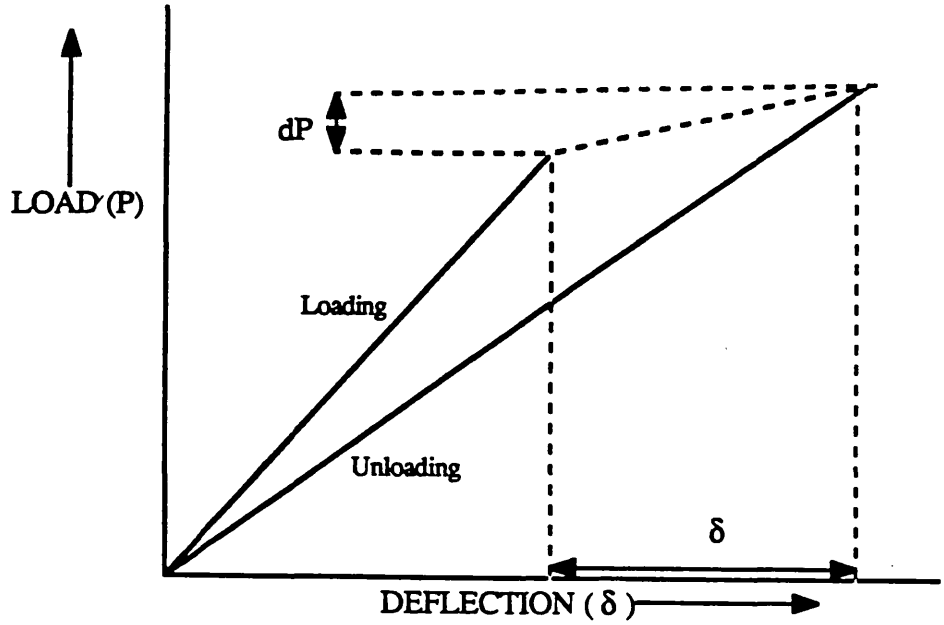


Figure A_1: Load against deflection curves for materials exhibiting linear elastic deformation.

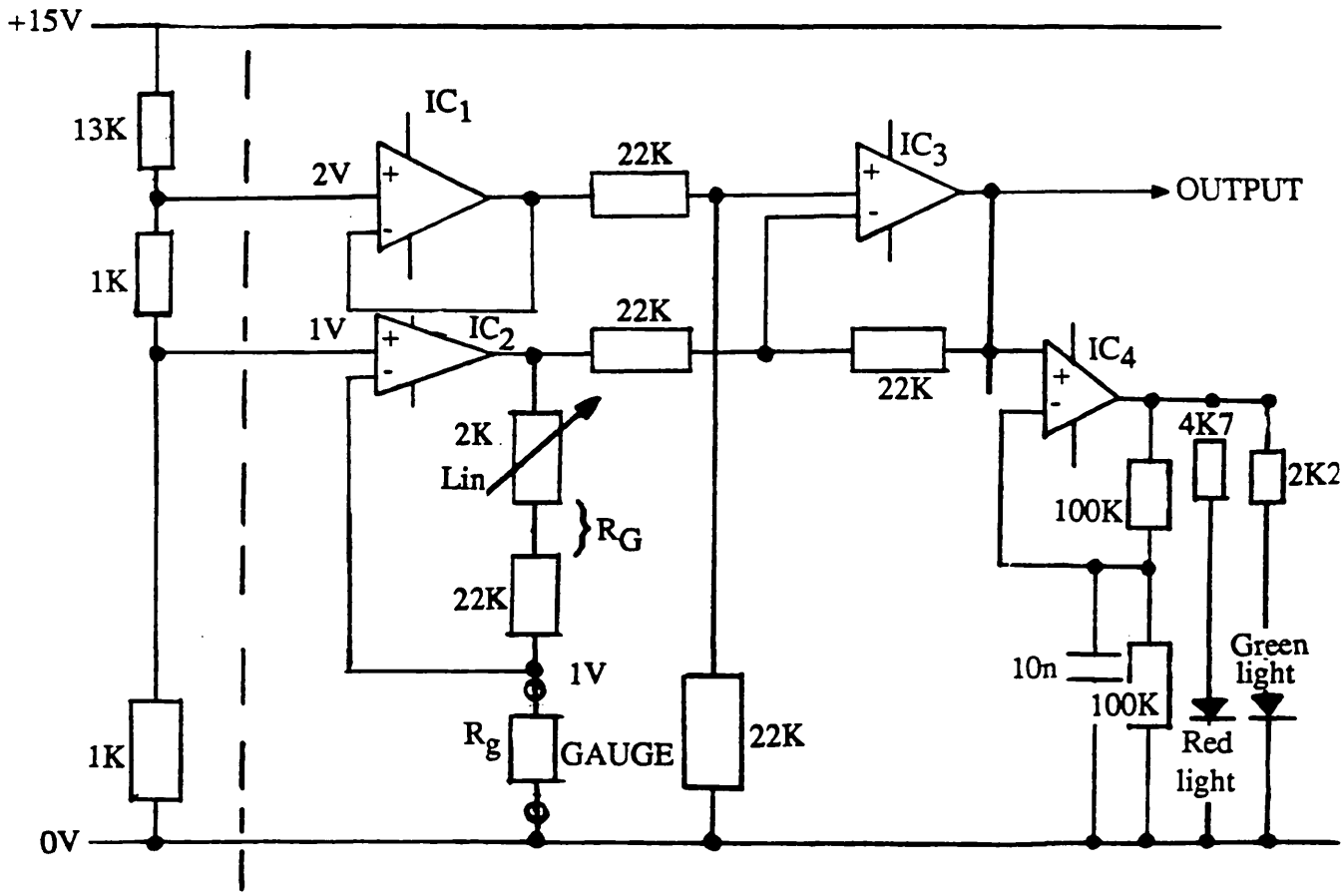


Figure A_2: Electrical circuit of potentiometer used in the present investigation.